

TOPICAL REVIEW

Testing general relativity with present and future astrophysical observations

To cite this article: Emanuele Berti *et al* 2015 *Class. Quantum Grav.* **32** 243001

View the [article online](#) for updates and enhancements.

Related content

- [Black hole based tests of general relativity](#)
Kent Yagi and Leo C Stein
- [I-Love-Q relations for neutron stars in dynamical Chern Simons gravity](#)
Toral Gupta, Barun Majumder, Kent Yagi et al.
- [TESTING UNIVERSAL RELATIONS OF NEUTRON STARS WITH A NONLINEAR MATTER GRAVITY COUPLING THEORY](#)
Y.-H. Sham, L.-M. Lin and P. T. Leung

Recent citations

- [Spontaneous tensorization from curvature coupling and beyond](#)
Fethi M. Ramazanolu
- [Scalar field as a null dust](#)
Valerio Faraoni and Jeremy Côté
- [Global monopole in Palatini \$f\(R\)\$ gravity](#)
J. R. Nascimento *et al*



IOP Astronomy ebooks

Part of your publishing universe and your first choice for astronomy, astrophysics, solar physics and planetary science ebooks.

iopscience.org/books/aas

Topical Review

Testing general relativity with present and future astrophysical observations

Emanuele Berti^{1,2}, Enrico Barausse^{3,4}, Vitor Cardoso^{2,5},
Leonardo Gualtieri⁶, Paolo Pani^{2,6}, Ulrich Sperhake^{1,7,8},
Leo C Stein^{8,9}, Norbert Wex¹⁰, Kent Yagi^{11,12}, Tessa Baker¹³,
C P Burgess^{5,14}, Flávio S Coelho¹⁵, Daniela Doneva¹⁶,
Antonio De Felice^{17,18}, Pedro G Ferreira¹³,
Paulo C C Freire¹⁰, James Healy¹⁹, Carlos Herdeiro¹⁵,
Michael Horbatsch¹, Burkhard Kleihaus²⁰, Antoine Klein¹,
Kostas Kokkotas¹⁶, Jutta Kunz²⁰, Pablo Laguna²¹,
Ryan N Lang^{22,23,24}, Tjonnie G F Li^{25,26}, Tyson Littenberg²⁷,
Andrew Matas²⁸, Saeed Mirshekari²⁹, Hirotada Okawa²,
Eugen Radu¹⁵, Richard O’Shaughnessy^{19,22},
Bangalore S Sathyaprakash³⁰, Chris Van Den Broeck³¹,
Hans A Winther¹³, Helvi Witek⁷, Mir Emad Aghili¹,
Justin Alsing³², Brett Bolen³³, Luca Bombelli¹,
Sarah Caudill²², Liang Chen¹, Juan Carlos Degollado¹⁵,
Ryuichi Fujita², Caixia Gao¹, Davide Gerosa⁷, Saeed Kamali¹,
Hector O Silva¹, João G Rosa¹⁵, Laleh Sadeghian²²,
Marco Sampaio¹⁵, Hajime Sotani³⁴ and Miguel Zilhao¹⁹

¹ Department of Physics and Astronomy, The University of Mississippi, University, MS 38677-1848, USA

² CENTRA, Departamento de Física, Instituto Superior Técnico, Universidade de Lisboa, Avenida Rovisco Pais 1, 1049 Lisboa, Portugal

³ CNRS, UMR 7095, Institut d’Astrophysique de Paris, 98bis Bd Arago, 75014 Paris, France

⁴ Sorbonne Universités, UPMC Univ Paris 06, UMR 7095, 98bis Bd Arago, 75014 Paris, France

⁵ Perimeter Institute for Theoretical Physics, Waterloo, Ontario N2L 2Y5, Canada

⁶ Dipartimento di Fisica, “Sapienza” Università di Roma & Sezione INFN Roma 1, P.le A. Moro 2, 00185 Roma, Italy

⁷ Department of Applied Mathematics and Theoretical Physics, Centre for Mathematical Sciences, University of Cambridge, Wilberforce Road, Cambridge CB3 0WA, UK

⁸ Theoretical Astrophysics 350-17, California Institute of Technology, Pasadena, CA 91125, USA

⁹ Cornell Center for Astrophysics and Planetary Science, Cornell University, Ithaca, NY 14853, USA

¹⁰ Max-Planck-Institut für Radioastronomie, Auf dem Hügel 69, D-53121 Bonn, Germany

¹¹ Department of Physics, Princeton University, Princeton, NJ 08544, USA

- ¹² Department of Physics, Montana State University, Bozeman, Montana 59717, USA
- ¹³ Astrophysics, University of Oxford, DWB, Keble Road, Oxford, OX1 3RH, UK
- ¹⁴ Department of Physics & Astronomy, McMaster University, Hamilton ON, Canada
- ¹⁵ Departamento de Física da Universidade de Aveiro and CIDMA Campus de Santiago, 3810-183 Aveiro, Portugal
- ¹⁶ Theoretical Astrophysics, Eberhard Karls University of Tübingen, Tübingen 72076, Germany
- ¹⁷ ThEP's CRL, NEP, The Institute for Fundamental Study, Naresuan University, Phitsanulok 65000, Thailand
- ¹⁸ Thailand Center of Excellence in Physics, Ministry of Education, Bangkok 10400, Thailand
- ¹⁹ Center for Computational Relativity and Gravitation, School of Mathematical Sciences, Rochester Institute of Technology, 85 Lomb Memorial Drive, Rochester, NY 14623, USA
- ²⁰ Institut für Physik, Universität Oldenburg, D-26111 Oldenburg, Germany
- ²¹ Center for Relativistic Astrophysics and School of Physics, Georgia Institute of Technology, Atlanta, GA 30332, USA
- ²² Leonard E Parker Center for Gravitation, Cosmology, and Astrophysics, University of Wisconsin-Milwaukee, Milwaukee, WI 53211, USA
- ²³ Department of Physics, University of Florida, Gainesville, FL 32611, USA
- ²⁴ Department of Physics, University of Illinois at Urbana-Champaign, Urbana, IL 61801, USA
- ²⁵ Department of Physics, The Chinese University of Hong Kong, Shatin, N. T., Hong Kong, People's Republic of China
- ²⁶ LIGO — California Institute of Technology, Pasadena, CA 91125, USA
- ²⁷ Center for Interdisciplinary Exploration and Research in Astrophysics (CIERA) & Dept. of Physics and Astronomy, Northwestern University, 2145 Sheridan Rd., Evanston, IL 60208, USA
- ²⁸ CERCA/Department of Physics, Case Western Reserve University, 10900 Euclid Ave, Cleveland, OH 44106, USA
- ²⁹ ICTP South American Institute for Fundamental Research & Instituto de Física Teórica, UNESP — Universidade Estadual Paulista, Rua Dr. Bento T. Ferraz 271 — 01140-070 São Paulo, SP, Brazil
- ³⁰ School of Physics and Astronomy, Cardiff University, 5, The Parade, Cardiff CF24 3AA, UK
- ³¹ Nikhef, Science Park, 1098 XG Amsterdam, The Netherlands
- ³² Imperial Centre for Inference and Cosmology, Imperial College London, Prince Consort Road, London SW7 2AZ, UK
- ³³ Department of Physics, Grand Valley State University, Allendale, MI 49401-9403, USA
- ³⁴ Yukawa Institute for Theoretical Physics, Kyoto University, Kyoto 606-8502, Japan

E-mail: eberti@olemiss.edu

Received 9 February 2015, revised 5 June 2015

Accepted for publication 3 August 2015

Published 1 December 2015



CrossMark

Abstract

One century after its formulation, Einstein's general relativity (GR) has made remarkable predictions and turned out to be compatible with all experimental tests. Most of these tests probe the theory in the weak-field regime, and there are theoretical and experimental reasons to believe that GR should be modified when

gravitational fields are strong and spacetime curvature is large. The best astrophysical laboratories to probe strong-field gravity are black holes and neutron stars, whether isolated or in binary systems. We review the motivations to consider extensions of GR. We present a (necessarily incomplete) catalog of modified theories of gravity for which strong-field predictions have been computed and contrasted to Einstein's theory, and we summarize our current understanding of the structure and dynamics of compact objects in these theories. We discuss current bounds on modified gravity from binary pulsar and cosmological observations, and we highlight the potential of future gravitational wave measurements to inform us on the behavior of gravity in the strong-field regime.

Keywords: general relativity, black holes, neutron stars, compact binaries, gravitational waves

Contents

1. Introduction	5
1.1. Taxonomy of proposed extensions of GR	7
1.2. Compact objects in modified theories of gravity	11
1.3. Present and future tests of strong gravity	12
2. Extensions of GR: motivation and overview	14
2.1. A compass to navigate the modified-gravity atlas	14
2.2. Scalar–tensor gravity	18
2.2.1. The Bergmann–Wagoner formulation	18
2.2.2. Scalar–tensor theories with multiple scalar fields	20
2.2.3. Horndeski gravity	20
2.3. Metric $f(R)$ theories	21
2.4. Quadratic gravity	23
2.4.1. EdGB gravity	25
2.4.2. Chern–Simons gravity	26
2.5. Lorentz-violating theories	27
2.5.1. Einstein-Æther	27
2.5.2. Khronometric theory	28
2.5.3. Hořava gravity	30
2.5.4. n -DBI gravity	31
2.6. Massive gravity and Galileons	32
2.7. Gravity with auxiliary fields	35
2.8. GR and quantum mechanics: an EFT approach	38
2.8.1. Power-counting and the semiclassical approximation	40
2.8.2. Modified gravity seen through EFT glasses	42
2.9. Open problems	43
3. Black holes	46
3.1. BHs in GR	46

3.2.	Scalar–tensor theories	47
3.2.1.	Real scalars and no-hair theorems.	47
3.2.2.	Complex scalars: new hairy rotating BHs	48
3.2.3.	Evading no-hair theorems in Horndeski/Gauss–Bonnet gravity	50
3.2.4.	BHs surrounded by matter.	52
3.2.5.	Stability	52
3.3.	$f(R)$ theories.	53
3.4.	Quadratic gravity	53
3.4.1.	Perturbative solutions in the slow-rotation limit	53
3.4.2.	EdGB theory	55
3.4.3.	dCS theory	58
3.5.	Lorentz-violating theories.	59
3.6.	Massive gravity	63
3.7.	Gravity with auxiliary fields.	64
3.8.	Parametrized phenomenological deviations from the Kerr metric.	64
3.9.	BH mimickers	66
3.10.	BHs as strong-gravity laboratories for exotic fields	68
3.10.1.	Collapse of self-interacting scalar fields.	68
3.10.2.	Superradiant instabilities: BHs as observatories for beyond- standard-model physics	70
3.11.	Open problems	73
4.	Neutron stars	74
4.1.	General-relativistic stellar models	74
4.2.	Scalar–tensor theories	75
4.3.	$f(R)$ theories.	79
4.4.	Quadratic gravity	83
4.4.1.	EdGB theory	84
4.4.2.	dCS theory	86
4.5.	Lorentz-violating theories.	87
4.6.	Massive gravity and Galileons	89
4.7.	Gravity with auxiliary fields.	90
4.8.	Strong-field tests of gravity with universal relations in NSs and quark stars (Qs)	93
4.9.	NS sensitivities in modified gravity.	99
4.10.	Open problems	102
5.	Compact binaries	104
5.1.	Scalar–tensor theories	104
5.1.1.	Analytical calculations	104
5.1.2.	Numerical relativity simulations	109
5.2.	$f(R)$ theories.	114
5.3.	Quadratic gravity	115
5.4.	Lorentz-violating theories.	120
5.5.	Massive gravity	122
5.6.	Open problems.	123

6. Binary pulsar and cosmological tests of GR	123
6.1. Tests of gravity from radio pulsars	123
6.1.1. Open problems	129
6.2. Testing GR with cosmology	130
6.2.1. Theory: the linear regime	131
6.2.2. Theory: the nonlinear regime	134
6.2.3. Observations, current and future	138
6.2.4. Open problems	138
7. Gravitational wave tests	139
7.1. Science opportunities	140
7.2. Parameter estimation and model selection	142
7.3. Direct versus parametrized tests of gravity	143
7.3.1. Implementation of direct tests: the TIGER pipeline	147
7.4. Waveform and astrophysical systematics	153
7.4.1. Stellar mass objects	153
7.4.2. Supermassive BHs	157
8. Discussion and conclusions	160

1. Introduction

Einstein's theory of general relativity (GR), together with quantum mechanics, is one of the pillars of modern physics. The theory has passed all precision tests to date with flying colors. Most of these tests—with the possible exception of binary pulsar observations—are probes of *weak-field* gravity; more precisely, they probe gravity at intermediate length ($1 \mu\text{m} \lesssim \ell \lesssim 1 \text{AU} \sim 10^{11} \text{m}$) and therefore intermediate energy scales. Laboratory experiments and astrophysical observations verify the so-called 'Einstein equivalence principle' (i.e. the weak equivalence principle supplemented by local Lorentz invariance and local position invariance) and they set constraints on hypothetical weak-field deviations from GR, as encoded in the parametrized post-Newtonian (PPN) formalism (see [1] for an introduction, and [2] for a review of the state of the art on experimental tests of GR).

The conceptual foundations of GR are so elegant and solid that when asked what he would do if Eddington's expedition to the island of Principe failed to match his theory, Einstein famously replied: 'I would feel sorry for the good Lord. The theory is correct.' Chandrasekhar made a similar private remark to Clifford Will when Will was a postdoc in Chicago: 'Why do you spend so much time and energy testing GR? *We know* that the theory is right.' Giving up the fundamental, well tested principles underlying Einstein's theory has dramatic consequences, often spoiling the beauty and relative simplicity of Einstein's theory. However, there is growing theoretical and experimental evidence that modifications of GR at small and large energies are somehow inevitable.

From a theoretical point of view, GR is a purely classical theory. Power-counting arguments indicate that GR is not renormalizable in the standard quantum field theory sense. Strong-field modifications may provide a solution to this problem: it has long been known that the theory becomes renormalizable if we add quadratic curvature terms—i.e., high-energy/high-curvature corrections—to the Einstein–Hilbert action [3]. Furthermore, high-energy corrections can avoid the formation of singularities that are inevitable in classical GR, as shown by the Hawking–Penrose singularity theorems [4]. Candidate theories of quantum

gravity (such as string theory and loop quantum gravity) make specific and potentially testable predictions of *how* GR must be modified at high energies.

From an observational point of view, cosmological measurements are usually interpreted as providing evidence for dark matter and a nonzero cosmological constant ('dark energy'). This interpretation poses serious conceptual issues, including the cosmological constant problem ('Why is the observed value of the cosmological constant so small in Planck units?') and the coincidence problem ('Why is the energy density of the cosmological constant so close to the present matter density?'). No dynamical solution of the cosmological constant problem is possible within GR [5]. It seems reasonable that ultraviolet corrections to GR would inevitably 'leak' down to cosmological scales, showing up as low-energy (infrared) corrections.

The arguments summarized above suggest that GR should be modified at both low and high energies. This is a serious challenge for theorists. Einstein's theory is the unique interacting theory of a Lorentz-invariant massless helicity-2 particle [6, 7], and therefore new physics in the gravitational sector must introduce additional degrees of freedom. Any additional degrees of freedom must modify the theory at low and/or high energies while being consistent with GR in the intermediate-energy regime, i.e. at length scales $1 \mu\text{m} \lesssim \ell \lesssim 10^{11} \text{ m}$, where the theory is extremely well tested. Laboratory, Solar System and binary-pulsar experiments verify the Einstein equivalence principle to remarkable accuracy; they force PPN parameters to be extremely close to their GR values; and (as we will see below) they place stringent bounds on popular extensions of GR, such as scalar-tensor theories and Lorentz-violating theories (see [2, 8] for reviews).

Some confusion exists about how to link tests of gravity that take place in the very different regimes described above. For example, though it is agreed that strong-field constraints on GR do not rule out cosmological modifications (or vice versa), it is not immediately obvious how to express this statement quantitatively, except perhaps in specific models. One method of resolving this problem was recently put forward in [9]. There the authors place a wide range of laboratory, astrophysical and cosmological systems on a two-dimensional parameter space, where the axis quantities are the approximate gravitational potential and Kretschmann scalar of a system. The Kretschmann scalar is used because it gives a rough measure of how relativistic the system is and does not vanish in vacuum (the diagnostic power of the Ricci scalar is limited for this reason). Many orders of magnitude of Kretschmann curvature separate the classic PPN tests of gravity from both the strong-field regime and the cosmological regime, so we cannot simply take existing Solar System constraints as comprehensive.

The main focus of this review is on present and future tests of *strong-field gravity*. It is useful to classify 'tests of strong-field gravity' as belonging to two qualitatively different categories. 'External tests' are laboratory experiments, astrophysical and cosmological observations that can be used to determine whether GR (as opposed to any of the numerous proposed extensions) is the correct theory of gravity. 'Internal tests' are observations that tell us whether some key predictions of GR (e.g. the Kerr solution of the Einstein equations in vacuum, or the radiative dynamics of compact objects) are 'internally' consistent with astrophysical observations.

Compact objects such as black holes (BHs) and neutron stars (NSs) are our best natural laboratories to constrain strong gravity. In these celestial bodies gravity prevails over all other interactions, and collapse leads to large-curvature, strong-gravity environments (see e.g. [10]). The Kerr metric is a solution of the vacuum field equations in a large class of modified gravity theories, but theories that differ from GR generically predict different *dynamics* and different gravitational-wave (GW) signatures when compact objects are displaced from equilibrium and/or when they merge. This is the reason why a large part of this review will be devoted to the structure and dynamics of BHs and NSs, whether isolated or in binary systems.

1.1. Taxonomy of proposed extensions of GR

To frame external tests in terms of hypothesis testing, one would like to have one or more valid alternatives to GR. What constitutes a ‘valid alternative’ is, of course, a matter of taste. From our perspective (i.e., in terms of tests of strong-field gravity) the alternative should be a cosmologically viable fundamental theory passing intermediate energy tests, with a well-posed initial value formulation, and field equations that follow from an action principle. Furthermore, the theory should be simple enough to make definite, calculable prediction in the strong-field regime: ideally, it should allow us to predict the structure and dynamics of compact objects and the gravitational radiation that they emit, whether isolated or in binary systems.

This is a very stringent set of requirements. There are countless attempts to modify GR [11–17], but (for the reasons listed above) in several cases the modifications introduce some screening mechanism in order to be viable at intermediate energies. Screening mechanisms include chameleons, symmetrons, dilatons, MOND-like dynamics, the Vainshtein mechanism, etcetera, depending on whether the screening is set by the local value of the field or by its derivatives [18].

Section 2 reviews various theories that have been explored in some detail as phenomenological alternatives to GR in the strong-field regime. The section begins with a discussion of Lovelock’s theorem, a ‘uniqueness theorem’ for the field equations of GR. Uniqueness is based on a small set of definite assumptions. The interest of Lovelock’s theorem from a pragmatic point of view is that it can be ‘turned around,’ and used to classify extensions of GR based on which of the underlying assumptions of Lovelock’s theorem they violate. Within this classification framework, we list and discuss several theories that have been seriously considered as plausible alternatives to GR in the context of strong-field tests. This selection is necessarily incomplete, and the authors of this review have different opinions on the intrinsic merits, viability and aesthetic appeal of these theories. The main criterion we used to choose these particular theories is that they are simple enough to make definite (and sometimes ‘orthogonal’) predictions for the strong-field dynamics of compact objects. The theories we discuss include:

- (1) scalar–tensor theories and their generalizations (including tensor-multiscalar and Horndeski theories);
- (2) $f(R)$ theories;
- (3) theories whose action contains terms quadratic in the curvature, including in particular Einstein-dilaton-Gauss-Bonnet (EdGB) and dynamical Chern-Simons (dCS) theories;
- (4) Lorentz-violating theories, including Einstein-Æther, Hořava and n -Dirac-Born-Infeld (n -DBI) gravity;
- (5) massive gravity theories;
- (6) theories involving nondynamical fields, including the Palatini formulation of $f(R)$ gravity and Eddington-inspired Born-Infeld (EiBI) gravity.

This broad classification will be a leitmotif of the review. Table 1 lists some key references to the literature on the various theories listed above, plus others that are not considered in depth here. The table is an incomplete (but hopefully useful) ‘bird’s eye’ reference guide for further study. Similar tables following the same classification scheme will support our discussion of the structure and stability of compact objects.

Since we do not have a full theory of quantum gravity, an effective field theory (EFT) approach is often invoked when constructing phenomenological alternatives to GR [19, 20]. For example, not all theories of gravity with action quadratic in the curvature (item 3 in the

Table 1. Catalog of several theories of gravity and their relation with the assumptions of Lovelock’s theorem. Each theory violates at least one assumption (see also figure 1), and can be seen as a proxy for testing a specific principle underlying GR.

Theory	Field content	Strong EP	Massless graviton	Lorentz symmetry	Linear $T_{\mu\nu}$	Weak EP	Well- posed?	Weak-field constraints
Extra scalar field								
Scalar–tensor	S	×	✓	✓	✓	✓	✓[34]	[35–37]
Multiscalar	S	×	✓	✓	✓	✓	✓[38]	[39]
Metric $f(R)$	S	×	✓	✓	✓	✓	✓[40, 41]	[42]
Quadratic gravity								
Gauss–Bonnet	S	×	✓	✓	✓	✓	✓?	[43]
Chern–Simons	P	×	✓	✓	✓	✓	×✓? [44]	[45]
Generic	S/P	×	✓	✓	✓	✓	?	
Horndeski	S	×	✓	✓	✓	✓	✓?	
Lorentz-violating								
Æ-gravity	SV	×	✓	×	✓	✓	✓?	[46–49]
Khronometric/ Hořava–Lifshitz	S	×	✓	×	✓	✓	✓?	[48–51]
n -DBI	S	×	✓	×	✓	✓	?	none ([52])
Massive gravity								
dRGT/Bimetric	SVT	×	×	✓	✓	✓	?	[17]
Galileon	S	×	✓	✓	✓	✓	✓?	[17, 53]
Nondynamical fields								
Palatini $f(R)$	—	✓	✓	✓	×	✓	✓	none
Eddington–Born–Infeld	—	✓	✓	✓	×	✓	?	none
Others, not covered here								
TeV e S	SVT	×	✓	✓	✓	✓	?	[37]
$f(R)\mathcal{L}_m$?	×	✓	✓	✓	×	?	
$f(T)$?	×	✓	×	✓	✓	?	[54]

Note. See text for details of the entries. Key to abbreviations: S: scalar; P: pseudoscalar; V: vector; T: tensor; ?: unknown; ✓?: not explored in detail or not rigorously proven, but there exist arguments to expect ✓. The occurrence of ×✓? means that there exist arguments in favor of well-posedness within the EFT formulation, and against well-posedness for the full theory. Weak-field constraints (as opposed to strong-field constraints, which are the main topic of this review) refer to Solar System and binary pulsar tests. Entries below “Others, not covered here” are not covered in this review.

Table 2. Catalog of BH properties in several theories of gravity. The column ‘solutions’ refers to asymptotically-flat, regular solutions. Legend: ST—‘scalar-tensor’; \equiv GR—‘same solutions as in GR’; \supset GR—‘GR solutions are also solutions of the theory’; NR—‘non rotating’; SR—‘slowly rotating’; FR—‘fast rotating/generic rotation’; ?—unknown or uncertain.

Theory	Solutions	Stability	Geodesics	Quadrupole
Extra scalar field				
Scalar-tensor	\equiv GR [55–60]	[61–67]	—	—
Multiscalar/Complex scalar	\supset GR [56, 68, 69]	?	?	[68, 69]
Metric $f(R)$	\supset GR [58, 59]	[70, 71]	?	?
Quadratic gravity				
Gauss–Bonnet	NR [72–74]; SR [75, 76]; FR [77]	[78, 79]	SR [75, 80, 81]; FR [77]	[76, 82]
Chern–Simons	SR [83–85]; FR [86]	NR [87–90]; SR [79]	[74, 91]	[85]
Generic	SR [80]	?	[80]	equation (3.12)
Horndeski	[92–94]	? [95, 96]	?	?
Lorentz-violating				
\mathcal{A} -gravity	NR [97–99]	?	[98, 99]	?
Khronometric/ Hořava–Lifshitz	NR, SR [98–101]	? [102]	[98, 99]	?
n -DBI	NR[103, 104]	?	?	?
Massive gravity				
dRGT/Bimetric	\supset GR, NR [105–108]	[109–112]	?	?
Galileon	[113]	?	?	?
Nondynamical fields				
Palatini $f(R)$	\equiv GR	—	—	—
Eddington–Born–Infeld	\equiv GR	—	—	—

6

Table 3. Catalog of NS properties in several theories of gravity. Symbols and abbreviations are the same as in table 2.

Theory	Structure			Collapse	Sensitivities	Stability	Geodesics
	NR	SR	FR				
Extra scalar field							
Scalar–tensor	[26, 114–118]	[116, 119, 120]	[121–123]	[124–131]	[132]	[133–143]	[122, 144]
Multiscalar	?	?	?	?	?	?	?
Metric $f(R)$	[145–157]	[158]	[159]	[160, 161]	?	[162, 163]	?
Quadratic gravity							
Gauss–Bonnet	[164]	[164]	[82]	?	?	?	?
Chern–Simons	\equiv GR	[27, 45, 165–167]	?	?	[166]	?	?
Horndeski	?	?	?	?	?	?	?
Lorentz-violating							
\mathcal{A} -gravity	[168, 169]	?	?	[170]	[48, 49]	[162]	?
Khronometric/ Hořava–Lifshitz	[171]	?	?	?	[48, 49]	?	?
n -DBI	?	?	?	?	?	?	?
Massive gravity							
dRGT/Bimetric	[172, 173]	?	?	?	?	?	?
Galileon	[174]	[174]	?	[175, 176]	?	?	?
Nondynamical fields							
Palatini $f(R)$	[177–181]	?	?	?	—	?	?
Eddington–Born–Infeld	[182–188]	[182, 183]	?	[183]	—	[189, 190]	?

list) are acceptable: the equations are of second order in the strong-coupling limit (a very desirable feature, given that higher-order derivatives are vulnerable to the so-called Ostrogradskii instability [21]) only if the quadratic invariants appear in the special ‘Gauss–Bonnet’ combination. To avoid higher-order derivatives in the equations of motion one must generally assume that couplings are small, and work in an EFT framework. A more detailed discussion of EFTs and further references can be found in section 2.8.

1.2. Compact objects in modified theories of gravity

Investigations of compact objects, binary pulsars, cosmology and gravitational radiation vary in depth and scope for the various classes of theories listed above. The best studied examples include scalar–tensor theories and some forms of quadratic gravity. Sections 3–5 are devoted to a discussion of isolated BHs, isolated NSs and compact binary systems in various theories.

Isolated BHs. In section 3 we discuss BHs, one of the most striking predictions of GR. There is a consensus in the astronomy community that the massive compact objects in galactic centers, as well as the compact objects with mass larger than about $3M_{\odot}$ found in some low-mass x-ray binaries, are well described by the Kerr solution in GR. However, this ‘BH paradigm’ rests on somewhat shaky foundations.

From a theorist’s point of view, one of the most convincing arguments in favor of the BH paradigm is that the alternatives are either unstable (as in the case of dense star clusters, fermion stars or naked singularities), unnatural (e.g. ‘exotic’ matter violating some of the energy conditions), contrived (such as gravastars), more implausible than BHs as the endpoint of gravitational collapse (boson stars) or nearly indistinguishable from Kerr.

The experimental evidence that astronomical BH candidates possess event horizons (more correctly, apparent horizons) rather than solid surfaces usually rests on plausibility arguments based on accretion physics [22, 23]. All of these arguments are model-dependent, and they leave room for some skepticism (see e.g. [24]).

Strictly speaking, any tests that probe the Kerr *metric* alone (such as tests based on matter accretion or ray tracing of photon trajectories) are of little value as internal tests of GR. The reason is that a large number of extensions of GR admit the Kerr metric as a solution, and the theories that do not (e.g. EdGB, dCS and some Lorentz-violating gravity theories) predict BH solutions that differ from GR by amounts that may not be astrophysically measurable. Despite this somewhat pessimistic caveat, many ‘quasi-Kerr metrics’ have been proposed to perform GR tests, and we will review these proposals in section 3. Most deformations of the Kerr metric should be viewed as unnatural strawmen: they often have serious pathologies, and they are therefore unacceptable even for the limited scope of parametrizing deviations from the Kerr metric [25].

The prospects for testing GR with BHs look brighter when we recall that all extensions of GR predict different *dynamics* and different GW signatures when compact objects are perturbed away from equilibrium and/or when they merge. These arguments suggest that the most promising way to verify whether the compact objects in galactic centers or low-mass x-ray binaries are actually Kerr BHs is via direct observation of gravitational radiation, especially in the strong-field merger/ringdown phase.

Last but not least, astrophysical BHs can be used to constrain modifications of GR in a different way. Many proposed modifications of Einstein’s theory and extension of the standard model of particle physics predict the existence of light bosonic degrees of freedom. Light bosons can trigger a superradiant instability, that extracts angular momentum from rotating BHs. By setting the superradiant instability timescale equal to the typical timescale

for accretion to spin up the hole (say, the Salpeter time) one can get very stringent constraints on the allowed masses of light bosons (e.g. axions, Proca fields or massive gravitons).

Table 2 is a quick reference guide to BH solutions and stability in various modified theories of gravity, organized in the same way as table 1.

Isolated NSs. In section 4 we discuss NS solutions and their stability in various extensions of GR. Among other topics, we review the possibility that NSs in scalar–tensor theory may significantly deviate from their GR counterparts in the presence of ‘spontaneous scalarization’ (a phase transition akin to spontaneous magnetization [26]), we discuss controversial claims on the existence of NSs in $f(R)$ theories, and we review the somewhat surprising ‘no-hair’ properties of NSs in quadratic gravity.

A major problem in carrying out strong-gravity tests with NSs is the degeneracy between our ignorance of the equation of state (EOS) of high-density matter and strong-gravity effects. A possibility to lift the degeneracy consists of using universal relations between the moment of inertia, Love number (a measure of tidal deformability) and quadrupole moment of a NS—the so-called ‘I–Love–Q’ relations [27]—as well as EOS-independent relations between the lowest three multipole moments and those of higher order [28, 29]. Section 4.8 overviews the promises and challenges of this approach.

A property of isolated NSs that plays an important role in many extensions of GR is their ‘sensitivity.’ The sensitivity is a measure of how the gravitational mass of the NS (or any self-gravitating object) varies as it moves within the nonhomogeneous extra field(s) mediating the gravitational interactions—or in other words, a measure of the violation of the strong equivalence principle (SEP) in the theory in question. Section 4.9 is a review of sensitivity calculations, that play an important role in binary dynamics.

In table 3 we give a quick reference guide to NS solutions and their stability in various modified theories of gravity.

Compact binaries. In preparation for binary pulsar tests (covered in section 6) and GW tests (section 7), in section 5 we review calculations of compact binary dynamics in some extensions of GR. The equations of motion and GW fluxes have been derived using the post-Newtonian (PN) expansion—an expansion in powers of v/c , where v is the orbital velocity of the binary—in scalar–tensor theory, $f(R)$ gravity, specific forms of quadratic gravity (including EdGB and dCS) and Lorentz-violating theories. In comparison, numerical work is much less developed: at the moment of writing this review, simulations of compact binary mergers were carried out only for some of the simplest scalar–tensor theories.

1.3. Present and future tests of strong gravity

Sections 6 and 7 capitalize on the material covered in previous sections. Section 6 reviews *present* astrophysical tests of GR, more specifically those coming from binary pulsar and cosmological observations. Section 7 focuses on the potential payoff of *future* GW observations, and on how astrophysical modeling will affect our ability to perform tests of strong-field gravity in this context.

The first part of section 6 is an overview of the spectacular progress of GR tests from binary pulsars. These extraordinary natural laboratories can be utilized to probe with high precision various nonradiative strong-field effects, as well as radiative aspects of gravity [30]. For instance, pulsars are now able to test Einstein’s quadrupole formula for GW emission to an accuracy of less than 0.1%. They provide stringent bounds on dipolar radiation and on violations of the SEP by strongly self-gravitating bodies (the best tests coming from pulsar-

white dwarf systems), and they tightly constrain hypothetical violations of local Lorentz invariance of gravity. The near future in this field is particularly bright. Facilities such as the five-hundred meter aperture spherical radio telescope (FAST) and the Square Kilometer Array (SKA) are expected to come online soon. They should provide drastic improvements in the precision of current tests, qualitatively new tests with already known systems, and the discovery of many new ‘pulsar laboratories’ (possibly including the first pulsar-BH system).

The second part of section 6 reviews cosmological tests of GR. In the last few decades, a remarkable wealth of astronomical data has constrained the expansion rate of the Universe and provided accurate maps of large-scale structure and the cosmic microwave background, placing ever-tightening constraints on cosmological parameters. In particular, anisotropies in the cosmic microwave background encode information on the geometry of the Universe, its material constituents and the initial conditions for structure formation. If GR is assumed to be correct, 96% of the material content of the Universe must consist of dark matter and dark energy. Since the evidence for these dark constituents of the Universe is purely gravitational, there have been countless attempts at finding theories in which dark matter and dark energy arise from modifications of gravity. These modifications affect the expansion rate of the Universe, but they should also affect gravitational clustering in a way that might be distinguishable from GR. The proliferation of alternative theories of gravity has led to the development of model-independent cosmological tests of modified gravity somewhat similar to the PPN framework, which are now one of the primary drivers for future surveys of large scale structure. In the linear regime, these model-independent tests can be grouped in three classes, corresponding to three manifestations of a gravity theory: the action, the field equations derived from that action, and the combinations of those field equations which influence observable quantities. Section 6 reviews these tests as well as recent progress in the nonlinear regime, where screening effects are important and numerical simulations are necessary.

Last but not least, in section 7 we turn our attention to the future of strong-gravity tests, focusing on the promise of GW observations by Earth- and space-based detectors. The main target for both classes of detectors is the inspiral and merger of compact binaries. A technique called matched filtering, based on a careful monitoring of the GW phase to extract the (generally weak) signal from the detector’s noise, is used to observe these systems and to measure their parameters. GR makes very specific and testable predictions on the GW phasing of compact binaries as they inspiral, and on the oscillation frequencies of the compact objects that they produce as a result of the merger. If observed, any deviations from these predictions may identify problems in Einstein’s theory, and even point us to specific ways in which it could be modified.

There are several comprehensive reviews on GW-based tests of GR. In particular, the recent *Living Reviews in Relativity* article by Yunes and Siemens [31] provides an excellent introduction to the literature on GR tests with Earth-based detectors (such as Advanced LIGO/Virgo, LIGO-India and KAGRA) and Pulsar Timing Arrays, and the review by Gair *et al* [32] expounds the great potential of future space-based detectors such as eLISA. We find it unnecessary to reproduce that material here, and therefore we focus on aspects that are not covered in detail in those reviews, namely: (1) the data analysis implementation of GR tests in advanced Earth-based detectors (the TIGER framework), arguably our best hope to constrain modified gravity using GW observations in the near future; and (2) an analysis of how astrophysical effects can limit (or sometimes enhance) our ability to test strong-field gravity with GW observations.

As a rule, in this paper we use geometrical units where the gravitational constant and the speed of light are set to unity: $G_N = c = 1$. Factors of G_N and c are occasionally reinstated for clarity, and in isolated cases (e.g. in section 2.8) we switch to units such that $\hbar = c = 1$. We adopt the mostly positive signature for the metric, and the same conventions as in Misner *et al* [33] for the Riemann tensor.

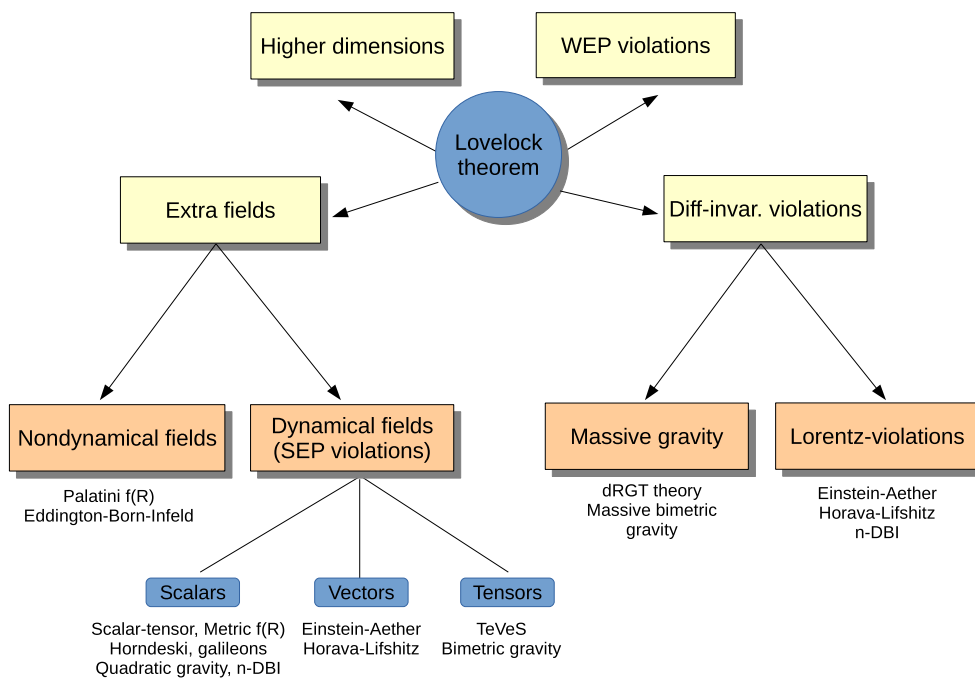


Figure 1. This diagram illustrates how Lovelock’s theorem serves as a guide to classify modified theories of gravity. Each of the yellow boxes connected to the circle represents a class of modified theories of gravity that arises from violating one of the assumptions underlying the theorem. A theory can, in general, belong to multiple classes. See table 1 for a more precise classification.

2. Extensions of GR: motivation and overview

2.1. A compass to navigate the modified-gravity atlas

There are countless inequivalent ways to modify GR, many of them leading to theories that can be designed to agree with current observations. Cosmological observations and fundamental physics considerations suggest that GR must be modified at very low and/or very high energies. Experimental searches for beyond-GR physics are a particularly active and well motivated area of research, so it is natural to look for a guiding principle: if we were to find experimental hints of modifications of GR, which of the assumptions underlying Einstein’s theory should be abandoned?

Such a guiding principle can be found by examining the building blocks of Einstein’s theory. Lovelock’s theorem [191, 192] (the generalization of a theorem due to Cartan [193]) is particularly useful in this context. In simple terms, the theorem states that GR emerges as the unique theory of gravity under specific assumptions. More precisely, it can be articulated as follows:

In four spacetime dimensions the only divergence-free symmetric rank-2 tensor constructed solely from the metric $g_{\mu\nu}$ and its derivatives up to second differential order, and preserving diffeomorphism invariance, is the Einstein tensor plus a cosmological term.

Lovelock's theorem suggests a natural route to Einstein's equations

$$G_{\mu\nu} + \Lambda g_{\mu\nu} = 8\pi T_{\mu\nu}, \quad (2.1)$$

where $G_{\mu\nu} \equiv R_{\mu\nu} - \frac{1}{2}Rg_{\mu\nu}$ is the Einstein tensor and $T_{\mu\nu}$ is the matter stress–energy tensor. Indeed, the divergence-free nature of the Einstein tensor (that follows from the Bianchi identities) implies that $T_{\mu\nu}$ is also divergence free, $\nabla_{\mu}T^{\mu\nu} = 0$. This property is necessary for geodesic motion and it guarantees the validity of the weak equivalence principle, i.e. the universality of free fall (see [194, 195] for further discussion). If we assume that the equations of motion for the gravitational field and the matter fields follow from a Lagrangian, the arguments above single out the Einstein–Hilbert action

$$S = \frac{1}{16\pi} \int d^4x \sqrt{-g} R + S_M[\Psi, g_{\mu\nu}], \quad (2.2)$$

where Ψ collectively denotes the matter fields, which couple minimally to $g_{\mu\nu}$, so that S_M reduces to the standard model action in a freely falling frame.

As it stands, Lovelock's theorem seems to leave little room for modifying the gravitational theory (2.2). However, when analyzed in detail, the theorem contains a number of nontrivial assumptions [196]. Giving up each of these assumptions provides a way to circumvent the theorem and gives rise to different classes of modified theories of gravity, as illustrated in figure 1. Specifically, there are at least four inequivalent ways to circumvent Lovelock's theorem:

(1) **Additional fields.**

Dynamical fields. The simplest and most beaten path to circumvent Lovelock's theorem consists of adding extra degrees of freedom. This leaves more options to construct the left-hand side of Einstein's equations (2.1), including more than just the metric and connection. Lifting this assumption paves the way for countless possibilities, where the metric tensor $g_{\mu\nu}$ is coupled to extra fundamental (scalar, vector, tensor) fields. Similar corrections arise from lifting the assumption of second differential order³⁵. Because of the coupling with extra dynamical fields, these theories usually violate the SEP [2]. It is not straightforward to construct theories with extra fields nonminimally coupled to gravity that avoid instabilities associated to the new degrees of freedom, as generically predicted by Ostrogradski's theorem [21]. Because such degrees of freedom remain undetected to date, a major challenge for these theories has been to tame the behavior of the extra fields, so as to evade current experimental constraints related to their existence [2].

Nondynamical fields. Lovelock's theorem implicitly assumes that the matter stress–energy tensor $T_{\mu\nu}$ enters the field equations (2.1) *linearly*. By dropping this assumption, it is possible to construct theories where the left-hand side of equation (2.1) is precisely the Einstein tensor, whereas the right-hand side is a nonlinear combination of $T_{\mu\nu}$ such that its covariant divergence vanishes, i.e., that $\nabla_{\mu}T^{\mu\nu} = 0$ remains an identity [197]. These theories satisfy the weak equivalence principle and are equivalent to GR in vacuum, but differ from it in the coupling to matter. Due to such nonlinear couplings, they resolve some of the curvature singularities that afflict fluid collapse and early time cosmology in GR [198]. The only theories belonging to this class known to date are special classes of theories which modify GR by adding only auxiliary (i.e. nondynamical) fields, the prototypical example being the Palatini formulation of $f(\mathcal{R})$ gravity [11, 199]. Here

³⁵ Indeed, higher-order equations can always be brought to second-order form by adding an arbitrary number of (effective) extra fields. A representative example is metric $f(R)$ gravity [11], see section 2.3.

$\mathcal{R} = g^{\mu\nu}\mathcal{R}_{\mu\nu}$, where $\mathcal{R}_{\mu\nu}$ denotes the Ricci tensor built from the connection, to distinguish it from the Ricci tensor $R_{\mu\nu}$ in the metric formalism: see the discussion below equation (2.50).

(2) **Violations of diffeomorphism invariance.**

Lorentz invariance. One particular form of diffeomorphism invariance, namely Lorentz invariance, has been tested with remarkable precision in the standard model sector, and it is widely believed to be a necessary ingredient of viable gravitational theories. However, if we assume that Lorentz invariance is just an emergent symmetry that is broken at high energies in the gravitational sector, a new class of gravity theories can be built. Some of these theories were found to possess a better ultraviolet behavior than GR [200]. Violations of Lorentz invariance are typically encoded in some extra field(s), so that theories of this class usually also belong to category (1) above.

Massive gravity. The assumption of diffeomorphism invariance is also crucial because it implies that gravity should be mediated by a *massless* spin-2 field. Understanding how the graviton can acquire mass is a century-old problem, and strong constraints on the graviton mass are in place [201]. Massive gravity theories are currently under intense scrutiny, mostly because of their applications in the context of the cosmological constant problem (see [17] for a review).

(3) **Higher dimensions.**

Even retaining all other assumptions of Lovelock's theorem, the Einstein–Hilbert action (2.2) is not unique in higher dimensions. Gravitational theories built in dimensions other than four have a strong theoretical interest for several reasons, including the formulation of consistent string theories or understanding how the field equations depend on an extra parameter, i.e. the spacetime dimension³⁶. These theories may even offer a resolution of the hierarchy problem, because they predict that the fundamental Planck mass can be several orders of magnitude smaller than the effective four-dimensional $M_{\text{Pl}} \approx 10^{19}$ GeV. Some extra-dimensional models are severely constrained from an experimental point of view (see e.g. [205]), and their relevance for beyond-GR effects in astrophysics is limited. However, some quantum-gravity corrections might be accessible through astrophysical observations, as we discuss in section 2.8. GR in higher dimensions leads naturally to additional fields if the theory is reduced to $D = 4$ dimensions: additional scalar and gauge fields emerge by performing a Kaluza–Klein or dimensional reduction from $D > 4$ to $D = 4$ dimensions. We discuss theories in higher dimensions only marginally and refer the interested reader to other reviews, e.g. [15].

(4) **WEP violations.**

The requirement that the left-hand side of Einstein's equation be divergence-free is dictated by the desire of having a divergence-free $T_{\mu\nu}$ and, in turn, by the weak equivalence principle. Various classes of theories that circumvent Lovelock's theorem only by postulating a nonminimal coupling to the matter sector (and thus violating the weak equivalence principle) have been proposed (see e.g. [206], and [14] for a review). Nevertheless, because the equivalence principle has been tested with the astonishing precision of one part in 10^{13} [207], we will seldom discuss theories where it is violated.

³⁶ The Cauchy problem in D -dimensional Gauss–Bonnet gravity was first investigated by Choquet-Bruhat in [202] (see also [38]). Reall *et al* showed that Lovelock theories in $D > 4$ spacetime dimensions allow for acausal propagation of physical degrees of freedom in some backgrounds, including BH spacetimes [203]. They concluded that higher-dimensional Lovelock theories may or may not be hyperbolic depending on the background spacetime. Willison [204] showed that Lovelock gravity is locally well-posed in arbitrary backgrounds, but global hyperbolicity is still an open problem.

Although rather elementary, the classification proposed above has the virtue of simplicity. In this review we are mainly interested in understanding *how to test GR*, and especially *what* we can test, rather than attempting a comprehensive classification of alternative theories. Our point of view is therefore very practical: any modified theory of gravity will necessarily fall into one of the categories above, and therefore it will violate one or more of the fundamental principles underlying GR; these violations will determine the new effects predicted by the theory, and the payoff of a hypothetical observation of these effects.

In table 1 we give a schematic (and necessarily incomplete) summary of proposed extensions of GR that are of interest for astrophysics, i.e. those that provide potential means to test the fundamental principles of GR with current and near-future astrophysical observations. In the rest of this review we discuss these theories (and their implications for experimental verifications of GR in the weak-field and strong-field regimes) in more detail.

Regardless of the manner in which Lovelock's theorem is violated, all these theories face a common challenge: how to modify the behavior of gravity at extreme energy scales, while leaving the (tightly constrained) intermediate energy regime unchanged? The hypothetical solution to this problem is termed 'screening.' When used in a general sense, the word is simply a label for unknown physics, much like the phrase 'dark energy.' Three concrete kinds of screening mechanisms are known, corresponding to density-dependent modifications of the three kinds of terms appearing in the action of a scalar field: (i) kinetic terms (including derivative self-interactions), (ii) potential terms, and (iii) couplings to matter fields [18]. These modifications lead to, respectively, the symmetron/dilaton screening mechanisms, the chameleon mechanism and the Vainshtein mechanism; see section 6.2 for further mathematical details.

It is likely that these exhaust the possibilities for a gravity theory with one additional scalar field. However, it is far from clear that one of these three mechanisms can be embedded in every gravity theory in the current literature. One could argue that any theory lacking an 'in-built' screening mechanism is disfavored or, at best, incomplete. However, given the rapidly evolving nature of this research area, it would seem hasty to discard all nonscreening theories at this stage.

If GR is not the fully correct theory of gravity, then we are forced to accept one of the following propositions:

- (a) the true theory must incorporate one of the three known mechanisms; or
- (b) there exist yet-unknown screening mechanisms, which require more than a single scalar field to operate; or
- (c) deviations from GR do exist in the intermediate energy regime, but are below the current detection threshold of PPN and binary pulsar constraints.

It is worth noting that, in addition to the strong-field and cosmological tests of gravity described in this review, screening mechanisms have spawned a wave of new laboratory and astrophysical tests of gravity. Laboratory examples include experiments to detect the chameleon mechanism using cold atom interferometry [208, 209], and the 'afterglow' of a chameleon field interacting with the electromagnetic field inside a radio frequency cavity [210]. New astrophysical tests include searches for a potential mismatch between distance indicators such as cepheid variables and tip-of-the-red-giant-branch stars in unscreened dwarf galaxies [211].

2.2. Scalar–tensor gravity

One of the most natural extensions of GR is *scalar–tensor gravity*, in which one or more scalar degrees of freedom are included in the gravitational sector of the theory, through a *nonminimal coupling* (i.e., the Ricci scalar in the Einstein–Hilbert action is multiplied by a function of the scalar field(s)). Several reviews provide extensive discussions on the subject, see e.g. [39, 196, 212–214].

Scalar fields with nonminimal couplings to gravity appear in several contexts, such as in string theory [215], in Kaluza–Klein-like theories [216] or in braneworld scenarios [217, 218]. They also have important applications in cosmology [15]. Therefore, scalar–tensor gravity is a good framework to study phenomenological aspects of several possible fundamental theories.

2.2.1. The Bergmann–Wagoner formulation. The most general action of scalar–tensor gravity with one scalar field which is at most quadratic in derivatives of the fields was studied by Bergmann and Wagoner [219, 220], and can be written (after an appropriate field redefinition) as:

$$S = \frac{1}{16\pi} \int d^4x \sqrt{-g} \left[\phi R - \frac{\omega(\phi)}{\phi} g^{\mu\nu} (\partial_\mu \phi)(\partial_\nu \phi) - U(\phi) \right] + S_M[\Psi, g_{\mu\nu}], \quad (2.3)$$

where ω and U are arbitrary functions of the scalar field ϕ , and S_M is the action of the matter fields Ψ . When $\omega(\phi) = \omega_{\text{BD}}$ is constant and $U(\phi) = 0$, the theory reduces to (Jordan–Fierz-) Brans–Dicke gravity [221–223], an extension of GR which was proposed in the mid-20th century (see [224–226] for a historical account).

The Bergmann–Wagoner theory (2.3) can be expressed in a different form through a scalar field redefinition $\varphi = \varphi(\phi)$ and a conformal transformation of the metric $g_{\mu\nu} \rightarrow g_{\mu\nu}^* = A^{-2}(\varphi) g_{\mu\nu}$. In particular, fixing $A(\varphi) = \phi^{-1/2}$, the action (2.3)—generally referred to as the *Jordan-frame* action—transforms into the *Einstein-frame* action

$$S = \frac{1}{16\pi} \int d^4x \sqrt{-g^*} \left[R^* - 2g^{*\mu\nu} (\partial_\mu \varphi)(\partial_\nu \varphi) - V(\varphi) \right] + S_M[\Psi, A^2(\varphi) g_{\mu\nu}^*], \quad (2.4)$$

where g^* and R^* are the determinant and Ricci scalar of $g_{\mu\nu}^*$, respectively, and the potential $V(\varphi) \equiv A^4(\varphi)U(\phi(\varphi))$. The price paid for the minimal coupling of the scalar field in the gravitational sector is the nonminimal coupling in the matter sector of the action: particle masses and fundamental constants depend on the scalar field.

We remark that the actions (2.3) and (2.4) are just different representations of the same theory: the outcome of an experiment will not depend on the chosen representation, as long as one takes into account that the units of physical quantities do scale with powers of the conformal factor A [194, 227]. It is then legitimate, when modeling a physical process, to choose the conformal frame in which calculations are simpler: for instance, in vacuum the Einstein-frame action (2.4) formally reduces to the GR action minimally coupled with a scalar field. It may then be necessary to change the conformal frame when extracting physically meaningful statements (since the scalar field is minimally coupled to matter in the Jordan frame, test particles follow geodesics of the *Jordan-frame* metric, not of the Einstein-frame metric).

The relation between Jordan-frame and Einstein-frame quantities is simply $\phi = A^{-2}(\varphi)$, $3 + 2\omega(\phi) = \alpha(\varphi)^{-2}$, where $\alpha(\varphi) \equiv d(\ln A(\varphi))/d\varphi$ [2]. Note that the theory is fixed once the function $\omega(\phi)$ —or, equivalently, $\alpha(\varphi)$ —is fixed, and the form of the scalar potential is chosen. Moreover, many phenomenological studies neglect the scalar potential. This

approximation corresponds to neglecting the cosmological term, the mass of the scalar field and any possible scalar self-interaction. In an asymptotically flat spacetime the scalar field tends to a constant ϕ_0 at spatial infinity, corresponding to a minimum of the potential. Taylor expanding $U(\phi)$ around ϕ_0 yields a cosmological constant and a mass term for the scalar field to the lowest orders [36, 220].

Scalar–tensor theory with a vanishing scalar potential is characterized by a single function $\alpha(\varphi)$. The expansion of this function around the asymptotic value φ_0 can be written in the form

$$\alpha(\varphi) = \alpha_0 + \beta_0(\varphi - \varphi_0) + \dots \quad (2.5)$$

As mentioned above, the choice $\alpha(\varphi) = \alpha_0 = \text{constant}$ (i.e., $\omega(\phi) = \text{constant}$) corresponds to Brans–Dicke theory. A more general formulation, proposed by Damour and Esposito-Farèse, is parametrized by α_0 and β_0 [26, 116]. Another simple variant is massive Brans–Dicke theory, in which $\alpha(\varphi)$ is constant, but the potential is nonvanishing and has the form $U(\phi) = \frac{1}{2}U''(\phi_0)(\phi - \phi_0)^2$, so that the scalar field has a mass $m_s^2 \sim U''(\phi_0)$. Note that since the scalar field φ in the action (2.4) is dimensionless, the function $\alpha(\varphi)$ and the constants α_0, β_0 are dimensionless as well.

The field equations of scalar–tensor theory in the Jordan frame are (see e.g. [228, 229])

$$\begin{aligned} G_{\mu\nu} = & \frac{8\pi}{\phi} T_{\mu\nu} + \frac{\omega(\phi)}{\phi^2} \left(\partial_\mu \phi \partial_\nu \phi - \frac{1}{2} g_{\mu\nu} \partial_\lambda \phi \partial^\lambda \phi \right) \\ & + \frac{1}{\phi} \left(\nabla_\mu \nabla_\nu \phi - g_{\mu\nu} \square_g \phi \right) - \frac{U(\phi)}{2\phi} g_{\mu\nu}, \end{aligned} \quad (2.6a)$$

$$\square_g \phi = \frac{1}{3 + 2\omega(\phi)} \left(8\pi T - 16\pi\phi \frac{\partial T}{\partial \phi} - \frac{d\omega}{d\phi} \partial_\lambda \phi \partial^\lambda \phi + \phi \frac{dU}{d\phi} - 2U(\phi) \right), \quad (2.6b)$$

where $T^{\mu\nu} = -2(-g)^{-1/2} \delta S_M(\Psi, g_{\mu\nu}) / \delta g_{\mu\nu}$ is the Jordan-frame stress–energy tensor of matter fields, and $T = g^{\mu\nu} T_{\mu\nu}$.

In the Einstein frame, the field equations are

$$G_{\mu\nu}^* = 2 \left(\partial_\mu \varphi \partial_\nu \varphi - \frac{1}{2} g_{\mu\nu}^* \partial_\sigma \varphi \partial^\sigma \varphi \right) - \frac{1}{2} g_{\mu\nu}^* V(\varphi) + 8\pi T_{\mu\nu}^*, \quad (2.7a)$$

$$\square_{g^*} \varphi = -4\pi \alpha(\varphi) T^* + \frac{1}{4} \frac{dV}{d\varphi}, \quad (2.7b)$$

where $T^{*\mu\nu} = -2(-g)^{-1/2} \delta S_M(\Psi, A^2 g_{\mu\nu}^*) / \delta g_{\mu\nu}^*$ is the Einstein-frame stress–energy tensor of matter fields and $T^* = g^{*\mu\nu} T_{\mu\nu}^*$ (see e.g. [39]). Equation (2.7b) shows that $\alpha(\varphi)$ couples the scalar fields to matter [230], as does $(3 + 2\omega(\phi))^{-1}$ in the Jordan frame: see equation (2.6b).

Astrophysical observations set bounds on the parameter space of scalar–tensor theories. In the case of Brans–Dicke theory, the best observational bound ($\alpha_0 < 3.5 \times 10^{-3}$) comes from the Cassini measurement of the Shapiro time delay. In the more general case with $\beta_0 \neq 0$, current constraints on (α_0, β_0) have been obtained by observations of NS–NS and NS–WD binary systems [37], and will be discussed in section 6 (see figure 37). Observations of compact binary systems also constrain massive Brans–Dicke theory, leading to exclusion regions in the (α_0, m_s) plane [36].

An interesting feature of scalar–tensor gravity is the prediction of certain characteristic physical phenomena which do not occur at all in GR. Even though we know from observations that $\alpha_0 \ll 1$ and that GR deviations are generally small, these phenomena may

lead to observable consequences. There are at least three possible smoking guns of scalar–tensor gravity. The first is the emission of dipolar gravitational radiation from compact binary systems [228, 231], which will be discussed in section 5.1. Dipolar gravitational radiation is ‘pre-Newtonian,’ i.e. it occurs at lower PN order than quadrupole radiation, and it does not exist in GR. The second is the existence of nonperturbative NS solutions in which the scalar field amplitude is finite even for $\alpha_0 \ll 1$. This *spontaneous scalarization* phenomenon [26, 116] will be discussed in detail in section 4.2. Here we only remark that spontaneous scalarization would significantly affect the mass and radius of a NS, and therefore the orbital motion of a compact binary system, even far from coalescence. The third example is also nonperturbative, and it involves massive fields. The coupling of massive scalar fields to matter in orbit around rotating BHs leads to a surprising effect: because of superradiance, matter can hover into ‘floating orbits’ for which the net gravitational energy loss at infinity is entirely provided by the BH’s rotational energy [232].

The phenomenology of scalar–tensor theory in vacuum spacetimes, such as BH spacetimes, is less interesting. When the matter action S_M can be neglected, the Einstein-frame formulation of the theory is equivalent to GR minimally coupled to a scalar field. BHs in Bergmann–Wagoner theories satisfy the same *no-hair theorem* as in GR, and thus the stationary BH solutions in the two theories coincide [56, 59]. Moreover, dynamical (vacuum) BH spacetimes satisfy a similar *generalized no-hair theorem*: the dynamics of a BH binary system in Bergmann–Wagoner theory with vanishing potential are the same as in GR [39], up to at least 2.5PN order for generic mass ratios [233] and at any PN order in the extreme mass-ratio limit [234] (see section 5.1.1). These no-hair theorems will be discussed in section 3.2.

2.2.2. Scalar–tensor theories with multiple scalar fields. When gravity is coupled with more than one scalar field, the action (2.3) has the more general form [39]

$$S = \frac{1}{16\pi} \int d^4x \sqrt{-g} \left(F(\phi) R - \gamma_{ab}(\phi) g^{\mu\nu} \partial_\mu \phi^a \partial_\nu \phi^b - V(\phi) \right) + S_M[\Psi, g_{\mu\nu}], \quad (2.8)$$

where F, V are functions of the N scalar fields ϕ^a ($a = 1 \dots N$). The scalar fields live on a manifold (the *target space*) with metric $\gamma_{ab}(\phi)$. The action (2.8) is invariant not only under space–time diffeomorphisms, but also under target-space diffeomorphisms, i.e. scalar field redefinitions. These theories have a richer structure than those with a single scalar field, since the geometry of the target space can affect the dynamics. For instance, the theories with a complex scalar field discussed in section 3.2.2, in which the no-hair theorems can be circumvented, can also be seen as multiscalar–tensor theories with $N = 2$.

2.2.3. Horndeski gravity. The most general scalar–tensor theory with second-order field equations (and one scalar field) is Horndeski gravity [235]. The action of Horndeski gravity can be written in terms of Galileon interactions (see [236] and section 2.6) as

$$\begin{aligned} S = \int d^4x \sqrt{-g} \{ & K(\phi, X) - G_3(\phi, X) \square \phi \\ & + G_4(\phi, X) R + G_{4,X}(\phi, X) [(\square \phi)^2 - (\nabla_\mu \nabla_\nu \phi)(\nabla^\mu \nabla^\nu \phi)] \\ & + G_5(\phi, X) G_{\mu\nu} \nabla^\mu \nabla^\nu \phi - \frac{G_{5,X}(\phi, X)}{6} [(\square \phi)^3 - 3 \square \phi (\nabla_\mu \nabla_\nu \phi)(\nabla^\mu \nabla^\nu \phi) \\ & + 2(\nabla_\mu \nabla_\nu \phi)(\nabla^\mu \nabla_\sigma \phi)(\nabla^\nu \nabla^\sigma \phi)] \}, \end{aligned} \quad (2.9)$$

where K and the G_i ’s ($i = 3 \dots 5$) are functions of the scalar field ϕ and of its kinetic term $X = -1/2 \partial^\mu \phi \partial_\mu \phi$, and $G_{i,X}$ are derivatives of G_i with respect to the kinetic term X . For a

particular choice of these functions, this theory coincides with Gauss–Bonnet gravity (see section 2.4).

As we shall discuss in section 3.2, in Horndeski theory the no-hair theorem can be circumvented, and thus stationary BH solutions can be different from GR.

2.3. Metric $f(R)$ theories

The standard paradigm to explain the acceleration of the cosmic expansion is to postulate the existence of a diffuse form of dark energy described by an exotic EOS ($P \approx -\rho$) and amounting to roughly 70% of the critical energy density. The cosmological constant is the most natural candidate for this dark ‘fluid,’ although its tiny value (as inferred by cosmological observations) clashes with the value of vacuum energy as inferred from particle physics. As mentioned above, this is one of the main problems in theoretical physics: the cosmological constant problem [5, 237, 238].

As an alternative to the standard Λ CDM (Λ -cold dark matter) model, it has been proposed that infrared modifications of gravity could be the explanation for the cosmic acceleration. In this context, so-called $f(R)$ modified gravities have a long history [239] and have been widely explored as prototypical infrared corrections to GR. The action for $f(R)$ gravity reads

$$S = \frac{1}{16\pi} \int d^4x \sqrt{-g} f(R) + S_M[\Psi, g_{\mu\nu}], \quad (2.10)$$

where Ψ collectively denotes all matter fields and $f(R)$ is a function of the scalar curvature R . It is customary to use a simplified notation where $f_R \equiv f'(R)$, $f_{RR} \equiv f''(R)$ and so on. We shall focus for the moment on the theory obtained from the action above through a metric variational principle. Palatini $f(R)$ gravity is a completely different theory, that will be discussed in section 2.7 below.

Primarily, $f(R)$ theories attracted attention for their potential to describe the cosmological acceleration of the Universe without a fine-tuned cosmological constant [11]. Viable $f(R)$ models are usually chosen by ensuring that the field equations admit a de Sitter solution with curvature radius R_{dS} . We refer the reader to specialized reviews [11, 12, 14] for a more detailed discussion of the theoretical aspects and of current experimental constraints.

Viable $f(R)$ theories. If one wishes to modify GR at cosmological scales, while leaving the large curvature behavior essentially unaffected, very stringent constraints are in place. Solar System observations and local tests strongly constrain viable $f(R)$ models and rule out many candidates (see [12] for a review). In general, $f(R)$ models must be described by monotonically growing and convex functions, i.e. $f_R > 0$ and $f_{RR} > 0$, in order to avoid ghosts (i.e., negative kinetic energy states) and tachyons. Furthermore, $f(R)$ gravity theories are introduced to modify the infrared behavior of GR when $R \lesssim R_c$, R_c being some cosmological curvature scale of the order of R_{dS} . In order to recover Einstein’s theory at higher curvature and to pass Solar System tests, viable models usually have, at leading order

$$f \rightarrow R, \quad f_R \rightarrow 1, \quad f_{RR} \rightarrow 0, \quad R \gg R_c. \quad (2.11)$$

In the following, we shall focus on classes of $f(R)$ theories of gravity that satisfy the above requirements.

Different formulations of $f(R)$ theories. It is well known that $f(R)$ theories are dynamically equivalent to a specific class of scalar–tensor theories [240–243] (see [11] for a review), so they propagate an additional scalar degree of freedom. These theories allow for different formulations depending on which quantity is identified as the scalar field. At least three different approaches to the study of $f(R)$ theories have been proposed. While equivalent in principle, each approach has different features and practical drawbacks. A common choice in

the literature is to transform the $f(R)$ action (2.10) into a Brans–Dicke theory with $\omega = 0$ in the Jordan frame. If $f_{RR} \neq 0$, the action (2.10) is dynamically equivalent to

$$S_J = \frac{1}{16\pi} \int d^4x \sqrt{-g} [\phi R - V_{\text{KM}}(\phi)] + S_M[\Psi, g_{\mu\nu}], \quad (2.12)$$

where $\phi = f_R$ and $V_{\text{KM}}(\phi) = Rf_R - f$ (the reason for the KM subscript will be apparent shortly). It should be stressed that, if $f_{RR} = 0$ at some point, the equivalence is not guaranteed and must be checked on a case-by-case basis. Scalar–tensor theories with a vanishing kinetic term of the form (2.12) were also studied by O’Hanlon [244] and others (see e.g. [245]).

In the context of compact objects, Kobayashi and Maeda [145, 147] integrated the field equations arising from the action (2.12), which read

$$\phi R_{\mu\nu} - \frac{1}{2} f g_{\mu\nu} - \nabla_\mu \nabla_\nu \phi + g_{\mu\nu} \square \phi = 8\pi T_{\mu\nu}, \quad (2.13)$$

$$\square \phi = \frac{8\pi}{3} T + \frac{1}{3} [2f(R(\phi)) - \phi R(\phi)] \equiv \frac{8\pi}{3} T + \frac{dV_{\text{KM}}}{d\phi}, \quad (2.14)$$

where the evolution equation for the scalar degree of freedom ϕ is obtained from the trace of equation (2.13) above, and R is now an implicit function of ϕ .

It is possible to recast $f(R)$ theory as a scalar–tensor theory in the Einstein frame for a new scalar field $\varphi \propto \log \phi$ [240, 246]. By defining

$$\varphi \equiv \frac{\sqrt{3}}{2} \log f_R, \quad g_{\mu\nu}^* = A^{-2} g_{\mu\nu}, \quad A^{-2} \equiv f_R = e^{2\varphi/\sqrt{3}}, \quad (2.15)$$

the action (2.12) becomes

$$S_E = \frac{1}{16\pi} \int d^4x \sqrt{-g^*} [R^* - 2\partial_\alpha \varphi \partial^\alpha \varphi - V_{\text{BL}}(\varphi)] + S_M[\Psi, A^2 g_{\mu\nu}^*], \quad (2.16)$$

where the new scalar potential reads

$$V_{\text{BL}}(\varphi) = \frac{Rf_R - f}{f_R^2}, \quad (2.17)$$

Here $R = R(\varphi)$, and we introduced a subscript ‘BL’ because this formulation was used by Babichev and Langlois in their study of compact stars [148, 149].

Besides the standard approaches discussed above, another formulation of the theory was proposed by Jaime *et al* [151]. In this approach, the Ricci curvature R is considered as an independent scalar degree of freedom. By introducing a new scalar field ψ , the action (2.10) is dynamically equivalent to

$$S_R = \frac{1}{16\pi} \int d^4x \sqrt{-g} [f'(\psi)R - V_{\text{JPS}}(\psi)] + S_M[\Psi, g_{\mu\nu}], \quad (2.18)$$

where $V_{\text{JPS}}(\psi) \equiv \psi f'(\psi) - f$. Variation with respect to ψ leads to $\psi = R$, if $f_{RR} \neq 0$. In fact, this is usually considered as an intermediate step in reducing the action (2.10) to the scalar–tensor theory (2.12): see e.g. [11]. As in the case of Brans–Dicke theory in the Jordan frame, the field equations for the scalar field simply impose $\psi = R$, but the scalar evolution arises from the trace of Einstein’s equation. The field equations read

$$\begin{aligned}
G_{\mu\nu} &= \frac{1}{f_R} \left[f_{RR} \nabla_\mu \nabla_\nu R + f_{RRR} (\nabla_\mu R) (\nabla_\nu R) - \frac{g_{\mu\nu}}{6} (Rf_R + f + 16\pi T) + 8\pi T_{\mu\nu} \right], \\
\Box R &= \frac{dV_{\text{JPS}}^{\text{eff}}}{dR} \equiv \frac{8\pi}{3f_{RR}} T - \frac{f_{RRR}}{f_{RR}} (\nabla R)^2 + \frac{dV_{\text{JPS}}}{dR},
\end{aligned} \tag{2.19}$$

with $dV_{\text{JPS}}/dR \equiv (2f - Rf_R)/3f_{RR}$. As pointed out in [151], in this formulation the potential is as well defined as the function $f(R)$.

The field equations of $f(R)$ gravity are of fourth differential order, but the theory admits a well-posed initial value problem by virtue of its equivalence with scalar–tensor gravity [40, 41].

2.4. Quadratic gravity

One of the most pressing problems in theoretical physics is to accommodate GR in the framework of quantum field theories. It has long been known that Einstein’s theory is not renormalizable in the standard quantum field theory sense, and this is a major obstacle on the route to quantum gravity. The situation changes if the Einstein–Hilbert action is assumed to be only the first term in an expansion containing all possible curvature invariants, as also suggested by low-energy effective string theories. Already in the 1970s, Stelle showed that including quadratic curvature terms in the action makes the theory renormalizable [3]. This comes at the cost of having higher-derivative terms in the field equations, which generically introduce ghosts or other pathologies (but see [247, 248] for recent progress in constructing a class of ghost-free, higher-derivative extensions of GR).

At second order in the curvature, the only independent algebraic curvature invariants are

$$R^2, \quad R_{\mu\nu}^2, \quad R_{\mu\nu\rho\sigma}^2, \quad {}^*RR, \tag{2.20}$$

where $R_{\mu\nu}^2 \equiv R_{\mu\nu} R^{\mu\nu}$, $R_{\mu\nu\rho\sigma}^2 \equiv R_{\mu\nu\rho\sigma} R^{\mu\nu\rho\sigma}$, ${}^*RR \equiv \frac{1}{2} R_{\mu\nu\rho\sigma} \epsilon^{\nu\mu\lambda\kappa} R^{\rho\sigma}{}_{\lambda\kappa}$ is the Pontryagin scalar, and $\epsilon^{\mu\nu\rho\sigma}$ is the Levi-Civita tensor. Of particular interest are the Gauss–Bonnet scalar $R_{\text{GB}}^2 \equiv R^2 - 4R_{\mu\nu}^2 + R_{\mu\nu\rho\sigma}^2$ and the Pontryagin scalar (also referred to as the Chern–Simons scalar) defined above, because these terms can be shown to emerge in low-energy realizations of string theory [215, 249]. The Pontryagin scalar also appears in loop quantum gravity [250]. However, these terms alone do not yield modifications to Einstein’s equations in four spacetime dimensions, because their integrals are four-dimensional topological invariants and only account for boundary terms in the action. To circumvent this problem one is thus forced to add extra dynamical fields, i.e., extra propagating degrees of freedom (but see section 2.7 below for a different strategy using nondynamical fields). The simplest way to introduce nontrivial higher-order curvature corrections is via coupling with a scalar field.

The most generic class of four-dimensional theories obtained by including all quadratic algebraic curvature invariants coupled to a single scalar field reads [74, 80]

$$\begin{aligned}
S &= \frac{1}{16\pi} \int \sqrt{-g} d^4x \left[R - 2\nabla_\mu \phi \nabla^\mu \phi - V(\phi) \right. \\
&\quad \left. + f_1(\phi) R^2 + f_2(\phi) R_{\mu\nu} R^{\mu\nu} + f_3(\phi) R_{\mu\nu\rho\sigma} R^{\mu\nu\rho\sigma} + f_4(\phi) {}^*RR \right] \\
&\quad + S_{\text{mat}} \left[\Psi, \gamma(\phi) g_{\mu\nu} \right],
\end{aligned} \tag{2.21}$$

where $V(\phi)$ is the scalar self-potential, $f_i(\phi)$ ($i = 1, \dots, 4$) are coupling functions, and in the matter action S_{mat} we have included a nonminimal but universal metric coupling, which thus satisfies the weak (but in general not the strong) equivalence principle. The action (2.21) generically yields higher-order field equations that are prone to the Ostrogradski instability

and to the appearance of ghosts, unless the various terms appear in the special combination corresponding to the four-dimensional Gauss–Bonnet invariant (discussed in section 2.4.1 below). To avoid this instability, the theory (2.21) must be considered as an *effective* action, obtained as the truncation of a more general theory, valid only up to second order in curvature³⁷. In the *decoupling limit* (where the effective theory is valid, see section 2.8), a perturbative approach is applicable and the field equations remain of second differential order for generic combinations of the curvature invariants. For example, it has been shown that dCS gravity (introduced in section 2.4.2 below) does not exhibit any ghost-like instabilities when treated order-by-order in the perturbation scheme and, in fact, can be cast into a well-posed Cauchy problem in the decoupling limit [44]. We expect a similar argument to hold for EdGB gravity (see section 2.4.1), but a rigorous proof in this case is still missing.

The EFT approach is not only motivated by the desire to avoid higher-order derivatives in the field equations, but it arises naturally in some low-energy expansion in string theory, which indeed contains the Gauss–Bonnet and Chern–Simons terms coupled respectively to the dilaton and axion at second order in the curvature. In this approach the Einstein–Hilbert term is considered as the first-order term in a (possibly infinite) series expansion containing all possible curvature corrections. In this sense, GR may be only accurate up to second-order terms in the curvature.

In the geometrical units adopted here, the scalar field entering the action (2.21) is dimensionless, whereas the coupling functions $f_i(\phi)$ have the dimensions of a length squared, i.e. of an inverse curvature. Thus, at variance with the scalar–tensor theories previously discussed, quadratic-gravity corrections may require introducing a new fundamental length scale. If the length scale is taken to be the Planck length, quadratic-gravity corrections would be negligible at the scales of compact objects: they would be suppressed by a factor of

$$\frac{\ell_{\text{Planck}}^2}{\ell_{\text{BH}}^2} \sim 10^{-78}, \quad (2.22)$$

where $\ell_{\text{Planck}} \sim 10^{-35}$ m is the Planck length, and $\ell_{\text{BH}} \sim 10$ km is the typical scale of a compact object. However, as discussed in the introduction, the region close to compact objects has been poorly probed, particularly when the spacetime is highly dynamical. Moreover, assuming that GR is correct all the way down to the Planck scale, with no new gravitational physics along the way, would be a tremendous extrapolation³⁸. When considering quadratic gravity, the standard approach is to assume the existence of this new fundamental scale, unrelated to the Planck scale, and proceed with calculations of observables from compact objects. For experimental observations to differ from GR predictions the ‘new’ length scale must be comparable to astrophysical scales. Here we will adopt this agnostic phenomenological point of view.

In this approach, quadratic-curvature terms may be important when dealing with non-linear, relativistic solutions. Clearly, within this perturbative context we can only consider corrections which are small compared to the leading Einstein–Hilbert term. In practice, the

³⁷ Alternatively, one can circumvent the Ostrogradski instability by expanding the phase-space of the (dynamical) variables if the resulting equations of motion constitute a closed system of PDEs that are at most second order [251, 252].

³⁸ As an illustration, the gravitational potential at the Earth’s surface, where Newtonian gravity proved to be extremely successful, is only four orders of magnitude smaller than the gravitational potential at the Sun’s surface, where relativistic effects are relevant, as shown by the classical tests of GR. In a particle physics context, even a very successful theory such as quantum electrodynamics cannot be extrapolated from atomic to nuclear energy scales, where the strong interaction dominates over electromagnetism; and again, these two scales are separated by just six orders of magnitude.

coupling functions f_i are expanded as

$$f_i(\phi) = \eta_i + \alpha_i \phi + \mathcal{O}(\phi^2), \quad (2.23)$$

where η_i and α_i ($i = 1, 2, 3, 4$) are dimensionful coupling constants. When the coupling functions are constant, i.e. $\alpha_i = 0$, the theories above admit all vacuum GR solutions [74, 253]. However, even in this case the background solutions generically have a different linear response with respect to GR: for example, these theories predict a different GW emission [88, 254, 255]. We will mostly be interested in theories that modify the structure of BHs and NSs, and we will consider the generic case $\alpha_i \neq 0$. At any rate, it is remarkable that in the weak-coupling limit (and provided that the f_i 's are analytic functions) all viable quadratic theories of gravity boil down to a small number of coupling *constants* that parametrize strong-curvature deviations from GR.

2.4.1. EdGB gravity. When $f_2 = -4f_1 = -4f_3$ and $f_4 = 0$, the theory (2.21) reduces to EdGB gravity [73], with action

$$S = \frac{1}{16\pi} \int \sqrt{-g} d^4x \left[R - 2\nabla_\mu \phi \nabla^\mu \phi - V(\phi) + f_1(\phi) R_{\text{GB}}^2 \right], \quad (2.24)$$

where $f_1(\phi)$ is a generic coupling function and the Gauss–Bonnet invariant R_{GB}^2 has been defined below equation (2.20). This is the only quadratic theory of gravity whose field equations are of second differential order for *any* coupling, and not just in the weak-coupling limit. Indeed, when $f_1(\phi) = \alpha_{\text{GB}} e^{-2\phi}$, the theory reduces to the bosonic sector of heterotic string theory [256]. Gauss–Bonnet gravity can also be seen as a particular case of Horndeski gravity [257], as mentioned in section 2.2.3. For instance, in the case $f_1(\phi) = \alpha\phi$, the action (2.24) can be shown to be equivalent to the action (2.9) with $K = X/2$, $G_3 = 0$, $G_4 = 1/2$, $G_5 = -2\alpha \ln|X|$ [92].

As in all of these theories, the coupling parameter is *dimensionful* and, specifically, it has dimensions of an inverse curvature. It is thus natural to expect that the strongest constraints on the theory should come from physical systems involving high curvature: BHs, NSs and the early Universe. We postpone a discussion of BHs and NSs to sections 3 and 4, respectively. Here we anticipate the observational bounds that have been derived.

Most bounds have been derived in the weak-coupling approximation, where one expects

$$\sqrt{|\alpha_{\text{GB}}|} \lesssim \mathcal{O}(L), \quad (2.25)$$

where L is the typical curvature radius in the system under consideration. Thus, Solar System constraints—such as those derived by measuring the Shapiro time delay of the Cassini probe [35]—give a mild bound $\sqrt{|\alpha_{\text{GB}}|} \lesssim 10^{13}$ cm, which is in fact of the order of an astronomical unit. On the other hand, as we shall discuss in section 3, BHs in this theory carry a scalar charge, and observations of BH low-mass x-ray binaries give a constraint which is six orders of magnitude stronger [43]:

$$\sqrt{|\alpha_{\text{GB}}|} \lesssim 5 \times 10^6 \text{ cm} \quad (2.26)$$

(in the units of equation (2.24)). As expected, this constraint is comparable to the typical size of a stellar-mass BH. On the other hand, the only bound on EdGB gravity as an *exact* theory is of theoretical nature, because the existence of BH solutions implies that $\sqrt{|\alpha_{\text{GB}}|}$ be smaller than the BH horizon size [73]; this bound implies $\alpha_{\text{GB}}/M^2 \lesssim 0.691$ [75]. Thus, the observational constraint (2.26) is likely to be a good estimate also for the exact EdGB gravity.

As previously mentioned, the bounds listed above are clearly satisfied if one assumes that quadratic curvature corrections become relevant only at the Planck scale. Nonetheless, they represent the best constraints on quadratic gravity to date, and they were obtained without any *a priori* assumptions on the regime in which deviations from GR should be relevant.

2.4.2. Chern–Simons gravity. While the terms proportional to f_1, f_2 and f_3 in the action (2.21) are all associated with qualitatively similar corrections to GR, the term proportional to f_4 is peculiarly different, to the extent that the special case $f_1 = f_2 = f_3 = 0$ describes a specific theory (Chern–Simons gravity) which has been widely scrutinized in recent years (see [258] for a review). At variance with EdGB gravity, to avoid higher-order derivatives in the field equations Chern–Simons theory must be considered as an EFT. Almost all work so far has focused on the special case $f_4 = \alpha_{\text{CS}}\phi$, working perturbatively in the coupling constant α_{CS} . Then the action reads

$$S = \frac{1}{16\pi} \int \sqrt{-g} d^4x [R - 2\nabla_\mu\phi\nabla^\mu\phi - V(\phi) + \alpha_{\text{CS}}\phi {}^*RR], \quad (2.27)$$

and most of the literature considered the case of a vanishing scalar potential: $V(\phi) = 0$. Like the Gauss–Bonnet term, the Chern–Simons term *RR is also a topological invariant, so that if $f_4 = \text{const}$ the theory is equivalent to GR.

For historical reasons, Chern–Simons gravity comes in two flavors: (i) a nondynamical version in which the scalar kinetic term in (2.27) is absent, and (ii) a theory where the scalar is a true dynamical degree of freedom, that goes under the name of dCS gravity. These two theories are actually very different from each other. Despite some confusion in the literature, only the nondynamical theory is parity breaking, whereas dCS gravity simply has different solutions than GR for spacetimes which are not reflection-invariant, as in the case of spinning objects. Furthermore, the nondynamical version introduces a constraint, ${}^*RR = 0$, arising from the variation of the CS action with respect to the nondynamical scalar field [259]. This constraint limits the space of solutions of the modified gravitational equations and introduces other problems [258]. For these reasons, the dynamical version of the theory has received much more attention in recent years.

It can be shown that any spherically symmetric solution of GR is also a solution of dCS gravity [254], and this makes it challenging to distinguish between the two theories. On the other hand, dCS gravity is almost unique as an extension of GR, as it predicts corrections only in the presence of a parity-odd source such as rotation. Among the most studied predictions of the theory are an amplitude birefringence in GW propagation [258] and modified spinning solutions, including corrections to Kerr BHs and rotating NSs, to be discussed in detail in sections 3 and 4.

To lowest order in the rotation rate, the CS modification to GR only affects the gravitomagnetic sector of the metric. Tests of the theory might therefore rely on frame-dragging effects. Using the results of Gravity Probe B [260], [45] derived the bound

$$\sqrt{|\alpha_{\text{CS}}|} < \mathcal{O}(10^{13})\text{cm}. \quad (2.28)$$

As mentioned above, dCS gravity should be interpreted as an EFT, and to have perturbative control requires $\alpha_{\text{CS}}/M^2 \ll 1$. This requirement is stronger than the bound (2.28) for BHs with masses $M \lesssim 10^8 M_\odot$.

Similar bounds come from the Lense–Thirring effect as measured by the LAGEOS satellites, which have also been used to constrain the nondynamical version of the theory [258]. Note that these bounds are of the order of an astronomical unit, as expected from the previous dimensional analysis. The detection of GWs from an extreme mass-ratio inspiral

(EMRI) can potentially yield constraints of the order $\sqrt{|\alpha_{\text{CS}}|} < \mathcal{O}(10^{10})\text{cm}$ or even determine the Chern–Simons parameter with fractional errors below 5% [261]. Since large-curvature environments are expected to put stronger bounds on the theory, the optimal systems to constrain quadratic gravity are compact binaries. Indeed, [262] derived projected bounds that are six orders of magnitude more stringent than the one above by considering future GW detection of the late inspiral of BH binaries. Similar bounds were also recently estimated in [86] by analyzing CS corrections of rapidly spinning Kerr BHs. Such corrections could be constrained from electromagnetic observations of accreting stellar mass BHs such as those in low-mass x-ray binaries, e.g. GRO J1655–40 (see e.g. [263]).

2.5. Lorentz-violating theories

While Lorentz invariance has been tested to high precision in the matter sector [201, 264–267], constraints in the gravity sector are much weaker. Constraints on Lorentz invariance in gravity beyond those obtainable in the Solar System have received much interest after Hořava [200] pointed out that a power-counting renormalizable theory can be constructed by giving up Lorentz invariance in gravity. We will focus here on Einstein-Æther and khronometric gravity, which are the most generic theories violating boost symmetry in gravity at low energies. A very clear review of these theories can be found in [268]³⁹.

2.5.1. Einstein-Æther. To break boost invariance in the most generic way, one can describe the gravitational degrees of freedom by means of a metric and a timelike vector field, \mathbf{u} , usually referred to as the ‘æther.’ Up to total divergences, the most general action composed of the metric and two or fewer derivatives of the æther, and that couples the æther minimally to matter (so as to enforce the weak equivalence principle and experimental evidence against the existence of ‘fifth forces’) is given by the Einstein-Æther action [47, 274, 275]

$$S_{\text{E}} = \frac{1}{16\pi G_{\text{E}}} \int \sqrt{-g} \left(R - M^{\alpha\beta}{}_{\mu\nu} \nabla_{\alpha} u^{\mu} \nabla_{\beta} u^{\nu} \right) d^4x + S_{\text{mat}}[\Psi, g_{\mu\nu}], \quad (2.29)$$

where

$$M^{\alpha\beta}{}_{\mu\nu} = c_1 g^{\alpha\beta} g_{\mu\nu} + c_2 \delta_{\mu}^{\alpha} \delta_{\nu}^{\beta} + c_3 \delta_{\nu}^{\alpha} \delta_{\mu}^{\beta} - c_4 u^{\alpha} u^{\beta} g_{\mu\nu}, \quad (2.30)$$

c_i ($i = 1, \dots, 4$) are dimensionless couplings, and Ψ denotes the matter degrees of freedom. In this section we do not assume $G_{\text{N}} = 1$; the ‘bare’ G_{E} is related to the ‘Newtonian’ gravitational constant G_{N} measured locally by Cavendish-type experiments via [276]

$$G_{\text{N}} = \frac{2G_{\text{E}}}{2 - (c_1 + c_4)}. \quad (2.31)$$

To enforce the timelike character of the æther, one has to impose

$$g_{\mu\nu} u^{\mu} u^{\nu} = -1, \quad (2.32)$$

either implicitly or by adding a Lagrange multiplier $\ell(g_{\mu\nu} u^{\mu} u^{\nu} + 1)$ in the variation of the action above.

The field equations for Einstein-Æther theory can be derived by varying the action (2.29) with respect to $g^{\alpha\beta}$ and u^{μ} , while imposing the constraint (2.32). This results in the following

³⁹ An alternative parametrized EFT approach to Lorentz violations in both the gravity and matter sectors was developed by Kostelecky *et al* [264, 269–271]. For binary pulsar constraints in the EFT framework of [264, 269–271], see [272, 273].

modified Einstein equations:

$$E_{\alpha\beta} \equiv G_{\alpha\beta} - T_{\alpha\beta}^{\mathcal{E}} - 8\pi G_{\mathcal{E}} T_{\alpha\beta}^{\text{mat}} = 0, \quad (2.33)$$

where $T_{\alpha\beta}^{\text{mat}}$ is the matter stress–energy tensor

$$\begin{aligned} T_{\alpha\beta}^{\mathcal{E}} = & -\nabla_{\mu} \left(J_{(\alpha}{}^{\mu} u_{\beta)} - J^{\mu}{}_{(\alpha} u_{\beta)} - J_{(\alpha\beta)} u^{\mu} \right) \\ & - c_1 \left[(\nabla_{\mu} u_{\alpha})(\nabla^{\mu} u_{\beta}) - (\nabla_{\alpha} u_{\mu})(\nabla_{\beta} u^{\mu}) \right] \\ & + \left[u_{\nu} (\nabla_{\mu} J^{\mu\nu}) + c_4 \dot{u}^2 \right] u_{\alpha} u_{\beta} + c_4 \dot{u}_{\alpha} \dot{u}_{\beta} - \frac{1}{2} M^{\sigma\rho}{}_{\mu\nu} \nabla_{\sigma} u^{\mu} \nabla_{\rho} u^{\nu} g_{\alpha\beta}, \end{aligned} \quad (2.34)$$

$J^{\alpha}{}_{\mu} = M^{\alpha\beta}{}_{\mu\nu} \nabla_{\beta} u^{\nu}$, and $\dot{u}^{\alpha} \equiv u^{\beta} \nabla_{\beta} u^{\alpha}$. These are completed by the æther equations

$$\mathcal{E}_{\mu} \equiv (\nabla_{\alpha} J^{\alpha\nu} + c_4 \dot{u}_{\alpha} \nabla^{\nu} u^{\alpha}) (g_{\mu\nu} + u_{\mu} u_{\nu}) = 0. \quad (2.35)$$

Strong constraints on the coupling constants c_i come from Solar System tests. This is because Einstein-Æther theory predicts that the (dimensionless) preferred-frame parameters α_1 and α_2 of the PPN expansion will in general be nonzero functions of the c_i 's [46, 47]. Because Solar System experiments constrain $|\alpha_1| \lesssim 10^{-4}$ and $|\alpha_2| \lesssim 10^{-7}$ [2], one can expand the theory in α_1 and α_2 , and reduce the parameter space to just two independent couplings $c_{\pm} \equiv c_1 \pm c_3$. The remaining couplings are given by $c_2 = (-2c_1^2 - c_1 c_3 + c_3^2)/(3c_1) + \mathcal{O}(\alpha_1, \alpha_2)$, $c_4 = -c_3^2/c_1 + \mathcal{O}(\alpha_1, \alpha_2)$ [46, 47]. Further constraints on the two independent couplings c_{\pm} come from requiring that the theory should have positive energy (i.e. no ghosts) and that Minkowski space should be linearly stable (i.e. no gradient instabilities) [2].

Einstein-Æther theory predicts the existence of not only spin-2 gravitational perturbations (like in GR), but also spin-1 and spin-0 gravitational perturbations. All these propagating modes have speeds that are functions of the c_i , and which differ in general from the speed of light [277]. However, if these modes were propagating at speeds lower than the speed of light, photons (or relativistic particles) could Cherenkov radiate into the gravitational field and lose energy to these modes, and this would lead to (unobserved) experimental consequences [278]. Therefore, one has to impose that the speed of the spin-2, spin-1 and spin-0 gravitons is larger than (or equal to) the speed of light. Taking into account these constraints, one obtains the viable region plotted in cyan in figure 38 (left panel) for the two independent couplings c_{\pm} . As previewed in that figure and discussed in section 6.1, more stringent constraints on c_{\pm} come from binary pulsar data [48, 49].

2.5.2. *Khronometric theory.* If we impose that the æther is always hypersurface-orthogonal, one can express it as

$$u_{\alpha} = -\frac{\partial_{\alpha} T}{\sqrt{-g^{\mu\nu} \partial_{\mu} T \partial_{\nu} T}}, \quad (2.36)$$

where T is the hypersurface-defining scalar and the constraint (2.32) has already been enforced. By assumption, surfaces of constant T foliate the spacetime, and one can re-express the action (2.29) adapted to this ‘preferred time’ T . This yields a different theory, described by the ‘khronometric theory’ action [200, 279, 280]

$$S_K = \frac{1 - \beta}{16\pi G_E} \int dT d^3x N \sqrt{h} \left(K_{ij} K^{ij} - \frac{1 + \lambda}{1 - \beta} K^2 + \frac{1}{1 - \beta} {}^{(3)}R + \frac{\alpha}{1 - \beta} a_i a^i \right) + S_{\text{mat}}[\Psi, g_{\mu\nu}], \quad (2.37)$$

where $N = (-g^{TT})^{-1/2}$ is the lapse function, K^{ij} is the extrinsic curvature of $T = \text{constant}$ hypersurfaces, h_{ij} is the induced spatial metric on those hypersurfaces, ${}^{(3)}R$ their three-dimensional Ricci curvature, $a_i = \partial_i \ln N$, and the æther is now related to the lapse via $u_\alpha = -N\delta_\alpha^T$. We have also redefined the theory's parameters via

$$\lambda \equiv c_2, \quad \beta \equiv c_3 + c_1, \quad \alpha \equiv c_4 + c_1. \quad (2.38)$$

It should be stressed at this stage that the action (2.37) only depends on three couplings, as opposed to four in the action (2.29). This is because the hypersurface-orthogonality constraint (2.36) makes it possible to re-express one of those four couplings in terms of the remaining three without loss of generality.

The field equations of khronometric theory are obtained by replacing the hypersurface orthogonality constraint (2.36) in the action (2.29), and then varying the action with respect to $g_{\alpha\beta}$ and T ; they are

$$E_{\alpha\beta} + 2\mathcal{E}_{(\alpha}u_{\beta)} = 0, \quad (2.39)$$

$$\nabla_\mu \left(\frac{\mathcal{E}^\mu}{\sqrt{-\nabla^\alpha T \nabla_\alpha T}} \right) = 0. \quad (2.40)$$

Note that equation (2.40) actually follows from equation (2.39) and from the conservation of the matter stress–energy tensor, i.e. the only independent equations are the modified Einstein equations and the equations of motion of matter [280]. By comparing this set of equations with the Einstein-Æther equations (2.33) and (2.35), it is easy to see that the hypersurface-orthogonal solutions of Einstein-Æther theory will also be solutions of khronometric theory. The converse is true in spherical symmetry [50, 102, 280, 281], but not in more general situations. For instance, slowly rotating BH solutions are different in the two theories [99, 101, 281].

As in the Einstein-Æther case, in Khronometric theory the PPN preferred-frame parameters α_1 and α_2 are nonzero and functions of the couplings. In light of the bounds $|\alpha_1| \lesssim 10^{-4}$ and $|\alpha_2| \lesssim 10^{-7}$ [2], one can expand khronometric theory in α_1 and α_2 . As a result, one is left with two independent parameters (say β and λ), while the third parameter α is related to the first two by⁴⁰ $\alpha = 2\beta + \mathcal{O}(\alpha_1, \alpha_2)$.

From the hypersurface orthogonality constraint (2.36), there are no propagating spin-1 gravitational modes. Requiring positive energies, linear stability of Minkowski space, and the absence of gravitational Cherenkov radiation for the remaining spin-0 and spin-2 degrees of freedom still selects a sizeable region of the parameter space (λ, β) [50, 98, 278], shown in cyan in figure 38 (right panel). Further constraints come from requiring that the theoretically predicted Big Bang nucleosynthesis elemental abundances agree with observations [48, 49, 276]; these constraints are much stronger for Khronometric theory than for Einstein-Æther [47, 276], and are represented by the orange region in figure 38 (right panel).

⁴⁰ Though it may seem that the conditions $\alpha_1 = \alpha_2 = 0$ would reduce the dimensionality of the parameter space to a one-dimensional subspace, both α_1 and α_2 happen to vanish for $\alpha = 2\beta$ in Khronometric theory. Thus, the conditions $\alpha_1 = \alpha_2 = 0$ still select a two-dimensional subspace. However, this only holds at the origin in α -space, and so saturating the bounds to $|\alpha_1| \approx 10^{-4}$ and $|\alpha_2| \approx 10^{-7}$ reduces to a one-dimensional subspace. We refer the reader to [49] for a detailed discussion.

As reviewed in that figure and discussed later in section 6.1, even more stringent constraints on λ and β come from binary pulsar observations [48, 49].

2.5.3. Hořava gravity. The khronometric theory action (2.37) is particularly interesting because it is the low-energy (or infrared) limit of Hořava gravity [200], a renormalizable quantum field theory which has only spatial diffeomorphism invariance. The complete action of Hořava gravity is [279]

$$S_H = \frac{1}{16\pi G_H} \int dT d^3x N \sqrt{h} \left(L_2 + \frac{\hbar^2}{M_*^2} L_4 + \frac{\hbar^4}{M_*^4} L_6 \right), \quad (2.41)$$

where

$$L_2 = K_{ij} K^{ij} - \frac{1 + \lambda}{1 - \beta} K^2 + \frac{1}{1 - \beta} {}^{(3)}R + \frac{\alpha}{1 - \beta} a_i a^i \quad (2.42)$$

is the Lagrangian density of Khronometric theory (see equation (2.37)), M_* is a mass scale, and L_4 and L_6 are terms of fourth and sixth order in the spatial derivatives, but contain no derivatives with respect to the preferred time T .

Complete constraints on M_* are somewhat elusive to obtain, and are probably one of the most important open questions in Hořava gravity [282]. The reason is that one would expect Lorentz violations to percolate from gravity into the matter sector, where Lorentz symmetry has been verified to high precision by particle physics and cosmic-ray experiments [201, 264–267]. However, several mechanisms have been put forward to suppress this percolation. For instance, it has been suggested that the operators that violate Lorentz symmetry in the matter sector might be finely tuned to much smaller values than those in the gravity sector. Also, Lorentz invariance in matter might be an emergent property at low energies [283], as an accidental symmetry [284] or due to renormalization group phenomena [285, 286]. Finally, it has been shown that two sectors with different Lorentz violation degrees can easily coexist if their interaction is suppressed by a high mass scale [287], and this could be the case for the gravity and matter sector. Therefore, taking into account only the gravitational bounds (i.e. assuming that percolation of Lorentz violation into the matter sector is efficiently suppressed), one obtains $M_* \gtrsim 10^{-2}$ eV from sub-millimeter gravitational experiments. Also, perhaps surprisingly, M_* has an upper bound ($M_* \lesssim 10^{16}$ GeV) from the requirement that the theory remains perturbative at all scales [288–290], so that the power-counting renormalizability arguments proposed in [200] apply.

Three things are worth stressing about the higher-order derivative terms L_4 and L_6 in the action. First, the presence of sixth-order spatial derivatives is essential for power-counting renormalizability [200]. Second, the fourth- and sixth-order terms in the spatial derivatives generally lead to nonlinear dispersion relations for the gravitational degrees of freedom of the theory, i.e. the spin-2 and spin-0 gravitons (the latter present in the theory because of the foliation-defining scalar T) satisfy

$$\omega^2 \propto k^2 + \alpha_4 \left(\frac{\hbar}{M_*} \right)^2 k^4 + \alpha_6 \left(\frac{\hbar}{M_*} \right)^4 k^6 + \dots, \quad (2.43)$$

where ω and k are respectively the frequency and the wave-number, while α_4 and α_6 are dimensionless constants. Because such a dispersion relation allows for infinite propagation speeds in the ultraviolet limit, the notion of a BH may appear problematic in these theories. However, we will return to this problem in section 3.5 and show that the presence of a dynamical foliation-defining scalar T actually allows for BHs to be defined in this theory as

well [98, 99, 102]. Third, aside from instantaneous propagation at very high energies, the higher-order terms L_4 and L_6 are typically negligible in astrophysical settings [99]. These terms induce corrections on the spacetime geometry around astrophysical objects that are of order $\mathcal{O}(G_N^{-2}M^{-2}M_*^{-2}) \sim \mathcal{O}(M_{\text{Pl}}^4/(MM_*)^2)$ for an object of mass M , which translates into an error $\lesssim 10^{-16}(M_\odot/M)^2$.

2.5.4. n -DBI gravity. Inspired by the approximate scale invariance of the Universe at early and late times, when it is believed to be approximately de Sitter, Herdeiro *et al* [103, 291] proposed a modification of GR that automatically results in inflation at early times, without the need for additional scalar fields. This model, dubbed n -DBI gravity, was designed so that it yields the Dirac–Born–Infeld type conformal scalar theory when the Universe is conformally flat and resembles Einstein’s gravity in weakly curved space–times. Interestingly, not only does it result in inflation, but it can also accommodate a smooth transition to radiation- and matter-dominated epochs, followed by late time acceleration. The two distinct accelerating periods, with two distinct effective cosmological constants, are a manifestation that the cosmological constant can vary in this theory. Moreover, a large hierarchy between these two cosmological constants can be naturally achieved if the naive cosmological constant appearing in a weak-curvature expansion of the theory is associated to the TeV scale, which also suggests a new mechanism to address the cosmological constant problem. The action for n -DBI gravity is [103]

$$S_{n\text{DBI}} = -\frac{3\lambda}{4\pi G_N^2} \int d^4x \sqrt{-g} \left\{ \sqrt{1 + \frac{G_N}{6\lambda}(R + \mathcal{K})} - q \right\}, \quad \mathcal{K} = -2\nabla_\mu(n^\mu \nabla_\nu n^\nu). \quad (2.44)$$

It contains two dimensionless parameters λ and q and an everywhere time-like vector field \mathbf{n} coupled to the gravitational sector which breaks Lorentz invariance and makes the theory invariant under *foliation preserving diffeomorphisms*, in a way similar to Hofava–Lifschitz gravity. Concretely, if we perform an Arnowitt–Deser–Misner (ADM) decomposition [292], then \mathbf{n} determines the lapse function N through $n_\mu = -N dt$. This gives rise to a scalar degree of freedom, in addition to the two tensor polarizations of GR [293]. Remarkably, the term \mathcal{K} in (2.44) allows for the equations of motion to remain at most second order in time derivatives, despite an infinite power series in the Ricci curvature.

Any solution of Einstein’s gravity with cosmological constant plus matter, admitting a foliation with constant $R + \mathcal{K}$, is also a solution of n -DBI gravity. Moreover, any Einstein space admitting a foliation with constant ${}^{(3)}R - N^{-1}\Delta N$ (where ${}^{(3)}R$ is the Ricci scalar of the three-dimensional hypersurfaces) is a solution of n -DBI gravity [103]. By requiring spherical symmetry, one can explicitly obtain the Schwarzschild, Reissner–Nordström and (anti-)de Sitter BH solutions, albeit in an unusual set of coordinates. Unlike GR, however, the cosmological constant is not determined at the level of the action, but appears instead as an integration constant. The foliation condition of constant ${}^{(3)}R - N^{-1}\Delta N$ can be interpreted as the *maximal slicing* gauge condition common in numerical relativity [294], and it is then straightforward to show that the Kerr metric in Boyer–Lindquist coordinates is also a solution of n -DBI gravity [104].

Since n -DBI gravity has a preferred foliation, one might expect the PPN preferred-frame parameters α_1 and α_2 to be nonvanishing. Then experimental bounds on the PPN parameters should provide a lower bound for λ which, together with the estimate coming from inflation, would in principle define a finite interval of viability $\lambda_{\text{PPN}} < \lambda < \lambda_{\text{inf}}$. However, in a perturbative expansion about Minkowski, solutions of n -DBI gravity coincide with those of

GR and exist for all values of λ, q [52]. Thus, at least to first PN order, we have $\alpha_1 = \alpha_2 = 0$, and n -DBI is indistinguishable from GR in the Solar System.

2.6. Massive gravity and Galileons

de Rham–Gabadadze–Tolley (dRGT) massive gravity is an infrared modification of GR in which gravity is described by a local, Lorentz-invariant, self-interacting, massive spin-2 field. If the mass of the graviton is of order the Hubble scale today, $m_g \sim 10^{-33}$ eV, massive gravity may explain the observed cosmic acceleration (see [17] for a recent review). For clarity of presentation, in this section we do not assume $G_N = 1$, but the gravitational constant is expressed in terms of the Planck mass $M_{\text{Pl}} = (8\pi G_N)^{-1/2}$.

Historically, one of the main challenges in constructing a consistent theory of massive gravity has been preventing the appearance of a scalar ghost mode in the spectrum. The existence of this spurious ghost mode follows from a simple counting argument: a massive spin-2 particle should have five degrees of freedom, but there are six possible polarizations for GWs carried by a symmetric tensor h_{ij} . Thus a theory of massive gravity needs to contain a constraint so that this sixth allowed mode is not present. At the linear level, this problem was solved by Fierz and Pauli by choosing a specific tuning in the mass term [295]. However, Boulware and Deser showed that the sixth mode generically reappears as a ghost at the nonlinear level [296]. When this mode arises nonlinearly, it is referred to as a Boulware–Deser (BD) ghost.

dRGT massive gravity, originally proposed in [297, 298], was constructed to avoid the BD ghost to all orders around any background. The action is

$$S_{\text{dRGT}} = \int d^4x \sqrt{-g} \left[\frac{M_{\text{Pl}}^2}{2} R + \frac{M_{\text{Pl}}^2 m_g^2}{4} \sum_{n=0}^4 \alpha_n \mathcal{L}_n(\mathcal{K}) \right], \quad (2.45)$$

where $\mathcal{K}^\mu{}_\nu \equiv \delta^\mu{}_\nu - \sqrt{g^{\mu\alpha} f_{\alpha\nu}}$, m_g is the graviton mass and α_i are constant coefficients⁴¹.

The Lagrangians \mathcal{L}_n are functions of symmetric tensors $X_{\mu\nu}$:

$$\mathcal{L}_n[X] = \epsilon^{\mu_1\mu_2\mu_3\mu_4} \epsilon_{\nu_1\nu_2\nu_3\nu_4} \prod_{k=1}^n X_{\mu_k}^{\nu_k} \prod_{k'=n+1}^4 \delta_{\mu_{k'}}^{\nu_{k'}}, \quad (2.46)$$

so that $\mathcal{L}_0[X] = 4!$, $\mathcal{L}_1[X] = 3! X_\mu^\mu$, $\mathcal{L}_2[X] = 2!(X_\mu^\mu X_\nu^\nu - X_\nu^\mu X_\mu^\nu)$, etc. The existence of two second-class constraints (and thus the absence of the BD ghost) has been confirmed by many authors, see for example [301, 302].

The metric $f_{\mu\nu}$ is a fixed, external metric called the ‘reference metric.’ The reference metric is needed because the only nontrivial scalar function that can be built out of a single metric is the determinant $\det(g)$ or functions of the determinant, which simply give a cosmological constant or a single new scalar mode [296]. Recently it has been shown that in certain frameworks the reference metric can be eliminated altogether [303]. We may also make the reference metric dynamical by adding a second Einstein–Hilbert term $S_f = \frac{M_f^2}{2} \int d^4x \sqrt{-f} R[f]$ to the action [304]. This is known as bigravity; in this case the spectrum consists of one massless and one massive graviton.

⁴¹ The matrix square root $\sqrt{g^{\mu\alpha} f_{\alpha\nu}} \equiv M^\mu{}_\nu$ is defined in such a way that $M^\mu{}_\rho M^\rho{}_\nu = g^{\mu\alpha} f_{\alpha\nu}$. For flat backgrounds, there is no problem defining the matrix square root in the action perturbatively around flat space using the infinite series expansion given in [298]. It is possible to avoid dealing with matrix square roots by defining massive gravity in the vielbein language [299, 300], in which case the mass term becomes a finite polynomial in the vielbeins, rather than a matrix square root. In this formalism there is no need to take any matrix square roots: see equations (6.1) and (6.2) of [17].

In the following we will mostly focus on massive gravity with a fixed Minkowski reference metric.

Decoupling limit. Many classic tests of gravity take place at length scales much shorter than the Hubble scale, and in regions where the gravitational field is weak: $|h/M_{\text{Pl}}| \ll 1$. In this regime, we may study massive gravity in a simple approximation of the fully nonlinear theory by considering the decoupling limit: $m_g \rightarrow 0$ and $M_{\text{Pl}} \rightarrow \infty$, with $\Lambda_3 = (m_g^2 M_{\text{Pl}})^{1/3}$ fixed. To be relevant for cosmology we need $m_g \sim 10^{-33}$ eV, so $\Lambda_3 \sim (1000 \text{ km})^{-1}$. In all cases where calculations have been done in the full theory and in the decoupling limit, the decoupling limit turned out to be an excellent approximation: see e.g. [172]. In this limit, we may decompose the metric perturbation $H_{\mu\nu} = g_{\mu\nu} - \eta_{\mu\nu}$ into helicity eigenstates: two helicity-2 modes, two helicity-1 modes and one helicity-0 mode (see [297] for a derivation of the decoupling limit). The helicity-2 modes have the same dynamics as in GR, while the helicity-1 modes are not sourced by matter in this limit. Therefore, we will focus exclusively on the helicity-0 mode, whose dynamics is governed by

$$S_{\text{gal}}[\pi] = \int d^4x \left\{ -\frac{3}{4}(\partial\pi)^2 + \sum_{n=3}^5 c_n \mathcal{L}_n^{(g)} \left[\frac{1}{\Lambda_3^3} \partial_\mu \partial_\nu \pi \right] + \frac{g_1}{M_{\text{Pl}}} \pi T + \frac{g_2}{M_{\text{Pl}} \Lambda_3^3} \partial_\mu \pi \partial_\nu \pi T^{\mu\nu} \right\}, \quad (2.47)$$

where $T_{\mu\nu}$ is an external stress–energy tensor, c_n , g_i are constant coefficients, $\mathcal{L}_n^{(g)} = \pi \mathcal{L}_{n-1}$, and \mathcal{L}_n are the same as those given in equation (2.46). The interactions for the π field are called the Galileon interactions [305]; $\mathcal{L}_3^{(g)}$, $\mathcal{L}_4^{(g)}$, $\mathcal{L}_5^{(g)}$ are called the Cubic, Quartic, and Quintic Galileons, respectively. The Galileon interactions ensure that π has second-order equations of motion, which reflects the fact that the BD ghost is not present.

As can be seen from equation (2.47), the helicity-0 mode remains coupled to matter in the decoupling limit, in which $m_g \rightarrow 0$. This surprising fact is known as the van Dam–Veltman–Zakharov (vDVZ) discontinuity [306, 307]. This would appear to rule out massive gravity because the helicity-0 mode would then source a fifth force of gravitational strength, so that, for example, the bending of light by the Sun in massive gravity would differ from the GR prediction by 25%.

Vainshtein mechanism. The resolution to the vDVZ discontinuity, as originally proposed by Vainshtein in [308], is that we cannot ignore the nonlinear self-interactions of the helicity-0 mode. These interactions serve to suppress the coupling to matter, restoring continuity with GR (see [309] for an introduction). This is why it was crucial to keep the scale Λ_3 fixed in the decoupling limit.

The Vainshtein mechanism was proved to work under specific assumptions (e.g. for spherically symmetric, static spacetimes). A general proof of its validity is still lacking, but there have been some studies of the Vainshtein mechanism in time-dependent situations, including binary pulsars [53, 310] and cosmology [311, 312]. Furthermore, there is by now a fair amount of numerical evidence that the Vainshtein mechanism operates even beyond the spherically symmetric static solutions for Galileons. For example, Koyama and collaborators carried out numerical simulations characterizing the strength of the Vainshtein mechanism [313, 314], considering in particular a two-body system that breaks spherical symmetry [315] and using N -body simulations to study the growth of structures, such as dark matter halos and cosmic webs [316, 317].

From a field-theoretic perspective, the Vainshtein mechanism may be understood by considering fluctuations in the Galileon ($\pi = \pi_0 + \phi$) in a regime where the background is

large, in the sense that $\partial^2\pi_0 \gg \Lambda_3^3$. Then, expanding to quadratic order, the fluctuations have the quadratic action (using the Cubic Galileon for definiteness)

$$S[\pi_0 + \phi] = \int d^4x Z [\pi_0]^{\mu\nu} \partial_\mu \phi \partial_\nu \phi + \frac{1}{M_{\text{Pl}}} \phi T + \dots, \quad (2.48)$$

where $Z \sim \partial^2\pi_0/\Lambda_3^3 \gg 1$. After canonically normalizing, $\phi \rightarrow \phi/\sqrt{Z}$, the effective coupling to matter is redressed: $M_{\text{Pl}} \rightarrow M_{\text{Pl}}\sqrt{Z} \gg M_{\text{Pl}}$. Thus the Galileon decouples from matter once this effect is taken into account.

Solutions for Galileons around a static, spherically symmetric source of mass M that exhibit the Vainshtein screening mechanism have been explicitly constructed in [305, 318, 319]. The field profile has a characteristic length scale called the Vainshtein radius, $r_V \equiv \Lambda_3^{-1}(M/M_{\text{Pl}})^{1/3}$. For the Sun, $r_{V,\odot} \sim 100$ pc. The Galileon generates a fifth force sourced by the mass. At distances large compared to the Vainshtein radius, the Galileon force is comparable to Newtonian gravity: $F_\pi/F_N \rightarrow 1$. Yet this force is highly suppressed at short distances: $F_\pi/F_N \sim (r/r_V)^\alpha$, where $\alpha = 3/2$ for the Cubic Galileon and $\alpha = 2$ for the Quartic Galileon (the Quintic Galileon interactions vanish in the spherically symmetric case). Perturbations to these solutions have been shown to be stable for a wide variety of parameters [305].

Hassan–Rosen bimetric theory and other nonlinear massive gravity theories. Recently, there has been revived interest in nonlinear theories of massive gravity. Here we mostly focus on dRGT theory and on the bimetric extension proposed by Hassan and Rosen [304]. In bimetric massive gravity both metrics are dynamical and the theory propagates seven degrees of freedom, corresponding to a massive graviton and to a massless graviton. A different proposal is nonlocal massive gravity [320], in which the field equations are nonlocal but respect causality. This theory propagates the five degrees of freedom of a massive graviton plus a scalar ghost which, however, has the same mass as the massive graviton. Therefore, the ghost is associated with a vacuum instability, which is irrelevant even at cosmological scales [320, 321]. Because of its nonlocal character, few phenomenological studies of this theory are available to date.

Observational tests. A classic observational way to constrain massive gravity is to consider constraints on the Yukawa force law in the Solar System. In the weak-field limit, the Yukawa gravitational potential of a point mass takes the form $V(r) \sim e^{-m_g r}/r$. Tests of deviations from the inverse square law from Solar System experiments set the bound $m_g < 0.5 \times 10^{-21}$ eV [2].

The best bounds on Galileons come from lunar laser ranging. In [322, 323] it was shown that the fifth force discussed above in the context of spherically symmetric solutions leads to an anomalous precession of the perihelion of the moon

$$\delta\phi \sim \frac{\delta\Phi}{\Phi} \sim \left(\frac{R}{r_V}\right)^\alpha \text{ rad/orbit}, \quad (2.49)$$

where Φ is the gravitational potential, $\delta\Phi$ is the extra contribution of the helicity-zero mode π to the potential, R is the semi-major radius, and α depends on the Galileon model (see [17] for a review). For the Cubic Galileon $\alpha = 3/2$, leading to $\delta\phi \sim 10^{-12}$ rad/orbit when using parameters relevant for cosmology. As the current observational precision is $\sim 0.5 \times 10^{-11}$ rad/orbit [2], next-generation experiments can potentially rule out the Cubic Galileon. For the Quartic Galileon, $\alpha = 2$. For $m_g \sim 10^{-33}$ this yields $\delta\phi \sim 10^{-16}$ rad/orbit,

which cannot be probed by current experiments. Turning this around and phrasing it as a bound on Λ , we find $\Lambda > 10^{-11}$ eV, or alternatively $m_g < 10^{-30}$ eV.

2.7. Gravity with auxiliary fields

All the theories previously discussed imply, in one way or another, the existence of extra *dynamical* fields. This is the most common way to circumvent Lovelock's theorem. There is, however, a more subtle way which does not require any additional degrees of freedom [197]. Specifically, it is possible to construct a theory which modifies only the right-hand side of Einstein's equations, adding another symmetric rank-2 tensor constructed solely from the metric and the matter fields (i.e. without introducing any new degrees of freedom). The additional term must be identically divergence-free so as to not compromise the weak equivalence principle.

These requirements may seem hard to satisfy simultaneously, but there is in fact a generic prescription to construct such theories. In some special theories that include *auxiliary* (i.e., nondynamical) fields, eliminating these fields leads precisely (and generically) to the type of modification of Einstein's equation just described, without modifying the field equations of matter. Two representative theories belonging to this class are Palatini $f(\mathcal{R})$ gravity [11, 199] and the so-called EiBI gravity [198], as discussed below.

Palatini $f(\mathcal{R})$ gravity. The action of $f(\mathcal{R})$ gravity in the Palatini formalism reads

$$S = \frac{1}{16\pi} \int d^4x \sqrt{-g} f(\mathcal{R}) + S_M[\Psi, g_{\mu\nu}], \quad (2.50)$$

where henceforth $\mathcal{R} = g^{\mu\nu} \mathcal{R}_{\mu\nu}$ and $\mathcal{R}_{\mu\nu}$ denotes the Ricci tensor built from the connection $\Gamma_{\mu\nu}^\sigma$ (which is assumed to be symmetric), to distinguish it from the Ricci tensor R built from the Levi-Civita connection of the metric $g_{\mu\nu}$, as in the metric formalism discussed in section 2.2. Recall that in the Palatini (or affine) approach the connection $\Gamma_{\mu\nu}^\sigma$ is considered as an independent field, which enters the action (2.50) on the same footing as the metric $g_{\mu\nu}$. This choice has dramatic consequences for the theory, which is in fact completely different from *metric $f(R)$ gravity*. By varying the action (2.50) with respect to the metric and the independent connection, the field equations can be cast in the form [11]

$$f'(\mathcal{R}) \mathcal{R}_{(\mu\nu)} - \frac{g_{\mu\nu}}{2} f(\mathcal{R}) = 8\pi T_{\mu\nu}, \quad (2.51)$$

$$\tilde{\nabla}_\mu [\sqrt{-g} f'(\mathcal{R}) g^{\mu\nu}] = 0, \quad (2.52)$$

where $\tilde{\nabla}_\mu$ is the covariant derivative associated with $\Gamma_{\mu\nu}^\sigma$, $T^{\mu\nu} \equiv -2(-g)^{-1/2} \delta S_M / \delta g_{\mu\nu}$ is the standard stress–energy tensor, whose indices are raised and lowered with $g_{\mu\nu}$, and a prime denotes derivative with respect to \mathcal{R} . GR is recovered when $f(\mathcal{R}) = \mathcal{R}$, because equation (2.52) becomes the definition of the Levi-Civita connection; this implies $\mathcal{R}_{\mu\nu} = R_{\mu\nu}$ and, in turn, equation (2.51) yields the standard Einstein equations. Remarkably, in this framework the fact that $\Gamma_{\mu\nu}^\sigma$ is the Levi-Civita connection of $g_{\mu\nu}$ emerges *dynamically*, and it is not imposed *a priori* as in the standard Einstein–Hilbert action.

Nevertheless, for generic functions $f(\mathcal{R})$ the field equations (2.52) imply that $\Gamma_{\mu\nu}^\sigma$ is the Levi-Civita connection of the conformal metric $h_{\mu\nu} = f'(\mathcal{R}) g_{\mu\nu}$, and the dynamical content of the theory is very different from *metric $f(R)$* . The connection can be expressed *algebraically* in terms of $g_{\mu\nu}$ and the matter fields, and the field equations in Palatini $f(\mathcal{R})$ gravity read [11]

$$G_{\mu\nu} = \frac{8\pi}{f'} T_{\mu\nu} - \frac{g_{\mu\nu}}{2} \left(\mathcal{R} - \frac{f}{f'} \right) + \frac{1}{f'} (\nabla_\mu \nabla_\nu - g_{\mu\nu} \square) f' - \frac{3}{2f'^2} \left[(\nabla_\mu f') (\nabla_\nu f') - \frac{g_{\mu\nu}}{2} (\nabla f')^2 \right], \quad (2.53)$$

where now ∇_μ is the covariant derivative associated with the Levi-Civita connection of the metric. Furthermore, by taking the trace of equation (2.51) one obtains the following algebraic equation for \mathcal{R} :

$$f'(\mathcal{R})\mathcal{R} - 2f(\mathcal{R}) = 8\pi T, \quad (2.54)$$

which reduces to the standard trace relation $R = -8\pi T$ in the GR limit. For a given f the equation above can be solved for \mathcal{R} , and by plugging the solution back into equation (2.53) one obtains a set of field equations that depend only on the metric $g_{\mu\nu}$ and on the stress-energy tensor $T_{\mu\nu}$, with no extra degrees of freedom.

Thus, the theory has effectively the same degrees of freedom as GR, i.e. it propagates only a massless spin-2 graviton. This is a striking difference with respect to metric $f(R)$ gravity, which propagates an extra scalar field and is in fact equivalent to scalar-tensor theory. It can be shown that Palatini $f(\mathcal{R})$ is also equivalent to a scalar-tensor theory in the form (2.3) with a potential that depends on the functional form of $f(R)$ and with $\omega(\phi) = 0$, i.e. the kinetic term is vanishing and the scalar field is nondynamical or *auxiliary* [11]. This theory is *equivalent* to GR in vacuum ($T_{\mu\nu} = 0$), but the gravitational field equations contain a nonlinear source through terms like $\square f'$. Nonetheless, $\nabla_\mu T^{\mu\nu} = 0$ identically, as can be seen by the fact that matter fields are minimally coupled to the metric in the action (2.50).

EiBI gravity. The idea behind EiBI gravity is to incorporate the Palatini approach into a gravitational analog of Born-Infeld nonlinear electrodynamics [324] which removes the divergence of the electron self-energy by introducing an upper bound of the electric field at the origin. Studies of similar proposals for a gravitational Born-Infeld-like action are thus motivated by the prospect of resolving the curvature singularities that afflict GR in a similar fashion.

Inspired by Born-Infeld theory, EiBI gravity is described by the action [198]

$$S = \frac{1}{8\pi\kappa} \int d^4x \left(\sqrt{|\det(g_{\mu\nu} + \kappa \mathcal{R}_{(\mu\nu)})|} - (1 + \kappa\Lambda)\sqrt{g} \right) + S_M[g_{\mu\nu}, \Psi], \quad (2.55)$$

where $g = |\det(g_{\mu\nu})|$, Λ is the cosmological constant and κ is a new EiBI parameter with dimensions of length squared. EiBI gravity is naturally based on the Palatini formulation because in the metric approach the field equations contain ghosts, which must be eliminated by adding extra terms to the action [325, 326]. Here we will focus on the original EiBI proposal [198] (see [184] for a discussion).

When expanded at second order in $\kappa \mathcal{R}_{\mu\nu}$, the action (2.55) takes the form

$$S = \frac{1}{16\pi} \int d^4x \sqrt{g} \left[\mathcal{R} - 2\Lambda + \frac{\kappa}{4} (\mathcal{R}^2 - 2\mathcal{R}_{(\mu\nu)}\mathcal{R}^{(\mu\nu)}) \right] + S_M[g_{\mu\nu}, \Psi] + \mathcal{O}(\kappa^2), \quad (2.56)$$

and to lowest order EiBI gravity reduces to the Palatini formulation of GR with a cosmological constant. To next-to-leading order, quadratic corrections in the curvature tensor built from the independent connection appear in the action (2.56). The Palatini formulation guarantees that, despite these extra terms, no higher derivatives of the metric would appear in

the field equations. When expanded order by order in κ , the action (2.55) takes the form of a specific Palatini $f(\mathcal{R}, \mathcal{R}_{\mu\nu})$ theory.

Beyond the perturbative level, independent variation of the action (2.55) with respect to the metric and the connection yields

$$\sqrt{q} q^{\mu\nu} = \sqrt{g} [(1 + \kappa\Lambda)g^{\mu\nu} - 8\pi\kappa T^{\mu\nu}], \quad (2.57)$$

$$0 = \tilde{\nabla}_\sigma [\sqrt{q} q^{(\mu\nu)}] - \tilde{\nabla}_\gamma [\sqrt{q} q^{\gamma(\mu} \delta^{\nu)}_\sigma], \quad (2.58)$$

where we have defined $q_{\mu\nu} \equiv g_{\mu\nu} + \kappa\mathcal{R}_{(\mu\nu)}$, $\tilde{\nabla}_a$ is the covariant derivative associated with $\Gamma_{\mu\nu}^\sigma$, and $q^{\mu\nu}$ is the inverse of $q_{\mu\nu}$. After some manipulation, equation (2.58) implies that $\Gamma_{\mu\nu}^\sigma$ is the Levi-Civita connection of $q_{\mu\nu}$ and, by using equation (2.57), one obtains an *algebraic* equation that determines $q_{\mu\nu}$ in terms of $g_{\mu\nu}$ and $T_{\mu\nu}$. Similarly to the case of Palatini $f(\mathcal{R})$ gravity, one can eliminate $\Gamma_{\mu\nu}^\sigma$ from the field equations. The final set of equations is of second differential order in the metric $g_{\mu\nu}$ and contains second derivatives of $T_{\mu\nu}$. This is true in the full theory, but it becomes more explicit by working perturbatively in the $\kappa\mathcal{R}_{\mu\nu} \ll 1$ limit. To first order, the field equations read [184]

$$\begin{aligned} R_{\mu\nu} = & \Lambda g_{\mu\nu} + 8\pi \left(T_{\mu\nu} - \frac{1}{2} T g_{\mu\nu} \right) \\ & + \kappa \left[S_{\mu\nu} - \frac{1}{4} S g_{\mu\nu} \right] + \frac{\kappa}{2} \left[\nabla_\mu \nabla_\nu \tau - 2 \nabla_\sigma \nabla_{(\mu} \tau_{\sigma\nu)} + \square \tau_{\mu\nu} \right] + \mathcal{O}(\kappa^2), \end{aligned} \quad (2.59)$$

where $S_{\mu\nu} \equiv 64\pi^2 [T^\sigma{}_\mu T_{\sigma\nu} - \frac{1}{2} T T_{\mu\nu}]$ and $\tau_{\mu\nu} \equiv 8\pi (T_{\mu\nu} - \frac{1}{2} g_{\mu\nu} T) + \Lambda g_{\mu\nu}$. Einstein's theory is recovered when $\kappa \rightarrow 0$. For $\kappa \neq 0$, equation (2.59) contains second derivatives of $T_{\mu\nu}$. This is in contrast to Einstein's theory, where the stress–energy tensor appears on the right-hand side of Einstein's equations at zero differential order. This different structure is also evident in the Newtonian limit of the theory. The modified Poisson equation sourced by a matter density ρ is [183, 198]

$$\nabla^2 \Phi = 4\pi\rho + 2\pi\kappa \nabla^2 \rho, \quad (2.60)$$

whose solution reads $\Phi = \Phi_N + 2\pi\kappa\rho$, where Φ_N is the standard Newtonian potential.

Generalized auxiliary field gravity. It has recently been pointed out that Palatini $f(\mathcal{R})$ and EiBI gravity are only two examples of a generic class of theories with auxiliary fields that can be constructed in a derivative expansion. Up to 4th order in derivatives, the field equations of this theory read [197]

$$\begin{aligned} G_{\mu\nu} = & 8\pi T_{\mu\nu} - \Lambda g_{\mu\nu} - 8\pi\beta_1 \Lambda g_{\mu\nu} T + 16\pi^2 (1 - 2\beta_1 \Lambda) (\beta_1 - \beta_4) g_{\mu\nu} T^2 \\ & + 64\pi^2 \left[\beta_4 (1 - 2\beta_1 \Lambda) - \beta_1 \right] T T_{\mu\nu} + 64\pi^2 \left[\frac{1}{2} \beta_4 g_{\mu\nu} T_{\sigma\gamma} T^{\sigma\gamma} - 2\beta_4 T^\sigma{}_\mu T_{\sigma\nu} \right] \\ & + 8\pi \left[\beta_1 \nabla_\mu \nabla_\nu T - \beta_1 g_{\mu\nu} \square T - \beta_4 \square T_{\mu\nu} + 2\beta_4 \nabla^\sigma \nabla_{(\mu} T_{\nu)\sigma} \right] + \dots \end{aligned} \quad (2.61)$$

Remarkably, to this order the theory contains only two extra coupling constants, β_1 and β_4 , which completely parametrize *any* theory belonging to this class. In this parametrization, EiBI gravity and Palatini $f(\mathcal{R})$ theories belong to ‘orthogonal’ classes: the small-coupling limit of EiBI gravity corresponds to $\beta_1 = 0$ and $\beta_4 \propto \kappa$, whereas generic Palatini $f(\mathcal{R})$ theories correspond to $\beta_4 = 0$, with Λ and β_1 depending on the specific $f(\mathcal{R})$ model.

Main results. Most applications of these theories were worked out for Palatini $f(\mathcal{R})$ gravity. EiBI gravity has been investigated to a lesser extent, despite a recent surge of activity. We list some of the main findings below:

- As mentioned, this class of theories is *equivalent* to GR in vacuum. Hence, no BH-based tests can distinguish these theories from GR. However, nonperturbative effects can replace the singular interior of a *charged* BH by a regular wormhole geometry [327], similarly to the resolution of the point-charge singularity in Born–Infeld electrodynamics.
- When applied to early cosmology, the Big Bang singularity that appears generically in GR cosmological models is replaced by a regular behavior [198, 328].
- The critical mass of a NS can be much larger in these theories than in GR [182] and gravitational collapse is suppressed [183], as discussed in section 4.7.
- When matter is described by a perfect fluid with a barotropic EOS $P = P(\rho)$, the modified field equations are equivalent to GR sourced by an effective perfect fluid with a different EOS, where the dependence $P(\rho)$ is highly nonlinear [329]. This allows for interesting configurations: for example a fluid may satisfy all energy conditions in flat spacetime but, when coupled to gravity, the effective stress–energy tensor (the right-hand side of equation (2.61)) can violate some energy conditions. Furthermore the degeneracy between different EOSs and beyond-GR corrections is maximal in these theories [329].
- As we discuss in more detail in section 4, these theories lead to curvature singularities when there are discontinuities in energy density, e.g. at the interface between a solid body and vacuum [179, 180, 184, 197, 330, 331]. Whether or not this is a consequence of the often employed polytropic approximation, or whether such singularities can be avoided in other ways, is currently unclear [332].
- An analysis of the Newtonian limit of this class of theories was performed in [197], with the result that the lowest-order PN solution does not fit into the standard PPN framework [2]. The PPN framework should therefore be extended to accommodate these theories.
- Flanagan [333] pointed out that Palatini $f(\mathcal{R})$ gravity can produce unacceptable deviations in the matter sector, and therefore it would be in conflict with the standard model of particle physics. This result is debated (see [227, 334] and [199] for a review) but, if correct, it should also apply to EiBI gravity and other theories belonging to this category [184, 197]. Another potential shortcoming of these theories is related to the averaging problem in cosmology [333, 335]. More detailed studies in these directions are necessary to assess the viability of theories with auxiliary fields.

2.8. GR and quantum mechanics: an EFT approach

Since gravity is nonrenormalizable, a useful alternative point of view on modifications of GR is provided by EFT, since this is the framework widely used for understanding non-renormalizable theories elsewhere in physics. This approach recognizes that such theories arise when one focuses on observables involving only the lower of two well-separated scales, and so make sense (even at the quantum level) only within the context of a low-energy approximation. (Indeed this is arguably the only way known yet to make sense of such theories at the quantum level, and this provides their main motivation.) Typically quantum effects are suppressed by the small ratio of scales, and so the classical approximation itself fails if applied at too high energies. For gravity the higher scale might be the mass of some hitherto undiscovered particle, but—for the reasons given below—cannot be higher than the Planck scale: energies comparable to $M_{\text{Pl}} \sim 10^{19}$ GeV. However, for some theories of gravity (e.g. higher-dimensional theories) this scale can be much smaller. Consequently quantum

gravity corrections may be important at lower energies, and so be accessible to astrophysical observations. In most of the strong-field modifications of GR discussed in this review one implicitly assumes the existence of a new fundamental scale, smaller than M_{pl} , at which the modifications set in. As we now discuss, EFT is extremely powerful in this context: simply by assuming the existence of two different scales, the EFT framework provides a prescription to obtain all viable corrections to the classical action, even when the full quantum theory is unknown.

If a system involves two very different energy (or mass) scales, $M_1 \ll M_2$, a drastic simplification occurs when observables are expanded in powers⁴² of the small ratio M_1/M_2 . The EFT formulation is designed to exploit this simplification as early in a calculation as possible, focusing on observables that directly involve energies only at the lower of the two scales, $E \lesssim M_1$. In this case, because no ‘heavy’ states at scale M_2 appear directly in the observables, they can only influence the result as virtual states. As a result their effects on longer wavelengths can always be incorporated as corrections to the ‘effective’ Lagrangian (or Hamiltonian) used to describe the evolution of the low-energy states. In particular, the same corrected Lagrangian can be used to compute *all* low-energy observables, so it is much more efficient to first compute the effective Lagrangian once and for all, and later use this to compute implications for any observables of interest.

In formulae, suppose a system is described by a theory having both ‘heavy’ and ‘light’ fields, h and l , described by a classical action $S(h, l)$. Suppose also that measurements are performed at low energies, using quantities $\mathcal{O}_k(l)$ involving only the lighter fields l . Observables can then be expressed in terms of functional integrals of the form

$$\begin{aligned} \langle \mathcal{O}_1 \cdots \mathcal{O}_n \rangle &= \int \mathcal{D}h \mathcal{D}l [\mathcal{O}_1(l) \cdots \mathcal{O}_n(l)] \exp [iS(h, l)] \\ &= \int \mathcal{D}l [\mathcal{O}_1(l) \cdots \mathcal{O}_n(l)] \exp [iS_{\text{eff}}(l)], \end{aligned} \quad (2.62)$$

where the \mathcal{O}_k ’s independence of h allows the $\mathcal{D}h$ integration to be performed once and for all, ensuring all its effects arise through the combination

$$\exp [iS_{\text{eff}}(l)] \equiv \int \mathcal{D}h \exp [iS(h, l)]. \quad (2.63)$$

Expanding in powers of $1/M_2$ in $S_{\text{eff}}(l)$ then amounts to writing it as a local expansion in derivatives of l , with more complicated interactions being suppressed by higher powers of $1/M_2$.

For instance, if the light field is the metric, this leads to an expansion of the form

$$\begin{aligned} S_{\text{eff}} = - \int d^4x \sqrt{-g} & \left[c_4 + c_{(2,1)} R + c_{(0,1)} R^2 + c_{(0,2)} R_{\mu\nu} R^{\mu\nu} + c_{(0,3)} R_{\mu\nu\lambda\rho} R^{\mu\nu\lambda\rho} \right. \\ & \left. + c_{(-2,1)} R^3 + c_{(-2,2)} R R_{\mu\nu} R^{\mu\nu} + \cdots \right], \end{aligned} \quad (2.64)$$

where all possible terms consistent with symmetries (such as general covariance) are included⁴³. The subscript d on the constants $c_{(d,k)}$ means that they have dimension (mass) ^{d} in ‘fundamental’ units (for which $\hbar = c = 1$); k simply labels the possible terms for each value of d .

⁴² It can sometimes happen that a Taylor expansion is inadequate (e.g. when infrared divergences occur), and then more singular functional forms—such as a logarithmic dependence $\sim \log(M_1/M_2)$ —can also arise.

⁴³ Not all such terms need be independent of one another, making it useful in practice to identify a minimal basis of interactions of each dimension. For some reviews of gravity formulated as an EFT, see [19, 336, 337].

By integrating out a heavy field with mass M_2 , as in equation (2.63), one typically gets a contribution to $c_{(d,k)}$ of order $c_{(d,k)} = \tilde{c}_{(d,k)} M_2^d$ (where the dimensionless coefficients, $\tilde{c}_{(d,k)}$, might depend logarithmically on M_2). It is because M_2 is assumed large and we are interested in expanding in powers of $1/M_2$ that only positive powers of curvature appear in this expression. If more than one such fields are integrated out one might find a sum of contributions of this form

$$c_{(d,k)} \sim \sum_f \tilde{c}_{(d,k)}^f M_f^d, \quad (2.65)$$

where M_f is the mass of the corresponding particle. Clearly the contribution coming from the field with the largest mass dominates in c_4 and $c_{(2,1)}$, while the *smallest* mass wins in $c_{(d,k)}$ for any $d < 0$. We therefore expect $c_{(d,k)}$ to be of order m^{-d} , where m is the mass of the lightest particle that has been integrated out, perhaps the electron in applications to the Solar System⁴⁴. By contrast, c_4 and $c_{(2,k)}$ should be potentially enormous, since they are most sensitive to the most massive particles that are present. This expectation is borne out for $c_{(2,1)}$, which can be identified with $M_{\text{Pl}}^2/2$, since $M_{\text{Pl}} \approx 10^{19}$ GeV is the highest fundamental energy scale we know in Nature. This argument seems to fail for c_4 , which cosmological observations indicate cannot be larger than on the order of $(10^{-3} \text{ eV})^4$. Why c_4 should be so small is a long-standing unsolved problem: the cosmological constant problem⁴⁵.

2.8.1. Power-counting and the semiclassical approximation. What does any of this have to do with the classical approximation? The connection to EFTs arises for two reasons. First, $S_{\text{eff}}(I)$ enters into expressions in precisely the same way as would a classical action; the influence of the heavy fields makes the system behave at low energies *as if* its classical action were $S_{\text{eff}}(I)$. Second, much of the nitty gritty of EFT techniques aims to identify how successive heavy-field corrections to S_{eff} propagate through to contribute to observables, to make their calculation as efficient as possible. The point is that these same techniques can be used to track which combinations of parameters arise order-by-order in the loop expansion, and so whose small size ultimately justifies this expansion. Since classical physics is just the leading (nonloop) contribution, such arguments also justify when it suffices to stop with a classical result.

It is worth illustrating this with a specific example. A particularly simple class of observables for a low-energy gravity theory consist of the scattering of weakly coupled gravitons moving through a weakly curved classical geometry. If $c_4 = 0$ we can take the background geometry to be flat space⁴⁶, allowing us to expand the metric around the Minkowski background: $g_{\mu\nu} = \eta_{\mu\nu} + h_{\mu\nu}$. We then ask how each of the terms in the gravitational action, equation (2.64), contribute. In particular, with a view to asking how large quantum corrections can be, we can ask about the relative size of different contributions to the amplitude, $\mathcal{A}(E)$, for two gravitons to scatter into another two with energy E .

As shown in [19, 336, 337] in some detail, the contribution to this amplitude of an L -loop Feynman graph built using $V_{i,r}$ vertices built from a term in S_{eff} involving r powers of the curvature tensor, involving the emission or absorption of i gravitons, is of order

⁴⁴ Notice that these arguments indicate that for practical applications $c_{(d,k)}$ is almost certainly *not* of order M_{Pl}^d when $d < 0$, unlike the choice often made.

⁴⁵ A classic review of the cosmological constant problem is given in [5]. A review with a sturdy defense of anthropic approaches and issues raised by the ‘landscape’ of solutions to quantum gravity theories is in [338]; see also [339].

⁴⁶ The assumption of flatness here is purely for convenience, and the conclusions below apply equally well to curved spaces, since they rely essentially on dimensional arguments.

$$\mathcal{A}(E) \sim \left(\frac{E}{M_{\text{Pl}}}\right)^2 \left(\frac{E}{4\pi M_{\text{Pl}}}\right)^{2L} \prod_i \prod_{r \geq 2} \left[\frac{E^2}{M_{\text{Pl}}^2} \left(\frac{E}{M}\right)^{(2r-4)} \right]^{V_{i,r}}. \quad (2.66)$$

Here M is the mass that sets the dimensions of the coefficients $c_{(d,k)} \propto M^d$ for $d < 0$, which is assumed for simplicity to be the same order of magnitude for all negative d . Equation (2.66) has several useful consequences.

First, because $r \geq 1$ for all terms in equation (2.64) the contribution to \mathcal{A} contains no negative powers of E . This illustrates how S_{eff} encapsulates how observables simplify in the hierarchical low-energy limit, where $E \ll M$, $E \ll M_{\text{Pl}}$. In particular, this expression quantifies why the weakness of the graviton's coupling follows purely from the low-energy approximation, $E \ll M_{\text{Pl}}$ and $E \ll M$.

Second, these expressions identify precisely which kinds of interactions dominate scattering amplitudes at low energies. The minimum suppression by powers of E comes when $L = 0$ and we choose $V_{i,r} = 0$ unless $r = 1$, and so is given by arbitrary tree graphs constructed purely from the Einstein–Hilbert action. This tells us what we would be inclined to believe in any case: it is $L = 0$ (no-loop) graphs built only from the Einstein–Hilbert action—i.e. classical GR—which govern the low-energy dynamics of GWs, giving a result of order $(E/M_{\text{Pl}})^2$.

But we may also identify the next-to-leading contributions. These are proportional to $(E/M_{\text{Pl}})^4$ and can appear in one of two ways:

- (i) either: $L = 1$ and $V_{i,r} = 0$ for any $r \neq 1$,
- (ii) or: $L = 0$ with $\sum_i V_{i,2} = 1$ and $V_{i,1}$ arbitrary, and $V_{i,r} = 0$ for all $r \geq 3$.

That is, the next-to-leading contribution is obtained by computing the one-loop corrections using only Einstein gravity, or by working to tree level and including precisely one curvature-squared interaction in addition to any number of interactions from the Einstein–Hilbert term. Both are suppressed compared to the leading term by a factor of $(E/M_{\text{Pl}})^2$. At this order the ultraviolet divergences that famously plague gravitational loops in option (i) above are absorbed into renormalizations of the coefficients of the curvature-squared contributions that appear in option (ii), and so on further down the E/M_{Pl} expansion.

These conclusions are borne out by explicit calculations. At tree level the only nonzero amplitudes are related by crossing symmetry to the amplitude for which all graviton helicities have the same sign, and this is given by [340–342]:

$$-i\mathcal{A}_{(++++)}^{\text{tree}} = 8\pi G \left(\frac{s^3}{tu} \right), \quad (2.67)$$

where s , t and u are the usual Mandelstam invariants built from inner products of the graviton four-momenta, all of which are proportional to the square of the center-of-mass energy, E_{cm} . This shows that it is the frame-independent center-of-mass energy that appears in the E/M_{Pl} expansion of \mathcal{A} . The one-loop corrections are also computed [343], and are infrared divergent. These infrared divergences cancel in the usual way with tree-level bremsstrahlung diagrams [344], leading to a finite result [345], which is suppressed as expected relative to the tree contribution by terms of order $(E/M_{\text{Pl}})^2$, up to logarithmic corrections.

It is expressions like the amplitude scaling (2.66) that make the explicit connection between EFTs and the domain of validity of the semi-classical (or loop) approximation. This expression reveals that the loop expansion for gravity is secretly a low-energy approximation. This turns out to be generic for any nonrenormalizable field theory [346]. For such theories

the only known way to extract sensible quantum corrections is within a low-energy approximation, for which the classical action should be regarded as a general derivative expansion along the lines of equation (2.64). All terms in this action consistent with symmetries and field content are compulsory, since their presence is required to renormalize the ultraviolet divergences that are generated by loops involving terms arising at lower orders in the derivative expansion.

2.8.2. Modified gravity seen through EFT glasses. We can now return to our road map of modified gravity theories to see what it leads us to expect. Following [347], we argue that EFT can provide useful guidelines.

New particles and/or dimensions. The most conservative modifications simply involve the addition of new light particles or the addition of more dimensions (or both), with the new additions resembling those about which we already know. It is certainly true that such modifications can be sensible in principle, and explicit examples exist (such as string theory) for higher-energy physics that can produce such modifications. It makes sense to constrain such possibilities observationally.

There are also issues that can be expected to arise in such theories if the new particles are light enough to be relevant over astrophysical or cosmological distances. This is true in particular for proposals meant to describe present-epoch dark energy [5, 338, 339]. Such particles are so close to massless that many of the constraints on massless particles in practice are likely to apply. In particular, it can be expected that in the Lorentz-invariant framework of special relativity the new particles must be spin zero, half or must be gauge particles with spin one or $\frac{3}{2}$ or smaller.

Another problem potentially can also arise, associated with the size of quantum corrections to the mass, particularly for spinless particles represented by a scalar field, ϕ . Then the low-energy EFT contains a mass term of the form $\mathcal{L}_{\text{eff}} = -c_{(2,2)} \sqrt{-g} \phi^2$ whose coefficient $c_{(2,2)} \propto M^2$ should be large, for the same reasons (given above) that lead one to expect $c_{(2,1)}$ and c_4 are large. This is a ‘hierarchy’ problem, similar to the cosmological constant problem; very light spinless particles very rarely arise as the low-energy limit of something more fundamental because their masses are sensitive to quantum contributions from every heavy state at higher energies that is integrated out.

A similar problem does not occur for spin-half particles, because for these the particle mass can be forbidden by a chiral symmetry, under which the fermion’s left- and right-handed components rotate differently: $\psi \rightarrow i\gamma_5\psi$. Because of this it can only receive quantum corrections from particles that also break this symmetry. Only very few symmetries (supersymmetry and scale invariance) are known that can forbid a scalar mass, making this mechanism more challenging to use at low energies for spinless particles.

Modifications to the Einstein equations. Short-distance modifications to the left-hand side of Einstein’s equations are also very plausible, since these can easily be generated by integrating out various kinds of heavy fields. In well understood situations these usually lead to modified actions along the lines of equation (2.64) that are local polynomials of the metric and its derivatives, and involve all possible kinds of interactions allowed by the assumed symmetries. In particular, it should be noted that generic higher-derivative interactions are allowed, and explicit calculations [348] show these need not take the specific Horndeski or Lovelock forms that are sometimes advocated as being required to avoid the presence of ghosts. What is hard to achieve in this way are modifications like $f(R)$ gravity where $f(R)$ is an unusual function,

such as $1/R$. Proposals such as this one step away from the underlying EFT understanding of the validity of the semi-classical approximation, and so the onus is on proponents to justify the regime of validity of any classical approximation. This is particularly so in situations like dark energy proposals, where one of the basic problems (the cosmological constant problem) cannot be seen until quantum effects are examined.

Breaking diffeomorphism invariance. As described above, it is ultimately the consistency of Lorentz invariance and quantum mechanics that drives many of the consistency conditions for massless (and very light) particles, including the requirements for the gauge invariance of their interactions. However the constraints are no longer quite as exacting once the particles are not exactly massless. In this case the general consistency issues can be expected to persist if the particle is light enough compared with the higher scales of the theory, $m \ll M$, but can be evaded if this hierarchy is not too large.

This observation has prompted some to put aside until later understanding the embedding into higher-energy physics, and instead to explore the implications of relaxing the assumptions of gauge invariance (and so usually also Lorentz invariance) at low energies. The hope is to find a consistent low-energy effective description that applies only up to relatively low energy scales, and hope that once this is done a consistent ultraviolet completion can be found. In most cases of this type, no candidate ultraviolet extension is yet known.

Modifications to gravity provide a rich theoretical laboratory as to how quantum field theories work, that display their tight consistency issues in new and instructive situations. Sensible modifications—i.e. those that can be embedded into well-understood ultraviolet completions—are the goal, but are also not that easy to come by. Together with their success in describing astrophysical and cosmological observations, theoretical soundness should be regarded as one part of the evidence to be used when assessing the likelihood of such theories describing Nature.

2.9. Open problems

Here we give a (necessarily biased) list of open problems regarding the modified theories of gravity discussed in this section:

Scalar–tensor gravity and metric $f(R)$ theories.

- Multiscalar–tensor theories with a nontrivial target space geometry offer a barely explored, uncharted territory (see [39] for pioneering work). The presence of different nonperturbative phenomena and richer phenomenology awaits exploration.
- Building $f(R)$ theories which are observationally viable in the weak-field limit and differ from GR at cosmological scales (as needed to alleviate the difficulties associated with a cosmological constant: see section 6.2) is a challenging task [12, 349, 350]. Indeed, it seems that in $f(R)$ gravity one cannot produce any drastically different behavior at cosmological scales without simultaneously compromising the Newtonian limit at small scales [349]. If confirmed, this quite general result would cast serious doubts on the attractiveness of $f(R)$ gravity as an alternative to GR.
- Even cosmologically viable $f(R)$ models seem to be disfavored against the Λ CDM paradigm. On the other hand, the simplest inflationary models can be framed as $f(R)$ theories, where the inflaton is the extra scalar degree of freedom.

Quadratic gravity.

- At variance with GR and scalar–tensor theories, a well-posed formulation of quadratic gravity is not available yet. This is important for the theoretical viability of the theory and for numerical simulations, as discussed in the remainder of this review. In fact, while a well-posed formulation is expected to exist in the small-coupling limit, it is unclear whether these theories are well posed in their exact form (see [44] for an analysis of this problem in dCS gravity).
- Because very few studies have analyzed quadratic gravity beyond the perturbative regime, it is unknown whether such theories predict strong-field effects (akin to spontaneous scalarization in scalar–tensor theories) that are not captured by a perturbative analysis in the small-coupling regime. The results of [164] seem to suggest that such effects may not occur, at least for isolated stars.
- To the best of our knowledge, the effects of a scalar self-potential (and in particular of a mass term) have not been explored yet.
- Higher-order terms are suppressed by powers of the (dimensionful) coupling constants. The latter depend on the system under consideration, and if $\alpha \sim L$ (recall that L is the typical size of the system) the perturbative analysis would break down, and higher-order curvature invariants would become increasingly more important. Furthermore, also other combinations of higher-order terms can give rise to second-order field equations, similarly to the Gauss–Bonnet term in quadratic gravity.
- Quadratic curvature terms might also be coupled to an extra fundamental vector (or higher-spin) field, which would allow for new scalar quantities in the action and presumably for a completely different phenomenology.
- A theory that received some interest is conformal gravity [351], where the Lagrangian $\mathcal{L} = R_{\mu\nu}R^{\mu\nu} - (1/3)R^2$ is constructed out of contractions of the Weyl tensor. This theory admits all *vacuum* solutions of Einstein gravity with a cosmological constant (see e.g. [352] and references therein for a study of the geodesic motion around spinning BHs in this theory). Having higher-order derivatives, the theory may be plagued by ghosts, but this issue is still debated. Another problem is that the field equations of conformal gravity imply $T = 0$, so that only conformal matter can be consistently coupled to gravity. It is presently unclear whether realistic models of stars—which are characterized by $T \neq 0$ —can be constructed in this theory.

Lorentz-violating theories.

- There are three main open issues in Lorentz-violating gravity. The first is the relation between violations of Lorentz symmetry and ultraviolet renormalizability. This relation has been shown only at the power-counting level and for scalar-field toy models [200, 353] (and not yet for spin-2 gravitons). The second open issue has to do with the percolation of Lorentz violations from the gravity sector into the matter sector, where Lorentz symmetry has been tested to high accuracy [264, 265]. Observations of the synchrotron radiation from the Crab Nebula show that some mechanism is needed to suppress this percolation [282]. While several mechanisms have been proposed (see e.g. [267] for a review), detailed studies are necessary to assess their viability. The third open problem has to do with the causal structure of BHs, and namely with the existence of a universal horizon. Universal horizons have only been found in spherical and slowly rotating BH solutions [98, 99, 102], but it is unclear whether they exist in generic situations and whether they are stable at the nonlinear level [102].

- At the moment, the most important challenge faced by n -DBI gravity, from a theoretical point of view, is the prediction of a clear and distinct observable signature that sets it apart from GR and might enable constraints to be imposed on its validity. How generic is the property that GR solutions are also solutions of n -DBI gravity (with the same matter content)? This question can be recast very objectively as the existence of a foliation with a specific property. How generically can such a foliation be found? This subclass of solutions has a self-contained perturbation theory that can be made to coincide with that of GR in the PN regime. The analysis performed in [52], however, was not exhaustive, in the sense that the solution provided, which matches that of GR, was not shown to be unique. This is an important open question.

Massive gravity and Galileon theories. In order to address tests of gravity beyond the decoupling limit, one needs exact or numerical solutions of the full nonlinear theory. Here we will briefly discuss some of the progress searching for BH and cosmological solutions in massive gravity.

- Any viable theory of modified gravity should have BH solutions. If we restrict ourselves to a flat reference metric and a dynamical metric $g_{\mu\nu}$ that is static and spherically symmetric, the most general solution is given by Schwarzschild-(anti-)de Sitter (see [108] for a review of BH solutions in massive gravity and in bigravity). The cosmological constant of the asymptotic solutions is set by the graviton mass. It is not possible to find asymptotically flat solutions. Additionally, as discussed in [17], there may be physically interesting BH solutions that do not have exact spherical symmetry.
- dRGT with a Minkowski reference metric has no nontrivial spatially flat FRW solutions [354]. There are several ways to address this problem. One approach is to look for backgrounds with spatial curvature, or where the reference metric is FRW. It has turned out that these backgrounds exhibit instabilities or are infinitely strongly coupled and cannot be trusted [17].
- Alternatively, one may accept that homogenous and isotropic solutions do not exist, and try to find inhomogeneous solutions. An exact solution of this kind is known [354, 355]. While the solution is infinitely strongly coupled, this solution is a proof of principle that there may be viable inhomogeneous cosmological solutions in massive gravity. As with BH solutions, the full space of possibilities is still being actively explored.
- Another approach is to look for FRW solutions in theories that add new degrees of freedom to massive gravity. For example, in bigravity (where the reference metric is a dynamical field) one can find stable FRW solutions, as shown in [356, 357]. Another idea along these lines is to consider adding a new scalar degree of freedom to massive gravity. Common examples are to allow the mass to be a dynamical scalar field [354], or to introduce a new scalar mode called the quasidilaton through the reference metric: see e.g. [358, 359].

Gravity with auxiliary fields. There are various open questions related to modified theories of gravity with auxiliary fields, since this is a relatively new research field.

- The issue of curvature singularities appearing at the surface of compact stars [179, 184, 197] is crucial to assess the theoretical viability of these theories. These singularities can be alleviated in some situations [332], but they seem to be ubiquitous. Solving this issue requires also an understanding of the ‘average problem’ [335]: given an

ensemble of fundamental particles, is the standard stress–energy tensor for a perfect fluid a valid approximation in these theories?

- Similar comments apply to the Cauchy problem in these theories, whose well-posedness is still under scrutiny [11, 40, 199].
- The fact that EiBI corrections due to a barotropic perfect fluid are completely degenerate with the EOS [329] makes it very difficult to test these theories or to rule them out with observations. To date it is unknown whether such degeneracy extends to other forms of matter.
- As discussed, Palatini $f(\mathcal{R})$ gravity and EiBI gravity are usually investigated under various assumptions, e.g. assuming a symmetric Ricci tensor and a symmetric connection. A metric-affine [360] version of EiBI gravity is still lacking.

3. Black holes

In this section we review BH solutions in the modified theories of gravity described earlier. The next section is devoted to a similar review of compact star solutions. Table 2 is meant to provide a practical guide to the literature on BH solutions and their stability in various theories at the time of writing.

3.1. BHs in GR

One of the most remarkable predictions of GR is that regular, stationary BHs in Einstein–Maxwell theory are extremely simple objects, being defined by at most three parameters: mass, angular momentum and electric charge. This was established by a series of uniqueness theorems due to Hawking, Carter and Robinson (see [361–364] for reviews), which imply that all isolated BHs in Einstein–Maxwell theory are described by the Kerr–Newman family. Astrophysical BHs are thought to be neutral to a very good approximation because of quantum discharge effects [365], electron–positron pair production [366–368] and charge neutralization by astrophysical plasmas. Therefore the geometry of astrophysical BHs in GR is simply described by the two-parameter Kerr metric [369], which in standard Boyer–Lindquist coordinates reads

$$ds^2 = - \left(1 - \frac{2Mr}{\rho^2} \right) dt^2 - \frac{4aMr \sin^2 \theta}{\rho^2} dt d\varphi + \frac{\rho^2}{\Delta} dr^2 + \rho^2 d\theta^2 + \left(r^2 + a^2 + \frac{2Ma^2r \sin^2 \theta}{\rho^2} \right) \sin^2 \theta d\varphi^2, \quad (3.1)$$

where $\Delta \equiv r^2 + a^2 - 2Mr$ and $\rho^2 \equiv r^2 + a^2 \cos^2 \theta$. This metric describes the gravitational field of a spinning BH of mass M and angular momentum $J = aM$. The roots of Δ correspond to the event horizon ($r_+ = M + \sqrt{M^2 - a^2}$) and the Cauchy horizon ($r_- = M - \sqrt{M^2 - a^2}$). The static surface $g_{tt} = 0$ defines the boundary of the ergosphere: $r_{\text{ergo}} = M + \sqrt{M^2 - a^2 \cos^2 \theta}$. The ‘angular velocity of the event horizon’ is

$$\Omega_{\text{H}} \equiv a / (r_+^2 + a^2). \quad (3.2)$$

Because of the uniqueness theorem, and because NSs in GR cannot be more massive than $\sim 3M_{\odot}$ [370], any observation of a compact object with mass larger than $\sim 3M_{\odot}$ with metric different from the Kerr geometry would inevitably signal a departure from standard physics (either in the gravitational or in the matter sector). Therefore tests of strong-field gravity targeting BH systems aim at verifying the ‘Kerr hypothesis’ in various ways.

Teukolsky [371] recently compiled an excellent review on the discovery of the Kerr metric and the impact of this discovery in astrophysics. We refer interested readers to Teukolsky's review and standard textbooks [372–374] for surveys of our current understanding of BHs in GR; here we summarize some considerations on the stability and no-hair properties of GR BHs that should be kept in mind when we discuss BH solutions in modified theories of gravity.

The key theoretical developments after Kerr's discovery were the derivation of a separable equation—the 'Teukolsky master equation'—describing perturbations of scalar, neutrino, electromagnetic and gravitational fields [375]; the use of this master equation to assess the mode stability of the metric [376–378]; and Whiting's work, that conclusively excluded the possibility of exponentially growing modes [379]. The free oscillation modes of Kerr BHs under the boundary conditions of ingoing waves at the horizon and outgoing waves at infinity (whose frequencies form the so-called 'quasinormal mode' (QNM) spectrum [380]) were investigated extensively by Leaver [381] and several other authors. The spectrum consists of an infinite discrete set of complex-frequency modes (hence 'quasinormal'); the nonzero imaginary part is due to gravitational radiation damping. QNMs find important applications in various areas of physics, ranging from quantum gravity to the gauge-gravity duality (see [382–385] for reviews). The Teukolsky equation is not self-adjoint, and QNMs do not form a complete set. The absence of unstable modes may be a good enough stability proof for a physicist, but not for a mathematician: mode stability does not imply linear stability. A rigorous proof of linear stability was carried out by Kay and Wald for Schwarzschild BHs [386], but the extension of this analysis to Kerr is still work in progress [387–391], and there is now evidence for instability in extremal Kerr BHs [392] (see also [393–396]). For our purposes, and with the previous caveats, we will consider the absence of unstable modes as a physically satisfactory stability criterion.

In the rest of this section we will first review the properties of BHs in various extensions of GR, and then turn to a discussion of possible ways to verify the Kerr hypothesis.

3.2. Scalar–tensor theories

3.2.1. Real scalars and no-hair theorems. Theoretical studies impose remarkable constraints and limitations on BH solutions in scalar–tensor theories. No-scalar-hair theorems for the simplest scalar–tensor theories were proved by various authors [55, 397–399], and state that stationary BH solutions in Brans–Dicke theory are the same as those in GR. In other words, the scalar must be trivial and the geometry must be described by the Kerr metric.

One way to understand this property is to recall our discussion in section 2.2. By means of field redefinitions, it is always possible to reformulate the action of a scalar–tensor theory as the action (2.4) of a minimally coupled sigma-model, where matter fields have a nontrivial coupling with the scalar field. However, in vacuum (and in particular in BH spacetimes) the matter action can be discarded, and equation (2.4) reduces to the Einstein–Hilbert action with a minimally coupled scalar field.

Extensions of these uniqueness theorems to multiple scalars and to more generic scalar–tensor theories have been established more recently [56, 59]. These results assume the scalar field to be time-independent, a requirement recently shown to be unnecessary for any scalar–tensor theory with a *real* scalar [60]. The no-scalar-hair theorems have also been confirmed by numerical studies of gravitational collapse to nonrotating BHs [124–128, 130].

In summary, the Kerr family of vacuum BH solutions in GR is also the most general vacuum solution in a rather general class of scalar–tensor theories, although some exceptions exist, as we discuss in the next sections.

Furthermore, alternative theories with the same equilibrium solutions as GR have, in general, different dynamics. The theorems summarized above imply that Kerr BHs in GR are linearly stable, but they are unstable because of superradiance in massive scalar–tensor theories (including minimally coupled massive scalars) [62–67]. Superradiance extracts energy from rotating BHs, and transfers this energy to the perturbing field. For a monochromatic wave of frequency ω , the condition for superradiance is [67, 400, 401]

$$0 < \omega < m\Omega_{\text{H}}, \quad (3.3)$$

where $m > 0$ is the azimuthal harmonic index and the angular velocity of the BH horizon Ω_{H} was defined in equation (3.2). If the scalar is massive, superradiance triggers an instability [62–66, 402]: the ergoregion amplifies the field, and the mass term ‘traps it.’ The linear stages of the instability lead to the growth of a non-spherically symmetric scalar ‘cloud’ outside the horizon (because the mechanism requires nontrivial azimuthal dependence, as seen from (3.3)). For a single *real* scalar field, this leads to a nonzero quadrupole moment of the cloud resulting in periodic GW emission. Thus, the end-state is thought to be a Kerr BH with lower spin [67, 403–405]. Note, however, that the instability time scale depends on the scalar field’s mass, and may be of the order of the Hubble time, leading to what in practice amounts to hairy BH configurations.

3.2.2. Complex scalars: new hairy rotating BHs. When the scalar is time-dependent, the assumptions behind the no-hair theorems do not apply. Of course, the backreaction of a generic time-dependent scalar field will lead to a time-dependent geometry and not an equilibrium BH state. But for a *complex scalar field* (which is equivalent to two scalar fields) there is a special type of time dependence that yields a time-independent stress–energy tensor and hence is compatible with a stationary metric. This time dependence is simply a phase evolution, analogous to that of stationary states in quantum mechanics: $\Psi(t, \mathbf{x}) = e^{-i\omega t} \phi(\mathbf{x})$. As shown in [406], however, no spherically symmetric BHs exist even with this time dependence. With the wisdom of hindsight this is easy to understand. The null generator of the horizon $\chi = \partial_t$ does not preserve Ψ . As such there is scalar flux through the horizon and hence there can be no static geometry.

The latter argument can be circumvented by introducing rotation for the BH spacetime and thus making the geometry axisymmetric. Then, the null generator of the horizon gains an additional term $\chi = \partial_t + \Omega_{\text{H}}\partial_\varphi$, where Ω_{H} is the angular velocity of the horizon (given in equation (3.2)), and ∂_φ the Killing vector field which generates the axial symmetry. We must also introduce an azimuthally dependent phase for the scalar field, $\Psi(t, \varphi, \mathbf{x}) = e^{-i\omega t} e^{im\varphi} \phi(\mathbf{x})$, where $m \in \mathbb{Z}^\pm$ since φ is periodic with $\varphi \sim \varphi + 2\pi$. Observe that, again, the azimuthal dependence vanishes in the stress–energy tensor. Then, $\mathcal{L}_\chi \Psi = 0$, as long as

$$\omega = m\Omega_{\text{H}}. \quad (3.4)$$

Thus there is no scalar field flux through the horizon as long as (3.4) is obeyed, regardless of the value of $\phi(\mathbf{x})$ on the horizon. This argument suggests the existence of asymptotically flat rotating BHs with complex scalar hair. Such solutions were indeed found in [68]. The ultimate physical reason for the existence of these equilibrium states—in the sense that the geometry has an asymptotically timelike Killing vector field, just like Kerr—is that GW emission is halted due to cancellations in the stress–energy tensor, which becomes independent of the time and azimuthal variables, thus avoiding GW emission and consequent angular momentum losses.

The condition (3.4) for the existence of hairy BHs lies precisely at the threshold of the superradiant condition (3.3). This is no accident. A test-field analysis of the type that leads to condition (3.3), for a complex scalar field on the Kerr background, reveals that *real frequency* bound states are possible precisely in between amplified modes, which obey the superradiant condition (3.3), and decaying modes, which obey $\omega > m\Omega_{\text{H}}$. These are stationary scalar clouds [68, 407–410]. The hairy BHs found in [68] can be thought of as nonlinear realizations of these clouds, when the scalar field becomes ‘heavy’ and backreacts (see also [411]).

The solutions found in [68] correspond to a five-parameter family of the Einstein–(massive)–Klein–Gordon theory. Three of the parameters are continuous: the ADM mass M , the ADM angular momentum J , and a Noether charge Q . The latter is obtained by integrating the time component of the scalar field four-current on a spacelike slice and may be regarded as measuring the amount of scalar hair outside the horizon. In fact, it proves convenient to introduce a normalized Noether charge $q \equiv Q/2J$. Then, q is a compact parameter in the full space of solutions: $0 \leq q \leq 1$. The value $q = 0$ corresponds to Kerr BHs, showing that these hairy BHs are continuously connected to the standard Kerr family. This is why the solutions in [68] were dubbed ‘Kerr BHs with scalar hair.’ The value $q = 1$ corresponds to asymptotically flat, rotating boson stars [412, 413]. These are (horizonless) gravitating solitons, which are kept in equilibrium by a balance between the scalar field self-gravity and its wave-like dispersive nature. Rotating boson stars sustained by a complex, massive field have $Q = 2J$, which justifies the normalization taken. The two remaining parameters of the solutions found in [68] are discrete: the aforementioned azimuthal harmonic index $m \in \mathbb{Z}^{\pm}$ and the node number $n \in \mathbb{N}_0$. The latter counts the number of zeros of the scalar field radial profile. One may regard $n = 0$ as the fundamental configuration and $n \geq 1$ as excited states.

The line element and scalar distribution describing Kerr BHs with scalar hair reads:

$$ds^2 = e^{2F_1} \left(\frac{dR^2}{N} + R^2 d\theta^2 \right) + e^{2F_2} R^2 \sin^2 \theta (d\varphi - W dt)^2 - e^{2F_0} N dt^2, \quad N \equiv 1 - \frac{R_{\text{H}}}{R},$$

$$\Psi = \phi(r, \theta) e^{i(m\varphi - \omega t)}.$$
(3.5)

In this ansatz there are five functions of (R, θ) : F_0, F_1, F_2, N, ϕ . To obtain them one numerically solves five nonlinear, coupled PDEs, with appropriate boundary conditions that ensure both asymptotic flatness and regularity at the horizon. The latter requirement actually implies condition (3.4). The parameter R_{H} is the location of the event horizon in this coordinate system. We remark that these are *not* Boyer–Lindquist coordinates in the Kerr limit. In order to write Kerr in the form (3.5) one must change the radial coordinate r in (3.1) by the transformation $R = r - a^2/r_{\text{H}}$, where $r_{\text{H}} = M + \sqrt{M^2 - a^2}$ is the event horizon location in Boyer–Lindquist coordinates.

The parameter and phase space for the solutions with $n = 0, m = 1$ were discussed in detail in [68] and are summarized in figure 2. There is a region of overlap of hairy and Kerr BHs with the same (M, J) . In that sense there is nonuniqueness. The degeneracy seems to be raised, however, by the introduction of q : no two solutions were found with the same (M, J, q) . In the region of nonuniqueness, hairy BHs have larger entropy than the corresponding Kerr BHs. As such the former cannot decay into the latter adiabatically. Also, hairy BHs can violate the Kerr bound: $J \leq M^2$. This violation is not surprising since it is known to occur for rotating boson stars [414], and hairy BHs are continuously connected to boson stars. It is indeed a generic feature that hairy BHs are more star-like, i.e. less tightly constrained in their physical properties than Kerr BHs. This observation also has implications for possible astrophysical phenomenology of hairy BHs, an aspect of special relevance for this review. It

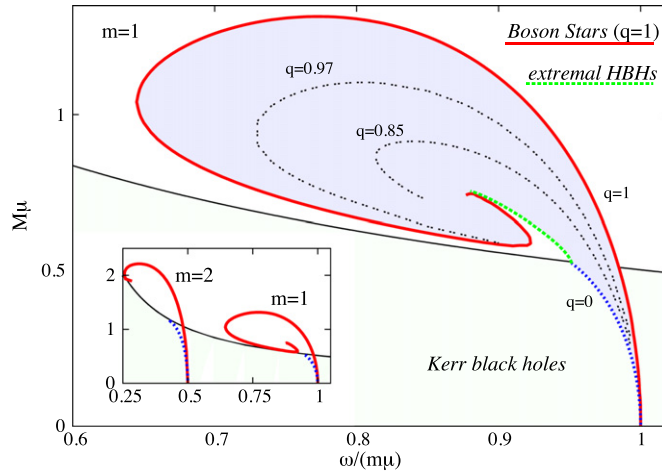


Figure 2. Domain of existence of hairy BHs for $n = 0$, $m = 1$ in M - ω space (shaded blue region). The black solid curve corresponds to extremal Kerr BHs, which obey $M = 1/(2\Omega_H)$; Kerr BHs exist below it. For $q = 0$, the domain of existence connects to Kerr solutions (dotted blue line). For $q = 1$, R_H vanishes and hairy BHs reduce to boson stars (red solid line). The final line that delimits the domain of existence of the hairy BHs (dashed green line) corresponds to extremal BHs, i.e. with zero temperature. (Inset) Boson star curves for $m = 1, 2$. The units in the axes are normalized to the scalar field mass μ . (Adapted from [68].)

was observed in [68] that both the quadrupole moment and the angular frequency at the ISCO can differ significantly for hairy BHs, as compared to the standard Kerr values. Finally, hairy BHs have a richer structure of ergo-regions than Kerr, with the occurrence of *ergo-Saturns*, besides ergo-spheres, in a region of parameter space [415].

In figure 3 we plot the five functions in (3.5) for an example of a Kerr BH (left panel, for which case $\phi = 0$) and also for a hairy Kerr BH solution (right panel), on the equatorial plane $\theta = \pi/2$ and in terms of a compactified radial coordinate $1 - R_H/R$. The behavior observed here is quite generic. All metric functions are monotonic functions of R . The scalar field profile function is nonzero on the horizon, has one maximum and tends to zero asymptotically, also a generic behavior for $n = 0$ solutions. A set of ten example solutions (including the two just mentioned) are available online as a supplement to this review [416]. The files provide all five metric functions (F_0, F_1, F_2, N, ϕ) on a fine grid (see also [69] for a detailed computation of these solutions).

The stability of these solutions and the formation mechanism of hairy BHs that deviate significantly from Kerr remain urgent open issues. A recent analysis suggests that, should these solutions arise from a superradiant instability of the Kerr metric, the energy-density of the scalar field would be negligible and the geometry would be well described by the Kerr solution [405].

3.2.3. Evading no-hair theorems in Horndeski/Gauss-Bonnet gravity. Hawking's no-hair theorem for stationary BHs in Brans-Dicke theory [55] was recently extended by Sotiriou and Faraoni to more general scalar-tensor theories [59]. Hui and Nicolis [113] further extended these proofs to the most general scalar-tensor theory leading to second-order field equations, i.e. Horndeski's theory (introduced in section 2.2.3). Hui and Nicolis claimed that static,

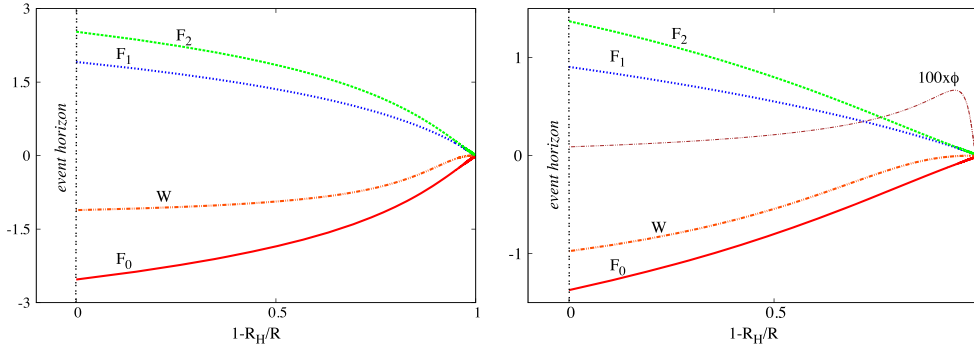


Figure 3. Left panel: the metric functions in (3.5) for a Kerr BH in the region of nonuniqueness. We have chosen its mass and angular momentum to be $M = 0.415$, $J = 0.172$; this corresponds to $r_{\text{H}} = 0.066$. Right panel: the metric and scalar field functions for a hairy BH in the region of nonuniqueness with the same M, J as the Kerr BH. This hairy BH is Kerr-like and has $\omega = 0.975$ and $r_{\text{H}} = 0.2$. The value of the scalar field profile function has been multiplied by a factor of 100.

spherically symmetric, asymptotically flat BHs in vacuum have no hair in Horndeski’s theory, provided that the scalar exhibits shift symmetry—i.e., symmetry under $\phi \rightarrow \phi + \text{constant}$. The conclusion follows from the fact that the scalar field equation can be written as a conservation equation for the Noether current J^μ associated with the shift symmetry, namely

$$\nabla_\mu J^\mu = 0. \quad (3.6)$$

In a nutshell, the argument is the following. If the scalar field respects the symmetries of the metric,

$$ds^2 = -f(r)dt^2 + f(r)^{-1}dr^2 + R(r)^2(d\theta^2 + \sin^2\theta d\phi^2), \quad (3.7)$$

then the only nonvanishing component of J^μ is the radial one, which gives the value of the invariant $J^\mu J_\mu = (J^r)^2/f$. Because $f = 0$ at the horizon, J^r must also vanish there. Then the conservation equation (3.6) implies that J^r must be zero everywhere. Finally, the last step of the proof is to argue that $J^r = 0$ everywhere implies that the scalar field must be constant, and therefore the metric must satisfy Einstein’s equations in vacuum.

This last step was criticized in [92], where it was shown that there exists a counterexample where the scalar field has a nontrivial profile even though $J^r = 0$. This happens precisely when the scalar field is *linearly coupled to the Gauss–Bonnet invariant* R_{GB} (see section 2.4), i.e. for a theory with action

$$S = \frac{1}{16\pi} \int \sqrt{-g} d^4x \left[R - 2\nabla_a \phi \nabla^a \phi + \alpha \phi R_{\text{GB}}^2 \right]. \quad (3.8)$$

This special case of Horndeski’s theory is also a special case of the quadratic gravity theories discussed in section 2.4.1. BHs in this theory are indeed endowed with a nontrivial scalar profile (see section 3.4). The scalar charge is not an independent quantity, but it depends on the BH mass, so these BHs are said to have ‘hair of the second kind,’ but they are nevertheless different from their Schwarzschild counterparts. These solutions were discussed in [93]. They are the only vacuum, spherically symmetric hairy BHs in Horndeski’s theory with shift symmetry for which the scalar field respects the symmetries of the metric.

If the scalar field is time-dependent, it is possible for BHs to develop hair both in scalar–tensor theories [57] and in Horndeski theories [94]. Furthermore, as discussed below, BHs in scalar–tensor theories can grow hair in the presence of matter.

3.2.4. BHs surrounded by matter. Isolated BHs in scalar–tensor theories are the same as in GR, but the situation changes completely in the presence of matter. Reference [417, 418] have investigated the effects of simple models of accretion disks and halos around BHs in generic scalar–tensor theories. In these theories the Klein–Gordon equation on a Kerr BH surrounded by matter takes the form

$$\left[\square - \mu_{\text{eff}}^2 \right] \Psi = 0, \quad (3.9)$$

where the effective mass μ_{eff} depends on the specific scalar–tensor theory, and it is proportional to the trace of the stress–energy tensor.

Depending on the sign of the scalar coupling, μ_{eff}^2 can either be positive or negative. In the latter case the system is prone to a *tachyonic* instability and spontaneously develops a scalar hair supported by matter. This phenomenon is akin to the spontaneous scalarization phenomenon in NSs (see section 4.2 below). On the other hand, when $\mu_{\text{eff}}^2 > 0$ the scalar field acquires a real effective mass and can trigger a ‘spontaneous superradiant instability’ similar to the one discussed previously. The instability is much stronger than in the vacuum case, because the presence of matter drastically affects the amplification of scalar waves. In fact, superradiant amplification from spinning BHs is strongly enhanced when Breit–Wigner resonances occur [417, 418]. Possible astrophysical implications of this amplification have not been investigated yet, but they may yield phenomenological constraints on the parameter space of scalar–tensor theories.

The effect of a matter distribution around BHs in scalar–tensor theory was studied in [419] in the context of theories with a screening mechanism. In scalar–tensor theory, screening occurs when the conformal factor $A(\varphi)$ and/or the potential $V(\varphi)$ suppress the effect of modified gravity in dense environments (such as those of the Solar System or of our Galaxy), allowing for modifications on a cosmological scale which are not in conflict with the bounds from Solar System and binary pulsar tests [420] (see section 6.2.2). Using a simple spherically symmetric model of an accretion disk or a galactic halo, and neglecting the effect of matter and of the scalar field on the spacetime metric, [419] shows that matter induces a nontrivial, spherically symmetric scalar field profile. Their estimates suggest that the effect of the ‘scalar fifth force’ on test particles should be much smaller than effects due to the quadrupole emission of GWs, and therefore that it is unlikely to reveal the presence of a fifth force in this context.

3.2.5. Stability. The stability of BHs in scalar–tensor theories is a nontrivial issue. No-hair theorems do not apply to BH dynamics, which is different from GR even in the simplest scalar–tensor theories.

To our knowledge, there are very few works on BH stability in scalar–tensor theories. Kobayashi, Motohashi and Suyama studied the linear perturbations of static, spherically symmetric BHs in Horndeski gravity [95, 96] finding a set of necessary conditions for BH stability. Quite interestingly, these conditions impose restrictions on the general Horndeski action. The stability of static, spherically symmetric BHs with respect to linear odd-parity perturbations was demonstrated in the case of GR minimally coupled with a scalar field (with an arbitrary potential) [61]; their result also applies to Bergmann–Wagoner theory (see section 2.2). On the other hand, it has long been known that rotating BHs in GR

minimally coupled with a *massive* scalar field are unstable. We will return to this point in section 3.10.2.

3.3. $f(R)$ theories

Scalar–tensor theories include $f(R)$ theories as a special case. The vacuum Kerr spacetime is a solution in $f(R)$ gravity by virtue of the theorems that apply to generic scalar–tensor theories [59]. Typically $f(R)$ theories propagate massive degrees of freedom [71]. As a consequence, rotating BHs may be prone to superradiant instabilities: this possibility was discussed as early as 1985 by Hersh and Ove [70]. Interestingly, in this case the effective scalar field is related to the scalar curvature of the metric, which grows exponentially through superradiance. This suggests that, at variance with the case of real massive fields previously discussed, the end-state of superradiant instabilities in $f(R)$ gravity might be different from a Kerr BH [70].

3.4. Quadratic gravity

New BH solutions can be found in theories with quadratic curvature terms in the action. We first discuss the perturbative approach in generic quadratic theories before focusing on results specific to the EdGB and dCS theories.

3.4.1. Perturbative solutions in the slow-rotation limit. Consider the action (2.21), that includes EdGB and dCS as special cases. BH solutions in this theory are not known in full generality (with the exception of EdGB gravity, see section 3.4.2 below), but perturbative solutions were obtained analytically when the coupling functions f_i admit the expansion (2.23) and the BH is slowly rotating (numerical solutions for rapid rotation will be discussed below). The solution describing a static, spherically symmetric BH is a limiting case (vanishing rotation) of this family. Consider the following metric ansatz for the stationary, slow-rotation limit:

$$ds^2 = -f(r, \theta)dt^2 + g(r, \theta)^{-1}dr^2 - 2\omega(r)\sin^2\theta dtd\varphi + r^2\Theta(r, \theta)d\theta^2 + r^2\sin^2\theta\Phi(r, \theta)d\varphi^2, \quad (3.10)$$

and let the scalar field have the dependence $\phi = \phi(r, \theta)$. By solving the field equations one finds the following metric functions that describe a slowly rotating BH solution [80]:

$$\begin{aligned} f(r, \theta) &= f^{(0)} + \frac{\alpha_3^2}{4} \left[-\frac{49}{40M_0^3 r} + \frac{1}{3M_0 r^3} + \frac{26}{3r^4} + \frac{22M_0}{5r^5} + \frac{32M_0^2}{5r^6} - \frac{80M_0^3}{3r^7} \right], \\ g(r, \theta) &= g^{(0)} + \frac{\alpha_3^2}{4} \left[-\frac{49}{40M_0^3 r} + \frac{r + M_0}{M_0^2 r^3} + \frac{52}{3r^4} + \frac{2M_0}{r^5} + \frac{16M_0^2}{5r^6} - \frac{368M_0^3}{3r^7} \right], \\ \omega(r) &= \frac{2aM_0}{r} - \frac{a\alpha_3^2}{4} \left[\frac{3}{5M_0 r^3} + \frac{28}{3r^4} + \frac{6M_0}{r^5} + \frac{48M_0^2}{5r^6} - \frac{80M_0^3}{3r^7} \right] \\ &\quad - a\alpha_4^2 \frac{5}{2} \left[\frac{1}{r^4} + \frac{12M_0}{7r^5} + \frac{27M_0^2}{10r^6} \right], \\ \Theta(r, \theta) &= 1 + \frac{\cos^2\theta}{r^2} a^2, \quad \Phi(r, \theta) = 1 + \frac{r + 2M_0 \sin^2\theta}{r^3} a^2. \end{aligned}$$

The scalar field solution is given by

$$\begin{aligned} \phi(r, \theta) = & \alpha_3 \left[\frac{1}{2M_0 r} + \frac{1}{2r^2} + \frac{2M_0}{3r^3} \right] + a\alpha_4 \frac{5 \cos \theta}{8M_0} \left[\frac{1}{r^2} + \frac{2M_0}{r^3} + \frac{18M_0^2}{5r^4} \right] \\ & - \frac{\alpha_3 a^2}{2} \left[\frac{1}{10r^4} + \frac{1}{5M_0 r^3} + \frac{M_0 + r}{4M_0^3 r^2} + \cos^2 \theta \left(\frac{48M_0^2 + 21M_0 r + 7r^2}{5M_0 r^5} \right) \right]. \end{aligned}$$

Here $f^{(0)} \equiv 1 - 2M_0/r + 2a^2 M_0 \cos^2 \theta / r^3$ and $g^{(0)} \equiv 1 - 2M_0/r + a^2(r - (r - 2M_0)\cos^2 \theta) / r^3$ are the expansions of the Kerr metric coefficients of equation (3.1) up to terms of order $\mathcal{O}(a^2)$. Note that, as discussed in section 2.4, α_3 is the EdGB coupling constant, and α_4 is the dCS coupling constant.

The curvature invariants are regular in the exterior spacetime. The angular momentum is $J = aM_0$, whereas the physical (ADM) mass of the BH is [72, 74]

$$M = M_0 \left[1 + \frac{49\alpha_3^2}{320M_0^4} \right]. \quad (3.11)$$

The above solution is accurate up to order $\mathcal{O}(a^2/M^2, \alpha_i^2/M^4, a\alpha_i^2/M^5)$ in the metric, and up to order $\mathcal{O}(a^2/M^2, \alpha_i^2/M^4, a\alpha_i^2/M^5, a^2\alpha_i/M^3)$ in the scalar field.

Using the second-order in spin corrections obtained in [76, 85], the corrections to the Kerr quadrupole moment Q_{Kerr} arising in quadratic gravity read

$$Q = Q_{\text{Kerr}} \left(1 + \frac{4463}{2625} \frac{\alpha_3^2}{M^4} - \frac{201}{448} \frac{\alpha_4^2}{M^4} \right), \quad (3.12)$$

where the quadrupole moment is defined through a large-distance expansion of the metric as

$$g_{tt} \rightarrow -1 + \frac{2M}{r} + \frac{\sqrt{3}}{2} \frac{Q}{r^3} Y_{20}(\theta), \quad (3.13)$$

and Y_{20} is a spherical harmonic with $l = 2$ and $m = 0$.

Constraints on BH solutions are mostly derived by understanding how matter moves in the vicinity of the BH. Geodesic motion can be derived from the matter action for a point particle:

$$S_{\text{mat}} = -m \int dt \sqrt{-\gamma(\phi) g_{\mu\nu} \dot{x}^\mu \dot{x}^\nu}, \quad (3.14)$$

where m is the mass of the particle, and $\gamma(\phi)$ is the coupling function between the matter and the scalar field. For the low-energy limit of heterotic string theory, $\gamma = e^\phi$. In the small-coupling limit we have

$$\gamma(\phi) = 1 + 2b\phi + \mathcal{O}(\phi^2), \quad (3.15)$$

where $b = 0$ for minimal coupling and $b = 1/2$ in heterotic string theory. We focus on equatorial motion ($\theta = \pi/2, \dot{\theta} \equiv 0$). Expanding geodesic quantities to the same order as the metric itself, we find the following expressions for the ISCO location and the frequency at the ISCO (both normalized by the physical mass M):

$$\begin{aligned}
\frac{R_{\text{ISCO}}}{M} &= 6 - 4\sqrt{\frac{2}{3}} \frac{a}{M_0} - \frac{7a^2}{18M_0^2} + \frac{8b\alpha_3}{9M_0^2} - \frac{17}{54}\sqrt{\frac{2}{3}} \frac{ba\alpha_3}{M_0^3} \\
&\quad - \left(\frac{16\,297}{38\,880} - \frac{22\,267a}{17\,496\sqrt{6}M_0} \right) \frac{\alpha_3^2}{M_0^4} + \frac{77a}{216\sqrt{6}M_0^5} \alpha_3^2, \\
M\Omega_{\text{ISCO}} &= \frac{1}{6\sqrt{6}} + \frac{11a}{216M_0} + \frac{59a^2}{648\sqrt{6}M_0^2} - \frac{12\,113a}{5225\,472M_0^5} \alpha_3^2 \\
&\quad - \frac{29}{432\sqrt{6}} \frac{b\alpha_3}{M_0^2} - \frac{169}{7776} \frac{ba\alpha_3}{M_0^3} + \left(\frac{32\,159}{2099\,520\sqrt{6}} - \frac{49\,981a}{75\,582\,720M_0} \right) \frac{\alpha_3^2}{M_0^4}. \tag{3.16}
\end{aligned}$$

We have kept only dominant terms in b , and for simplicity we focused on corotating orbits (the result for counterrotating orbits is trivially obtained by inverting the sign of a). Note that a/M_0 is not the physical dimensionless angular momentum, J/M^2 , but it can be easily related to the latter to second order in α_3/M^2 using equation (3.11) [421].

The behavior of the ISCO frequency depends on several coupling parameters. For $b = 0$, the dominant correction is of order $\mathcal{O}(\alpha_3^2)$ and tends to increase the ISCO frequency. The first corrections proportional to the BH spin are $\mathcal{O}(a\alpha_3^2)$ and $\mathcal{O}(a\alpha_4^2)$, and they contribute to lower the frequency. However, when a nonminimal coupling is turned on, its effect is dominant [75]. When $b \neq 0$, the ISCO frequency gets corrections of order⁴⁷ $\mathcal{O}(b\alpha_3)$.

For null geodesics, the light-ring frequency $\Omega_{\text{LR}} = L_{\text{LR}}/E_{\text{LR}}$ (related to the real part of the ringdown frequency of the BH in the eikonal limit [422]) and the light-ring radius R_{LR} do not depend on the coupling γ :

$$\frac{R_{\text{LR}}}{M} = 3 - \frac{2a}{\sqrt{3}M_0} - \frac{2a^2}{9M_0^2} + \frac{31}{81\sqrt{3}} \frac{a\alpha_4^2}{M_0^5} - \left(\frac{961}{3240} - \frac{33\,667a}{174\,960\sqrt{3}M_0} \right) \frac{\alpha_3^2}{M_0^4}, \tag{3.17}$$

$$\begin{aligned}
M\Omega_{\text{LR}} &= \frac{1}{3\sqrt{3}} + \frac{2a}{27M_0} + \frac{11a^2}{162\sqrt{3}M_0^2} - \frac{131}{20\,412} \frac{a\alpha_4^2}{M_0^5} \\
&\quad + \left(\frac{4397}{262\,440\sqrt{3}} + \frac{24\,779a}{4723\,920M_0} \right) \frac{\alpha_3^2}{M_0^4} \tag{3.18}
\end{aligned}$$

The dominant correction is $\mathcal{O}(\alpha_3^2)$ and increases the frequency, whereas the $\mathcal{O}(a\alpha_3^2)$ and $\mathcal{O}(a\alpha_4^2)$ corrections have opposite relative signs.

3.4.2. EdGB theory

Static and slowly rotating solutions. Perturbative BH solutions in EdGB gravity can be obtained as special cases of the results discussed above. Besides these perturbative results, an exact static solution in EdGB gravity (i.e., a solution going beyond the perturbative level in α_3) is also known [73]. It has the form

$$ds^2 = -f(r)dt^2 + g(r)^{-1}dr^2 + r^2d\theta^2 + r^2 \sin^2\theta d\varphi^2, \tag{3.19}$$

where the metric functions $f(r)$, $g(r)$ and the scalar field $\phi(r)$ can be found by solving a system of ordinary differential equations. The solution (regular at the horizon and at infinity) only exists when [73, 75]

⁴⁷ Note that a nonminimal coupling to the matter sector violates the weak equivalence principle. Since the latter is tested within the astonishing precision of 1 part in 10^{13} [2], a very stringent bound on b can be derived: $b\alpha_i/M^2 < 10^{-13}$.

$$0 < \alpha_3/M^2 \lesssim 0.691. \quad (3.20)$$

Reference [75] extended these results to the slow-rotation case, analyzing geodesics and QNMs in the eikonal limit. Reference [81] studied the epicyclic frequencies of this solution, with the aim of constraining EdGB gravity through observations of BH quasi-periodic oscillations. Reference [76] analyzed corrections of second order in the spin working in the small-coupling limit. The character of the solution changes quite dramatically: the solution at first order in spin is algebraically special (i.e. of Petrov type D, just like the Kerr metric), while the second-order solution is of Petrov type I. The Petrov type of the metric is very important, because it is related to the separability of the field equations. This example illustrates the importance of obtaining *exact* BH solutions (rather than perturbative expansions) when analyzing their features in modified theories of gravity.

Rapidly rotating solutions. Rapidly rotating BHs in EdGB theory have been obtained numerically [77] using the Lewis–Papapetrou ansatz for a stationary, axially symmetric spacetime. The line element can be parametrized as

$$ds^2 = -e^{2\nu_0} dt^2 + e^{2(\nu_1 - \nu_0)} \left[e^{2\nu_2} (dr^2 + r^2 d\theta^2) + r^2 \sin^2 \theta (d\varphi - \omega dt)^2 \right], \quad (3.21)$$

where ν_0 , ν_1 , ν_2 and ω are functions of r and θ only. BH solutions are asymptotically flat and possess the expansion

$$\nu_0 = -\frac{M}{r} + \frac{D_1 M}{3r^3} - \frac{M_2}{r^3} P_2(\cos \theta) + \mathcal{O}(r^{-4}), \quad (3.22)$$

$$\nu_1 = \frac{D_1}{r^2} + \mathcal{O}(r^{-3}), \quad (3.23)$$

$$\nu_2 = -\frac{4M^2 + 16D_1 + q^2}{8r^2} \sin^2 \theta + \mathcal{O}(r^{-3}), \quad (3.24)$$

$$\omega = \frac{2J}{r^3} + \mathcal{O}(r^{-4}), \quad (3.25)$$

$$\phi = \frac{q}{r} + \mathcal{O}(r^{-2}), \quad (3.26)$$

where $P_2(\cos \theta)$ is a Legendre polynomial, and ϕ denotes the dilaton field. The expansion constants M , J , and q denote the (ADM) mass, the angular momentum and the dilaton charge, respectively. The expansion (3.22)–(3.26) also depends on the constants D_1 , M_2 .

The quadrupole moment Q of EdGB BHs reads [82]

$$Q = -M_2 + \frac{4}{3} \left[\frac{1}{4} + \frac{D_1}{M^2} + \frac{q^2}{16M^2} \right] M^3. \quad (3.27)$$

This has been obtained by extending the formalism of Geroch and Hansen [423, 424]⁴⁸.

The domain of existence of EdGB BHs is illustrated by the shaded area in the left panel of figure 4. The figure shows the scaled horizon area $a_H = A_H/M^2$ (where A_H is the BH area) as a function of the scaled angular momentum $j = J/M^2$. The upper-left edge corresponds to Schwarzschild BHs, which are all mapped to the point $a_H = 1, j = 0$. Likewise, Kerr BHs lie

⁴⁸ The scalar field of the static BH in EdGB gravity decays as $1/r$ at large distances, similarly to the electric field of a Reissner–Nordström BH. The Geroch–Hansen formalism to compute multipole moments was extended to stationary electrovacuum spacetimes in [425, 426]. Using the fact that the Gauss–Bonnet curvature term R_{GB} decays very quickly at large distances, the structure of the first multipoles can be shown to be equivalent to that of a Reissner–Nordström BH with a suitable identification of the scalar charge.

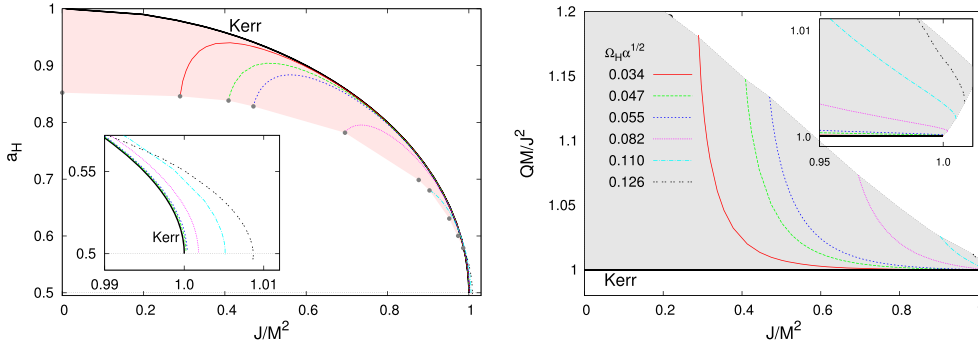


Figure 4. The domain of existence of EDBG BHs (shaded area). We plot the scaled horizon area $a_H = A_H/M^2$ (left panel) and the scaled quadrupole moment $\hat{Q} = QM/J^2$ (right panel) as functions of the scaled angular momentum $j = J/M^2$. Different curves correspond to families of EDBG BHs with fixed scaled horizon angular velocity $\Omega_H \alpha_3^{1/2}$. (From [77, 82].)

on a curve in this plot, i.e. the upper boundary of the domain of existence (except for $j \approx 1$: see inset). The lower boundary of the domain of existence corresponds to critical BH solutions. These arise when the argument of a square root in the expansion of the dilaton function at the horizon vanishes [73, 77, 427]. For a given value of the coupling constant α_3 and of the mass, EdGB BHs possess lower horizon area than Kerr BHs. A remarkable feature is that EdGB BHs can slightly exceed the Kerr bound ($j \leq 1$) for the dimensionless angular momentum. Only the metric functions for EdGB solutions with $j \geq 1$ are well defined, while the dilaton field diverges at the poles at the horizon.

The right panel of figure 4 shows the rescaled quadrupole moment $\hat{Q} = QM/J^2$ [82]. \hat{Q} is largest for slow rotation, and decreases with increasing j . The deviations of \hat{Q} from the corresponding Kerr values can be up to 20% and more. Superspinning EdGB BHs with $j > 1$ always have $\hat{Q} > 1$.

Figure 5 exhibits the scaled moment of inertia $\hat{I} = J/(\Omega_H M^3)$ versus the scaled quadrupole moment \hat{Q} for fixed values of j [82]. The Kerr values $\hat{I}_{\text{Kerr}} = 2(1 + \sqrt{1 - j^2})$ and $\hat{Q}_{\text{Kerr}} = 1$ are indicated by dots on the vertical axis of the plot, and represent the minimum possible values for \hat{Q} . Families of EdGB solutions terminate at the critical solutions represented by the dotted curve. For comparison, straight, dotted lines show the perturbative results of [76], derived for small α_3 and small j . The inset shows the region $j > 1$, not present in GR. The extraction of higher multipole moments from the numerical solutions is still an open problem.

The study of geodesic motion around rapidly rotating EdGB BHs unveiled some interesting features [75, 77]. Timelike geodesics for circular motion are obtained from the Lagrangian $2\mathcal{L} = e^{2b\phi} g_{\mu\nu} \dot{x}^\mu \dot{x}^\nu = -1$, where again the constant b fixes the coupling between the matter and the dilaton field ($b = 1/2$ corresponds to the low-energy limit of heterotic string theory).

Figure 6 shows the scaled circumferential ISCO radius R_{ISCO}/M versus the scaled angular momentum $j = J/M^2$ for a coupling constant $b = 1/2$. The Kerr solutions and the extremal EdGB solutions possess the smallest values for the scaled ISCO radius R_{ISCO}/M , whereas the maximal values of R_{ISCO}/M are found for the critical EdGB solutions. Note that the ISCO radius is not given in Boyer–Lindquist coordinates. When the rescaled angular momentum is large, the deviation of R_{ISCO}/M from the Kerr value can be as large as 10% for

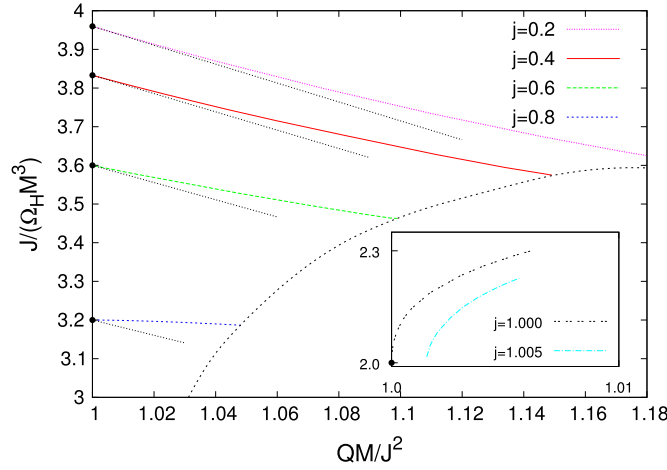


Figure 5. The scaled moment of inertia $\hat{I} = J/(\Omega_H M^3)$ is shown versus the scaled quadrupole moment \hat{Q} for fixed values of j . The Kerr BHs are indicated by the fat dots on the \hat{I} -axis. The straight dotted lines represent the perturbative results of [76]. The critical BHs are represented by the dotted curve. (From [82].)

$b = 1/2$. Similarly, for large angular momentum the orbital frequencies at the ISCO exhibit deviations from the Kerr frequencies as large as 60% (see (3.16) for a small-spin expansion). Note, however, that the weak equivalence principle imposes $b = 0$, so that the corrections to the geodesic quantities are expected to be smaller.

Future space-based observations of the gravitational signal emitted by EMRIs [428] and observations of the electromagnetic signal associated to quasi-periodic oscillations in low mass x-ray binaries [91, 429, 430] can be used to map the spacetime around a BH. The key information is encoded in the orbital frequency Ω_{ISCO} and, more generally, in the epicyclic frequencies $(\Omega_r, \Omega_\theta, \Omega_\phi)$. These quantities have been computed in [91] in the case of dCS gravity, and in [81] for the case of EdGB gravity.

Stability. In the special cases investigated so far, BHs in EdGB gravity were found to be linearly stable. Reference [431] studied radial perturbations of static BHs, and [75] considered axial gravitational perturbations. The stability against polar gravitational perturbations is an open problem.

3.4.3. dCS theory. The field equations of dCS gravity in spherical symmetry reduce to GR [88, 259], so static BH solutions are given by the Schwarzschild metric.

Spinning BHs in dCS gravity are more interesting, because they are endowed with a nontrivial scalar field sourced by a nonvanishing Pontryagin density ($*RR \neq 0$). Spinning solutions at first order in a slow-rotation expansion were computed in [83, 84]. These solutions can be obtained from the general slowly rotating BH solution for quadratic gravity discussed in section 3.4.1 by setting $\alpha_3 = 0$, and they have been extended to second order in the BH spin [85].

In the slow-rotation limit, the scalar field is dominated by a dipole moment which is proportional to the spin of the BH. The correction to the metric quadrupole moment was computed in [85]. The geometry is of Petrov type D at first order in rotation, and of Petrov type I at higher order. For arbitrary rotation, the scalar field profile and trace of the metric

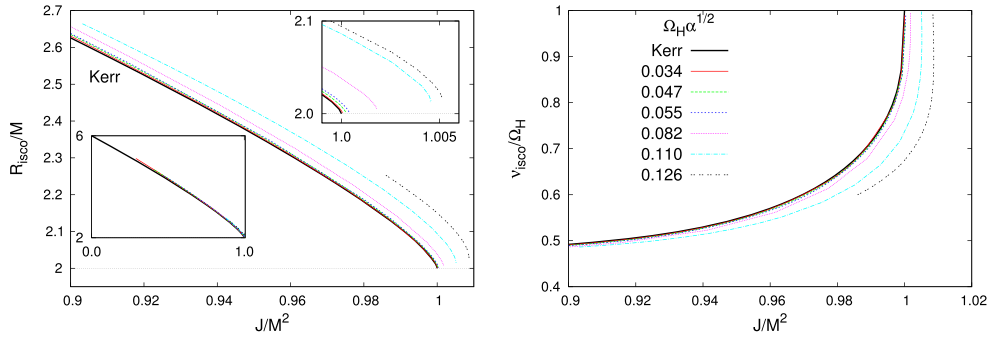


Figure 6. (Left) The scaled circumferential ISCO radius R_{ISCO}/M and (right) the scaled ISCO frequency $\nu_{\text{ISCO}}/\Omega_{\text{H}}$ are shown versus the scaled angular momentum $j = J/M^2$ for dilaton matter coupling constant $b = 1/2$ for families of EDBG BHs with fixed scaled horizon angular velocity $\Omega_{\text{H}}\alpha_3^{1/2}$. (From [82].)

deformation were computed in [86]. As rotation increases, the higher multipole moments of the scalar field are sourced more strongly, as seen in figure 7.

Stability. The linear stability of Schwarzschild BHs in dCS gravity was studied in [87, 88], where it was found that these solutions are mode-stable against all gravitational and scalar perturbations. The stability of slowly rotating solutions has not been studied yet, but see [79, 89] for a high-frequency analysis.

3.5. Lorentz-violating theories

The notion of a BH in Lorentz-violating gravity is at first glance less clear-cut than in GR. As mentioned in section 2.5, in the infrared limit the most generic Lorentz-violating gravity theories are Einstein-Æther and khronometric theory, which allow for spin-2 gravitons (like in GR), but also for spin-0 and (in Einstein-Æther theory but not in khronometric gravity) also spin-1 gravitons. These propagating gravitational modes have speeds that are functions of the coupling parameters c_i of the theories, and are generally different from the speed of light appearing in the Maxwell equations and regulating the propagation of the electromagnetic field. As a result, BHs in these theories, provided they exist, will present multiple horizons, namely: a ‘matter horizon’ for the electromagnetic field and the other matter fields, which do not couple directly to the Lorentz violating æther or khronon field (so as to enforce the weak equivalence principle, see section 2.5); a spin-2 horizon for the spin-2 gravitons; a spin-0 horizon for the spin-0 gravitons; and (for Einstein-Æther theory only) a spin-1 horizon for the spin-1 gravitons. These horizons will generally lie at different locations, depending on the propagation velocity of the corresponding field. However, because of the requirement that there be no gravitational Cherenkov radiation in these theories (see discussion in section 2.5), for viable values of the coupling constants the propagation speeds of the spin-2, spin-0 and (when present) spin-1 modes will be larger than (or equal to) the speed of light, and therefore the spin-2, spin-1 and (when present) spin-0 horizons will be enclosed by the matter horizon.

The situation gets even more complicated if one interprets Einstein-Æther and khronometric theory as low-energy limits of a more generic Lorentz-violating gravity theory containing higher-order spatial derivative terms in the action. This is the case for instance in Hořava gravity, whose action (2.41) reduces to that of khronometric gravity in the infrared limit, but which contains fourth- and sixth-order spatial derivative terms that are crucial for

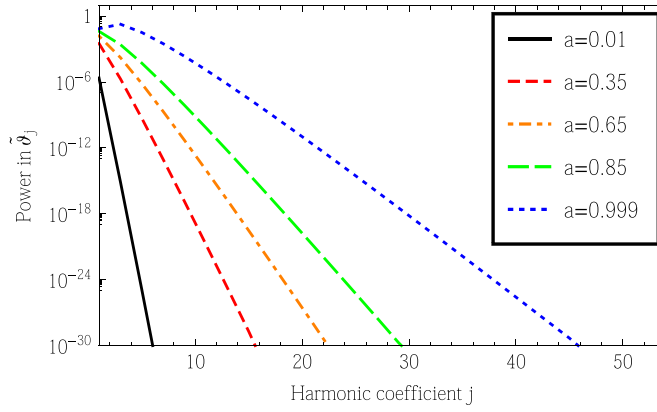


Figure 7. ‘Power’ in different multipole moments of the scalar field $\tilde{\theta}$ (rescaled with α_4/M^2) around a rotating BH in dCS. The horizontal axis is the multipole moment number j , i.e. the coefficient of $P_j(\cos\theta)$ (only the odd coefficients are plotted). The vertical axis is the L^2 norm of $\tilde{\theta}_j$ on a log scale. As spin increases, the exponential convergence slows down, and there is more power in higher multipole moments. (From [86].)

the power-counting renormalizability of the theory. The presence of those terms, as mentioned in section 2.5, causes gravitons to obey nonlinear dispersion relations (see equation (2.43)). The matter degrees of freedom (and photons in particular) will also satisfy similar nonlinear dispersion relations, although the coefficients of the nonlinear terms may be smaller than for gravitons, and in particular sufficiently small to satisfy particle physics tests of Lorentz invariance [201, 264–267], if the theory efficiently suppresses percolation of the Lorentz violations from gravity to the matter sector (see discussion in section 2.5). From a conceptual point of view, however, equation (2.43) makes the very concept of an event horizon meaningless in the ultraviolet limit, because it implies diverging propagation speeds $d\omega/dk$ in the limit $k \rightarrow \infty$. Therefore, the question arises of whether the multiple event horizons discussed above are simply low-energy artifacts.

To answer this question, [98] (building on [97]) looked first at BH solutions in the infrared limit of Lorentz-violating gravity, i.e. in Einstein-Æther and khronometric theory. As mentioned in section 2.5, the two theories have exactly the same solutions for static, spherically symmetric, asymptotically flat BHs. More specifically, using ingoing Eddington–Finkelstein coordinates, the most generic static and spherically symmetric ansatz for the metric and the æther is given by

$$ds^2 = -f(r)dv^2 + 2B(r)dvdr + r^2d\Omega^2, \quad (3.28)$$

$$\mathbf{u} = A(r)\partial_v - \frac{1 - f(r)A^2(r)}{2B(r)A(r)}\partial_r. \quad (3.29)$$

Solving the field equations perturbatively near spatial infinity, and imposing asymptotic flatness, one obtains the series-expanded solution [97, 98]

$$f(r) = 1 - \frac{r_g}{r} - \frac{c_1 + c_4}{48} \frac{r_g^3}{r^3} + \dots, \quad (3.30)$$

$$B(r) = 1 + \frac{c_1 + c_4 r_g^2}{16 r^2} + \frac{c_1 + c_4 r_g^3}{12 r^3} + \dots, \quad (3.31)$$

$$A(r) = 1 + \frac{1}{2} \frac{r_g}{r} + \frac{A_2 r_g^2}{r^2} - \left(\frac{1}{16} - \frac{c_1 + c_4}{96} - A_2 \right) \frac{r_g^3}{r^3} + \dots, \quad (3.32)$$

where $r_g = 2G_N M/c^2$ (the locally measured gravitational constant G_N being related to the ‘bare’ one appearing in the action by equation (2.31)), M is the mass of the BH as measured by an observer far from the system, and A_2 is a dimensionless ‘æther charge.’ The latter can in principle take arbitrary values, but if one attempts to construct the BH solution corresponding to a given A_2 value by integrating the field equations inwards starting from the asymptotic solution (3.30)–(3.32), one obtains a solution that presents a finite-area singularity on the spin-0 horizon [97, 98]. Only for a specific value $A_2 = A_2^{\text{reg}}$ (a function of the theory’s coupling constants) is the BH regular everywhere except for the central $r = 0$ singularity. We stress that fully nonlinear numerical simulations [170] have shown that spherically symmetric gravitational collapse does indeed select the regular $A_2 = A_2^{\text{reg}}$ BH solution. In practice, this regular BH solution is found by solving the field equations perturbatively near the spin-0 horizon, imposing that the solution be regular there, and then selecting the solution that matches the asymptotically flat perturbative solution (3.30)–(3.32) by a shooting procedure (see [98, 99] for more details). After the shooting procedure has selected the asymptotically flat solution, the behavior in the interior can be obtained by integrating inwards from the spin-0 horizon.

The resulting solutions will therefore describe the BHs of infrared Lorentz-violating gravity and present multiple horizons, as discussed above. However, in spite of the causal structure differing from GR, the BH geometry outside the outermost horizon (i.e. the matter one) is very similar to GR as far as astrophysical tests are concerned. As two representative examples, figures 8 and 9 show the fractional deviation from GR of the dimensionless combinations $\omega_{\text{ISCO}} r_g$ and b_{ph}/r_g , where ω_{ISCO} is the orbital frequency of the innermost stable circular orbit (ISCO) and b_{ph} is the impact parameter of the circular photon orbit. The former is measurable, at least in principle, with GW observations of the inspiral of binary BH systems or with observations of iron-K α emission lines from accretion disks, while the latter regulates the size of the BH ‘shadow’ observable with future electromagnetic telescopes, as well as the BH ringdown frequencies, in principle measurable with GW detectors. For values of the couplings allowed by binary pulsar observations (see the purple region in figure 38), deviations from GR are below the percent level, and thus outside the reach of electromagnetic observations (see e.g. [432]), although probably within the reach of space-based detectors such as eLISA [433].

The behavior of these BH solutions is however very different from GR inside the matter horizon. Figure 10 shows a spacetime diagram that captures schematically the causal structure of the BH solutions studied in [98]. Hypersurfaces of constant preferred time T are represented by green lines that get darker and darker as the value of T increases (i.e. a darker green means that the curve is farther in the future). Also shown (in red) are two very special hypersurfaces of constant T , namely ones that are also hypersurfaces of constant radius. Those hypersurfaces lie within the matter, spin-2, spin-0 and (when present) spin-1 horizons, and act as *universal* horizons for signals of *arbitrary* speed [98, 99, 102]. This can be understood because a signal emitted at the universal horizon must propagate into the future, as defined by the preferred time T . As a result, as can be seen from figure 10, such a signal must propagate inwards (i.e. towards smaller radii). Note that the solutions of [98] present multiple universal

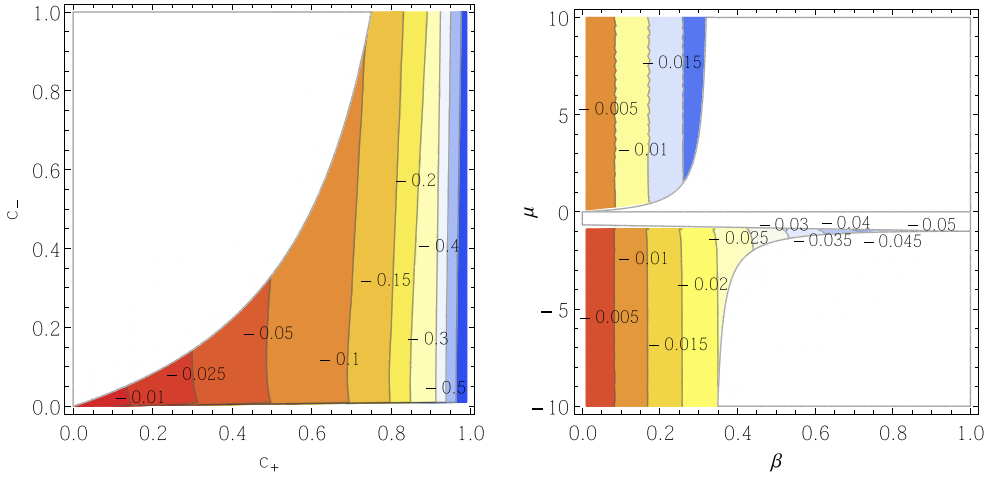


Figure 8. Fractional deviation of the dimensionless combination $\omega_{\text{ISCO}}r_g$ from its GR value, in Einstein-Æther (left) and khronometric theory (right). Negative values denote smaller values in Lorentz-violating gravity than in GR. The quantities c_{\pm} , μ , β are defined in section 2.5. (From [98, 99].)

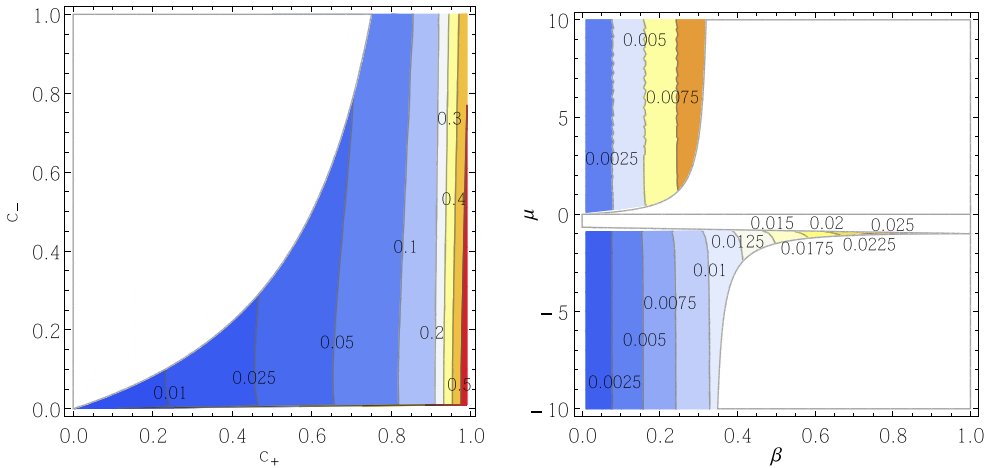


Figure 9. Fractional deviation of the dimensionless combination b_{ph}/r_g from its GR value, in Einstein-Æther (left) and khronometric theory (right). Postive values denote larger values in Lorentz-violating gravity than in GR. The quantities c_{\pm} , μ , β are defined in section 2.5. (From [98, 99].)

horizons, but we are truncating figure 10 to show just the outermost two. Also, it is clear that the concept of a universal horizon only makes sense in the presence of the *ultraviolet* higher-order spatial derivative terms in the action, which produce the nonlinear dispersion relation (2.43), thus allowing for the infinite-speed signals for which the universal horizon is relevant. As mentioned earlier, the BH solutions of [98] were instead derived by solving the field equations for the *infrared* limit of Lorentz-violating gravity theories. Nevertheless, the universal horizon of those solutions lies very close to the matter horizon and far from the central singularity, and thus in a region of small curvature for the BH masses that are relevant in

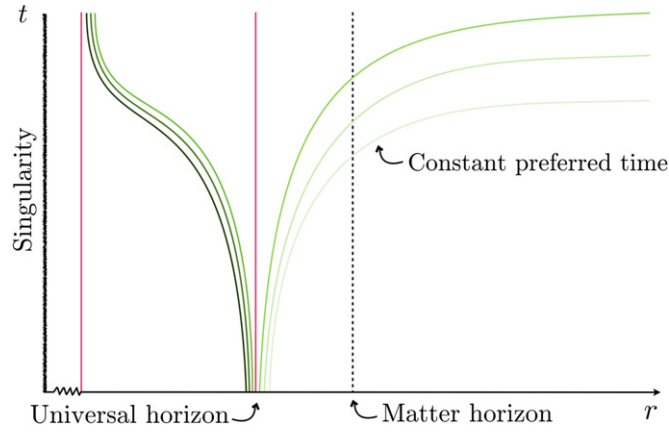


Figure 10. Sketch of the causal structure of a BH possessing a universal horizon, marked with a red vertical line. The green curves are hypersurfaces of constant preferred time T (the darker the color, the larger T). The universal horizon itself is a hypersurface of constant T . As can be seen, a signal emitted at the universal horizon has to travel inwards, simply because it has to propagate in the future direction as defined by the preferred time T . Note that multiple universal horizons are generally present, but here we are truncating the region between the first two and the central singularity. (From [99].)

astrophysics. Indeed, simple dimensional arguments show that for astrophysical BHs the effect of the higher-order derivative terms is tiny at the location of the universal horizon, leading to corrections $\lesssim 10^{-16} (M_{\odot}/M)^2$ (M being the BH mass) away from the results obtained with the infrared limit of the theory. Universal horizons have been shown to be compatible with the first [434]—and possibly the second [435]—law of BH thermodynamics.

Finally, we stress that while the presence of such a universal horizon is a remarkable feature of the theory, clues of its instability to nonlinear perturbations have been reported in the decoupling limit (i.e. neglecting the backreaction of the æther/khronon on the metric) and for the low-energy limit of Hořava gravity (i.e. khronometric theory) [102]. A fully nonlinear analysis accounting for the æther’s/khronon’s backreaction has not been performed yet, and it is needed to draw definitive conclusions about stability. Similarly, the effect of the higher-order spatial derivative terms on the stability of the universal horizon is unknown.

3.6. Massive gravity

BH solutions in massive-gravity theories are still largely unexplored. In massive bigravity theories there are asymptotically flat solutions for which the reference metric $f_{\mu\nu}$ equals the spacetime metric ($f_{\mu\nu} = g_{\mu\nu}$). One such family of solutions includes the Kerr metric.

The superradiant instability responsible for hairy BH solutions in theories of minimally coupled massive gravity (see section 2.6) also destabilizes Kerr BHs in massive gravity [110]. Because of this instability, astrophysical BH spin measurements imply that the graviton mass μ in any theory of massive gravity must be smaller than 5×10^{-23} eV [110] (see section 3.10.2 for a discussion of similar constraints on the masses of ultralight scalar and vector fields).

Graviton masses μ smaller than a threshold value $\mu M \leq 0.438$ (in $G = c = \hbar = 1$ units, with M the BH mass) trigger yet another instability against monopole fluctuations, that plagues even nonrotating BHs [109–111]. Quite remarkably, the mass coupling μM is well

within the instability region for values of M and μ that are phenomenologically relevant. In a cosmological context it is natural to consider the graviton mass to be of the order of the Hubble constant, i.e. $\mu \sim H \sim 10^{-33}$ eV [16]. Such a tiny graviton mass would destabilize any Schwarzschild BH with mass smaller than $10^{22}M_{\odot}$!

Instabilities often signal the existence of a new family of equilibrium solutions. Because there are no complex fields in massive gravity, the superradiant instability presumably drives rotating BHs to slower rotation rates. However, the monopole instability affecting nonrotating BHs hints at the existence of a truly new family of BH solutions [105, 111]. These ‘hairy’ solutions have metrics of the form

$$g_{\mu\nu} dx^{\mu} dx^{\nu} = -F(r)^2 dt^2 + B(r)^{-2} dr^2 + r^2 d\Omega^2,$$

$$f_{\mu\nu} dx^{\mu} dx^{\nu} = -p(r)^2 dt^2 + [U'(r)]^2 / Y(r)^2 dr^2 + [U(r)]^2 d\Omega^2,$$

where $' \equiv d/dr$. Such asymptotically flat, hairy BH solutions were indeed found numerically in [105]; their properties depend on the particular theory under consideration, i.e. on the values of the parameters α_3 and α_4 as defined in equation (2.45). Notebooks to generate these hairy solutions are available online [436].

Additional BH solutions may exist when the fiducial metric is not proportional to the spacetime metric. The only asymptotically flat solutions found so far belong to the Kerr family [107, 108] and monopole fluctuations are *stable* for these configurations [112]. Stability against nonradial modes and superradiant amplification has not been studied at the time of writing.

3.7. Gravity with auxiliary fields

As discussed in section 2.7, gravitational theories that modify GR by adding solely non-dynamical fields are *equivalent* to Einstein’s theory in vacuum. In these theories, vacuum BH solutions and their dynamics are the same as in GR. In particular, any stationary, regular and asymptotically flat geometry is described by the Kerr family. However, corrections to GR appear in the coupling with matter. An interesting aspect of these theories is that singularities may not form during gravitational collapse [182] and in early cosmology [198]. Nonvacuum solutions—such as charged BHs—are generally different from GR [198]. Furthermore, similarly to the regularization of the Coulomb field generated by a point charge in Born–Infeld electromagnetism, the curvature singularity hosted in the BH interior in EiBI gravity may be replaced by a regular, wormhole-like geometry due to nonperturbative effects [327].

3.8. Parametrized phenomenological deviations from the Kerr metric

BH solutions and their properties are obviously dependent on the theory they are derived from. Although many theories—some of which were described previously—share the Schwarzschild and Kerr geometry as stationary solutions, even in these cases their dynamical properties (stability, GW emission, etc), depend on the field content of the theory. Unfortunately, in the context of alternatives to Einstein’s theory, the possibilities are endless. Each theory has its own family (or families) of BH solutions, and in the absence of observational data in the strong-field regime, choosing one’s favorite theory is largely a matter of taste.

Thus, some efforts focus on *parametrizing* generic spacetimes, rather than exploring specific theories. These efforts are in many ways parallel to the PPN expansion, designed to parametrize asymptotically flat spacetimes in the weak-field regime [437–439]. The PPN approach facilitates tests of the weak-field regime of GR and is particularly well suited to perform tests in the Solar System, which translate into constraints on alternative theories of

gravity. For example, one can show that any metric theory of gravity yielding an asymptotically flat spacetime admits the expansion [2]:

$$-g_{tt} \rightarrow 1 - \frac{2M}{r} + 2(\beta - \gamma)\frac{M^2}{r^2} + \mathcal{O}(1/r^3), \quad (3.33)$$

$$g_{ij} \rightarrow \delta_{ij} \left[1 + 2\gamma\frac{M}{r} + \mathcal{O}(1/r^2) \right], \quad (3.34)$$

where M is the ADM mass, and the indices (i, j) run over asymptotically Cartesian coordinates. The PPN parameters are very well constrained by observations, $|\gamma - 1| \lesssim 10^{-5}$ and $|\beta - 1| \lesssim 2.3 \times 10^{-4}$ [2]. The success of the PPN approach is rooted in the existence of an extensively studied, unique reference metric, the Minkowski geometry. Because the metric is post-Minkowskian, the meaning of the coordinates is clear, and so are the physical predictions one can draw from the metric.

A comparable ‘reference metric’ is lacking in the strong-field regime. For this reason, developing a parametrized approach to quantify deviations from GR is a nontrivial problem. Existing attempts deal with the construction of a generic parametrization of spinning geometries which can be matched continuously onto the Kerr metric in the strong- *and* in the weak-field regime. This is a formidable task with no unique solution. Several approaches have been proposed, each of them with their own limitations, but all very similar in spirit (see e.g. [25, 440, 441]). The original ‘bumpy BH’ formalism assumes Einstein’s equations, and perturbs the Kerr metric to find BHs *in GR* distorted by small amounts of unspecified matter [442, 443]. The metric computed within this approach is supposed to be valid only in vacuum. This formalism cannot be extended in a straightforward manner to test alternative theories of gravity (but see [444] for some improvements over the analysis of [445]). A similar approach was used to build ‘quasi-Kerr’ spacetimes, by expanding generic slowly rotating spacetimes up to the lowest nontrivial quadrupole moment [446]. These solutions are not regular at the horizon. Stationary, axisymmetric and asymptotically flat solutions of the vacuum Einstein equations which do *not* describe BHs, most notably the so-called Manko–Novikov spacetimes [447], have also been used by several authors to model spacetimes in alternative theories and to parametrize deviations from the Kerr geometry [432, 448].

To overcome some of the limitations of the parametrizations above—while introducing others—it was recently proposed to build on the ‘Newman–Janis algorithm’⁴⁹ to generate spinning BH solutions in arbitrary theories of gravity [450]. Using suitable choices of parameters, these solutions consist of small deformations of the Kerr geometry. At variance with previous studies, this approach does not assume the validity of Einstein’s equations, nor the existence of an approximate Carter constant [445]. Even though the procedure makes use of the—unjustified, because the field equations are unknown—Newman–Janis transformation (see e.g. [451] for some criticism), the final transformed metric could as well be the ad-hoc starting point for the investigation of deviations from GR [441]. Such parametrized metrics can *in principle* be suitable for tests involving observations of the images of inner accretion flows, x-ray observations of relativistically broadened iron lines or of the continuum spectra of accretion disks, for which a regular behavior very close to the event horizon is crucial [452].

The generalized deformed Kerr metric in this approach is [440]

$$g_{tt} = -F(1 + h^t), \quad (3.35)$$

⁴⁹ The Newman–Janis algorithm allows one to generate the Kerr family of BH starting from the Schwarzschild family [449]. This approach works in GR, but is bound to fail in general for modified theories of gravity.

$$g_{rr} = \frac{(r^2 + a^2 \cos^2 \theta)(1 + h^r)}{\Delta + a^2 \sin^2 \theta h^r}, \quad (3.36)$$

$$g_{\theta\theta} = r^2 + a^2 \cos^2 \theta, \quad (3.37)$$

$$g_{\phi\phi} = \sin^2 \theta \left\{ r^2 + a^2 \cos^2 \theta + a^2 \sin^2 \theta [2H - F(1 + h^t)] \right\}, \quad (3.38)$$

$$g_{t\phi} = -a \sin^2 \theta [H - F(1 + h^t)], \quad (3.39)$$

where $F \equiv 1 - 2M_0 r / \Sigma$, we have introduced $H \equiv \sqrt{(1 + h^r)(1 + h^t)}$,

$$h^i(r, \theta) \equiv \sum_{k=0}^{\infty} \left(\epsilon_{2k}^i + \epsilon_{2k+1}^i \frac{M_0 r}{\Sigma} \right) \left(\frac{M_0^2}{\Sigma} \right)^k \quad (3.40)$$

are the small deformation quantities parametrizing deviations from the Kerr geometry in terms of dimensionless numbers ϵ_k^i , and $\Sigma = r^2 + a^2 \cos^2 \theta$, $\Delta = r^2 + a^2 - 2M_0 r$.

Imposing asymptotic flatness requires only $\epsilon_0^t = \epsilon_0^r = 0$, but does not imply any constraint on ϵ_1^t and ϵ_1^r . Expanding the metric elements (3.35) and (3.36) at infinity and comparing with the PPN expansions (3.33) and (3.34), we can identify

$$M = M_0 (1 - \epsilon_1^t / 2), \quad (3.41)$$

$$\epsilon_1^t = -2 - \gamma (\epsilon_1^t - 2), \quad (3.42)$$

$$2\epsilon_2^t = (\beta - \gamma) (\epsilon_1^t - 2)^2 + 4\epsilon_1^t. \quad (3.43)$$

Therefore, even imposing the GR values $\beta = \gamma = 1$ supported by observations, the parameters $\epsilon_1^t, \epsilon_2^r$ and all the ϵ_k^i 's with $k > 2$ ($i = t, r$) are left unconstrained. Figure 11 shows the shifts of the ISCO frequency for the generalized metric (3.35)–(3.39) in the small- ϵ_k^i limit. For low rotation rates the corrections associated to ϵ_k^t are larger than those associated to ϵ_k^r , while the converse is true for rapid rotation, i.e. when $a/M \gtrsim 0.85$. An exception to this behavior are the ϵ_1^i parameters, for which the t -correction is larger than the r -correction for any spin. The dominant corrections are the ones associated with ϵ_1^t , although in the fast-spinning case the corrections $\delta\Omega_k^r$ for different values of k are all comparable to each other, and they are also comparable to $\delta\Omega_1^t$. However, at least for moderately large spin, the corrections $\delta\Omega_1^t$ and $\delta\Omega_2^r$ are dominant. Note that both ϵ_1^t and ϵ_2^r are currently unconstrained by observations, so that their contribution would likely dominate the near-horizon geometry of the deformed Kerr metric (3.35)–(3.39). A more detailed analysis of this parametrization has recently appeared in [452, 453].

The approach summarized above relies on a Taylor expansion of the unknown functions $h^t(r), h^r(r)$ in powers of M/r . Continued-fraction resummations based on a compactified radial coordinate have been recently proposed and explored for nonrotating BHs [454].

3.9. BH mimickers

Despite growing experimental evidence (see e.g. [455]), at the moment an incontrovertible proof that dark compact objects are indeed BHs (i.e. that they possess an event horizon or, at least, an apparent horizon) is lacking. In fact, concerns have been raised on whether such a proof is possible at all with electromagnetic observations [24].

Our current understanding of stellar evolution strongly suggests that even extreme forms of matter cannot support the enormous self-gravity of massive and ultracompact objects, so

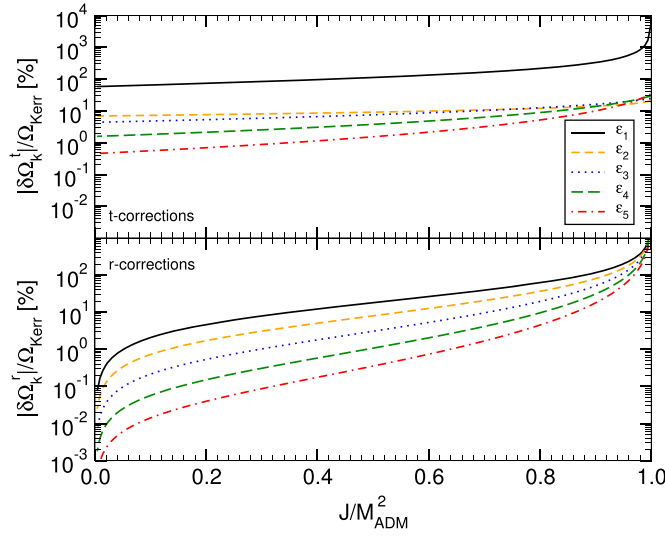


Figure 11. Relative corrections $\delta\Omega_k/\Omega_0$ to the ISCO frequency as a function of J/M^2 for the metric (3.35)–(3.39) to linear order in $\epsilon_k \ll 1$ up to $k = 9$. The ISCO frequency reads $\Omega = \Omega_0 + \sum_k \delta\Omega_k \epsilon_k$, where Ω_0 is the ISCO frequency of a Kerr geometry. The small-coupling approximation requires $(\delta\Omega_k/\Omega_0)\epsilon_k \ll 1$ for consistency. Each ϵ_k – line is built by setting to zero all other ϵ_i , $i \neq k$. The two panels refer to the corrections associated to ϵ_k^t (upper panel) and ϵ_k^r (lower panel), respectively. For ease of comparison, the range of the vertical axis is the same for both panels. In this case the total ISCO frequency reads $\Omega = \Omega_0 + \sum_k \delta\Omega_k^t \epsilon_k^t + \sum_k \delta\Omega_k^r \epsilon_k^r$. The small-coupling approximation requires $(\delta\Omega_k^i/\Omega_0)\epsilon_k^i \ll 1$ for consistency. (From [440].)

that the latter are naturally expected to be BHs. The above picture has been challenged by the construction of exotic objects—so-called ‘BH mimickers’—relying on different support mechanisms. These objects are all (almost) as compact as BHs, but do not possess horizons. Among others, they include *boson stars*, consisting of self-gravitating massive scalar fields [456, 457]; gravitational condensate stars or *gravastars* [458], supported by an exotic EOS of the form $P(\rho) \approx -\rho$; and *superspinars* [459], objects with angular momentum exceeding the Kerr bound and with some form of matter replacing the singular BH interior.

The key observational distinction between genuine BHs and ‘mimickers’ is the presence of a surface. Experimental tests of this property are challenging in the electromagnetic spectrum, but they should become simpler in the context of future GW observations: the oscillation modes of BHs have a very precise and well-known structure, which can be tested against observations [384, 460, 461], while the presence of a surface will leave an imprint on the GWs generated during the merger of two objects [457, 462, 463] (but see the discussion about QNMs and ringdown modes in section 7.4.2 and [464]).

Some BH mimickers can be ruled out by purely theoretical arguments, that generally rely on instabilities related to the absence of the event horizon. Mimickers can be ruled out when these instabilities grow on time scales much shorter than the age of the Universe.

The theoretical foundation for the presence of these instabilities is the work of Friedman, that showed how any spacetime with an ergoregion but without a horizon is linearly unstable [465]. The instability is due to long-lived modes that exist for ultracompact objects whose radius is $R \lesssim 3M$, and that might turn unstable because of the effects of rotation [466, 467].

Ultracompact objects such as gravastars and boson stars become linearly unstable when they possess an ergoregion [466, 468], with an instability time scale that depends strongly on the compactness and spin [469]. The same instability affects also superspinars [470, 471].

In addition to the ergoregion instability, a new mechanism could exclude *any* ultracompact ‘star’ on the grounds that such an object would be nonlinearly unstable [472]. In this case the instability is due to the existence of long-lived modes in the linearized spectrum. These modes are trapped between the center of the object and the light ring, and they are localized near a second, *stable* null geodesic [467]. The long-lived modes may become unstable under fragmentation via a Dyson–Chandrasekhar–Fermi mechanism at the nonlinear level. Alternatively, nonlinear interactions over their long life time may lead to the formation of small BHs close to the stable light ring [467].

If confirmed, the nonlinear instability results could soon give further support to the BH hypothesis: the mere observation of a light ring—a much simpler task than the observation of the event horizon, and something that is within the reach of upcoming facilities [473–475]—would be conclusive evidence for the existence of BHs.

3.10. BHs as strong-gravity laboratories for exotic fields

Besides being the optimal testbed for tests of GR in the strong-curvature regime, BHs can also be used to study exotic fields, as those appearing in extensions of the standard model of particle physics and as dark-matter candidates. This possibility stems from a surprising connection between strong-field gravity and particle physics. Although not immediately related with tests of GR, we conclude this section by discussing two examples in which the interplay between BHs and exotic fields is particularly dramatic. We consider the dynamics of scalar fields in the framework of Einstein’s GR but—as it will be clear below—the qualitative aspects of this analysis are mostly independent of the underlying theory of gravity.

3.10.1. Collapse of self-interacting scalar fields. One of the most important phenomena in GR where the nonlinearity of the theory plays a crucial role is that of gravitational collapse (for a review, see [476] and references therein). A particularly intriguing result in this context has recently been discovered numerically by Bizoń and Rostworowski [477], namely the collapse to a BH of arbitrarily small spherically symmetric, massless scalar field configurations in asymptotically anti-de Sitter (AdS) spacetimes. The AdS boundary plays a key role for the dynamics because, in contrast to asymptotically flat spacetimes, the scalar field pulses reach spatial infinity in finite time and get reflected back onto the coordinate origin. This effective *confinement* of the spacetime combined with the nonlinear interaction of the wave modes results in a resonant transfer of energy to higher frequencies, i.e. shorter wavelengths [477–479] (see also [480]). On the other hand, there exist asymptotically AdS scalar-field solutions which do not collapse into a BH, such as time-periodic solutions or boson stars [481–483]. Gravitational collapse in these spacetimes could also be prevented by the formation of nonlinear bound states of *massive* fields. Such bound states have been studied extensively in asymptotically flat spacetimes [403, 404, 484–490].

To study the possibility of asymptotically flat spacetimes being unstable in the context of confinement mechanisms [491, 492], consider the action

$$S = \int d^4x \sqrt{-g} \left(\frac{R}{16\pi} - \frac{1}{2} \partial^\mu \varphi \partial_\mu \varphi - \frac{1}{2} \mu^2 \varphi^2 \right). \quad (3.44)$$

This choice corresponds to the special case $V(\varphi)/16\pi = \frac{1}{2}\mu^2\varphi^2$ and to a one-dimensional (hence flat) target space in equation (2.4), i.e., to a minimally coupled massive scalar field of

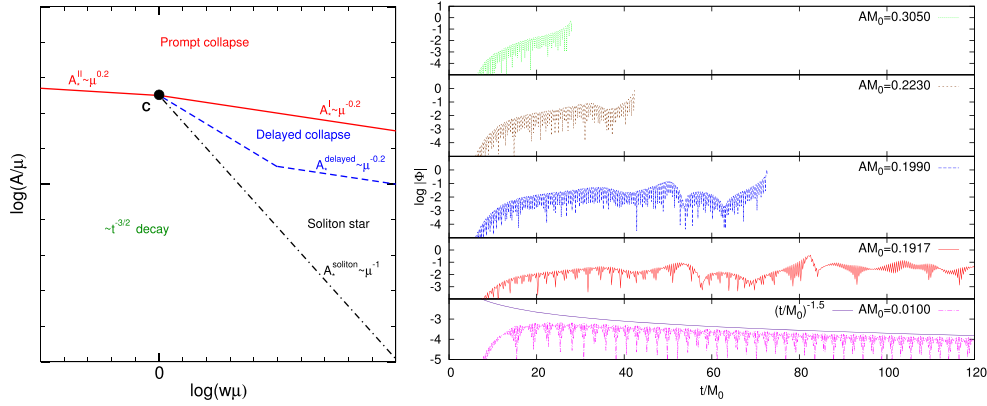


Figure 12. Left panel: qualitative phase diagram for the spherically symmetric collapse of a massive scalar field in the amplitude (A) versus width (w) plane. Right panel: the scalar field amplitude at the coordinate origin as a function of time is shown for selected values of the amplitude A . M_0 denotes the ADM mass of the spacetime. (Adapted from [493].)

mass μ . Applying the Arnowitt–Deser–Misner (ADM) decomposition to the field equations resulting from (3.44) for the special case of spherical symmetry, one obtains two constraint equations and a set of evolution equations which are given explicitly in equations (3), (4) of [493]. Initial data are constructed by analytically solving the constraint equations for a Gaussian scalar pulse in a Minkowski background.

The results of the numerical time evolutions are summarized in figure 12. The left panel of the figure shows the phase diagram for the collapse of a massive scalar field in the $w\mu$ – A/μ plane, where $w\mu$ and A/μ represent the initial pulse width to Compton wavelength ratio and the pulse amplitude, respectively. For small values of the width, the phase diagram reveals a behavior similar to the massless case: collapse above a threshold initial amplitude, and dispersion below that threshold. For large $w\mu$, however, the phase diagram exhibits a much richer phenomenology. This is also demonstrated in the right panel of the figure, where the scalar field amplitude at the coordinate origin is shown as a function of time for several configurations with varying initial amplitude. For large initial amplitude the scalar field collapses promptly to a BH, irrespective of whether a mass term $U(\phi) = \frac{1}{2}\mu^2\phi^2$ is included in the action or not. For smaller amplitudes, however, this mass term leads to a delayed collapse, similar to that observed in the AdS case. The mass term introduces an effective confinement of the scalar field, which gets reflected off the potential barrier instead of escaping to infinity, and thus collapses after some number of reflections: see the top three plots in the right panel. Additionally, there exist meta-stable, long-lived oscillations (second lowest plot in the right panel) which occur for smaller values of the initial amplitudes. Finally, for very small A , the scalar field decays (bottom plot).

In summary, the numerical evolutions demonstrate that for a massive scalar field coupled to gravity there exist nonlinear bound states, i.e. meta-stable oscillations [484, 486, 493, 494]. This implies that the mass term of the scalar field can lead to a confinement-induced gravitational collapse similar to the AdS case, but that in the asymptotically flat case, energy can escape to some extent from the potential, which results (for some values of the initial parameters) in a bound state, rather than BH formation through gravitational collapse. Indeed, a rather generic class of arbitrarily small initial data evolving in a totally confined geometry

seems to be generically unstable to BH formation [495]. If confirmed, this result might have interesting implications for the nonlinear stability of compact stars, whose fluid perturbations are effectively confined within the stellar surface.

3.10.2. Superradiant instabilities: BHs as observatories for beyond-standard-model physics.

One of the main reasons why BHs represent interesting laboratories for the exploration of the properties of light bosonic fields is the superradiant instability of spinning BHs [65, 400, 402] (for a recent exhaustive overview on the subject, see [496]). As previously discussed, superradiance occurs in the interaction between BHs and fundamental fields with frequencies $\omega \leq m\Omega_H$, where Ω_H is the angular velocity of the BH horizon, and m denotes the azimuthal mode number. The interaction provides a *classical* mechanism to reduce the mass and spin of the rotating hole as the field taps into the rotational energy and gets amplified. A gedanken experiment first proposed by Press and Teukolsky [402] suggests that a superradiant system can be rendered unstable by a run-away amplification of the field if it is immersed inside a reflective cavity: this is a superradiant instability, or ‘BH bomb.’

Such a configuration naturally arises for the case of massive fields, as in the action (3.44): as discussed above, the mass term μ leads to a potential barrier, and thus acts as a ‘mirror’ [62–64]. In that case, modes with $\omega \lesssim \mu$ are trapped inside the potential well, and the rotating BH can become (superradiantly) unstable against these modes. The growth rate of the BH-bomb instability is regulated by the coupling between the field’s mass μ and the BH mass M , and it is strongest when these parameters satisfy the condition $M\mu \sim \mathcal{O}(1)$. In other words, the interaction is maximized when the Compton wavelength of the field is comparable to the size of the BH. More specifically, perturbative calculations predict that the strongest growth rates of scalar fields surrounding a BH with dimensionless spin parameter $a/M \sim 0.99$ are realized for the dipole mode with a coupling $M\mu \sim 0.42$. The e -folding times in this case are $\tau \sim 50M/M_\odot$ [487, 488]. That time scale can decrease by several orders of magnitude if we consider massive vector fields [403, 489, 497] or gravitons [110].

While the BH bomb mechanism is negligible for known composite or fundamental scalar particles interacting with astrophysical BHs (the mass coupling is $M\mu \geq 10^{18}$, yielding time scales longer than the age of the Universe), it can play a significant role if the field’s mass is $10^{-22} \text{ eV} \leq \mu \leq 10^{-8} \text{ eV}$, as might be the case for dark-matter candidates, ultra-light axions [498, 499] or fundamental fields in modified gravity theories [11, 15, 31]. Given that the superradiant amplification provides a mechanism to reduce the energy and spin of a BH, one can argue that BHs with certain parameters (M , a/M) should not exist if they interact with fields of mass μ . Conversely, the observation of BHs [500–502] within these exclusion regions allows us to constrain the allowed field masses. This effect has indeed been used to constrain the mass of Proca fields by comparing the superradiant instability time scale with the Salpeter time scale, which gives (roughly) the time it takes to spin up and feed a BH through accretion. The bound obtained from this study constrains the mass of a hypothetical light vector field, $\mu_\gamma \leq 10^{-20} \text{ eV}$ [489]. Strictly speaking, superradiant instabilities only exclude mass intervals (superradiance is ineffective at large boson masses [496]), but the quoted upper limit on the vector field mass takes into account previous constraints obtained by other means. In principle this bound also applies to a hypothetical massive photon, but in this case it may be necessary to model the interaction of the photons with the surrounding accretion disk and plasma.

More solid bounds are in place for massive gravitons [110], which are only weakly coupled to matter. The superradiant instability under massive spin-2 perturbations is the strongest instability of the Kerr metric known to date and, together with observations of

Table 4. Current bounds on the mass of ultralight bosonic degrees of freedom arising from BH superradiant instabilities within a linearized approximation (see [496] for details).

Field	Bounds		Reference
Scalar	$\mu \lesssim 5 \times 10^{-20}$ eV	U	$\mu \gtrsim 10^{-11}$ eV [504, 505]
Vector	$\mu_\gamma \lesssim 5 \times 10^{-21}$ eV	U	$\mu_\gamma \gtrsim 10^{-11}$ eV [489]
Tensor	$\mu_g \lesssim 5 \times 10^{-23}$ eV	U	$\mu_g \gtrsim 10^{-11}$ eV [110]

rapidly spinning supermassive BHs, imposes the constraint $\mu_g \lesssim 5 \times 10^{-23}$ eV on the mass μ_g of the graviton [503].

Table 4 summarizes the current bounds on the mass of ultralight bosonic degrees of freedom arising from BH superradiant instabilities (see [496] for details).

These results follow from perturbative calculations, and leave various questions unanswered. (i) What is the fate of the system if we include back reaction? Does the instability persist or is the system driven towards a stable regime? (ii) Is it possible to form in this manner a ‘gravitational atom’ or ‘pulsar,’ as has been suggested in [498, 504]? (iii) What would be the observational signatures, including modifications of GW signals and the radiation emitted by the field itself?

Reference [405] has recently addressed these questions by performing a quasi-adiabatic, fully relativistic evolution of the superradiant instability of a Kerr BH including GW emission and gas accretion. It turns out that GW emission does not have a significant effect on the evolution of the BH, although it contributes to dissipate the dipolar bosonic cloud that forms as a result of the instability. The mass of the cloud can be a sizeable fraction of the total BH mass, but its energy density is very low, because the cloud typically extends over very large distances. This implies that backreaction effects are always negligible: even in the presence of effective bosonic ‘hair’ (both for real and for complex fields), the geometry remains close to Kerr. Thus, the prospects of imagining deviations from Kerr due to superradiantly produced bosonic clouds in the electromagnetic band are low, but such systems are a primary source for observations aiming at testing the Kerr hypothesis through GW detection. Finally, the role of gas accretion is very important. On the one hand, accretion competes against superradiant extraction of mass and angular momentum. On the other hand, accretion might produce the optimal conditions for superradiance, for example by increasing the BH spin before the instability becomes effective or by increasing the superradiant coupling $M\mu$.

In order to verify the theoretical bounds on the existence of light bosons [110, 489, 504, 506], a relevant problem concerns the *final* BH state at the time of observation in realistic situations. In other words, given the observation of an old BH and the measurement of its mass and spin, would these measurements be compatible with the evolution driven by superradiance, accretion and GW emission? This problem is addressed in figure 13, which shows the final BH mass and spin in the Regge plane [504] (i.e. a BH mass–spin diagram) for $N = 10^3$ Monte Carlo evolutions for a scalar field mass $\mu = 10^{-18}$ eV. We consider three different accretion rates f_{Edd} (defined as the fraction of mass accretion rate relative to the Eddington limit) and, in each panel, we superimpose the bounds derived from the linearized analysis, i.e. the threshold line when the instability time scale equals the accretion time scale. As a comparison, in the same plot we include the experimental points for the measured mass and spin of some supermassive BHs listed in [507]. These results confirm that a very solid prediction of the existence of ultralight bosons is the appearance of ‘holes’ in

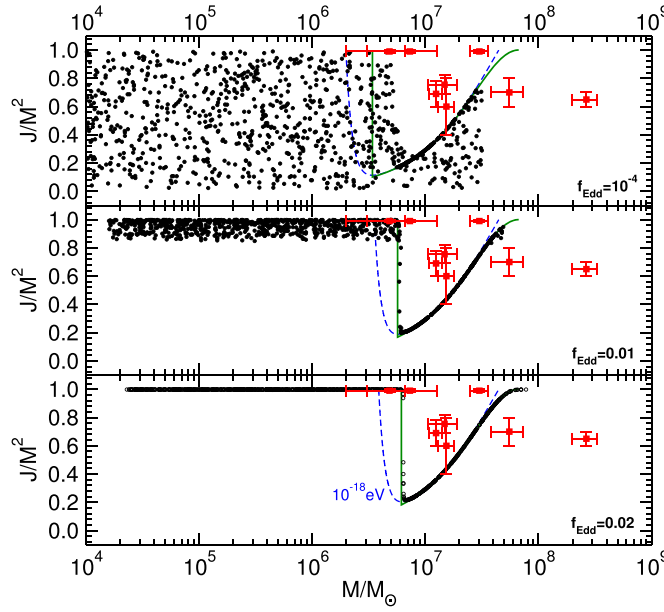


Figure 13. The final BH mass and spin in the Regge plane [504] for initial data consisting of $N = 10^3$ BHs with initial mass and spin randomly distributed between $\log_{10} M_0 \in [4, 7.5]$ and $J_0/M_0^2 \in [0.001, 0.99]$. The BH parameters are then extracted at $t = t_F$, where t_F is distributed on a Gaussian centered at $\bar{t}_F \sim 2 \times 10^9$ yr with width $\sigma = 0.1\bar{t}_F$. As an example we considered $\mu = 10^{-18}$ eV, but similar results hold for other masses. The dashed blue line is the prediction of the linearized analysis obtained by comparing the superradiant instability time scale with the accretion time scale [110, 489, 504], whereas the solid green line is a new prediction computed in [405]. Old BHs do not populate the region above the green threshold curve, especially for high accretion rates. The experimental points with error bars refer to the supermassive BHs listed in [507]. (From [405].)

the Regge plane [504], i.e. regions of the BH mass–spin diagram which should not be populated by old BHs. We refer to [405] for a detailed discussion.

A quasi-adiabatic evolution is well suited to studying superradiant instabilities because of the existence of two very different scales [405]. One is dictated by the oscillation time $\tau_S \sim 1/\mu$, the other by the instability growth time scale, $\tau \gg \tau_S$. In the most favorable case for the instability (that of a massive scalar field), $\tau \sim 10^6 \tau_S \sim 10^6 M$ is the minimum evolution time scale required for the superradiant effects to become noticeable. Thus, fully numerical simulations that capture the effects of the instability are extremely challenging to perform.

The first fully nonlinear evolutions of massive scalars coupled to Kerr BHs [404] have found evidence for superradiant scattering in the early stages of the interaction, which has also been observed in simulations modeling the infall of GWs into a rotating BH [508]. After this scattering, however, the spin of the BH decreases so much that the system is driven out of the superradiant regime, and slow accretion of the scalar field dominates the ensuing evolution⁵⁰. These features are illustrated in the left panel of figure 14. Because of the mass term and the

⁵⁰ Note that these evolutions focused only on an isolated BH–scalar field system, neglecting the effects due to the presence of ordinary matter or accretion disks.

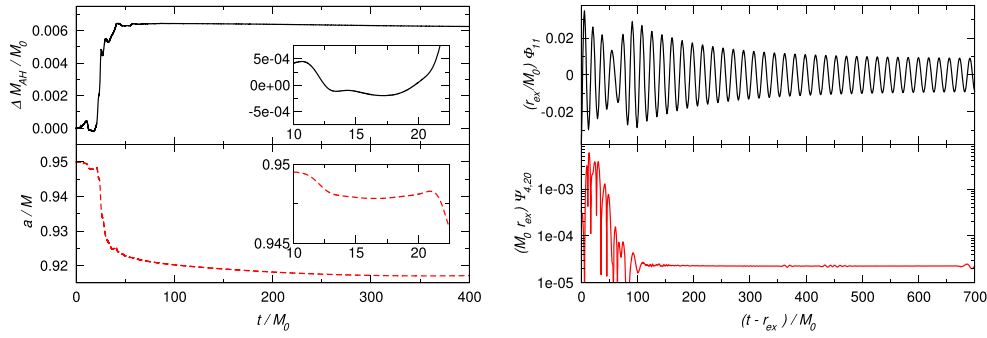


Figure 14. Nonlinear evolutions of a scalar cloud with $M\mu = 0.3$ around a BH with initial spin $a/M = 0.95$. Left: fractional variation in the BH mass (top) and dimensionless spin of the hole (bottom). At early times (shown in the inset), both quantities *decrease* hinting at superradiance scattering. At later times, the superradiance condition is no longer satisfied, resulting in an increase of the BH mass due to accretion of the scalar cloud. Right: dominant scalar (top) and induced gravitational waveforms (bottom). (From [404].)

resulting potential barrier the scalar field is trapped inside a region near the BH, and therefore forms a scalar cloud which continuously leaks into the rotating hole. This induces long-lived scalar and gravitational radiation: see right panel in figure 14 (as well as the animations available online at [436]). Although the gravitational radiation itself is not sensitive to the mass potential barrier, the continued interaction between the BH and the scalar cloud excites a GW signal with about twice the scalar-field frequency, which follows the beating pattern exhibited in the scalar modes [403, 404]. Moreover, the frequencies in both the scalar and GWs are of the order $f \sim \mathcal{O}(10) \text{ kHz}(M/M_\odot)^{-1}$, implying that the signals generated by stellar-mass or supermassive BHs are potentially observable with the Advanced LIGO/VIRGO network [509] or future space-based detectors such as eLISA [502], respectively (see [505] for recent work on GW signatures of bosonic clouds around BHs).

In addition to interesting constraints on particle masses, superradiant mechanisms have the potential to test the existence and geometry of extra dimensions [510]. Finally, the possibility of indirect observation of superradiance in a BH-pulsar system has recently been proposed. The idea is that the pulsar's GW and electromagnetic luminosities may exhibit a characteristic modulation due to superradiant scattering that depends on the pulsar position relative to the BH [511]. If observed, this would be the first—albeit indirect—observation of rotational superradiance, which forms the basis of all the superradiant instabilities discussed here [496].

3.11. Open problems

Here we give a (necessarily biased) list of open problems regarding BH physics in the context of tests of gravity:

- The stability of the hairy BH solutions found in [68], as well as their formation mechanism in astrophysical scenarios remain urgent open issues.
- In the context of stationary solutions, BHs in dCS gravity are known only for low spin and were obtained analytically within a perturbative scheme. Highly spinning dCS BHs have not been constructed numerically yet.

- The stability of BHs in quadratic gravity has been only partially investigated. Notable missing investigations include: polar gravitational perturbations of static EdGB BHs, any perturbations of slowly rotating EdGB BHs, and the gravito-scalar perturbations of slowly rotating dCS BHs. The latter might be relevant in the context of Ostrogradski instabilities and the well-posedness of dCS gravity.
- Similarly, the stability of BHs in Lorentz-violating theories under gravitational perturbations has not been studied, even in the static case. Such an analysis might be interesting in the context of stability of the universal horizons.
- The phenomenology of BHs in Horndeski theory, Galileon theory and massive gravity has not been studied in detail yet. In theories admitting BH solutions other than Kerr, it would be interesting to understand whether such solutions are formed as the result of gravitational collapse.
- Despite various attempts, a solid strong-field parametrization of spinning BHs in generic modified gravity is not yet available.
- The endpoint of the superradiant instability of spinning BHs triggered by massive bosons in full GR is unknown, due to the long time scales of the problem. Nonlinear effects, such as bosonova collapse [512], should be taken into account in numerical simulations.

4. Neutron stars

Our discussion of BH solutions in modified theories of gravity shows that there is a significant problem in testing GR with present and future astrophysical observations: the Kerr metric is a solution of the field equations in many proposed alternatives to GR, and even when it is not, deviations from the structure and dynamics of the Kerr metric are expected to be suppressed by some (typically small) coupling constant. Unlike BHs, the structure of compact stars depends on the coupling of gravity with matter in strong-field regions. Therefore NSs are a valuable alternative to BHs in tests of strong-field gravity, because they can probe (and possibly rule out) those theories that are close to GR in vacuum, but differ in the description of the coupling between matter and gravity. In fact, the enormous gravitational field of NSs, the high density of matter at their cores and the existence of pulsars with fast spin and large magnetic fields make them ideal laboratories to study all fundamental interactions [513–519].

The study of compact stars in alternative theories of gravity has a long history. In this section we give a concise overview of what we consider to be the state of the art, and for each specific theory we present a catalog of all⁵¹ the NS observables that have been computed at the moment of writing. Table 3 is meant to provide a practical guide to the literature. A glance at the table shows that while NS equilibrium configurations have been explored in many classes of modified theories of gravity, their stability and their dynamical properties are still largely unknown.

4.1. General-relativistic stellar models

Before discussing equilibrium stellar solutions in modified gravity, it is convenient to present a brief summary of the basic properties of relativistic stars in Einstein's theory (we refer the reader to [372, 520, 521] for excellent treatments of the subject).

⁵¹ One exception are the so-called NS 'sensitivities': extra charges that the NS can acquire in modified gravity due to the violation of the SEP. These are discussed in section 4.9, in preparation for our review of binary dynamics in modified gravity (section 5).

In GR, the equilibrium of spherically symmetric, static (nonrotating) stars is governed by the Tolman–Oppenheimer–Volkoff (TOV) equations, that follow from Einstein’s equations for a perfect-fluid stress energy tensor. When supplemented with an EOS relating the fluid’s density and pressure, Einstein’s equations form a closed system of ordinary differential equations. The NS EOS encodes the thermodynamical behavior of matter in the extreme conditions prevailing in the NS interior. Despite recent progress (see e.g. [513–519]), the EOS is still largely unknown at the supranuclear densities characterizing the NS core.

The solutions to the TOV equations are obtained, in general, by numerical integration. They form a single-parameter family, where the parameter labeling different solutions can be chosen to be (say) the central density. Relativistic equilibrium configurations are characterized by a maximum mass and a maximum compactness that depend on the EOS. Uncertainties in the EOS translate into uncertainties in the NS mass–radius relation. For example, for a typical NS mass $M \sim 1.4M_{\odot}$, EOSs compatible with our current knowledge of nuclear physics predict radii ranging from ~ 6 to ~ 16 kilometers [517].

Generic rotating stellar models are more difficult to construct. However, ‘old’ NSs are expected to rotate rather slowly, unless they are spun up by accretion from a companion; therefore, perturbative calculations using a slow-rotation expansion are reliable in many situations of astrophysical interest. The formalism to construct slowly rotating NS models, developed in the seminal work by Hartle and Thorne [522, 523], has been pushed up to fourth order in rotation [29]. Various works [29, 524, 525] have shown that the equilibrium properties of slowly rotating solutions compare favorably with numerical codes that solve Einstein’s equations in full generality to construct models of relativistic stars with arbitrary rotation rates (see [520, 521] for reviews).

Linear perturbations of stellar configurations are complex and interesting, even for static objects. Because of GW emission, the modes of relativistic NSs (just like the modes of BHs) have a dissipative component, i.e. they are QNMs. In addition to the standard fluid modes, that have well studied counterparts in the Newtonian limit [526], compact stars also possess characteristic modes of oscillation (the so-called w -modes) associated to pure spacetime perturbations, rather than fluid displacements (see [382, 521, 527, 528] for reviews). These w -modes are similar in nature to BH QNMs. Therefore NS QNMs carry information about the stellar geometry (as in the BH case), but in addition they can also be used to infer the properties of the NS EOS. In fact, one of the main scientific goals of third-generation Earth-based GW detectors is their potential to fulfill the promise of ‘GW asteroseismology’ [528–530]: accurate GW measurements of the oscillation frequencies would allow us to reconstruct the properties of the NS (something that is routinely done in helioseismology) and therefore to constrain nuclear physics in regimes that are out of reach for laboratory experiments. Rotating compact stars are characterized by various instabilities (most notably, the Chandrasekhar–Friedman–Schutz instability [531, 532] and the related r -mode instability [533]) that have important implications for their spin rate and evolution. This topic is largely unexplored in modified gravity, but there is a very large body of work on these instabilities and their implications in GR [382, 521, 528, 534].

4.2. Scalar–tensor theories

It should come as no surprise that most of the work on NSs in modified theories of gravity has focused on the simplest and arguably most natural extensions of GR, namely scalar–tensor theories. In these theories, the properties of static and spinning NSs and of their oscillation modes are well understood.

The modified TOV equations of hydrostatic equilibrium in Brans–Dicke theory were first studied by Salmona [114]. Soon after, Nutku [133] explored the radial stability of stellar models using a PN treatment. Hillebrandt and Heintzmann [115] analyzed incompressible (constant density) configurations. These studies found that corrections to NS structure are typically suppressed by a factor $1/\omega_{\text{BD}}$, where ω_{BD} is the Brans–Dicke coupling constant. The current best bound $\omega_{\text{BD}} > 40,000$ [2] implies that the bulk properties of NSs in the original Brans–Dicke theory deviate from GR by unmeasurable amounts.

However, as pointed out by Damour and Esposito-Farèse [26, 116], for a particular class of scalar–tensor theories that is indistinguishable from GR in the weak field regime [more precisely, when $\alpha_0 = 0$ and $\beta_0 < 0$ in the expansion of the Einstein-frame coupling function (2.5)], a nonlinear phenomenon called ‘spontaneous scalarization’ can occur, introducing macroscopically (and observationally) significant modifications to the structure of the star⁵². In addition the solutions become nonunique: for certain ranges of the parameter space, NS solutions in GR coexist with scalarized NSs. One of the most interesting observations in [26, 116] is that scalarized configurations are energetically favored over their GR counterparts. Scalarization occurs also for BHs in the presence of matter fields [417, 418, 536, 537].

A simple way to illustrate the principle behind spontaneous scalarization is by taking the limit in which the scalar field φ is a small perturbation around a GR solution. Expanding around the constant value φ_0 to first order in $\hat{\varphi} \equiv \varphi - \varphi_0 \ll 1$, the field equations in the Einstein frame (2.7a), (2.7b) read (see e.g. [234])

$$G_{\mu\nu}^* = 8\pi T_{\mu\nu}^*, \quad (4.1)$$

$$\square^* \hat{\varphi} = -4\pi\alpha_0 T^* - 4\pi\beta_0 \hat{\varphi} T^*. \quad (4.2)$$

Here we have assumed analyticity around $\varphi \sim \varphi_0$ and used equation (2.5), where $A(\varphi)$ is the nonminimal coupling to the matter fields in the Einstein frame, as defined by the action (2.4).

It is clear from equation (4.2) that α_0 controls the effective coupling between the scalar and matter. Various observations, such as weak-gravity constraints and tests of violations of the SEP, require α_0 to be negligibly small when the scalar tends to its asymptotic value [37, 116, 538]. This implies that a configuration in which the scalar $\varphi \approx \varphi_0$ and $\alpha_0 \approx 0$ should be at least an approximate solution in most viable scalar–tensor theories. A detailed study of the connection between the perturbative and nonperturbative scalarized solutions can be found in [536, 537].

With $\alpha_0 = 0$, any background GR solution solves the field equations above at first order in the scalar field. At this order, the Klein–Gordon equation reads

$$\left[\square^* - \mu_s^2(x^\nu) \right] \hat{\varphi} = 0, \quad \mu_s^2(x^\nu) \equiv -4\pi\beta_0 T^*. \quad (4.3)$$

Thus, the coupling of the scalar field to matter is equivalent to an effective position-dependent mass. Depending on the sign of $\beta_0 T^*$, the effective mass squared can be negative. Because $-T^* \approx \rho^* > 0$, this happens when $\beta_0 < 0$. When $\mu_s^2 < 0$ in a sufficiently large region inside the NS, scalar perturbations of a GR equilibrium solution develop a tachyonic instability (i.e., the perturbations propagate superluminally, as particles with imaginary mass). This instability is associated with an exponentially growing mode, which causes the growth of scalar hair in a process akin to ferromagnetism [26, 116].

Spherically symmetric NSs develop spontaneous scalarization for $\beta_0 \lesssim -4.35$ [135]. Detailed investigations of stellar structure [116, 118], numerical simulations of collapse [126–

⁵² For a comprehensive study of analytic solutions and an extensive bibliography, see [535]. Note in particular that Tsuchida *et al* [117] extended the Buchdahl inequality ($M/R \leq 4/9$ for incompressible stars) to generalized scalar–tensor theories.

[128] and stability studies [134, 135] confirmed that spontaneously scalarized configurations would indeed be the end-state of stellar collapse in these theories. In fact, spontaneously scalarized configurations may also be the result of semiclassical vacuum instabilities [138–141].

The nonradial oscillation modes of spontaneously scalarized, nonrotating stars were studied in [136, 137, 142, 143]. The bottom line of these studies is that the oscillation frequencies can differ by a large amount from their GR counterparts if spontaneous scalarization modifies the equilibrium properties of the star (e.g., the mass–radius relation) by appreciable amounts. However, current binary pulsar observations yield very tight constraints on spontaneous scalarization, and the oscillation modes of scalarized stars for viable theory parameters are unlikely to differ from the corresponding GR modes by any measurable amount.

Spontaneous scalarization and quantum instabilities in scalar–tensor theories with a conformal coupling. An interesting class of scalar–tensor theories that has been recently investigated in the context of NS physics is the following:

$$S = \frac{1}{16\pi} \int d^4x \sqrt{-g} \left[R - 2g^{\mu\nu} \varphi_{,\mu} \varphi_{,\nu} - \xi R \varphi^2 \right] + S_{\text{perfect fluid}}, \quad (4.4)$$

where ξ is the conformal coupling parameter. For $\xi = 1/12$ the scalar field equations are invariant under conformal transformations ($g_{\mu\nu} \rightarrow \gamma^2 g_{\mu\nu}$, $\varphi \rightarrow \gamma^{-1} \phi$), whereas for $\xi = 0$ one recovers the usual minimally coupled massless scalar. The theory above can be obtained as a particular case of the action (2.3) after a field redefinition.

Lima, Matsas and Vanzella showed that the vacuum expectation value of nonminimally coupled scalar fields can grow exponentially in relativistic stars [138]. At the classical level, this quantum instability can be interpreted in terms of the spontaneous scalarization discussed above [139]. The instability can occur for both positive and negative values of ξ . When $\xi < 0$ and $|\xi|$ is large enough, the instability can occur even for Newtonian stars. For a detailed analysis of the approach to the classical limit and of the relation between the quantum and classical nature of the final state, see [140, 141].

Slowly rotating solutions. Spinning NSs at first order in the Hartle–Thorne slow-rotation approximation were studied by Damour and Esposito-Farèse [116] and later by Sotani [119]. At first order in rotation, the scalar field only affects the moment of inertia, mass and radius of the NS. Second-order calculations [120] are necessary to compute corrections to the spin-induced quadrupole moment, tidal and rotational Love numbers, as well as higher-order corrections to the NS mass and to the scalar charge. Figure 15 shows representative examples of the properties of NSs in a scalar–tensor theory with spontaneous scalarization at second order in the rotation parameter.

Rapidly rotating solutions. Rapidly rotating NSs in scalar–tensor theories were recently constructed in [121] by extending the RNS code [520]. The results shown in figure 16 illustrate that scalarization effects are stronger for rapidly rotating stars, and deviations from GR are sensibly larger for fast-spinning NSs. One of the reasons is that the stress–energy tensor (which acts as a source for the scalar field) gets a contribution from the rotational energy of the star. The nontrivial scalar field has a strong effect also on the NS angular momentum and moment of inertia, which can differ by as much as a factor of two from their GR values at the Kepler limit [121]. In addition, there exists a larger range of parameters for which scalarization occurs, and the critical value of the coupling constant β_0 where a

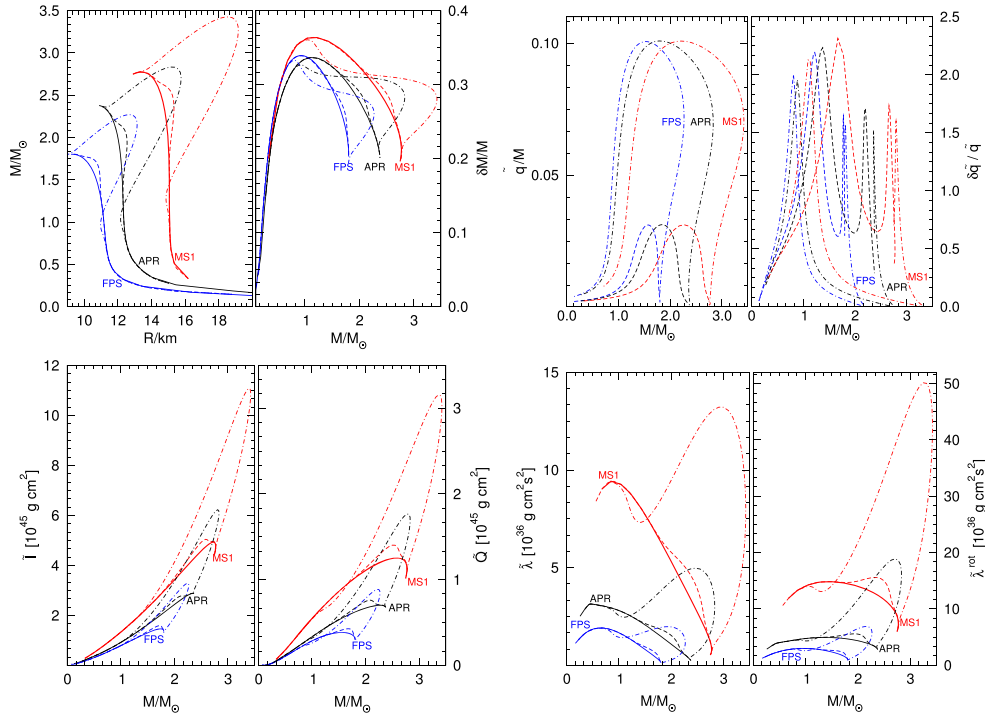


Figure 15. NS configurations in GR (solid lines) and in two scalar–tensor theories defined by equation (2.4) with $A(\varphi) \equiv e^{\frac{1}{2}\beta_0\varphi^2}$ and $V(\varphi) \equiv 0$. Dashed lines refer to $\beta_0 = -4.5$, $\varphi_0^\infty/\sqrt{4\pi} = 10^{-3}$; dashed–dotted lines refer to $\beta_0 = -6$, $\varphi_0^\infty/\sqrt{4\pi} = 10^{-3}$. Each panel shows results for three different EOS models (FPS, APR and MS1). Top-left panel, left inset: relation between the nonrotating mass M and the radius R in the Einstein frame. Top-left panel, right inset: relative mass correction $\delta M/M$ induced by rotation as a function of the mass M of a nonspinning star with the same central energy density. Top-right panel, left inset: scalar charge \tilde{q}/M as a function of M . Top-right panel, right inset: relative correction to the scalar charge $\delta\tilde{q}/\tilde{q}$ induced by rotation as a function of M . Bottom-left panel: Jordan-frame moment of inertia \tilde{I} (left inset) and Jordan-frame quadrupole moment \tilde{Q} (right inset) as functions of M . Bottom-right panel: Jordan-frame tidal ($\tilde{\lambda}$) and rotational ($\tilde{\lambda}^{\text{rot}}$) Love numbers as functions of M . (From [120].)

nontrivial scalar field can develop increases substantially. For example, for the polytropic EOS considered in [121] the critical value of β_0 increases from $\beta_0 \gtrsim -4.35$ in the nonrotating case to $\beta_0 \gtrsim -3.9$ for rapid rotation. For realistic EOSs scalarization can occur for even larger β_0 [122]. Binary pulsar observations imply $\beta_0 \gtrsim -4.5$ (see section 6). For a marginally allowed β_0 , nonrotating scalarized NSs would not differ considerably from the GR solutions, whereas rapid rotation can produce significant deviations that can potentially set even stronger astrophysical constraints on scalar–tensor theories [122, 123]. Other proposed mechanisms that can amplify the effects of scalarization include anisotropy [539] and ‘dynamical scalarization’ for merging NSs in scalar–tensor theories, that will be discussed in section 5 [540–543]. In the last stages before merger the rotational frequencies of each NS may approach the Kepler limit.

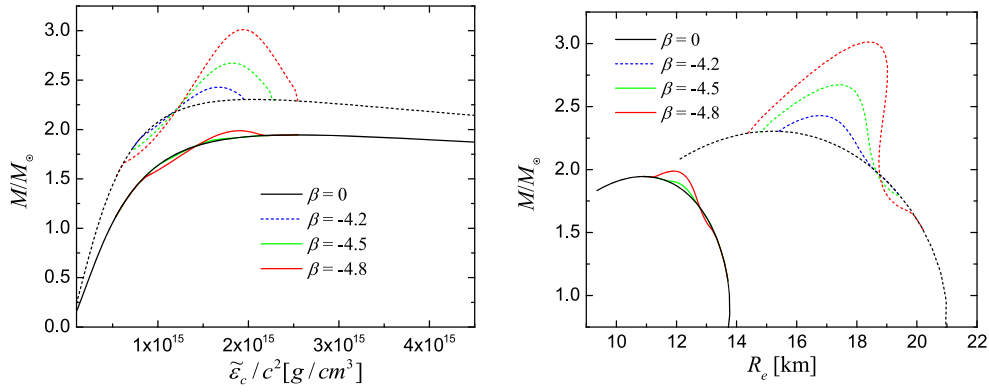


Figure 16. The NS mass as a function of the central energy density (left panel) and of the radius (right panel) for static sequences of NSs (solid lines) and sequences of stars rotating at the mass-shedding limit (dotted lines). The trivial solutions coincide with the GR limit ($\beta = \beta_0 = 0$). For $\beta = \beta_0 = -4.2$ nontrivial solutions do not exist in the nonrotating case. (From [121].)

4.3. $f(R)$ theories

In principle $f(R)$ theories can be mapped to a specific form of the action in scalar–tensor theory [11, 12], but this mapping involves subtleties and technicalities that justify a separate discussion of NS solutions in metric $f(R)$ gravity. In fact the literature on NS solutions in metric $f(R)$ gravity is quite extensive, and it contains several apparently controversial claims [145, 147–149, 151, 544].

The recent interest in $f(R)$ theories is due to their potential to explain cosmological observations without introducing dark matter or dark energy. In terms of compact objects, this means that one is usually interested in matching the stellar interior to a de Sitter metric with an effective cosmological constant

$$\Lambda_{\text{eff}} = R_{\text{dS}}/4, \quad (4.5)$$

where R_{dS} is the curvature at the de Sitter point, and $R \rightarrow R_{\text{dS}}$ far from the star. The problem involves two completely different density (or curvature) scales, because the central density of a NS ($\rho_0 \sim 10^{14} \text{ g cm}^{-3}$) is enormously larger than the density associated to the cosmological constant ($\rho_\Lambda = \Lambda/(8\pi G) \sim 10^{-29} \text{ g cm}^{-3}$): $\rho_\Lambda/\rho_0 \sim 10^{-43}$. In practice, only much larger values ($\rho_\Lambda/\rho_0 \sim 10^{-10} - 10^{-6}$) can be used in numerical codes. This issue is not specific to $f(R)$ theories: it would also arise in GR with a positive cosmological constant if one tries to match a NS interior with a de Sitter exterior. In fact, the large disparity in density (or curvature) scales is not a problem if one assumes that the cosmological scale has no sensible influence on local physics. In other words, one would expect local observables such as the NS mass and radius to be insensitive to ρ_Λ/ρ_0 , as long as this ratio is small enough: $\rho_\Lambda/\rho_0 \sim 10^{-10}$ (say) would be practically indistinguishable from $\rho_\Lambda/\rho_0 \sim 10^{-43}$, except for giving an unrealistically large cosmological constant.

Calculations of NS structure in $f(R)$ theory used different approaches, reaching different conclusions on the very existence of relativistic compact stars. Here we try to clarify some critical issues in the literature, pointing the reader to the original references for more details.

Singular potential. When $f(R)$ is reformulated as a scalar–tensor theory, the potential for the scalar degree of freedom can, and in general will, be singular [544]. The scalar-field equation (2.14) can be recast in the form

$$\square\phi = V'_{\text{KM}}(\phi) - \mathcal{F}, \quad (4.6)$$

where a prime denotes a derivative with respect to ϕ and $\mathcal{F} = 8\pi/3(\rho - 3P)$ plays the role of a matter-driven force term. For various solutions describing late-time cosmology or compact objects, the ‘force’ \mathcal{F} pushes the scalar field towards the unprotected curvature singularity, which is at finite distance (in field and energy space) from the equilibrium configuration. As discussed below, this happens precisely for those $f(R)$ models which are otherwise theoretically and observationally viable [544]. This singular character of the potential can cast doubts on the viability of $f(R)$ gravity and on the existence of compact objects in these theories. However, this premature conclusion depends on the choice of a specific scalar–tensor formulation of $f(R)$ gravity.

Kobayashi and Maeda [145] reported that the field equations inside relativistic stars are plagued by singularities, but subsequent work [147, 148] claimed that such singularities were unphysical and due to numerical instabilities. Indeed, the scalar field in the interior of compact objects can be very close to the value that corresponds to the singular potential, but does not necessarily need to end up in the singularity. This makes the integration challenging from a numerical point of view, but it does not necessarily imply a pathology in the underlying theory, as we show below.

First of all, note that any $f(R)$ model that meets the minimum requirements to satisfy Solar System constraints—i.e., it satisfies the requirements of equation (2.11)—is such that the first and second derivatives of the scalar potential defined in [145, 147, 148] are *divergent* in the $R \rightarrow \infty$ limit. This limit corresponds to a *finite* value of the scalar field and to a *finite* value of the potential at the singular point. In the following, we shall generically denote the scalar degree of freedom (in the various formulations discussed in section 2.3) by Φ and the scalar potential by V_Φ , whereas Φ_s denotes the value of the scalar at the singular point, i.e. $\Phi_s = \Phi(R \rightarrow \infty)$. Let us parametrize the large-curvature expansion by using the rather generic expression (see equation (2.11))

$$f(R) \sim R + R_c \left[a + b \left(\frac{R_c}{R} \right)^c + d \log \left(\frac{R_c}{R} \right) \right], \quad R \gg R_c, \quad (4.7)$$

where (a, b, c, d) are dimensionless real constants, $c \geq 0$, $d \geq 0$, R_c is some curvature scale of the order of R_{ds} , and we have kept only the dominant terms in a large-curvature expansion. Equation (4.7) is a good approximation in the interior of a NS, where the curvature is much larger than the cosmological curvature R_{ds} , and indeed most of the models considered in the compact object literature belong to this class. Using equation (4.7), it is straightforward to prove that

$$V_\Phi(R \gg R_c) \rightarrow R_c \left[\text{const} + d \log \left(\frac{R_c}{R} \right) \right] \quad (4.8)$$

up to a constant (that can be adjusted to eliminate the constant term above). In conclusion, in the limit $\Phi \rightarrow \Phi_s$ the potential V_Φ is finite if $d = 0$ and diverges logarithmically if $d \neq 0$, but its derivative $V'_\Phi \rightarrow \infty$ in any case. Therefore, the energy density needed to make the singularity energetically accessible is roughly

$$V'_\Phi(\Phi \rightarrow \Phi_s) \sim R. \quad (4.9)$$

In models in which corrections to GR are relatively small for $R \gg R_c$, this quantity is parametrically of the same order as the matter energy density ρ_c in the interior of a NS. This can be seen by taking the trace of the modified Einstein equations (see discussion around equation (4.12) below). This simple argument seems to suggest that the singularity should be accessible, as discussed in [544]. However, as we will see below, in $f(R)$ theories a subtle mechanism prevents such singularities to be accessible, at least in various situations. The price to pay is that numerical integrations for realistic values of the theory parameters are extremely challenging.

To this end, it is important to remark that the singular behavior of the scalar potential is not an *intrinsic* ingredient of the theory, but just a prerogative of specific formulations of $f(R)$ gravity. Indeed, this severe problem does not arise in the approach developed by Jaime *et al* [151], in which the potential defined in equation (2.19) is regular for finite curvature. When $R \gg R_c$, using equation (4.7) we get

$$V_{\text{JPS}}(R) \sim \begin{cases} R_c^3 (R/R_c)^{c+4}, & d = 0 \\ R_c^3 (R/R_c)^4, & d \neq 0 \end{cases}. \quad (4.10)$$

Remarkably, in this formulation the singularity at $R \rightarrow \infty$ is protected by an *infinite* potential well for any viable model satisfying equation (2.11). Furthermore, dimensional arguments show that in this case the energy density needed to reach the singularity is of order

$$V'_{\text{JPS}}(R)R^{-1} \sim \begin{cases} R_c (\rho_c/R_c)^{c+2}, & d = 0 \\ R_c (\rho_c/R_c)^2, & d \neq 0 \end{cases}, \quad (4.11)$$

which is always much larger than the internal energy density of a NS. In other words, in this formulation the singularity at infinity is protected by an infinite potential barrier [151], as in any well-behaved mechanical model (e.g. the harmonic oscillator).

Chameleon mechanism. The existence of singular scalar configurations accessible at finite energies is potentially dangerous. As we just discussed, in the case of $f(R)$ gravity it is not the theory itself to be potentially problematic, but only some particular formulations of the theory. Clearly, the viability of the theory cannot depend on the particular formulation chosen in [151], so there must exist a mechanism that prevents singular behavior also in other formulations. Indeed, even in these potentially ill-defined formulations, a subtle *chameleon mechanism* [545, 546] keeps the scalar field away from the singularity. The chameleon mechanism is related to the generation of an infinitely large mass term of the scalar field, due to self-interactions and to interactions with other matter fields (see e.g. [147]).

At high curvature $dV_{\Phi}/d\Phi \sim R$ and $dV_{\Phi}^{\text{eff}}/d\Phi \rightarrow R + 8\pi T$, so that the effective potential has a minimum at

$$R_{\text{min}} \sim -8\pi T, \quad (4.12)$$

which corresponds to some $\Phi_{\text{min}} = \Phi(R_{\text{min}})$. For any $f(R)$ gravity theory satisfying the viability conditions (2.11), assuming $T \sim \text{const}$, the scalar mass in the large-curvature limit reads

$$m_{\Phi}^2 \equiv \left. \frac{d^2 V_{\Phi}^{\text{eff}}(\Phi)}{d\Phi^2} \right|_{\Phi=\Phi_{\text{min}}} \sim \begin{cases} R_c (-8\pi T/R_c)^{c+2}, & d = 0 \\ R_c (-8\pi T/R_c)^2, & d \neq 0 \end{cases}. \quad (4.13)$$

It is crucial to realize that the dimensionless quantity $m_\Phi R^{-1/2}$ is an estimate of the ratio between the curvature lengthscale and the Compton wavelength of the graviton; therefore, it is proportional to the number of integration steps needed to resolve the dynamics of the chameleon field in a region of approximately constant curvature R [147]. Evaluating this quantity inside a NS, where $R \sim -8\pi T \sim \rho_c$, one obtains

$$m_\Phi^2 \rho_c^{-1} \sim \begin{cases} (x_{\text{dS}} \rho_c / \Lambda_{\text{eff}})^{c+1}, & d = 0 \\ (x_{\text{dS}} \rho_c / \Lambda_{\text{eff}}), & d \neq 0 \end{cases}, \quad (4.14)$$

where $x_{\text{dS}} = R_{\text{dS}}/R_c$. The larger the ratio $\rho_c/\Lambda_{\text{eff}}$, the larger the effective chameleon mass and the number of steps needed for the integration in the stellar interior. For a realistic NS embedded in a de Sitter Universe the effective mass is extremely large in cosmological units, and so is the number of integration steps. Such a heavy field is challenging to treat numerically. Indeed, as discussed by [147], Yukawa-like error modes grow as $e^{m_\Phi r}/r$, and dominate if the Compton scale m_Φ^{-1} becomes much smaller than the computational domain. Hence, in the ‘wrong’ formulations the integration of the field equations becomes practically impossible in realistic situations, but this does not imply that the solutions are singular.

Note also that the chameleon mass depends on powers of x_{dS} , which may be a large quantity, making the integration even more challenging. For example, the bound $x_{\text{dS}} \gtrsim 10^3$ must be imposed for a popular model (the simplest version of the Starobinsky model [547], where $f(R) = R[1 - \mu R_c R / (R_c^2 + R^2)]$) to satisfy local tests [147, 548]. Curiously, this fact is often overlooked and unrealistic values $x_{\text{dS}} = \mathcal{O}(1)$ are commonly used (but see [147] for an exception).

In summary, the challenge of constructing compact models in $f(R)$ gravity depends to a large extent on the formulation adopted and, in many cases, is usually overcome by restricting the discussion to unrealistic stars with $\rho_c \sim 10^2 \Lambda_{\text{eff}}$, which is much smaller than the realistic density one should use ($\rho_c \sim 10^{43} \Lambda_{\text{eff}}$), and even in this case numerical integrations can be very difficult. The chameleon mechanism provides an elegant way to keep the scalar field away from the singular point. In fact, it is remarkable that the same nonlinearities that make the scalar potential singular also keep the field away from the singularity. As Babichev and Langlois put it in their paper, the chameleon mechanism forces the scalar field to stay ‘attached to a track very near a precipice, without falling into it’ [149]. The distance of the track from the precipice can be tiny (as small as 10^{-43} in cosmological units), so that it is practically impossible to follow the evolution of the scalar field numerically without being contaminated by the nearby singularity.

Multivalued potential. Another known and controversial issue with the approaches by [147, 148] is multivaluedness. When we recast $f(R)$ theories as scalar–tensor theories, the scalar-field potential can be multi-valued [145, 151, 544]. This conclusion is model-dependent, but it applies e.g. to the Starobinsky model (see figure 1 of [544]) and to any model for which f_R is not a monotonic function of R . In particular, the cosmological branch of the Starobinsky potential is discontinuous at the singular point, i.e. as $\Phi \rightarrow \Phi_s$.

This problem is usually ignored on the grounds that stellar structure calculations only refer to the structure of the potential around a local minimum, and that possible multiple branches are harmless if the entire cosmological evolution of the scalar field is confined within a single-valued branch of the potential. While this is true, multivaluedness might seem to make $f(R)$ theories less natural and attractive, especially if the scalar field is extremely close to the singular and discontinuous point of the potential (as in the interior of compact objects).

However—similarly to the issue with the singular scalar potential—also multivaluedness is formulation-dependent, as pointed out in [151]. Indeed, it turns out that the potential (4.10) is *not* multivalued. This is simply due to the fact that the ‘true’ dynamical degree of freedom is the curvature R , not f_R , and no inversion $R = R(\Phi)$ is needed in the approach of [151].

Main results. The mapping of $f(R)$ gravity to scalar–tensor theories—both in the Jordan and in the Einstein frame—is plagued by several potentially dangerous issues, including singularities and multivaluedness in the scalar potential and a diverging effective mass for the field. These issues are intertwined, and in fact they can be seen as ‘features,’ as they are needed for the theoretical safety of the theory (an example being the chameleon mechanism that keeps the scalar field away from the singularity). The numerical challenges they introduce may also serve as a motivation to develop more efficient integration methods. These same issues make the study of compact objects in $f(R)$ gravity particularly difficult, especially for realistic configurations [146, 152, 153, 155–159].

Most studies of NS configurations in $f(R)$ gravity consider *perturbative* corrections to the Einstein–Hilbert action of the form $f(R) = R + \epsilon f_1(R)$, with $\epsilon \ll 1$ [146, 152, 153, 156, 157]. This expansion is similar in spirit to the EFT approach discussed elsewhere in this review, and it bypasses some of the difficulties listed above. Some of these models [152] predict NSs with large compactness (NS radii as small as ~ 9 km), which are difficult to obtain in GR, even taking into account current uncertainties in the EOS.

Yazadjiev *et al* [155] recently went beyond the perturbative level constructing static equilibrium models of NSs in a theory of the form $f(R) = R + \lambda R^2$, where the coupling λ is not necessarily small. They found that deviations from GR are comparable with the variations due to uncertainties in the EOS, even for large values of λ . Subsequent work by Staykov *et al* [158] extended the analysis to first order in the slow-rotation approximation, finding that the NS moment of inertia can be up to 30% larger than its GR counterpart. This correction is larger than that introduced by uncertainties in the EOS, and (in principle) it can be used to break the EOS degeneracy (see section 4.8 below). Yazadjiev *et al* [159] constructed rapidly rotating NSs in nonperturbative $f(R) = R + \lambda R^2$ gravity. For fast rotation, the maximum NS mass and moment of inertia can be up to $\sim 16\%$ and 60% larger than in GR, respectively. These corrections to the NS properties are large enough that, if observed, they may be used to constrain the parameter λ .

4.4. Quadratic gravity

A remarkable consequence of recent work is that, from the point of view of the properties of compact objects, scalar–tensor theories and quadratic gravity are ‘orthogonal’ extensions of GR. Isolated BHs in scalar–tensor theories are described by the Kerr solution, just like in GR, whereas NS configurations can acquire a scalar charge through spontaneous scalarization. On the contrary, BH solutions in quadratic gravity theories are endowed with a scalar field that is supported by the higher-order curvature terms, but a ‘no-scalar-monopole-hair’ theorem holds for NSs in EdGB and dCS gravity (at least in the *perturbative* regime).

There is a simple heuristic proof of the NS no-hair theorem in quadratic gravity [549]. Integrating the scalar equation of motion in EdGB gravity (within the perturbative EFT expansion) yields

$$\int d^4x \sqrt{-g} \square \phi \propto \int d^4x \sqrt{-g} R_{\text{GB}}^2, \quad (4.15)$$

where R_{GB}^2 is the Gauss–Bonnet term (a similar conclusion applies to dCS gravity, as long as we replace R_{GB}^2 with the Pontryagin density *RR). Because R_{GB}^2 (and *RR) are topological

invariants, the right-hand side of equation (4.15) vanishes identically for any simply connected, asymptotically flat domain. Furthermore isolated NSs are stationary, so the time dependence of the left-hand side can be neglected, yielding an integral over the volume. Finally, Stokes' theorem yields

$$\int \sqrt{-g} (\partial_i \phi) n^i dS = \int \sqrt{-g} (\partial_r \phi) dS = 0, \quad (4.16)$$

where the unit vector n^i is normal to the surface S , taken to be a two-sphere at infinity. In order to have finite energy, the scalar field must go to zero at large distances ($r \rightarrow \infty$). If we had $\phi \rightarrow Q/r$, where Q is a constant related to some hypothetical scalar charge, equation (4.16) would imply $Q = 0$. Therefore the scalar field must decay faster than $1/r$ at infinity, and isolated NSs in EdGB gravity and dCS gravity have no scalar monopole charge.

4.4.1. EdGB theory. The proof given above is valid only in the *perturbative* regime, i.e. when the R_{GB}^2 or $*RR$ terms in the action are coupled *linearly* to the scalar field, so that the right-hand side of equation (4.15) vanishes identically. If we consider the EdGB action of equation (2.24) with a generic coupling to the Gauss–Bonnet term, ‘baldness’ does not necessarily apply to NS solutions. Furthermore, even in the perturbative regime the proof does not exclude the possibility that NSs may be endowed with a nontrivial scalar field profile that just happens to have vanishing scalar monopole charge. Indeed, it is easy to check that the source term of the scalar field equation does not vanish in general ($R_{GB}^2 \neq 0$): a constant (or zero) scalar field is not a solution of the field equations, and therefore we would expect the NS properties to be affected by a nontrivial scalar field. These modifications were studied in [164] for the case of standard EdGB gravity with an exponential coupling of the form

$$f_1(\phi) = \alpha_{GB} e^{-\frac{\beta}{\sqrt{8\pi}}\phi} \quad (4.17)$$

(in the notation of (2.24)), where α_{GB} and β are coupling constants. For $\beta/\sqrt{8\pi} = 2$ the model reduces to the bosonic sector of heterotic string theory [256].

Static and slowly rotating solutions. Some properties of static and rotating solutions (computed at first order in the slow-rotation approximation) are shown in figure 17. Regardless of the EOS and for any value of α_{GB} , the coupling to the dilaton tends to *reduce* the importance of relativistic effects: this is again in contrast with the case of scalar–tensor theory, where spontaneous scalarization increases the relevance of relativistic effects (see e.g. the mass–radius curves in figure 15). This trend is confirmed in the left panel of figure 18, showing that the maximum gravitational mass M_{\max} decreases monotonically as a function of the product $\alpha_{GB}\beta$ of the EdGB coupling parameters. Thus in EdGB gravity—as in GR—soft EOS models should be ruled out by observations of high-mass NSs. As we will see, similar conclusions apply to other theories.

An interesting feature of EdGB gravity is that, for fixed values of α_{GB} and β , there exists a constraint on the central density ρ_c (or central pressure P_c) that allows for the existence of NSs. In the small-field limit, the constraint reads [164]

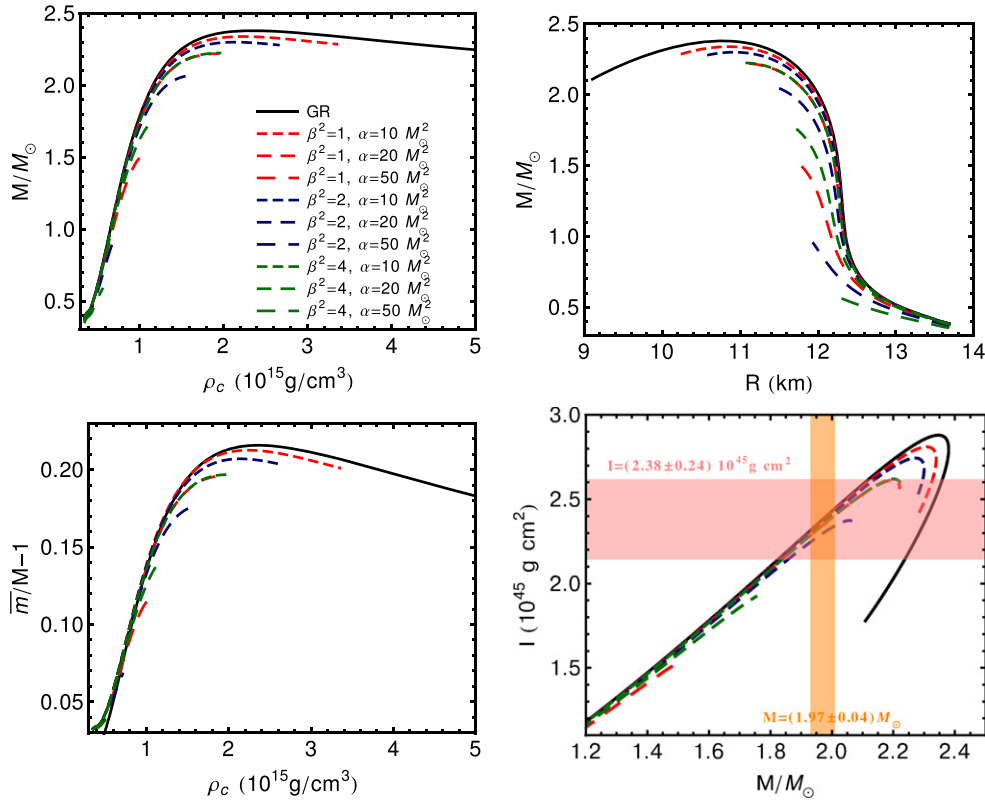


Figure 17. Compact star models in EdGB gravity for different values of the parameters α (denoted by α_{GB} in the text) and β , using the APR EOS. The bottom-left panel shows the NS binding energy as a function of its central energy density. The bottom-right panel displays the moment of inertia as a function of the NS mass, together with the observation of a NS with $M \approx 2M_{\odot}$ [550] (see also [551]) and a putative future observation of the moment of inertia in agreement with GR within 10% [552]. Curves terminate when the condition (4.18) is not fulfilled. (From [164].)

$$\alpha_{\text{GB}}^2 \beta^2 < \frac{1}{7776\pi P_c^4 \rho_c} \left[128\rho_c^3 - 27P_c^2 \rho_c + 288P_c \rho_c^2 + 54P_c^3 - 2\sqrt{(3P_c + \rho_c)(3P_c - 8\rho_c)^2(3P_c + 4\rho_c)^3} \right]. \quad (4.18)$$

If we fix $\alpha_{\text{GB}}\beta$, the condition above implies that no NSs exist above some critical maximum central density.

Quite interestingly, the requirement that the theory should support a maximum mass M_{max} larger than some fiducial observational value can place rather stringent upper bounds on the EdGB coupling. Under rather mild assumptions, Pani *et al* [164] estimated that $\alpha_{\text{GB}} \lesssim \mathcal{O}(10)M_{\odot}^2$, the precise number depending on the EOS and on the value of β . This bound is slightly more stringent than the purely theoretical bound that results from requiring the existence of BHs in the theory [73, 75].

Unfortunately, future observations of the moment of inertia are unlikely to place even tighter bounds on the theory. This is because deviations of the moment of inertia from its GR value are at most $\sim 5\%$, at least in the slow-rotation limit [164], while the precision of future

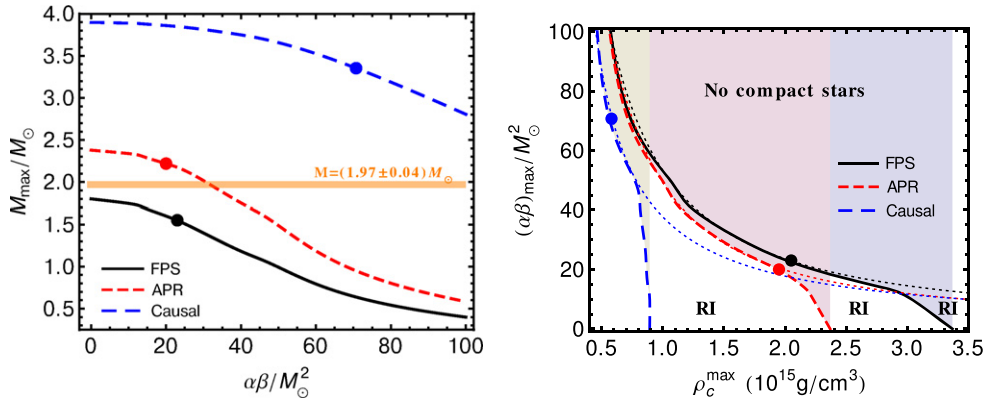


Figure 18. Left panel: maximum mass as a function of the product $\alpha_{\text{GB}}\beta$ of the EdGB coupling parameters, for different EOS models and in the nonrotating case. To the left of the filled circle, this maximum mass corresponds to the radial stability criterion; to the right, it corresponds to the maximum central density for which we can construct static equilibrium models. The maximum observed NS mass $M \approx 2M_{\odot}$ is marked by a horizontal line [550, 551]. Right panel: exclusion plot for the EdGB coupling in the small-field limit and for nonrotating models. In the region above the dotted lines no compact star solution can be constructed (see equation (4.18)). In the region above the thick lines (marked as ‘RI,’ Radial Instability), static configurations are unstable against radial perturbations. Markers indicate the maximum central density of radially stable stars in GR. (From [164].)

observations is expected to be $\sim 10\%$ in optimistic scenarios [552]. At least for EdGB gravity, we expect the most stringent constraints to come from mass measurements, rather than from measurements of the moment of inertia.

Rapidly rotating solutions. The previous analysis was limited to small (first-order) corrections in the NS spin. Rapidly rotating NSs in EdGB gravity were considered by Kleihaus *et al* [82]. Figure 19 shows the quadrupole moment Q in units of $M_{\odot} \cdot \text{km}^2$ for NSs at fixed angular momentum ($j \equiv J/M^2 = 0.4$) versus the angular velocity Ω . The EdGB results with coupling $\alpha_{\text{GB}}/M_{\odot}^2 = 1, 2$ are compared to the case of GR ($\alpha_{\text{GB}} = 0$) for two EOSs: the polytropic EOS from [553] (DI-II) and the FPS EOS [554] (fitted by a polytrope). The quadrupole moment is more sensitive to the EOS than to the Gauss–Bonnet coupling α_{GB} , so that even a putative measurement of the quadrupole moment of a fast-spinning NS can not be used to constrain the theory.

4.4.2. dCS theory. The CS term does not introduce any modification to GR for spherically symmetric configuration: isolated NSs differ from their GR counterparts only when they are rotating. So far, rotating solutions have been computed only in the slow-rotation approximation. The ‘baldness theorem’ discussed above implies that the scalar monopole will vanish, but NSs can still support a nontrivial scalar field. In fact, spinning NSs have a *scalar dipole* ‘hair,’ which modifies the geometry and the properties of the star. The CS correction to the NS moment of inertia was calculated in [45, 165] (at first order in slow rotation). Calculations of the CS correction to the NS quadrupole moment require going to second order in rotation, and they can be found in [166]. A summary of the main results is presented in figure 20. The plot shows: (1) the CS corrections to the moment of inertia, (2) the scalar dipole susceptibility (which is related to the NS sensitivity, discussed in section 4.9

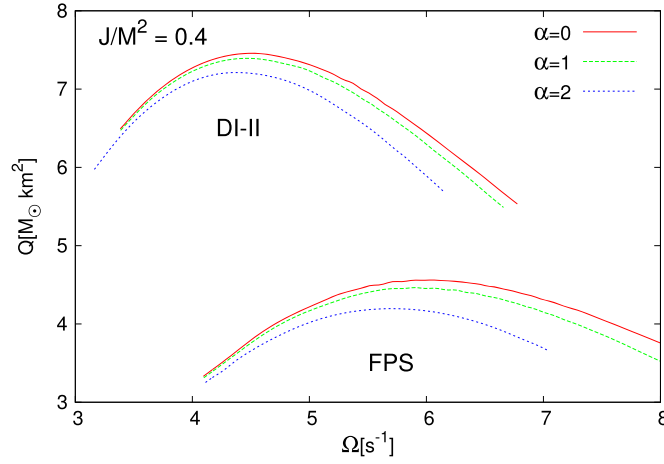


Figure 19. The quadrupole moment Q (in units of $M_{\odot} \cdot \text{km}^2$) is shown versus the angular velocity Ω (in Hz) for the scaled angular momentum $j = 0.4$ and EdGB couplings $\alpha \equiv \alpha_{\text{GB}}/M_{\odot}^2 = 0, 1$ and 2 [82]. The upper and lower sets of curves refer to the polytropic EOS DI-II [553] and to an approximation of EOS FPS [554], respectively.

below), (3) the CS corrections to the quadrupole moment and (4) the mass and angular momentum shifts induced by rotation at second order in the spin. The mass shift is always negative, while the quadrupole moment deformation is always positive.

4.5. Lorentz-violating theories

Static, spherically symmetric NS solutions in Einstein-Æther theory were first constructed by Eling *et al* [169] (see also [48, 49, 168, 171]). Figure 21 presents the mass–radius relation in Einstein-Æther theory for various coupling constants and EOSs. The NS mass decreases (at fixed radius) as a function of the coupling constant c_{14} . Spherically symmetric solutions in khronometric theory are identical to those of Einstein-Æther theory [50, 102, 280, 281], therefore the conclusions drawn for Einstein-Æther theory also apply to khronometric theory.

Stringent tests on Lorentz-violating theories come from binary dynamics, which depends on the NS sensitivity (see section 4.9 below). In preparation for a discussion of these tests, it is useful to examine stationary configurations of nonspinning NS solutions in slow motion with velocity v^i with respect to the Æther field.

To be specific, let us consider Einstein-Æther theory. Appropriately choosing a time coordinate⁵³, the metric and Æther-field ansatz read

$$\begin{aligned} ds^2 = & -e^{\lambda(r)} dt^2 + e^{\mu(r)} dr^2 + r^2(d\theta^2 + \sin^2\theta d\varphi^2) \\ & - 2vV(r, \theta) dt dr - 2vrS(r, \theta) dt d\theta + \mathcal{O}(v^2), \end{aligned} \quad (4.19)$$

⁵³ Following the analysis of [49], here we consider a coordinate system that is comoving with respect to the NS fluid elements by aligning the time coordinate vector to the fluid four-velocity U^μ . We adopt asymptotically spherical coordinates in which the velocity direction of the Æther field agrees with the polar axis, and impose invariance under the simultaneous reflection of $v^i \mapsto -v^i$ and $t \mapsto -t$.

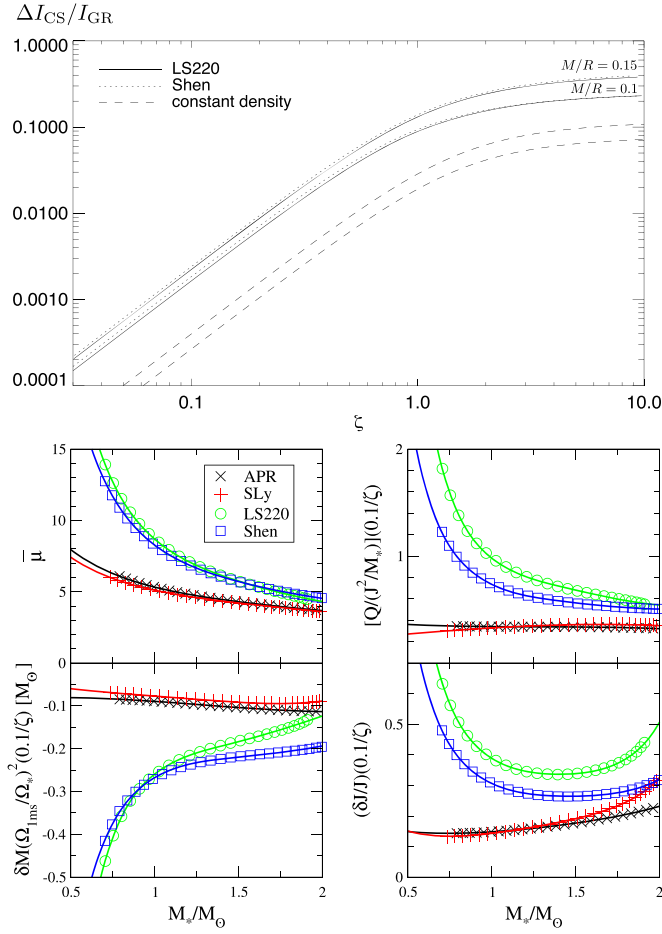


Figure 20. Properties of slowly rotating NSs in dCS gravity. The CS coupling ζ is related to α_{CS} , introduced in equation (2.27), by $\zeta \equiv 4\sqrt{2}\alpha_{\text{CS}}M/R^3$ in the top panel and $\zeta \equiv 4\alpha_{\text{CS}}^2M^2/R^6$ in the bottom panels. Top panel: change in the moment of inertia induced by the CS modification as a function of the CS coupling for two different EOSs and two different values of the NS compactness. The dashed lines show the analytic result for a nonrelativistic constant-density star [45]. Bottom panels: numerical (symbols) and fitted (curve) results for the dimensionless scalar dipole charge $\bar{\mu}$ (top left), the quadrupole correction Q (top right), the mass shift δM (bottom left), and the angular momentum shift δJ (bottom right), as functions of the NS mass M_* . The y-axes are rescaled as explained in [166]. (From [45, 166]).

$$u_\mu = -e^{\lambda(r)/2}\delta_\mu^t - vW(r, \theta)\delta_\mu^r + \mathcal{O}(v^2), \quad (4.20)$$

while the fluid four-velocity $U^\mu = e^{-\lambda(r)/2}\delta_t^\mu$ is the same as the static solution, since we are working in the comoving frame; μ and λ are of zeroth order in velocity, while V , S and W are linear in velocity. We decompose the latter set of functions using Legendre polynomials as $V(r, \theta) = \sum_\ell k_\ell(r)P_\ell(\cos \theta)$, $S(r, \theta) = \sum_\ell s_\ell(r)\frac{dP_\ell(\cos \theta)}{d\theta}$ and $W(r, \theta) = \sum_\ell w_\ell(r)P_\ell(\cos \theta)$ and insert them into the field equations, that reduce to a set of ordinary differential equations. One can show that all modes decouple [49]. Such equations are solved in both the interior and

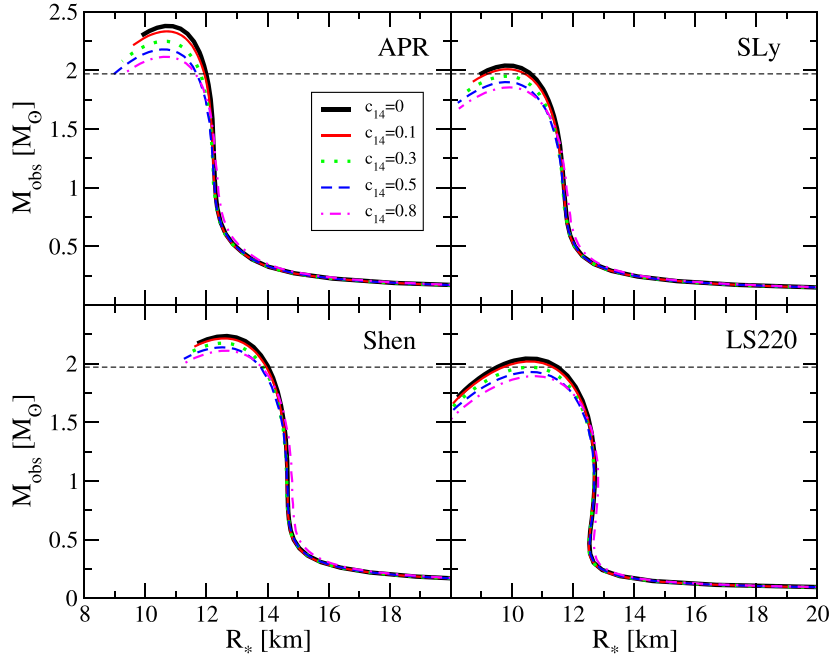


Figure 21. Mass–radius relations in Einstein-Æther theory with various coupling constants and EOS models APR [555] (top left), SLy [556] (top right), Shen [557, 558] (bottom left) and LS220 [559] (bottom right). The thick black curve is the GR result, and the horizontal dashed line corresponds to the lower mass bound from PSR J0348+0432 [551] (see also [550]). (From [49].)

exterior, imposing the matching condition that the solutions should be continuous and differentiable at the NS surface. As discussed in section 4.9, to extract the sensitivities, it is useful to consider the asymptotic behavior of $k_1(r)$ at spatial infinity given by

$$k_1(r) = -1 + A \frac{M}{r} + \mathcal{O}\left(\frac{M^2}{r^2}\right), \quad (4.21)$$

where A is a coefficient that is determined by the matching. In section 4.9 we will show that this coefficient defines the sensitivity in this theory: see equation (4.31).

In section 4.9 we will also discuss NS sensitivities in khronometric theory. In this case, thanks to the additional condition of hypersurface-orthogonality of the vector field, one can eliminate W from the vector field ansatz and repeat the same analysis as in the Einstein-Æther case (see [49] for details).

4.6. Massive gravity and Galileons

There are very few phenomenological studies of NSs in massive gravity. This is probably due to the technical difficulties related to the Vainshtein mechanism: see section 2.6, and [309] for a review. In a nutshell, the helicity-0 graviton mode becomes strongly coupled at distances smaller than the so-called ‘Vainshtein radius,’ a characteristic length scale that depends on both the theory parameters and the source. The Vainshtein effect resolves the vDVZ discontinuity afflicting Fierz–Pauli theory, but the presence of a new scale (which might be parametrically larger than the stellar radius and is much smaller than the Compton wavelength

of the graviton) makes it difficult to obtain nonvacuum solutions without resorting to approximations.

Before the recent developments in nonlinear, ghost-free massive gravity [298], Damour *et al* [560] reconsidered the vDVZ discontinuity problem and its possible resolution through Vainshtein's nonlinear resummation of nonlinear effects. As part of this study, the authors investigated the viability of spherically symmetric stars in a nonlinear version of Fierz–Pauli theory. They found that some solutions show physical singularities, but also that there exist regular solutions interpolating between a modified GR interior and a de Sitter exterior, with curvature proportional to the square of the graviton mass. Another relevant study in this context was performed by Babichev *et al*, who considered the problem of recovering GR from the decoupling limit of the theory in the case of static, spherically symmetric sources [172, 561]. To the best of our knowledge, the only attempt to construct static stellar configurations in full dRGT massive gravity was carried out by Gruzinov and Mirbabayi [173], but phenomenological studies of observational constraints (including stellar rotation and realistic EOSs) are still lacking. In the context of the cubic Galileon model (see section 2.6), in which the Vainshtein mechanism suppresses the scalar field interactions with matter, reference [174] studied nonrelativistic, slowly rotating stars and static relativistic stars, finding that deviations from GR are suppressed at high densities. Spherically symmetric gravitational collapse in Galileon theories was studied in [175, 176].

4.7. Gravity with auxiliary fields

Gravitational theories with auxiliary fields are equivalent to GR in vacuum and only differ from GR in their coupling to matter. Therefore these theories may look like the prototypical example of modified theories of gravity whose phenomenology can be explored using NSs, but not BHs. While this is true, it turns out that it is quite difficult to put observational constraints on these theories, due to a severe degeneracy between the nuclear matter EOS and beyond-GR effects. Furthermore these theories do not violate the SEP, and NSs do not acquire extra charges that could leave an imprint in binary dynamics. For this reason, the very concept of ‘sensitivity’ (discussed in section 4.9 below) is meaningless in these theories. We will now briefly review the literature on NSs in various theories with auxiliary fields.

Palatini $f(\mathcal{R})$. The Palatini formulation of $f(\mathcal{R})$ gravity has been investigated in detail in other respects, but the literature on NS solutions is not very extensive. Most studies dealt with the problem of curvature singularities (a problem shared with EiBI gravity: see [177–181] and below for a unified discussion), but there is no detailed analysis of NS properties in Palatini gravity and of possible strong-field tests. It is reasonable to expect that most of the phenomenology should be at least qualitatively similar to EiBI theory, reviewed below. This is confirmed by the findings of Pani *et al* [197], who showed that Palatini $f(\mathcal{R})$ gravity and EiBI gravity are only two representative examples of a *single* class of theories that modify GR by adding nondynamical fields.

EiBI gravity. Static and slowly rotating NSs in EiBI gravity were constructed in [182], and their phenomenology was studied in [183, 185, 186]. For a given EOS, the maximum mass of equilibrium NS configurations can be twice as large as the corresponding GR model for experimentally viable values of the EiBI parameter. An example of NS properties for a piecewise polytropic EOS [562] that reproduces the FPS EOS is shown in figure 22 (see [183] for details).

Within GR, the FPS EOS is ruled out by observations of NSs with masses $M = (1.97 \pm 0.04)M_{\odot}$ [550] (horizontal band in figure 22) and $M = (2.01 \pm 0.04)M_{\odot}$ [551]. In EiBI gravity the maximum mass of a NS can be much larger than in GR, and observations of high-mass NSs can be accommodated without invoking a stiffer EOS.

An interesting property of EiBI gravity is that, for a given value of κ , no self-gravitating objects can exist above some critical central density ρ_c (or pressure P_c). More specifically, one must have

$$P_c \kappa < 1 \quad \text{for } \kappa > 0, \quad (4.22)$$

$$\rho_c |\kappa| < 1 \quad \text{for } \kappa < 0, \quad (4.23)$$

where P_c and ρ_c are the central pressure and density, respectively [182]. Assuming that NSs can reach central densities $\rho_c \sim 10^{18} \text{ kg m}^{-3}$ and $P_c \sim 10^{34} \text{ N m}^{-2}$, these bounds would constrain the theory, yielding $|\kappa| \lesssim 1 \text{ m}^5 \text{ kg}^{-1} \text{ s}^{-2}$. Avelino [563] derived even stronger constraints, $|\kappa| < R^2$, from the existence of a self-gravitating astrophysical objects of size R . For a typical NS this translates into the bound

$$|\kappa| \lesssim 10^{-2} \text{ m}^5 \text{ kg}^{-1} \text{ s}^{-2}. \quad (4.24)$$

However these constraints are only indicative, because they are based on the (untestable) assumption that matter in the NS core reaches nuclear densities in EiBI gravity (as it does in GR). Furthermore, there is no constraint from causality (see the shaded region in the top-right panel of figure 22) because causality constraints are always satisfied, even for large values of κ . This is due to the existence of a maximum compactness ($M/R \lesssim 0.3$) and it can be understood by looking at the theory's effective stress–energy tensor [329].

Sham *et al* [189] studied the radial stability of relativistic stars in EiBI. Sotani [190] investigated nonradial oscillations in the Cowling approximation, finding that the observation of the fundamental mode frequency may be used to distinguish EiBI gravity from GR if the coupling is sufficiently large. Because of the peculiar nonlinear coupling to matter, exotic star-like solutions (such as pressureless stars [182, 183], wormholes [564] and geons [327]) exist in this theory. Furthermore (for $\kappa > 0$) the Chandrasekhar limit $M \lesssim 1.4M_{\odot}$ on the mass of white dwarfs is replaced by a minimum radius condition [183]: $R_{\text{WD}} > \sqrt{3\kappa/(16\pi)}$.

Pani *et al* [183] studied nonrelativistic stellar collapse in EiBI, finding that for any $\kappa > 0$ the final state of the collapse is a pressureless star (instead of a singularity, as in GR). No relativistic simulations of collapse in the full theory are available to date.

Degeneracy between NS EOS and nonlinear matter coupling. The degeneracy between beyond-GR effects and uncertainties in the NS EOS is an intrinsic limitation in our ability to carry out precision tests of gravity with NS observations. Uncertainties in the EOS often translate into uncertainties in macroscopic observables (such as masses, radii or oscillation frequencies) which are larger than putative deviations from GR. This is usually the case for theories (such as scalar–tensor theory) that are well constrained in the weak-field limit.

Because gravitational theories with auxiliary fields are essentially unconstrained in the weak-field limit, and they only modify GR in their coupling to matter, NSs may look like ideal laboratories to constrain them. Unfortunately, in this case GR modifications are ‘maximally degenerate’ with EOS uncertainties. The reason is that these theories do not contain extra dynamical fields, so the right-hand side of the gravitational field equations (2.61) can be interpreted as the stress–energy tensor of an ‘effective’ fluid with a contrived EOS. In particular, Delsate *et al* [329] proved analytically that EiBI gravity coupled to a perfect fluid is *equivalent* to GR with an ‘effective’ perfect fluid stress–energy tensor. If the original $T_{\mu\nu}$

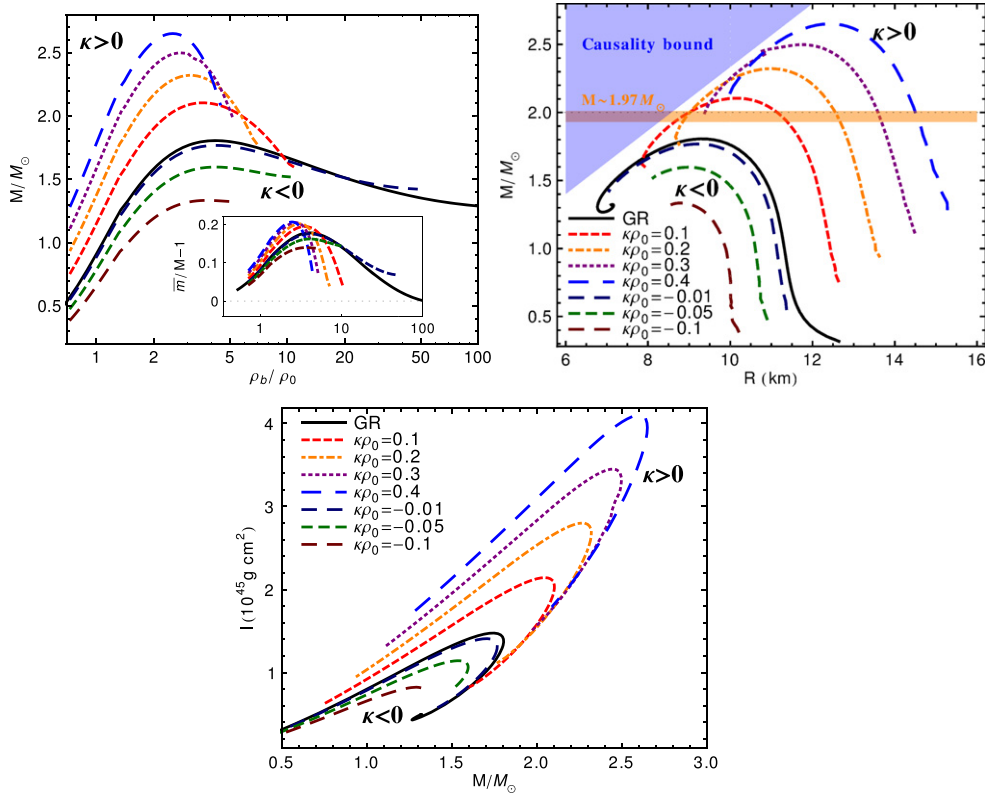


Figure 22. Compact stars in EiBI theory constructed using the FPS EOS and different values of the EiBI parameter κ (see equation (2.55)). Top-left panel: mass as a function of the central baryonic density ρ_b (inset: binding energy as a function of ρ_b). Top-right panel: mass–radius relation. Bottom panel: moment of inertia as a function of the stellar mass. The central density and coupling constant are normalized by the typical density of nuclear matter, $\rho_0 = 8 \times 10^{17} \text{ kg m}^{-3}$. Curves terminate when either condition (4.22) or (4.23) are not fulfilled, and self-gravitating objects can not exist. In the top-right panel, a horizontal band corresponds to the maximum observed NS mass $M \simeq 2M_\odot$ [550, 551], whereas the shaded region ($R \gtrsim 2.9M$) is excluded by causality [514]. (Adapted from [183].)

satisfies the energy conditions usually imposed in GR, the same is not necessarily true for the effective stress–energy tensor. For this reason the singularity theorems of GR do not apply [329], and theories with auxiliary fields have singularity-avoidance properties. The intrinsic ambiguity between modifications in the gravitational coupling and variations in the EOS makes it difficult (if not conceptually impossible) to constrain these theories.

Curvature singularities. Palatini $f(\mathcal{R})$ gravity and EiBI gravity are experimentally viable theories passing all weak-field tests. However, it has been pointed out that their peculiar coupling with matter might lead to the appearance of curvature singularities at the surface of macroscopic objects, where large gradients are present⁵⁴ [179, 184, 197]. The root of the

⁵⁴ As discussed in section 2.7, Palatini $f(\mathcal{R})$ gravity may be affected by other pathologies, including potential conflicts with the standard model [333] and issues with averaging in cosmology [333, 335]. These problems are still debated (see [199] for a review), but they cast serious doubts on the viability of this class of theories.

problem lies in the fact that equation (2.61) contains third-order derivatives of the matter fields. This is in contrast to GR, where at most first derivatives of the matter fields appear on the right-hand side of Einstein's equations.

This different structure is also evident in the Newtonian limit of the theory. The solution of the modified Poisson equation (2.60), $\Phi = \Phi_N + 2\pi\kappa\rho$, shows that the gravitational potential Φ is algebraically related to ρ . Any matter configuration which is discontinuous or just not smooth enough will produce discontinuities in the metric, as well as singularities in the curvature invariants that depend on the second derivatives of Φ , and ultimately lead to unacceptable phenomenology [179, 180, 184, 330]. For example, the Ricci curvature R of a self-gravitating barotropic perfect fluid would depend on the second derivatives of the pressure field, whereas in GR it simply reads $R = 8\pi(\rho - 3P)$. If the function $P(r)$ is continuous but not differentiable at the stellar surface, then $P'(r)$ would be discontinuous at the radius and $P''(r)$ would introduce an unacceptable Dirac-delta contribution to the curvature. This was shown explicitly in [179, 184] by assuming a polytropic EOS near the stellar surface: for rather standard values of the polytropic index, the scalar curvature is actually *divergent* near the NS radius due to the presence of higher-order derivatives of the matter fields. Strong deviations from GR are expected when the curvature becomes unbound near the stellar surface. For example, surface singularities would give rise to tidal forces which can be orders of magnitude larger than in Einstein's theory. This and other consequences of curvature singularities in theories with auxiliary fields are discussed in [179, 180, 184, 197, 330].

The appearance of curvature singularities may look like a fatal blow for these theories, but there is some controversy surrounding this issue. Kainulainen *et al* [178] criticized the analysis of Palatini $f(\mathcal{R})$ gravity carried out in [179], whereas [180, 330] argued that the original analysis is essentially correct. Olmo [181] showed that in a prototypical Palatini theory with $f(\mathcal{R}) = \mathcal{R} + \lambda\mathcal{R}^2$, where λ is of the order of the Planck length squared, the curvature invariant grows only at extremely small densities, so that the theory is practically viable (but in this case the macroscopic properties of NSs are indistinguishable from their GR counterparts, and no interesting phenomenology can be probed with astrophysical observations). Finally, Kim [332] pointed out that strong tidal forces near the stellar surface can modify the effective EOS in such a way that curvature singularities are removed. This result suggests that the gravitational backreaction on the matter dynamics can modify the effective description of the fluid. Further analysis is needed to test the generality of this conclusion and the viability of these theories.

4.8. Strong-field tests of gravity with universal relations in NSs and quark stars (QSs)

NSs and QSs are, in principle, excellent laboratories to test strong-field gravity [8, 565]. However, the EOS of matter prevailing in the interior of NSs and QSs is poorly known, and this poses an immediate difficulty if we want to probe the nature of gravity with observations of compact stars. Measurable macroscopic properties of these objects (such as the mass–radius relation) are sensitive to both the EOS and the underlying gravitational theory. Even if we could measure NS masses and radii with a precision comparable to the deviations induced by gravitational physics beyond GR, constraints on modifications of GR would demand a knowledge of the EOS that is currently unavailable. Recently, Yagi *et al* [27, 167] have shown that it is possible to use certain nearly universal (i.e., almost EOS-independent) relations between macroscopic observable properties of NSs to break this degeneracy and carry out test of strong-field gravity without prior detailed knowledge of the high-density EOS.

I–Love–Q and ‘three-hair’ relations in GR. Various nearly universal relations are known to hold in GR. For example, relations among NS oscillation mode frequencies and certain combinations of the NS mass and radius were found and discussed in [382, 529, 566, 567], and they were later extended to the case of rapid rotation in [568, 569]. Lau *et al* [570] found universal relations between the NS moment of inertia and oscillation frequencies. Ravenhall and Pethick [571] first proposed a possible relation between the moment of inertia and the stellar compactness $C = M/R$. Subsequently, more accurate relations were found in [552, 572, 573]. A relation between the quadrupole moment and the compactness for NSs and QSs was reported in [574]. A functional relation between the NS binding energy and the compactness was found in [575], confirmed in [576] and refined in [572]. For rotating stars, the mass-shedding (Keplerian) frequency was found to be related to the compactness of nonrotating equilibrium models in [513]. This relation was confirmed in [577], where the authors pointed out an additional relation between the equatorial radius for rotating configurations and the radius for nonrotating configurations.

Yagi and Yunes [27, 167] found new universal relations among macroscopic quantities that characterize slowly and uniformly rotating unmagnetized NSs and QSs. If M is the mass of a nonrotating model and $\chi = J/M^2$ the dimensionless spin of the star, the universal relations connect the following three quantities: the normalized moment of inertia $\bar{I} = I/M^3$, the normalized tidal Love number (a measure of stellar deformability) $\bar{\lambda} = \lambda/M^5$ and the normalized quadrupole moment $\bar{Q} = -Q/(M^3/\chi^2)$. For example, figure 23 shows the ‘I–Love’ relation. These ‘I–Love–Q’ relations are remarkably independent of the EOS—more so than the relations listed earlier⁵⁵.

Pappas and Apostolatos [28] studied the relation between the NS current octupole and mass quadrupole moments and found that it is insensitive to both, the EOS and the NS spin. Stein *et al* [586] confirmed and extended this finding by investigating relations among multipole moments for uniformly rotating, Newtonian polytropes, under the additional assumption that the isodensity contours are self-similar ellipsoids [587]. They found the following ‘Newtonian three-hair relation’ for the mass-multipole moments M_ℓ and the current-multipole moments S_ℓ :

$$M_\ell + i\frac{q}{a}S_\ell = \bar{B}_n \lfloor \frac{\ell-1}{2} \rfloor M_0 (iq)^\ell, \quad (4.25)$$

where $a \equiv S_1/M_0$, $iq \equiv \sqrt{M_2/M_0}$, $\lfloor x \rfloor$ stands for the largest integer that does not exceed x , and the $\bar{B}_n \lfloor \frac{\ell-1}{2} \rfloor$ ’s are constant coefficients determined by solving (in general numerically) the Lane–Emden equation. Equation (4.25) states that, given a polytropic EOS, all multipole moments are functions of the first three moments—namely the mass, spin and quadrupole moment. It is an approximate generalization of the BH no-hair relation [424], $M_\ell + iS_\ell = M_0 (ia)^\ell$, which states that all multipole moments of a stationary and axisymmetric (uncharged) BH in GR can be expressed in terms of its mass and spin.

⁵⁵ Several works relaxed some of the assumptions made in the original papers. The universality was first confirmed in [580] using a wider range of EOSs. Maselli *et al* [421] studied the I–Love relations for merging binary NSs, finding small deviations ($\sim 10\%$) from the relations that are valid for isolated NSs. Haskell *et al* [581] found that universality holds also for magnetized NSs, as long as the magnetic fields are smaller than $\sim 10^{12}$ G and the spin periods smaller than 0.1 s. Doneva *et al* [582] relaxed the slow-rotation approximation. Using the RNS code [583], they found that the I–Q relation is spin-dependent, and that for a fixed spin frequency, the universality only holds for a subclass of NS EOSs, concluding that the universality is lost for rapidly rotating NSs and QSs. However, subsequent work [28, 29, 584] showed that the universality is still preserved for fixed *dimensionless* spin parameters. Finally, Martinon *et al* [585] investigated universality for the nonbarotropic EOSs typical of proto-NSs. Deviations from universality can be as large as $\sim 30\%$ in the early stages of NS formation, but they decrease as soon as the entropy gradients smooth out.

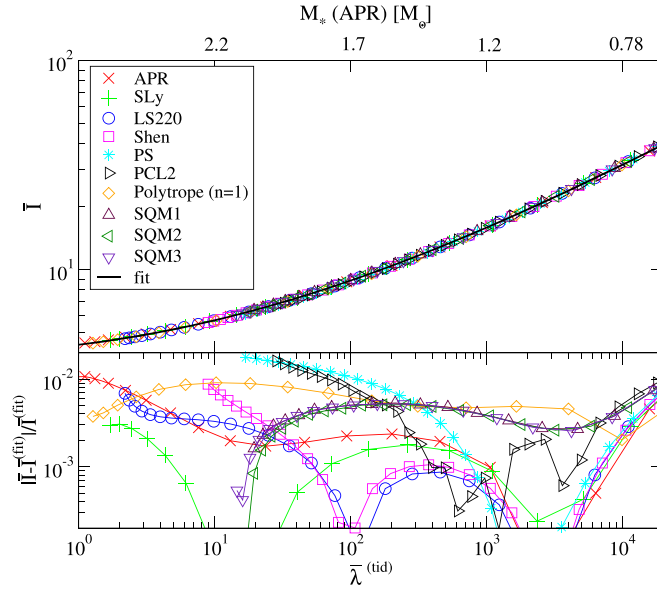


Figure 23. (Top) Universal relation between the dimensionless moment of inertia \bar{I} and the dimensionless tidal Love number $\bar{\lambda}^{(\text{tid})}$ for various EOSs (APR [555], SLy [556], LS220 [559], Shen [557, 558], PS [578], PCL2 [579] and the $n = 1$ polytropic EOS for NSs; SQM1-3 [579] for QSs), together with a fitting curve (solid). The top x-axis shows the corresponding NS mass for the APR EOS. The parameter varied along each curve is the NS or QS central density, or equivalently the stellar compactness, with the latter increasing to the left of the plots. (Bottom) Fractional errors between the fitting curve and numerical results. The EOS-independence holds within a few percent accuracy. (From [27].)

The dashed curves in the top panel of figure 24 show that this relation is EOS-independent to better than 10% accuracy for low-order multipoles ($\ell \leq 10$). Reference [588] showed that the relation also applies to Newtonian stars with piecewise polytropic EOSs (a good approximation to realistic NS EOSs [562]) and derived a purely analytic relation (solid curves in the top panel of figure 24) by perturbing $n = 0$ polytropes and using the perturbed Lane–Emden solution in [589]. The analytic relation approximates numerical results within $\mathcal{O}(1)\%$ accuracy, as shown in the bottom panel of figure 24. The validity of three-hair relations was confirmed in the relativistic regime up to hexadecapole order for both NSs and QSs [29], and its origin was investigated in [590].

The I–Love–Q relations and their generalizations to higher multipoles have various interesting applications. Any astrophysical measurement of either \bar{I} , $\bar{\lambda}$ or \bar{Q} will automatically yield the other two quantities, regardless of the uncertainty in the EOS. For instance, the tidal Love number λ may be measured with future GW observations (see section 7.4.1), and such a measurement would give information on I and Q . On the nuclear physics front, the universal relations allow us to break degeneracies among parameters in NS observations. For example, Psaltis *et al* [591] showed that the x-ray pulse profile emitted by hot spots on the NS surface depends not only on the NS mass and radius, but also on its moment of inertia, quadrupole moment, eccentricity, etcetera. By using the universal relations reported in [592], including the I–Q relation, one can eliminate some of the model parameters. This breaks degeneracies in parameter estimation and may allow future x-ray satellites such as NICER [593] and LOFT

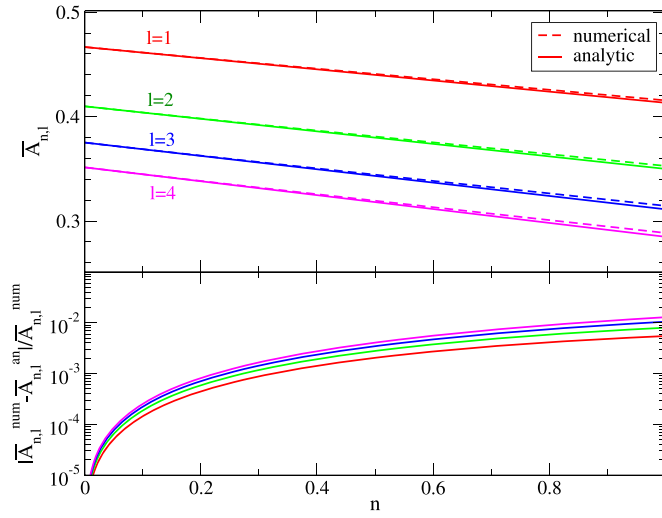


Figure 24. Top inset: $\bar{A}_{n,\ell} \equiv (\bar{B}_{n,\ell})^\ell$, where $\bar{B}_{n,\ell}$ represents the coefficient of the three-hair relation in equation (4.25), is plotted against the polytropic index n . Dashed lines are numerical solutions of the Lane–Emden equation; solid lines are analytic, perturbed Lane–Emden solutions around $n = 0$. Observe that $\bar{A}_{n,\ell}$ only changes by less than 10% from $n = 0$ to $n = 1$. Bottom inset: fractional differences between the numerical and analytic relations. The analytic result is within $\mathcal{O}(1)\%$ of the numerical result even for $n = 1$. (From [588].)

[429, 594] to measure the NS mass and radius within $\sim 5\%$ accuracy [519], as long as systematic errors are under control [595].

Universal relations in other theories of gravity and tests of GR. In the context of this review, the I–Love–Q and ‘three-hair’ relations are interesting because they can break the degeneracy between the uncertainties in nuclear and gravitational physics, and allow us to perform strong-field tests of gravity with NSs. Since in general the relations depend on the underlying gravitational theory (but see below for caveats), if one can measure *any two* of the I–Love–Q quantities independently, one can in principle perform a model-independent consistency test of GR or test a specific alternative theory [27]. Model-independent tests can also be obtained by measuring the first four multipole moments, i.e., mass, angular momentum, mass quadrupole and spin octupole [28].

As an example, [27, 167] studied the I–Love–Q relations in dCS gravity [83, 258, 596], whose action is given by equation (2.27). Corrections to the NS moment of inertia and quadrupole moment were calculated in [45, 165] and [166] by constructing slowly rotating NS solutions in dCS gravity that are valid to linear and quadratic order in the spin, respectively (the $\ell = 2$ electric tidal Love number is the same as in GR [549]). Yagi *et al* [27, 167] found that an EOS-independent I–Q relation holds in dCS gravity for a fixed $\xi^{\ell/4}/M_*$ (where $\xi \equiv 4\alpha_{\text{CS}}^2$ in the notation of equation (2.27)), as shown in the left panel of figure 25, and that this relation generally differs from GR. The dCS relation shown in figure 25 is the marginally allowed case, corresponding to $\xi^{\ell/4} = 1.85 \times 10^4 M_*$: this constraint is six orders of magnitude stronger than the current best bound from Solar System and table-top experiments [45, 85].

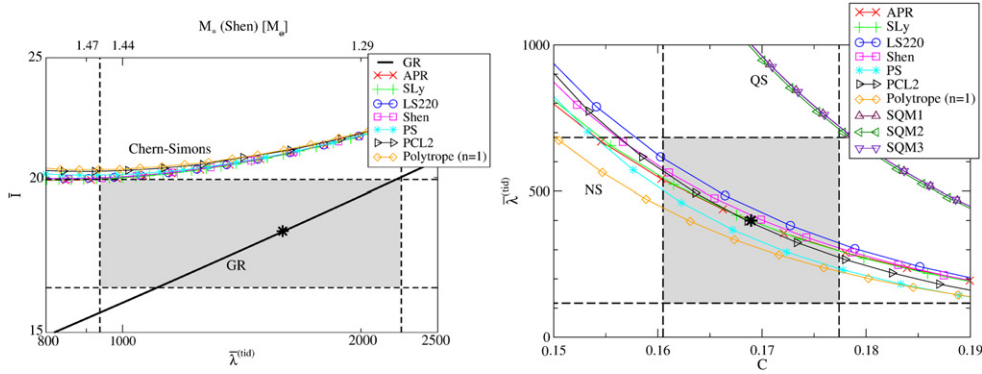


Figure 25. Left panel: the I–Love relation in dCS gravity for various EOSs. The shaded region represents a hypothetical error box in the I–Love plane resulting from independent measurements of the moment of inertia and of the tidal Love number (the black asterisk marks the hypothetically measured values). The black solid line shows the I–Love relation in GR. The top axis shows the NS mass M_* for the Shen EOS. An alternative theory is consistent with the measurement only if the modified I–Love relation passes through the error box. Right panel: Love–compactness relation in GR for various EOSs. The shaded region represents a hypothetical measurement error box in the Love–compactness plane. Different NS EOSs are consistent with the error box, and therefore it may be possible to carry out tests of GR (this conclusion does not apply to QSs). (From [27].)

This hypothetical test would not be so constraining for other theories of gravity. For example, Sham *et al* [597] calculated universal I–Love–Q relations (as well as similar relations involving f -mode oscillation frequencies) in EiBI gravity [198], finding that they are almost the same as in GR. The reason is that, in this theory, modified-gravity effects are equivalent to modifying the EOS within GR [329], and we already know that the relations are insensitive to the EOS.

Pani and Berti [120] studied the I–Love–Q relations using an extension of the Hartle–Thorne formalism [522, 523] to scalar–tensor theories. Working at second order in the spin, they focused on theories that allow for spontaneous scalarization [26, 116, 540–542]. As shown in figure 26, they found that the universal relations hold also in these theories, but they are essentially indistinguishable from the GR relations for values of the coupling parameters consistent with binary pulsar observations, even when spontaneous scalarization occurs. Doneva *et al* [123] extended this work to rapidly rotating stars, showing that deviations in the I–Q relation get larger for fast rotation rates. If one considers theory parameters that are consistent with observations, these deviations are still too small to discriminate GR from scalar–tensor theories with spontaneous scalarization via I–Love–Q-type tests. In [598], Pappas and Sotiriou extended the formalism of Geroch and Hansen [423, 424], providing a way to define and compute multipole moments of stationary, asymptotically flat spacetimes in scalar–tensor gravity. This approach may allow us to look for deviations from the three-hair relations in scalar–tensor theories of gravity, and, if such deviations occur, to use them as a tool to discriminate these theories from GR.

Reference [82] found a universal I–Q relation for rapidly rotating NSs in EdGB gravity, that is shown in figure 27 for a fixed dimensionless angular momentum $\chi \equiv J/M^2 = 0.4$. The figure shows that the EOS dependence in EdGB theory is (once again) weak: the relation remains similar to GR even for a theory which is marginally ruled out ($\alpha = 2$).

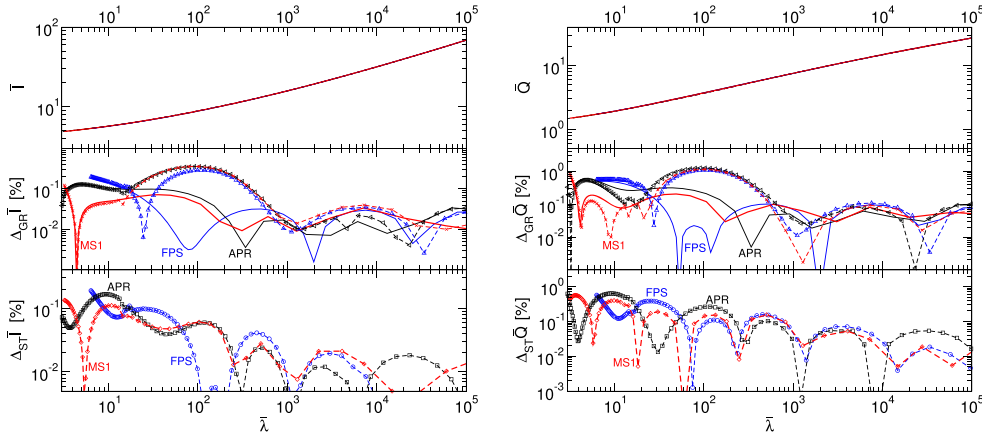


Figure 26. EOS-independent relations $\bar{I}(\bar{\lambda})$ (left) and $\bar{Q}(\bar{\lambda})$ (right). Solid linestyles refer to GR; dashed linestyles, to scalarized stars in a scalar–tensor theory that is only marginally allowed by current binary pulsar tests. In each panel, the top inset shows the relation itself; the middle and bottom insets show deviations from universality, as measured by the residual $\Delta X = 100[X/X_{\text{fit}} - 1]$. $\Delta_{\text{GR}}X$ means that the universal relation is obtained by fitting only pure GR solutions; $\Delta_{\text{ST}}X$ means that the fit is obtained only from scalarized solutions. The top panels show that both residuals are always smaller than 2%, and typically smaller than 1%, for scalar–tensor theories that are marginally ruled out by binary pulsar observations. (From [120].)

Staykov *et al* [158] constructed slowly rotating equilibrium models of NSs and strange stars (i.e., compact stars made up of deconfined up, down and strange quarks) in $f(R)$ gravity at first order in a slow-rotation approximation. For large values of the coupling parameter of the theory, the NS moment of inertia can be up to 30% larger than its GR counterpart. This deviation is much higher than the induced change in the maximum mass, and this allows for a breaking of the EOS degeneracy.

Other universality relations and tests of GR. Other universal relations besides the I–Love–Q relations can be used, in principle, to test GR. One approach is to consider the relation between the tidal Love number and the NS compactness C originally found in [599–601], as shown in the right panel of figure 25. This relation is not as EOS-independent as the I–Love–Q relations, but it can be treated as effectively universal if the EOS variation is smaller than the observational errors on the Love number and on the compactness. Such a relation can be more useful than the I–Love relation, as it may take more than 10 years to measure I from double binary pulsar observations [602], while the NS compactness (or the mass and radius) have already been constrained using type-I x-ray bursters with photospheric radius expansion [515, 516, 603–609] and thermal spectra from transient low-mass x-ray binaries [516, 610–625]. Assume that the tidal Love number can be measured to 75% accuracy with future GW observations (see section 7.4.1), and assume in addition that the NS compactness is measured to 5% accuracy with future x-ray observations by, e.g., NICER [593] or LOFT [429, 594]. One can then draw an error box in the Love-compactness plane, similar to that in the I–Love case (see the right panel of figure 25). The EOS-induced variation is smaller than this hypothetical error box, while the QS relation lies outside of the error box, suggesting that the relation is effectively universal for NSs. Then a specific modified theory of gravity can be

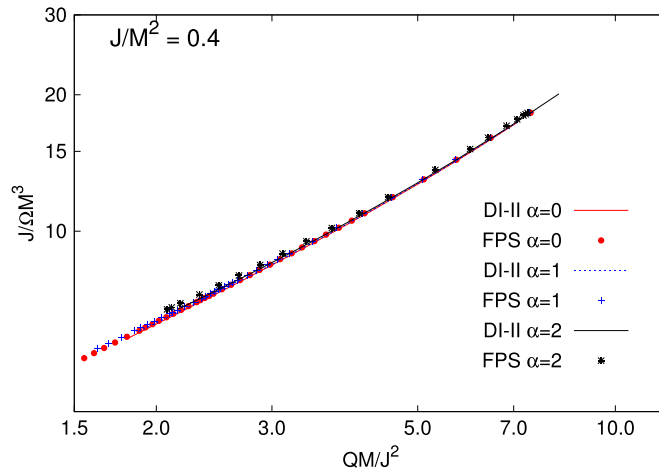


Figure 27. The universal relation between the (scaled) moment of inertia and quadrupole moment for rapidly spinning NSs with angular momentum $J = 0.4 > M^2$ in EdGB gravity using two different EOSs, namely DI-II EOS [553] and an approximation to the FPS EOS [554]. (From [82].)

ruled out (at least in principle) if the Love-compactness relation in that theory is inconsistent with the error box.

The tidal Love number λ discussed so far is, in technical jargon, the $\ell = 2$, electric-type Love number. Other Love numbers exist, including the so-called magnetic-type and shape Love numbers [599, 626, 627]. Yagi [628] found additional universal relations among different types of Love numbers. In principle these relations can be used to test GR, but in practice it seems very difficult to measure any two Love numbers independently from future GW observations, even if one considers third-generation interferometers such as the Einstein Telescope (ET) [629–632]. Chan *et al* [633] studied multipolar universal relations among the NS f -mode frequency f_ℓ and the electric-type tidal Love number $\lambda_{\ell'}$. They found that the universality is stronger for $\ell = \ell'$ than $\ell \neq \ell'$.

Another proposal is to use a universal relation between the radius of a $0.5M_\odot$ NS and the neutron skin thickness of ^{208}Pb [634] to constrain certain modified theories of gravity. Sotani [187] showed that the GR and EiBI relations are distinguishable if the radius of such low-mass NSs is measured with an accuracy of a few percent.

4.9. NS sensitivities in modified gravity

In preparation for our discussion of the dynamics of compact binaries, that will be the main topic of section 5, we conclude this section with a brief introduction to the so-called ‘sensitivities’ of extended self-gravitating objects in modified gravity.

In many extensions of GR the SEP is violated due to the presence of additional fields that mediate the gravitational interaction. Self-gravitating objects (and in particular compact objects) are not test particles, and violations of the SEP imply that the local value of the gravitational constant depends on the additional dynamical field(s). When self-gravitating bodies move in regions of spacetime where the extra fields are not constant, their internal gravitational energy, and therefore their total mass–energy, will change.

This effect can be described by endowing extended bodies in modified gravity with a macroscopic property (the ‘sensitivity’) measuring how the body’s internal energy depends

on the additional field(s) [228]. The sensitivity can be expected to be larger (and more relevant for, e.g., binary dynamics) for compact objects, such as NSs, because their self-gravity is stronger.

Scalar–tensor theories. How can we represent the stress–energy tensor for an extended object in scalar–tensor theories? Eardley [228] showed that it can be modeled as a normal point-particle stress–energy tensor, as long as we promote the (constant) mass of each body to a function of ϕ : $M_A = M_A(\phi)$.

More precisely, in order to describe the orbital dynamics of a widely separated binary system perturbatively in the size-to-separation ratio, it is useful to integrate out length scales smaller than the size of the bodies. We obtain an EFT in which the bodies are represented by point particles, whose dynamics are governed by an effective matter action

$$S_m = \sum_A \int_{\Gamma_A} \mathcal{L}_A ds_A. \quad (4.26)$$

Here A is an index that labels the bodies, Γ_A is the world-line of body A , and ds_A is the differential arclength along it. The effective Lagrangian \mathcal{L}_A encodes information about the internal structure of body A , and admits a derivative expansion

$$\mathcal{L}_A = -M_A(\phi) + \dots, \quad (4.27)$$

where the leading-order term describes the dependence of the mass–energy on the local scalar value, and subleading terms are discussed in the appendix of [538]. For bodies with negligible gravitational binding energy $M_A(\phi)$ is independent of ϕ , and so equation (4.26) reduces to the action of a collection of test particles, which move along geodesics of the Jordan-frame metric.

As will be discussed in section 5, the theoretical predictions for the orbital dynamics and emission of radiation in compact binaries depend on $M_A(\phi_0)$ and successive derivatives $M_A^{(k)}(\phi_0)$, where ϕ_0 is the asymptotic value of ϕ far away from the binary system. In particular, the sensitivity of body A is defined as

$$s_A \equiv \left(\frac{d \ln M_A(\phi)}{d \ln \phi} \right)_{\phi=\phi_0}. \quad (4.28)$$

Higher-order derivatives of $M_A(\phi)$ are used to define higher-order sensitivities, e.g. s'_A and s''_A .

The first detailed calculation of the NS sensitivities in scalar–tensor theories was carried out by Zaglauer [132]. The sensitivities are related to the gravitational binding energy, and therefore they depend on the microphysics of the specific self-gravitating object we consider. For ordinary stars and for white dwarfs the sensitivities are of order $\approx 10^{-6}$ and $\approx 10^{-4}$, respectively, because the gravitational binding energy of these objects is small. For compact objects (such as NSs and QSs) the sensitivities can be of the order of 0.1, and nonlinear phenomena (like spontaneous scalarization) can even produce arbitrarily large sensitivities. A special case are BHs: their mass in the Einstein frame is constant [39, 57], so BH sensitivities are constant for a given scalar–tensor theory ($s_{\text{BH}} = 1/2$ in Bergmann–Wagoner theories).

Quadratic gravity. Just like scalar–tensor theories, also quadratic gravity theories generically violate the SEP, and this violation can be described in terms of sensitivities. Due to an effective coupling between the matter fields and the scalar field, the observable NS properties depend on the local value of the scalar field near the object.

Yagi *et al* [166, 549] computed the sensitivities of compact objects in dCS theory. An important qualitative difference with scalar–tensor theories consists in the fact that in quadratic gravity BHs can carry a nontrivial scalar charge. BHs in dCS gravity have hair (and a nontrivial sensitivity) only if they are spinning; in EdGB gravity, this happens even for static BHs. On the other hand, the sensitivity of nonspinning NSs in EdGB gravity is vanishing, as argued at the beginning of section 4.4 (see appendix A of [549] for details). This is another example of how scalar–tensor theories and quadratic gravity are in some sense ‘orthogonal’ in the context of the structure and dynamics of compact objects.

The sensitivity (more precisely, the rescaled scalar dipole charge $\bar{\mu}$: see [166] for definitions and more details) of spinning NSs in dCS theory is shown in the top inset of the bottom-left panel of figure 20. To the best of our knowledge, the analogous calculation for spinning NSs in EdGB gravity is not available in the literature at the time of writing.

Lorentz-violating theories. In Lorentz-violating theories the sensitivities (also known as \mathcal{A} ether or khronon ‘charges’) characterize the amount of violation of the SEP due to the effective coupling between matter and the \mathcal{A} ether or khronon field in the strong-gravity regime. Due to this coupling, the compact object’s structure, binding energy and gravitational mass will be functions of the motion relative to the \mathcal{A} ether or khronon. The action describing the motion of a strongly gravitating body with gravitational mass \tilde{m} is given, in the point particle approximation, by [635]

$$S_{\text{pp}} = - \int d\tau \tilde{m}(\gamma) = -\tilde{m} \int d\tau \left\{ 1 + \sigma(1 - \gamma) + \mathcal{O}[(1 - \gamma)^2] \right\}, \quad (4.29)$$

where $\gamma \equiv u_\mu U^\mu$ represents the Lorentz factor of the body relative to the \mathcal{A} ether, and $d\tau$ is the proper time along the particle’s trajectory. In the second equality, we performed a slow-motion PN expansion with $\gamma \ll 1$ and $\tilde{m} \equiv \tilde{m}(1)$. The sensitivity parameter σ is defined by

$$\sigma \equiv - \left. \frac{d \ln \tilde{m}(\gamma)}{d \ln \gamma} \right|_{\gamma=1}. \quad (4.30)$$

For weakly gravitating objects, $\sigma \approx 0$. More in general, [48, 49] showed that the sensitivity of a star, whatever its compactness, can be extracted from the asymptotic behavior of the metric describing the star to *first* order in a perturbative expansion in the velocity relative to the \mathcal{A} ether or khronon. These *slowly moving* stellar solutions have been discussed in section 4.5, and it is possible to show that the sensitivities can be mapped to the parameter A appearing in those solutions (see equation (4.21)). Indeed, one can show that the sensitivity in Einstein- \mathcal{A} ether theory is

$$\sigma_{\mathcal{A}} = \frac{2c_1(2A - 4 - \alpha_1^{\mathcal{A}})}{c_-(8 + \alpha_1^{\mathcal{A}})}, \quad (4.31)$$

while in khronometric theory one has

$$\sigma^{\text{kh}} = \frac{2A - 4 - \alpha_1^{\text{kh}}}{8 + \alpha_1^{\text{kh}}}. \quad (4.32)$$

Here $\alpha_1^{\mathcal{A}}$ and α_1^{kh} are the weak-field PPN parameters given in terms of the theory’s coupling constants (see section 2.5). In the weak-field limit, one can show that the sensitivity scales as [635]

$$s_{\mathcal{E}}^{\text{wf}} = \left(\alpha_1^{\mathcal{E}} - \frac{2}{3} \alpha_2^{\mathcal{E}} \right) \frac{\Omega}{M} + \mathcal{O} \left(\frac{\Omega^2}{M^2} \right) \quad (4.33)$$

in Einstein-Æther theory, where Ω denotes the gravitational binding energy. One obtains a similar expression in khronometric theory by replacing $\alpha_{1,2}^{\mathcal{E}}$ with $\alpha_{1,2}^{\text{kh}}$.

The top-left panel of figure 28 presents the sensitivity as a function of the NS compactness for various EOSs [48, 49]. We also show the weak-field sensitivity for the APR EOS, as defined in equation (4.33). The PPN parameters $\alpha_{1,2}^{\mathcal{E}}$ are chosen to saturate the Solar System bounds, and the plot assumes $c_+ = c_- = 10^{-4}$. The bottom-left panel shows the fractional difference between the sensitivity defined in equation (4.31) and the weak-field sensitivity for each EOS: the two tend to the same limit for small compactness, and their fractional difference is of $\sim 20\%$ at most in the large-compactness limit. Observe also that the relation between the NS sensitivity and compactness is insensitive to the EOS. Similarly, the right panels of figure 28 present the NS sensitivity (and the fractional difference from the weak-field limit), with the PPN parameters $\alpha_{1,2}^{\text{kh}}$ again chosen to saturate the Solar System constraints, and $\beta = 10^{-4}$. As in Einstein-Æther theory, the weak-field and strong-field sensitivities have a common limit as the compactness decreases, but in the large-compactness regime their fractional difference can exceed 100%. The relation between the NS sensitivity and compactness in khronometric theory is also insensitive to the EOS.

4.10. Open problems

For the reader's convenience, here we list some important open problems in the context of strong-field tests of gravity using NSs:

- Except for a few special cases, the properties of NSs in the most general scalar–tensor theory with second-order equations of motion (Horndeski gravity) have not been explored, even in the static case.
- As discussed in section 4.3, the very existence of compact stars in $f(R)$ gravity is still a matter of debate. The generic consensus seems to be that while it is hard to construct NS equilibrium configurations in $f(R)$ gravity from a numerical point of view, there is no fundamental obstacle to their existence (but see [636] for a different point of view). Either way, NS configurations with realistic values of the physical parameters have never been constructed in viable $f(R)$ models.
- There are no calculations of fast-rotating NSs in dCS gravity.
- NS sensitivities have been computed only in scalar–tensor theories, quadratic gravity and Lorentz-violating theories, but not in other theories (such as massive gravity theories).
- Despite the vast literature on the Vainshtein effect, there is essentially no phenomenological study of NSs in massive gravity and Galileon theories, even for static models.
- Gravitational collapse in scalar–tensor theories has been considered under very idealized assumptions for the microphysics. Relativistic gravitational collapse in quadratic gravity has not been studied yet. The analysis of relativistic collapse in EiBI gravity and Palatini $f(\mathcal{R})$ gravity is crucial to clarify the issue of BH formation and singularity avoidance of these theories.
- The appearance of curvature singularities near the surface of macroscopical objects [179, 180, 184, 197, 330] in theories with auxiliary fields might be avoided using the arguments put forward in [332], but it is important to understand whether such effects are generic, and to devise tests to discriminate these theories from GR.

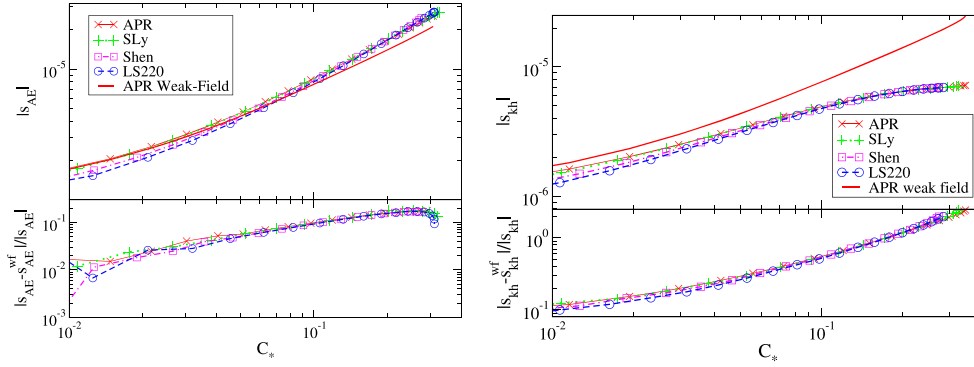


Figure 28. (Left) The top panel shows the absolute magnitude of the NS sensitivity in Einstein-Æther theory against the NS compactness for various EOSs, together with the weak-field expression in equation (4.33) with the APR EOS. The bottom panel presents the fractional difference between the sensitivity and the weak-field expression in equation (4.33). The PPN parameters α_1^E and α_2^E saturate the Solar System constraint, and $c_+ = c_- = 10^{-4}$. Observe that the weak-field result becomes inaccurate for realistic NS compactnesses, and that the relation is EOS-insensitive. (Right) Same as the left panels, but for khronometric theory with $\beta = 10^{-4}$. (From [49].)

- Studies of universal relations for NSs and QSs are not complete, even within GR. For example, there are no studies for differentially rotating stars. The experimental interest of differential rotation is probably limited, but differential rotation may provide a way to understand universality breaking, because it is expected to produce variations in the eccentricity of isodensity contours [586, 590]. Another topic that deserves further investigation are magnetic fields. Reference [581] found that the universality is lost for NSs with large magnetic fields, but it would be interesting to see if it can be somehow restored for fixed *dimensionless* magnetic field strength (e.g. by normalizing the magnetic field strength with the NS mass or radius, as is the case for rapidly rotating NSs [28, 29, 584]).
- Tests of GR with universal relations also deserve more study. Theories that have not been considered in the context of universal relations include quadratic gravity, Einstein-Æther and Hořava gravity. Static and slowly rotating NS solutions at first order in the slow-rotation parameter [164], as well as fast rotating solutions [82], are known for EdGB gravity, whereas the properties of spinning NSs in dCS theory are known only up at second order in rotation [27]. Static NS solutions have been constructed for Einstein-Æther gravity in [168, 169, 171]. Finally, slowly moving NS solutions were constructed for Einstein-Æther and Hořava gravity in [48, 49]. These works should be extended to at least quadratic order in rotation, because the quadrupole moment is a second-order quantity. It would also be interesting to consider massive scalar–tensor theories and $f(R)$ gravity.
- Universal relations among multipole moments are useful to measure the NS mass and radius with future x-ray observations [519, 592]. Using slowly rotating NS solutions and ray-tracing algorithms, it will be possible to compute x-ray pulse profiles from a rotating hot spot on the NS surface in modified theories of gravity [637, 638]. The number of parameters describing the profile can be reduced using the modified universal relations; then one could fit for the model parameters (such as the stellar mass and radius) together with the coupling constants in the modified theories. This analysis would reveal whether

future x-ray observations with NICER [593] and LOFT [429, 594] could constrain deviations from GR (see [595]).

5. Compact binaries

Binary systems containing BHs and/or NSs have played a crucial role in testing our understanding of strong-field gravitational physics (as we shall see in section 6), and they will play an even more decisive role in the future, when GW observations will become a reality (section 7). The two-body problem in GR has been a major focus of numerical and analytical work over the past few decades because of its relevance for GW detection, and there are several excellent reviews on this topic. We refer the reader to [1, 639–641] for overviews of analytical calculations within PN theory and the effective-one-body formalism, and to [642–647] for summaries of recent numerical work on compact binary mergers. In this section we focus on our current understanding of binary dynamics in some popular extensions of GR.

5.1. Scalar–tensor theories

Two complementary approaches are used to model compact binaries in GR: analytical calculations (usually PN expansions) and numerical relativity simulations. The first approach is valid at large separations, and for orbital velocities that are small compared to the speed of light; the second is necessary when the components of the binary system get close and merge. Both approaches have been extended to scalar–tensor theories and will be discussed in this section. We will focus mostly on the best studied case where the gravitational interaction is mediated by the metric and a single scalar field (see [39] for a pioneering study of binary dynamics in tensor-multiscalar theories).

5.1.1. Analytical calculations. Comprehensive studies of compact binaries in scalar–tensor theory were carried out by Eardley [228], Will and Zaglauer [231, 648] and Damour and Esposito-Farèse [39, 116, 538], among others. At present, the most accurate description of the orbital motion and GW emission in scalar–tensor theory is due to work by Mirshekari and Will [233] and Lang [649, 650], who derived the equations of motion and the radiation flux considering a single scalar field with vanishing potential (and therefore vanishing mass). The relevant field equations for this theory are given in equation (2.6), with $U(\phi) = 0$. Following Eardley [228], Mirshekari, Will and Lang describe the orbital motion of the binary in terms of the NS sensitivities (reviewed in section 4.9).

The calculation considers only the inspiral phase of the binary’s evolution. It is therefore appropriate to use the PN approximation, an expansion in powers of $v/c \sim (Gm/rc^2)^{1/2}$. The scalar–tensor equations are solved by adapting the ‘direct integration of the Einstein equations’ (DIRE) method developed by Will, Wiseman, and Pati [651–653], which has proven successful in GR and which has been extended to scalar–tensor theory (see [1] for a pedagogical introduction). To begin with, it is convenient to consider a rescaled version of the scalar field $\phi: \varphi \equiv \phi/\phi_0$, where ϕ_0 is the value of ϕ at infinity (assumed to be constant)⁵⁶. By introducing a new tensorial quantity

⁵⁶ The rescaled (Jordan-frame) field, denoted by φ in this section, should not be confused with the Einstein-frame field, denoted by the same symbol elsewhere in this review.

$$\tilde{h}^{\mu\nu} \equiv \eta^{\mu\nu} - \sqrt{-\tilde{g}} \tilde{g}^{\mu\nu}, \quad (5.1)$$

(where $\eta^{\mu\nu}$ is the inverse Minkowski metric, $\tilde{g}_{\mu\nu} \equiv \varphi g_{\mu\nu}$, and \tilde{g} is its determinant) and choosing the gauge condition $\tilde{h}^{\mu\nu}{}_{,\nu} = 0$, the field equations reduce to two *flat-spacetime* wave equations

$$\square_{\eta} \tilde{h}^{\mu\nu} = -16\pi\tau^{\mu\nu}, \quad (5.2)$$

$$\square_{\eta} \varphi = -8\pi\tau_s, \quad (5.3)$$

where the sources $\tau^{\mu\nu}$ and τ_s on the right-hand side contain terms depending not only on the matter stress–energy tensor $T^{\mu\nu}$, but also on the fields $\tilde{h}^{\mu\nu}$ and φ . The formal solution of these ‘relaxed’ Einstein equations can be written down using the usual flat-spacetime retarded Green’s function

$$\tilde{h}^{\mu\nu}(t, \mathbf{x}) = 4 \int \frac{\tau^{\mu\nu}(t', \mathbf{x}') \delta(t' - t + |\mathbf{x} - \mathbf{x}'|)}{|\mathbf{x} - \mathbf{x}'|} d^4x', \quad (5.4a)$$

$$\varphi(t, \mathbf{x}) = 2 \int \frac{\tau_s(t', \mathbf{x}') \delta(t' - t + |\mathbf{x} - \mathbf{x}'|)}{|\mathbf{x} - \mathbf{x}'|} d^4x'. \quad (5.4b)$$

The main qualitative difference with electromagnetism is that the sources in these integrals do not have compact support. In the DIRE method (and extensions thereof), spacetime is split into two regions, the ‘near zone’ and the ‘radiation zone.’ In the near zone close to the source (at distances smaller than the typical gravitational wavelength λ , $|\mathbf{x}'| < \mathcal{R}$ where $\mathcal{R} \sim \lambda$), the integral is calculated using a slow-motion approximation via the usual PN expansion in powers of v/c . In the radiation zone far from the source (at distances $|\mathbf{x}'| > \mathcal{R}$), a change of variables is used to evaluate the integral. The integration procedure is different depending on whether the field point \mathbf{x} itself lies in the near zone or the radiation zone, so there are four different classes of integrals. In general, the integrals will produce terms which depend on the arbitrary quantity \mathcal{R} , but it is safe to ignore these terms because any \mathcal{R} -dependent contributions from near-zone integrals must be completely canceled by contributions from radiation-zone integrals.

The first step to understanding compact binary systems is to find the equations of motion for the bodies. Mirshekari and Will [233] carried out this calculation up to 2.5PN order, or $O((v/c)^5)$. Their procedure requires evaluating the integrals (5.4) at field points in the near zone, where the bodies are located. The procedure is iterative: the lowest-order source, comprising only the compact object stress–energy, is used to find the lowest-order fields. These are then substituted in to find the next-highest-order source, which can then be used to find the next-highest fields, and so on. Once the fields, and thus the metric, have been calculated to the necessary order, the equations of motion are found from the geodesic equations (with a slight modification due to the ϕ -dependence of mass in the Eardley approach). Schematically, the relative acceleration $\mathbf{a} \equiv \mathbf{a}_1 - \mathbf{a}_2$ takes the form

$$\begin{aligned} a^i = & -\frac{G\alpha m}{r^2} \hat{n}^i + \frac{G\alpha m}{r^2} (A_{\text{PN}} \hat{n}^i + B_{\text{PN}} \dot{v}^i) + \frac{8}{5} \eta \frac{(G\alpha m)^2}{r^3} (A_{1.5\text{PN}} \dot{r} \hat{n}^i - B_{1.5\text{PN}} v^i) \\ & + \frac{G\alpha m}{r^2} (A_{2\text{PN}} \hat{n}^i + B_{2\text{PN}} \dot{v}^i), \end{aligned} \quad (5.5)$$

where $m \equiv m_1 + m_2$, $\eta \equiv m_1 m_2 / m^2$, r is the orbital separation, \hat{n} is a unit vector pointing from body 2 to body 1, and $\mathbf{v} \equiv \mathbf{v}_1 - \mathbf{v}_2$ is the relative velocity. The (typically time-dependent) coefficients A_{PN} , B_{PN} , $A_{1.5\text{PN}}$, $B_{1.5\text{PN}}$, $A_{2\text{PN}}$, and $B_{2\text{PN}}$ are given in [233]. We use

the symbol G to represent the combination $(4 + 2\omega_0)/[\phi_0(3 + 2\omega_0)]$ (with $\omega_0 \equiv \omega(\phi_0)$) because it appears in the metric component g_{00} in the same manner as the gravitational constant G in GR. However, the coupling in the Newtonian piece of the equations of motion is not simply G but $G\alpha$, where

$$\alpha \equiv \frac{3 + 2\omega_0}{4 + 2\omega_0} + \frac{(1 - 2s_1)(1 - 2s_2)}{4 + 2\omega_0} \quad (5.6)$$

and s_i ($i = 1, 2$) are the sensitivities of the two objects, defined in equation (4.28). Another important deviation from GR is the presence of a 1.5PN radiation-reaction contribution to the equations of motion. In GR, radiation reaction begins at 2.5PN order, with the lowest-order quadrupole radiation contribution. In scalar–tensor theory, radiation reaction begins at 1.5PN order, due to the presence of scalar dipole radiation.

Many other deviations from GR occur within the A and B coefficients: see [233] for details. Although the number of deviations is large, they can all be characterized using a fairly small number of parameters, all combinations of ϕ_0 , the Taylor coefficients of $\omega(\phi)$, and the sensitivities s_A , s'_A , and s''_A . The deviations are considerably simplified if one object in the system is taken to be a BH (with the other being a NS). Then the motion of the system is indistinguishable from the motion in GR up to 1PN order. All deviations beyond 1PN order depend only on a single parameter, which itself depends on ω_0 and the sensitivity of the NS. Unfortunately, this parameter does not depend on any more details of the scalar–tensor theory; if measured, it alone could not be used to distinguish between Brans–Dicke theory and a more general scalar–tensor theory.

The equations of motion simplify even more radically for a binary BH system: they are *identical* to the equations of motion in GR, except for an unobservable mass rescaling. This result is a generalization to binary systems of ‘no-scalar-hair’ theorems that apply to single BHs [55]. For generic mass ratio, Mirshekari and Will proved this ‘generalized no-hair theorem’ up to 2.5PN order, but they conjectured that it should hold at all PN orders. Indeed, Yunes *et al* have shown that the equations of motion are the same as in GR at any PN order if one considers an extreme mass-ratio system and works to lowest order in the mass ratio [234], and the conjecture is also supported by numerical relativity studies [654, 655] (see section 5.1.2). This ‘generalized no-hair theorem’ for binary BHs depends on some crucial assumptions: vanishing scalar potential, asymptotically constant value of the scalar field, and vanishing matter content. If any one of these assumptions breaks down, the BH binary’s behavior will differ from GR.

The next step is the calculation of gravitational radiation. The tensor part of the radiation, encoded in \tilde{h}^{ij} , was computed up to 2PN order by Lang [649]. The procedure requires evaluating equation (5.4a) for field points in the ‘far-away zone,’ a subset of the radiation zone which is very far ($R \equiv |\mathbf{x}| \gg \mathcal{R}$) from the source. When integrating over source points in the near zone, the main step is the calculation of certain moments of the source τ^{ij} , known as ‘Epstein–Wagoner moments.’ The first of these, the quadrupole moment, generates GW contributions at 0PN, 1PN, 1.5PN, and 2PN orders. (The 1.5PN order contribution does not occur in GR and is a direct result of scalar dipole radiation in this theory.) The next moment is the octupole moment, which generates GWs at 0.5PN, 1.5PN, and 2PN orders. In all, Epstein–Wagoner moments with up to six indices are required. The six-index moment contributes only 2PN GWs.

The final expression for the tensor waves is considerably more complicated than its GR equivalent; however, all deviations depend on the same small number of parameters that characterize the equations of motion. Most deviations appear as modifications to GR terms,

except for entirely new terms which depend on the existence of a scalar dipole moment. The tensor waves also show the same behavior as the equations of motion in special cases. For BH–NS systems, the waveform is indistinguishable from GR up to 1PN order; deviations at higher order depend only on the single parameter described earlier. For BH–BH systems, the waveform is completely indistinguishable from GR.

Scalar radiation has recently been computed by Lang [650] using a very similar procedure. The near-zone contribution requires the calculation of ‘scalar multipole moments’ similar to the Epstein–Wagoner moments, but involving τ_s instead of τ^{ij} . In this case, the lowest-order moment is not the quadrupole, but the monopole. Using the standard definition of PN orders, in which ‘0PN’ waves are generated by the tensor quadrupole, the scalar monopole moment generates a scalar field at -1 PN order. This field, however, turns out to be time-independent and not wavelike. The dipole moment generates the lowest-order scalar waves, which are of -0.5 PN order:

$$\varphi = \frac{4G\mu\alpha^{1/2}}{R}\zeta\mathcal{S}_-(\hat{N}\cdot\mathbf{v}), \quad (5.7)$$

where $\mu \equiv m_1m_2/m$ is the reduced mass, $\hat{N} \equiv \mathbf{x}/R$ is the direction from the source to the detector, $\zeta \equiv 1/(4 + 2\omega_0)$, and

$$\mathcal{S}_- \equiv \alpha^{-1/2}(s_2 - s_1). \quad (5.8)$$

Calculating the radiation up to 2PN order requires knowledge of the monopole moment to 3PN order (relative to itself) and knowledge of the dipole moment to 2.5PN order. Just constructing the 3PN expansion of the source τ_s is a challenging process. Evaluating the resulting integrals is even more difficult. For these reasons, Lang [650] computes the scalar waveform only to 1.5PN order, with the 2PN result saved for future work. The 1.5PN waveform turns out to be described by the same set of parameters that describes the 2.5PN equations of motion and the 2PN tensor waveform. Other similarities include the vanishing of the scalar waveform for binary BH systems (so that it is indistinguishable from GR) and tremendous simplifications in the mixed BH–NS case.

The tensor and scalar waveforms can be used to compute the total energy carried off to infinity using the expressions

$$\frac{dE_T}{dt} = \frac{R^2}{32\pi}\phi_0 \oint \dot{h}_{TT}^{ij}\dot{h}_{TT}^{ij}d^2\Omega, \quad (5.9)$$

$$\frac{dE_S}{dt} = \frac{R^2}{32\pi}\phi_0(4\omega_0 + 6) \oint \dot{\varphi}^2d^2\Omega, \quad (5.10)$$

for the tensor and scalar fluxes, respectively. Here TT refers to the transverse-traceless projection of the tensor. The existence of a -0.5 PN piece of the scalar waveform means that the scalar waveform must generally be known to $(N + 1/2)$ th PN order to find the flux at N th PN order. Lang [650] computes this flux to 1PN order. The result is

$$\frac{dE}{dt} = \dot{E}_{-1} + \dot{E}_0 + \dot{E}_{0.5} + \dot{E}_1, \quad (5.11)$$

where

$$\dot{E}_{-1} = \frac{4}{3}\frac{\mu\eta}{r}\left(\frac{G\alpha m}{r}\right)^3\zeta\mathcal{S}_-^2, \quad (5.12a)$$

$$\begin{aligned}
\dot{E}_0 = & \frac{8}{15} \frac{\mu\eta}{r} \left(\frac{G\alpha m}{r} \right)^3 \left\{ \frac{G\alpha m}{r} \left[-2 \frac{\delta m}{m} \zeta \mathcal{S}_+ \mathcal{S}_- \right. \right. \\
& + \left. \left(-23 + \eta - 10\bar{\gamma} - 10\bar{\beta}_+ + 10 \frac{\delta m}{m} \bar{\beta}_- \right) \zeta \mathcal{S}_-^2 \right] \\
& + v^2 \left[12 + 6\bar{\gamma} + 2\zeta \mathcal{S}_+^2 + 2 \frac{\delta m}{m} \zeta \mathcal{S}_+ \mathcal{S}_- + (6 - \eta + 5\bar{\gamma}) \zeta \mathcal{S}_-^2 \right. \\
& - \left. \frac{10}{\bar{\gamma}} \frac{\delta m}{m} \zeta \mathcal{S}_- (\mathcal{S}_+ \bar{\beta}_+ + \mathcal{S}_- \bar{\beta}_-) + \frac{10}{\bar{\gamma}} \zeta \mathcal{S}_- (\mathcal{S}_- \bar{\beta}_+ + \mathcal{S}_+ \bar{\beta}_-) \right] \\
& + \dot{r}^2 \left[-11 - \frac{11}{2} \bar{\gamma} + \frac{23}{2} \zeta \mathcal{S}_+^2 - 8 \frac{\delta m}{m} \zeta \mathcal{S}_+ \mathcal{S}_- + \left(-\frac{37}{2} + 9\eta - 10\bar{\gamma} \right) \zeta \mathcal{S}_-^2 \right. \\
& - \frac{80}{\bar{\gamma}} \zeta \mathcal{S}_+ (\mathcal{S}_+ \bar{\beta}_+ + \mathcal{S}_- \bar{\beta}_-) + \frac{30}{\bar{\gamma}} \frac{\delta m}{m} \zeta \mathcal{S}_- (\mathcal{S}_+ \bar{\beta}_+ + \mathcal{S}_- \bar{\beta}_-) \\
& \left. \left. - \frac{10}{\bar{\gamma}} \zeta \mathcal{S}_- (\mathcal{S}_- \bar{\beta}_+ + \mathcal{S}_+ \bar{\beta}_-) + \frac{120}{\bar{\gamma}^2} \zeta (\mathcal{S}_+ \bar{\beta}_+ + \mathcal{S}_- \bar{\beta}_-)^2 \right] \right\}, \tag{5.12b}
\end{aligned}$$

$$\begin{aligned}
\dot{E}_{0.5} = & -\frac{16}{9} \frac{\mu\eta}{r} \left(\frac{G\alpha m}{r} \right)^3 (\zeta \mathcal{S}_-)^2 \left(\mathcal{S}_+^2 + 2 \frac{\delta m}{m} \mathcal{S}_+ \mathcal{S}_- + \mathcal{S}_-^2 \right) \frac{G\alpha m}{r} \dot{r} \\
& - \frac{16}{3} \frac{\mu\eta}{r} \left(1 + \frac{1}{2} \bar{\gamma} \right) \zeta \mathcal{S}_-^2 \left\{ 2 \left(\frac{G\alpha m}{r} \right)^3 \frac{G\alpha m}{r} \dot{r} \right. \\
& + \left. \frac{(G\alpha m)^3}{r} \hat{n}^k \int_0^\infty ds \left[\frac{G\alpha m}{r^4} \left(\left(3v^2 - 15\dot{r}^2 - 2 \frac{G\alpha m}{r} \right) \hat{n}^k + 6\dot{r}v^k \right) \right] \right\}_{\tau-s} \\
& \times \ln \frac{s}{2R+s}, \tag{5.12c}
\end{aligned}$$

and \dot{E}_1 is given in [650]. Here we define $\delta m \equiv m_1 - m_2$,

$$\mathcal{S}_+ \equiv \alpha^{-1/2} (1 - s_1 - s_2), \tag{5.13a}$$

$$\bar{\gamma} \equiv -2\alpha^{-1} \zeta (1 - 2s_1)(1 - 2s_2), \tag{5.13b}$$

$$\bar{\beta}_\pm = \frac{1}{2} (\bar{\beta}_1 \pm \bar{\beta}_2), \tag{5.13c}$$

$$\bar{\beta}_1 \equiv \alpha^{-2} \zeta (1 - 2s_2)^2 (\lambda_1 (1 - 2s_1) + 2\zeta s_1'), \tag{5.13d}$$

$$\bar{\beta}_2 \equiv \alpha^{-2} \zeta (1 - 2s_1)^2 (\lambda_1 (1 - 2s_2) + 2\zeta s_2'), \tag{5.13e}$$

and

$$\lambda_1 \equiv \frac{(d\omega/d\varphi)_0 \zeta}{3 + 2\omega_0}. \tag{5.13f}$$

We also note that the subscript $\tau - s$ in (5.12c) means that the quantity should be evaluated at time $\tau - s$, where $\tau \equiv t - R$ is the retarded time. Equations (5.11) and (5.12) can be used to determine the phase evolution of a binary, the last step in producing a usable waveform for data analysis studies.

While future work in this area will certainly involve extending the current calculation to higher PN order, it may also be interesting to investigate theories with multiple scalars or a potential. A derivation of the quadrupole-order flux in tensor-multiscalar theories, that agrees with Lang's results in the single-scalar limit, can be found in [39]. The current state-of-the-art calculation for compact binaries in the massive Brans–Dicke theory was performed by Alsing *et al* [36] (see also [656, 657]). In the notation used by Lang, and correcting a mistake in [36], they found that the lowest-order flux is given by

$$\dot{E} = \frac{4}{3} \frac{\mu\eta}{r} \left(\frac{G\alpha m}{r} \right)^3 \zeta \mathcal{S}^2 \left[\frac{\omega^2 - m_s^2}{\omega^2} \right]^{3/2} \Theta(\omega - m_s), \quad (5.14)$$

where ω is the orbital frequency, m_s is the mass of the scalar field, and Θ is the Heaviside function. In massive Brans–Dicke theory, scalar dipole radiation is emitted only when $\omega > m_s$. Alsing *et al* continued their calculation to 1PN order; however, those terms are incomplete and we do not list them here.

5.1.2. Numerical relativity simulations. Numerical relativity (the use of numerical simulations to solve Einstein's equations in full generality in the nonlinear regime) is the most powerful tool at our disposal to understand strong gravity. Numerical relativity had a 40 year long gestation [658], and the main motivation behind its development was the description of high-energy astrophysical phenomena in the framework of GR. In recent years the theory has been extended beyond GR and it found unexpected applications in many other fields, ranging from high-energy physics to solid-state physics [659].

Even within GR, obtaining numerically stable and accurate time evolutions in the absence of high degrees of symmetry is a daunting task that requires an understanding of many complex issues, such as the well-posedness of the evolution system, the construction of initial data and gauge conditions [294, 660]. These same questions arise also in all proposed extensions of GR, and at present they remain unanswered for most of the theories discussed in this review.

Scalar–tensor theories represent a notable exception, because they can be formulated in close analogy to GR. As discussed in section 2.2, the action of scalar–tensor theories in the Einstein frame is the same as the Einstein–Hilbert action, except for a minimal coupling with the scalar field in the gravitational sector; a nonminimal coupling with the scalar field only appears in the matter sector.

The field equations in the Einstein frame—equations (2.7), that we reproduce here for the reader's convenience—are

$$G_{\mu\nu}^* = 2 \left(\partial_\mu \varphi \partial_\nu \varphi - \frac{1}{2} g_{\mu\nu}^* \partial_\sigma \varphi \partial^\sigma \varphi \right) - \frac{1}{2} g_{\mu\nu}^* V(\varphi) + 8\pi T_{\mu\nu}^*, \quad (5.15a)$$

$$\square_{g^*} \varphi = -4\pi \alpha(\varphi) T^* + \frac{1}{4} \frac{dV}{d\varphi}. \quad (5.15b)$$

In the Jordan frame the scalar field is minimally coupled to matter, free particles follow geodesics of the spacetime metric and the stress–energy tensor $T_{\mu\nu}$ of a given matter source (e.g., a perfect fluid) has formally the same expression as in GR. In the Einstein frame the stress–energy tensor is

$$T_{\mu}^{*\nu} = A^4(\varphi) T_{\mu}^{\nu}, \quad (5.16)$$

where $A(\varphi)$ is the conformal factor (see section 2.2). Therefore, as mentioned above, matter fields are coupled with φ in the Einstein frame. Energy–momentum conservation in the

Jordan frame, $\nabla_\mu T^{\mu\alpha} = 0$, translates to the Einstein-frame condition

$$\nabla_{g^*}^\mu T_{\mu\alpha}^* = \alpha(\varphi) T^* \partial_\alpha \varphi. \quad (5.17)$$

The time evolution of a physical system can then be obtained by solving equations (5.15a), (5.15b) and (5.17). Except for the addition of a minimally coupled scalar field and—when matter is present—for the nonminimal coupling of φ with the stress–energy tensor in equation (5.16), this system of equations is identical to the field equations of GR. This is the reason why scalar–tensor theories of gravity can be attacked using relatively minor generalizations of the numerical codes developed for GR. The evolution of the scalar field φ is dictated by equation (5.15b), a wave equation that manifestly preserves any hyperbolicity properties that are satisfied when equations (5.15a) and (5.17) are formulated as an initial-value problem.

Salgado *et al* [34, 661] showed that a strongly hyperbolic formulation can be obtained also in the physical (Jordan) frame. However, the Einstein frame is exceptionally convenient for applications to vacuum spacetimes. The reason is that in vacuum ($T^{*\alpha}_\beta = 0$) the evolution equations (5.15) are independent of the coupling function $A(\varphi)$. Therefore a single numerical evolution represents a whole class of theories characterized by different functional forms of $A(\varphi)$ for a given potential $V(\varphi)$. Different choices of $A(\varphi)$ result in different physical predictions (e.g. in terms of gravitational waveforms), but all of these predictions can be calculated by *post-processing* data from one and the same numerical simulation. This would not be possible in the Jordan frame, where the coupling function explicitly appears in the system of equations that are numerically evolved in time. At least for vacuum spacetimes, the Einstein frame allows for a considerable reduction in the computational cost of exploring different scalar–tensor theories.

Early numerical studies of gravitational systems in scalar–tensor theory focused on gravitational collapse in spherical symmetry, a 1 + 1 dimensional problem involving only time and one radial coordinate. These studies explored dust collapse in Brans–Dicke theory [124–126], the collapse and stability of NSs [128, 129], and stellar core-collapse [131] in more general scalar–tensor theories, with particular focus on the spontaneous scalarization phenomenon [26]. The recent breakthroughs in numerical relativity have opened up the realm of compact binary simulations in scalar–tensor theories of gravity. We now summarize the main findings for BH–BH and NS–NS binaries.

Black hole binaries. For BH–BH binaries, scalar–tensor theories represent conceptually simple modifications of GR. A downside of this simplicity is that introducing nontrivial BH binary dynamics in these theories (where by ‘nontrivial’ we mean dynamics differing from pure GR) requires somewhat contrived scenarios.

One obvious solution of the field equations (5.15) in the vacuum case ($T^\alpha_\beta = T^{*\alpha}_\beta = 0$) is the GR solution for the metric, plus a constant scalar field. This was realized a long time ago, and led to various no-hair theorems stating that *stationary* BH solutions in Brans–Dicke theory are the same as in GR (see e.g. [55, 397, 398], and [363] for a review). These results have recently been extended to Bergmann–Wagoner theories [59] (see section 3.2). Moreover, as discussed in section 5.1.1, the dynamics of BH binaries in scalar–tensor theories was shown to be indistinguishable from GR at all PN orders in the extreme mass-ratio limit, and up to 2.5PN order in the equations of motion in PN theory. This ‘generalized no-hair theorem’ relies on the following assumptions: (1) the spacetime contains no matter, (2) the potential $V(\varphi)$ vanishes, (3) the scalar–tensor action is truncated at second order in the derivative expansion, and (4) the metric is asymptotically flat and the scalar field is

asymptotically constant. Deviations from GR in the radiation from BH binaries can occur if we violate any of these four assumptions.

The most obvious way to obtain nontrivial dynamics is to violate hypothesis (1), i.e. to consider configurations involving matter, such as NS–NS binaries. Leaving this possibility aside for the moment, another way out of the no-hair theorems was suggested by Horbatsch and Burgess [662]: if the scalar field is not asymptotically stationary, the BHs in a binary could retain scalar hair [57] and emit dipole radiation, as long as their masses are not exactly equal. The introduction of higher-order derivatives in the action would also violate the hypotheses of the generalized no-hair theorem, but it would lead to substantially more complicated equations, whose well-posedness remains unclear at present (see section 1 of [655]).

Healy *et al* [654] investigated whether generalized no-hair theorems carry over to the nonlinear regime, i.e., whether the dynamics of BH binaries during the late inspiral and merger is the same as in GR. Their results show that the dynamics can differ if the scalar field evolves: the scalar field triggers energy loss that leads to a difference in the GW polarizations. In their evolutions, nontrivial dynamics is triggered by placing the BHs inside a scalar field ‘bubble,’ which in some cases includes a nonvanishing scalar field potential. As the bubble collapses, the BHs accrete the scalar field and grow. The increase in mass of the BHs has a dramatic effect on the binary dynamics.

Figure 29 shows the BH trajectories (in the Einstein frame) for the four cases considered in their study (cases A–D from top left to bottom right). Case A represents the binary evolution in GR. Cases B–D differ in the initial amplitude of the scalar field in the bubble, and case D furthermore contains a nonvanishing potential term: see table 1 in [654] for details. The left panel of figure 30 shows the $l = m = 2$ multipole of the Weyl scalar Ψ_4 (roughly speaking, the second time derivative of the GW signal) for each of the four initial configurations. There are obvious differences between the various time evolutions of Ψ_4 , in particular when compared against GR (case A). The $l = m = 0$ multipole of the so-called breathing mode $\tilde{\Phi}_{22}$ in the Jordan frame is shown for cases B–D in the right panel of figure 30. Notice that the inclusion of a potential term (as in case D) introduces longer lived dynamics in the scalar field mode; see also section 3.10 for long-term evolutions of the post-merger phase.

In summary, the study of Healy *et al* [654] supports the view that an evolving scalar field is required to bypass the generalized no-hair theorems for BH binaries. Inhomogeneities in the initial scalar field configuration could provide such a mechanism. This particular study considered a BH in a scalar field bubble, but the conclusions can be carried over to more generic scenarios. For the effects to be observable, the merging BHs must accrete enough scalar field to change their masses and modify the binary evolution.

A different mechanism to circumvent the no-hair theorems was considered by Berti *et al* [655], who relaxed assumption (4) in the list above by introducing non-asymptotically flat or constant boundary conditions. Conceptually, the main motivation for relaxing this assumption comes from cosmological considerations. Inhomogeneous scalar fields have been considered in cosmological models as an alternative to dark matter [663, 664], and also as models of supermassive boson stars [457]. For scalar-field profiles that vary on a lengthscale much larger than the BH binary separation, one effectively has a configuration with an approximately constant scalar-field gradient at large separation from the binary.

Reference [655] considered the quasi-circular inspiral of a nonspinning BH binary (with mass ratio 3 : 1) in a scalar field gradient of magnitude $M\sigma = 2 \times 10^{-7}$ perpendicular to the orbital angular momentum vector. The three lowest multipoles of the Newman–Penrose scalar Ψ_4 extracted from the Einstein metric are shown in the left panel of figure 31. These

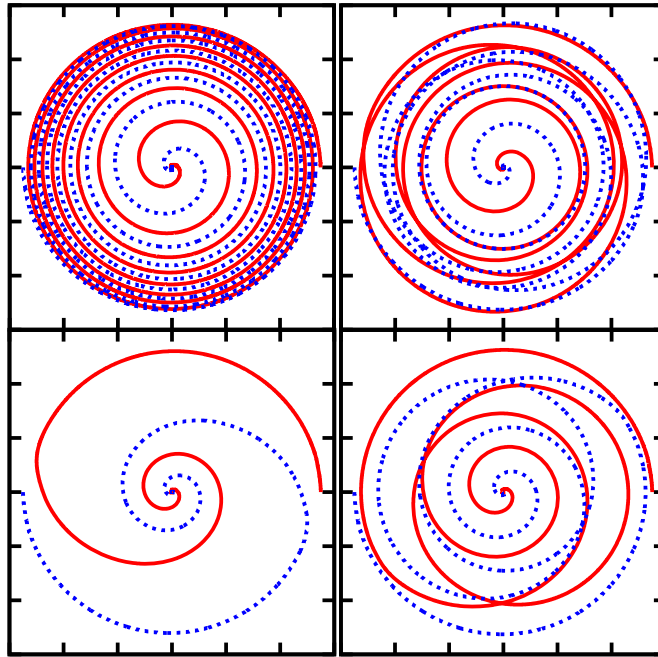


Figure 29. BH trajectories in the Einstein frame, assuming that the BHs are in a scalar field bubble. The upper-left panel corresponds to the GR limit; upper-right and lower-left panels correspond to different initial amplitudes of the scalar field. In the lower-right panel the evolution occurs in the presence of a nonzero quartic potential. (From [654].)

multipoles are effectively indistinguishable from their GR counterparts (see figure 5 of [655]). A nonvanishing ‘background’ scalar field does, however, lead to the (mostly dipolar) emission of scalar radiation, which is not present in GR. The time derivative of the real part of the dipole contribution is shown in the right panel of figure 31, and it displays the expected $1/r$ fall-off behavior. The oscillation frequency of this dipole mode is *twice* the orbital frequency. At first glance, it may appear surprising to see an $m = 1$ multipole oscillating at twice the orbital frequency (rather than at the orbital frequency). A simple calculation, however, reveals that this feature is a consequence of the interaction of the orbital motion with an $m = 1$ background field: see the discussion around equations (36)–(38) of [655]. In summary, these simulations demonstrate that non-asymptotically flat boundary conditions (here imposed in the form of a constant scalar-field gradient) provide a mechanism to generate scalar radiation in BH inspirals in scalar–tensor theories of gravity, thus circumventing the no-hair theorems. Unfortunately, there is little hope to observe scalar radiation of this nature in the near future for cosmologically realistic values of the scalar-field gradients.

NS binaries. The dynamics of scalar–tensor theories of gravity is different from GR whenever the spacetime contains matter sources. This is evident in the Einstein frame, where the stress–energy tensor explicitly depends on the scalar field (see equation (5.16)), but of course it is also true in the Jordan frame, by virtue of the physical equivalence of the two frames (see section 2.2). Violations of the SEP mean that self-gravitating objects follow

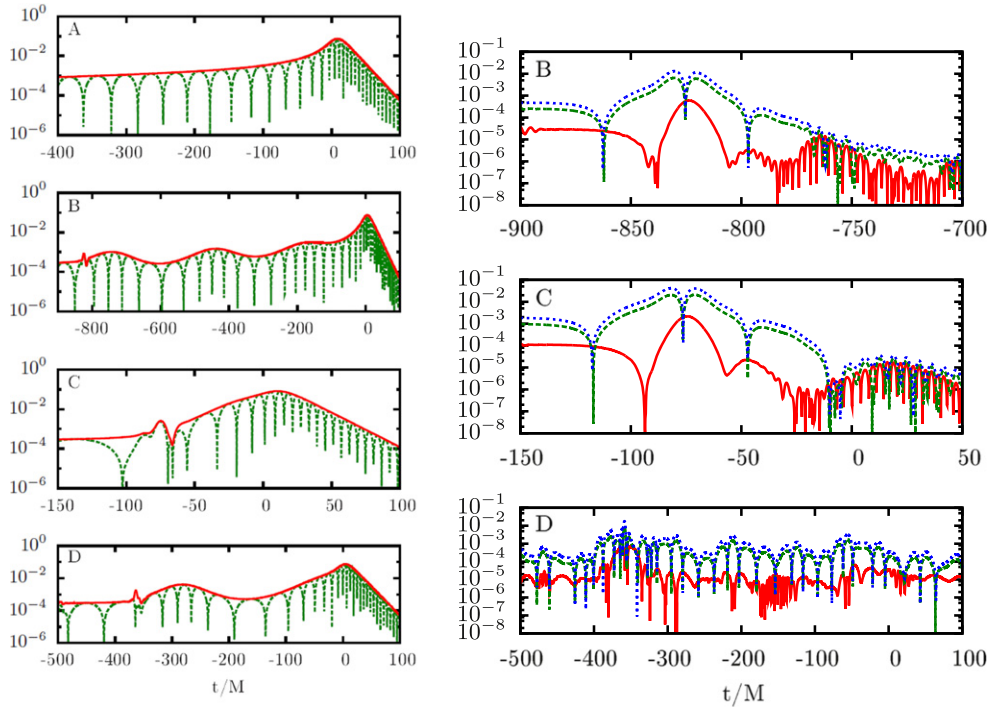


Figure 30. Left: The $l = m = 2$ multipole of the complex Weyl scalar Ψ_4 (the dashed line corresponds to the real part of Ψ_4 , and the solid line to its modulus). Right: the $l = m = 0$ multipole of the breathing mode $r M \tilde{\Phi}_{22}$, where r is the extraction radius and M is the total mass of the binary; solid, dashed and dotted lines correspond to different values of the parameter β_0 (see equation (2.5)). Merger occurs at $t/M = 0$. (From [654].)

trajectories that depend on their internal composition/structure: this is the well known ‘Nordtvedt effect’ [228, 665, 666].

For generic (Bergmann–Wagoner) scalar–tensor theories, the dimensionless coupling $\alpha(\varphi)$ between the scalar field and matter depends on the local value of the scalar field, and it can be Taylor expanded as (see equation (2.5))

$$\alpha(\varphi) \equiv \frac{d \ln A(\varphi)}{d\varphi} = \alpha_0 + \beta_0(\varphi - \varphi_0) + \mathcal{O}(\varphi)^2, \quad (5.18)$$

where $\alpha_0 = 1/\sqrt{3 + 2\omega_{\text{BD}}}$ and β_0 are dimensionless constants, and φ_0 is the asymptotic value of the scalar field. As discussed in section 4.2, the constant α_0 is severely constrained by Solar System experiments ($\omega_{\text{BD}} > 40\,000$, or $\alpha_0 < 3.5 \times 10^{-3}$) [2]. Observations of binary pulsars imply $\beta_0 \gtrsim -4.52$, because for sufficiently negative values of β_0 ($\beta_0 \lesssim -4.35$ for a static NS) spontaneous scalarization would set in (see section 4.2), and the motion of NSs in binary systems would be affected in ways that are severely constrained by binary pulsar data (see section 6.1). Note however that these constraints are somewhat degenerate with the EOS [542], i.e., a different EOS changes the value of β_0 below which dynamical scalarization appears.

Recently, reference [540] (using fully relativistic numerical simulations, performed in the Einstein frame) and [541] (using semi-analytical arguments) discovered a phenomenon

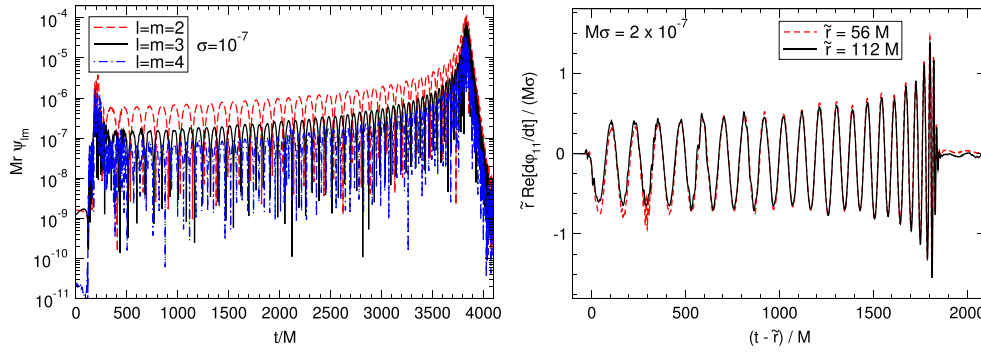


Figure 31. Numerical results for a ten-orbit inspiral of a nonspinning BH binary of mass ratio 3 : 1 inside a scalar field gradient of magnitude $M\sigma = 2 \times 10^{-7}$. Left: real part of the spin-weighted spherical harmonic components of the Newman–Penrose scalar Ψ_4 extracted at coordinate radius $\tilde{r} = 56 M$ for harmonic indices $l = m$ (the imaginary part is identical up to a phase shift). Right: time-derivative of the scalar field at the largest and smallest extraction radii, rescaled by radius and shifted in time. (From [655].)

similar to spontaneous scalarization in the late stages of the evolution of NS–NS binaries: ‘dynamical scalarization.’ Their results were independently confirmed by Shibata *et al* [542]. Even in cases in which the individual NSs would *not* spontaneously scalarize in isolation, the scalar field inside each star grows when the binary separation decreases to about 50–60 km (see e.g. figure 32). This growth has a strong effect on the binary dynamics, and produces an earlier plunge than in GR (see the upper panel of figure 33). The plunge is followed by the formation of a rotating bar-like matter configuration, which sheds angular momentum in GWs before collapsing to a BH. The resulting gravitational waveforms are significantly different from GR at frequencies ~ 500 –600 Hz, as shown in the lower panel of figure 33, as well as in figure 34 for a different system. Deviations at even lower frequencies are also possible for certain binary systems and theory parameters [541, 667]. Therefore, the effects of dynamical scalarization are in principle detectable (at least in some cases) with Advanced LIGO, Advanced VIRGO and KAGRA, for values of the coupling parameters ω_0 and β that are still allowed by all existing Solar System and binary pulsar tests, as recently shown in [667]. Deviations away from GR may also be observable in the electromagnetic signal (driven by magnetosphere interactions prior to merger) from binaries of magnetized NSs [668]. While these deviations are subtle, they might provide a way in which measurements of electromagnetic counterparts to GW sources can increase the confidence with which GR will be confirmed (or ruled out) by GW observations.

5.2. $f(R)$ theories

Compact binaries in $f(R)$ gravity have been studied by considering perturbative corrections to the Einstein–Hilbert action (i.e. $f(R) = R + aR^2$ with $aR \ll 1$) and linear perturbations of Minkowski spacetime. Berry and Gair [42] used this approach to compute the stress–energy pseudotensor and the parameters of the PPN expansion. Within the same framework, but exploiting the equivalence between $f(R)$ gravity and scalar–tensor theories, Naf and Jetzer [669] studied corrections to the periastron precession for compact binaries, and in a follow-up work [670] they also computed corrections to the GW flux formula up to $O((aR)^2)$. The flux formula derived in [670] predicts that the binary would produce monopole and dipole

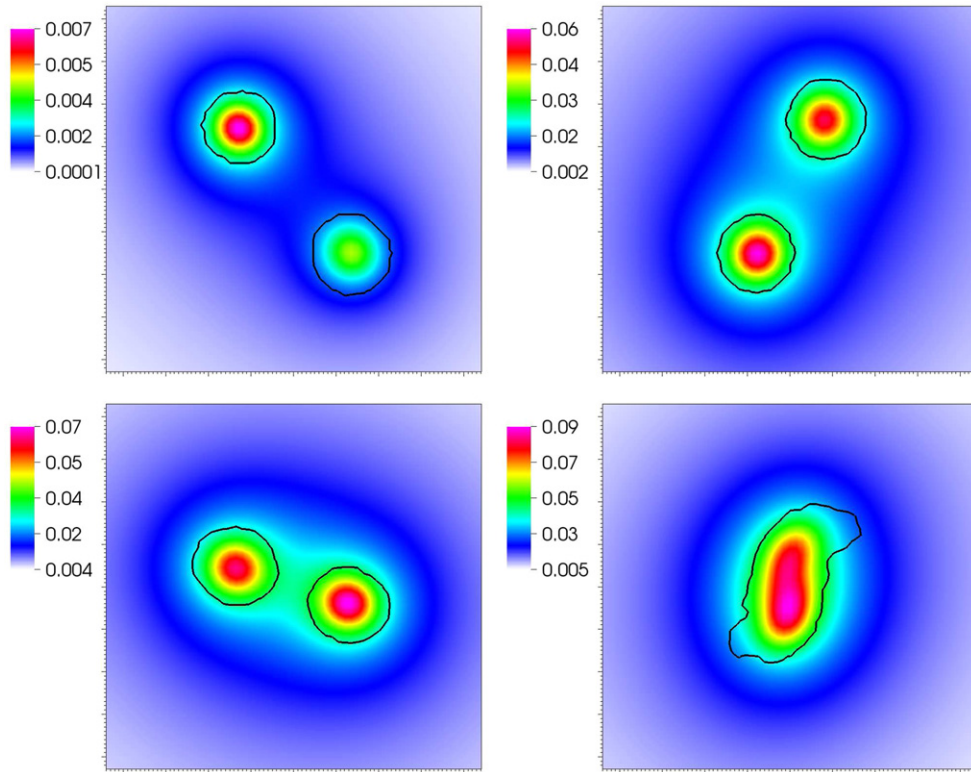


Figure 32. Snapshots of the scalar field value (color code) and the stellar surfaces (solid black line) at $t = [1.8, 3.1, 4.0, 5.3]$ ms for a binary system of NSs with gravitational masses $(1.64, 1.74)M_{\odot}$ in isolation, and a scalar–tensor theory with $\beta_0 = -4.5$. (From [540].)

radiation in addition to the ordinary quadrupolar radiation; these contributions are expected to dominate the non-GR part of the flux, because they enter at the lowest orders in a PN expansion. De Laurentis and Capozziello [671] derived a flux formula at $O(aR)$ in a similar perturbative expansion (see also [672]). At this order, gravitational radiation does not contain monopole or dipole contributions, but the quadrupole contribution has a correction linear in $f'' = 2a$. To the best of our knowledge, no calculation of the sensitivities in the context of $f(R)$ gravity has been performed yet. The results should be qualitatively similar to those in scalar–tensor theory, due to the equivalence between the two formulations.

At the moment of writing there are no numerical investigations of compact binaries in $f(R)$ gravity, but this is not due to pathologies in the theory. In fact, $f(R)$ gravity is equivalent to a special scalar–tensor theory, and as such it inherits the well-posedness properties of scalar–tensor theories (see section 5.1.2). Preliminary work on the feasibility of numerical relativity simulations in $f(R)$ gravity can be found in [41].

5.3. Quadratic gravity

The compact binary problem in quadratic gravity theories has been studied in [166, 549]. In [549], both parity-even and parity-odd theories were studied, for quasicircular orbits consisting of objects with yet-undetermined scalar monopole moments (parity-even theories) or

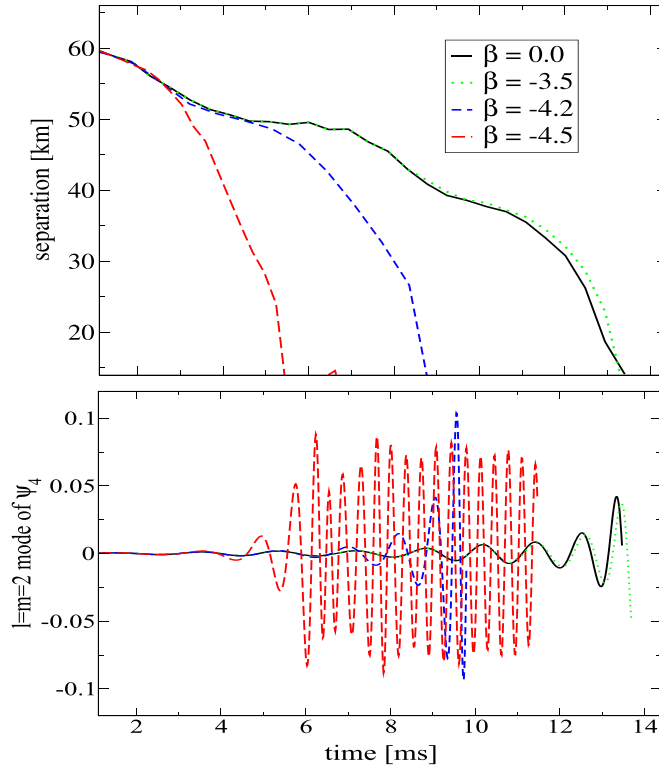


Figure 33. The separation and the dominant mode of the Ψ_4 curvature scalar (which encodes the detector's response to spin-2 GWs) for a binary system of NSs with gravitational masses $\{1.64, 1.74\}M_\odot$ in isolation, and for different values of β_0 . (From [540].)

scalar dipole moments (parity-odd theories). At that time, moments were only known for BHs, along with the result (see section 4.4) that NSs have no $1/r$ scalar hair in EdGB or dCS gravity. In [166], the authors focused on dCS. They first constructed numerical solutions for NSs to second order in rotation (these solutions include the leading dipole piece of the scalar field solution; see section 4.4 and specifically figure 20). With these dipole moments in hand, they were then able to study eccentric binaries consisting of either BHs or NSs.

There are four dominant physical corrections that arise in the compact binary problem in quadratic gravity theories.

- (1) The scalar field solutions sourced by both compact objects interact with each other, just as electric charges or magnetic dipoles interact through the electromagnetic field (scalar pole–pole interaction). This modifies the binding energy of the binary and hence the Kepler relation (orbital frequency as a function of separation).
- (2) All metric multipole moments are shifted. The mass monopole shift and mass–current dipole shift are unobservable, i.e. these shifts are absorbed back into the definition of physical mass and spin angular momentum. However, higher moments' shifts can not be absorbed and so they affect the motion. These also correct the binding energy, the Kepler relation, and cause additional precession.

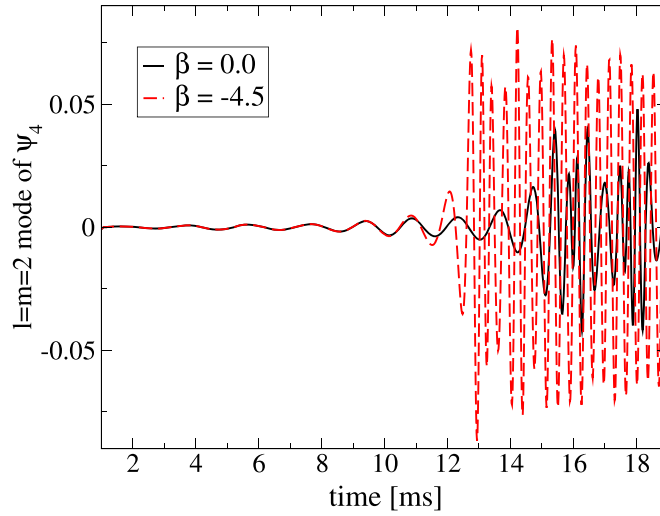


Figure 34. The dominant mode of the Ψ_4 scalar, for $\beta_0 = -4.5$ and an equal-mass binary with gravitational masses of $1.51M_\odot$ in isolation. Note that neither star undergoes spontaneous scalarization in isolation, but the GW signal is still different from GR in the late inspiral/plunge because of the dynamical scalarization of the system. (Adapted from [540].)

- (3) The scalar field is dynamical, and sourced by a configuration of scalar monopoles or dipoles (plus higher moments) which are orbiting. Thus, there may be a time-varying scalar dipole or quadrupole, which sources scalar radiation. This radiation carries away energy and thus the system inspirals at a different rate.
- (4) Finally, the GWs emitted by the system are also corrected. The change in the gravitational waveform leads to another change in the energy flux, and thus an additional correction to the inspiral rate.

Not all of the effects listed above can be directly physically observed. The three primary observables relevant to the compact binary problem are:

- (1) The correction to the precession of pericenter, $\delta \langle \dot{\omega} \rangle$.
- (2) The correction to the orbital decay $\delta \dot{P}_b$, or equivalently, the correction to the energy flux $\delta \dot{E}$.
- (3) The modification to the gravitational waveform, which can be parametrized via the parametrized post-Einsteinian (PPE) parameters $(\alpha_{\text{PPE}}, a_{\text{PPE}})$ for the amplitude and $(\beta_{\text{PPE}}, b_{\text{PPE}})$ for the phase of the waveform (see section 7.3 for more on the PPE parameterization).

The first two of these corrections are observables for pulsar timing, and the third is the observable for GW detection. As the authors of [549] only considered quasicircular orbits, they did not compute $\delta \langle \dot{\omega} \rangle$.

Almost the entire compact binary problem can be recovered by modeling compact objects as point particles with scalar hair. This amounts to replacing the scalar field's source term (in its equation of motion) with an *effective* source term τ_{eff} , which recovers the correct far-field solution [549]. There are some effects which are not captured, but they were shown to be subdominant. The effective equation of motion for the scalar field ϕ is then

$$\square\phi = \tau_{\text{eff}} = -4\pi q_1 \delta^{(3)}(\mathbf{x} - \mathbf{x}_1) + (1 \leftrightarrow 2) \quad (5.19)$$

when the bodies have scalar monopole charges q_A ($A = 1, 2$), as in the case of EdGB or other parity-even theories; or

$$\square\phi = +4\pi\mu_1^i \partial_i \delta^{(3)}(\mathbf{x} - \mathbf{x}_1) + (1 \leftrightarrow 2) \quad (5.20)$$

when the bodies have scalar dipole hair μ_A^i (the generalization to general ℓ -pole is covered in [673]). The quantities q_A or μ_A^i are found from the strong-field matching procedure, and are proportional to the small parameters α_i defined in equation (2.23). Thus, all of the above effects depend on powers of the α_i 's, which are the physical parameters that can be constrained from observations.

The scalar pole–pole interaction, correction (i), can be computed by ‘integrating out’ the scalar field at the level of the action. This gives, for the case of dCS (and correcting a sign error in [166]), an interaction potential

$$U_{\text{int}} = 4\pi \frac{1}{r_{12}^3} \left[3(\mu_1 \cdot n_{12})(\mu_2 \cdot n_{12}) - (\mu_1 \cdot \mu_2) \right], \quad (5.21)$$

where r_{12} is the distance between the two bodies, and $n_{12}^i = (x_1^i - x_2^i)/r_{12}$.

The general pole–pole interaction (again with a sign error) is given in [673]. The dependence on r_{12} is always as r_{12}^{-1-s-t} , where s and t are the ℓ 's of the dominant scalar moments of the two bodies, e.g. $s = 0$ for monopole, $s = 1$ for dipole, etc. Notice that for the case of a BH–BH binary in EdGB, where $s = t = 0$, the shift in binding energy is $1/r$, just as in the Kepler binding energy, and so this effect is completely absorbed by redefining the gravitational constant G .

The corrected metric multipole moments (correction (ii)) come from the strong-field matching calculation.

Computing corrections (iii) and (iv) now requires the far-field radiative parts of the scalar and the metric, as sourced by the dynamics of the binary. The far-field solution comes from the post-Minkowskian expansion of the retarded Green function for \square , e.g.

$$\phi^{\text{FZ}} = \frac{1}{r} \sum_m \frac{1}{m!} \frac{\partial^m}{\partial t^m} \int_{\mathcal{M}} \frac{-\tau'_{\text{eff}}}{4\pi} (n_j x'^j)^m d^3x', \quad (5.22)$$

where \mathcal{M} denotes a $t - r = \text{constant}$ hypersurface.

There is a similar expression for the GW correction. The orbit-averaged energy flux then comes from inserting ϕ^{FZ} into the stress–energy tensor $T_{\mu\nu}$ and evaluating

$$\dot{E}^{(\varphi)} = \lim_{r \rightarrow \infty} \int_{S_r^2} \langle T_{ii}^{(\varphi)} n^i \rangle_{\omega} r^2 d\Omega \quad (5.23)$$

on a two-sphere at $r \rightarrow \infty$ (here $\langle \cdot \rangle_{\omega}$ denotes the orbit-average operation). Again, there is a similar expression for the corrected energy flux from GWs.

As seen in equation (5.22), the radiative moments of ϕ come directly from time derivatives of the multipole moments of τ , and we must study which moment will dominate. The leading-in- α_i part of these corrections can be computed from the leading PN motion of the binary, i.e. simply Keplerian motion.

For a system containing a BH in EdGB, scalar dipole radiation will dominate, and is a pre-Newtonian effect (as in scalar–tensor theory, it contains fewer powers of v^2 than the GR quadrupolar energy flux). For circular orbits, this is [549]

$$\delta\dot{E}^{(\phi)} = -\frac{4\pi}{3} \frac{1}{m^4} (m_2 q_1 - m_1 q_2)^2 v^8. \quad (5.24)$$

For either BH or NS systems in dCS, the variation of the scalar dipole moment occurs on the spin-precession timescale, while the variation of the scalar quadrupole moment occurs on the orbital timescale, so the latter should dominate. For a binary with semimajor axis a and eccentricity e , this quadrupole contribution is [166]

$$\delta\dot{E}^{(\phi)} = -\frac{5}{768} \frac{\alpha_4^2}{\pi m^4} \left(\frac{m}{a}\right)^7 \frac{2\Delta_1^2 f_1(e) + 2\Delta_2^2 f_2(e) + \Delta_3^2 f_3(e)}{(1-e^2)^{11/2}}, \quad (5.25)$$

where $f_i(e) = 1 + \dots$ are $O(1)$ polynomials of degree 6, Δ_i is an $O(1)$ vector which depends on the bodies' scalar dipole moments (and hence their spin vectors), and where we have accounted for a difference in the convention for α_i between [166] and equation (2.21).

Equations (5.24) and (5.25) are correction (iii) listed above. In EdGB, since correction (iii) was pre-Newtonian, the GW effect (iv) is subdominant, so it was not computed in [549]. However, in dCS, correction (iv) is of the same PN order, and it is given by [166]

$$\delta\dot{E}^{(b)} = -\frac{15}{16} \frac{\alpha_4^2}{\pi m^4} \eta \left(\frac{m}{a}\right)^7 \frac{\chi_1 \chi_2 \bar{\mu}_1 \bar{\mu}_2 C_1^3 C_2^3 g_1(e) \hat{S}_1^x \hat{S}_2^x + g_2(e) \hat{S}_1^y \hat{S}_2^y + 2g_3(e) \hat{S}_1^z \hat{S}_2^z}{(1-e^2)^{11/2}}, \quad (5.26)$$

where $\eta = \mu/m$ is the symmetric mass ratio, $g_i(e) = 1 + \dots$ are $O(1)$ polynomials of degree 6, χ_A is the dimensionless spin angular momentum of body A , $\bar{\mu}_A$ is the dimensionless magnitude of the scalar dipole moment, C_A is the dimensionless compactness of body A , \hat{S}_A^i is the normalized spin vector of body A , and z is the direction orthogonal to the orbital plane.

We now turn to the observable signatures of the above effects. A detailed pulsar timing model does not exist, but it is still possible to compute the averaged additional precession of pericenter, $\delta\langle\dot{\omega}\rangle$. The standard way to do this averaged calculation is with the Gauss perturbation method [166, 229]. First, the perturbing acceleration is decomposed into components in an orthonormal frame which co-rotates with the binary, with two axes aligned with n_{12} and the unit angular momentum vector \hat{L} . The components are then inserted into standard formulae which are averaged over the orbital phase of the binary. Because [549] focused on quasi-circular orbits, this result was only computed in [166]. The additional precession arising from the effect (i) (the scalar pole–pole interaction) is

$$\delta\langle\dot{\omega}\rangle_\phi = \frac{75}{256} \frac{1}{\mu} \frac{\alpha_4^2}{\pi m^4} \frac{\chi_1 \chi_2}{(1-e^2)^2} C_1^3 C_2^3 \bar{\mu}_1 \bar{\mu}_2 \left(\frac{m}{a}\right)^{7/2} \left\{ \frac{1}{2} (\hat{S}_{1,x} \hat{S}_{2,x} + \hat{S}_{1,y} \hat{S}_{2,y}) - \hat{S}_{1,z} \hat{S}_{2,z} \right. \\ \left. - \cot \iota \left[\hat{S}_{1,z} (\hat{S}_{2,x} \sin \omega + \hat{S}_{2,y} \cos \omega) \right] \right\} + (1 \leftrightarrow 2), \quad (5.27)$$

where ι is the orbital inclination. The same calculation can be repeated for the perturbing acceleration arising from effect (ii), the shift in the metric quadrupole moment of each body, Q_1, Q_2 . This latter effect is estimated to be more important than $\delta\langle\dot{\omega}\rangle_\phi$, and it is given by

$$\delta \langle \dot{\omega} \rangle_h = \frac{3}{a^{7/2} \sqrt{m} (1 - e^2)^2} \mathcal{Q}_1 \left[-1 + \frac{3}{2} (\hat{S}_{1,x}^2 + \hat{S}_{1,y}^2) - \hat{S}_{1,z} \cot \iota (\hat{S}_{1,x} \sin \omega + \hat{S}_{1,y} \cos \omega) \right] + (1 \leftrightarrow 2). \quad (5.28)$$

The rate of a binary pulsar's pericenter precession, $\dot{\omega}$, is measured with much more precision than the rate of orbital decay, \dot{P}_b . Thus, observable (i) is much better for placing constraints than observable (ii). Regardless, it is algebraically straightforward to combine the Kepler binding energy, the shift in the binding energy (e.g. equation (5.21)), and the shift in the energy flux (e.g. equations (5.24), (5.25), or (5.26)) to find the leading-order in α_i correction to $\delta \dot{P}_b$. This has been computed for a circular BH–BH binary in dCS in [262] (this is not sufficient for pulsar timing constraints, but the calculation is very similar), giving $\dot{f} = \dot{f}_{\text{GR}} (1 + \delta C u^4)$, where $u \equiv (\pi m f)^{1/3}$, f is the GW frequency (twice the orbital frequency) and

$$\delta C = \frac{313\,345}{1107\,456} \frac{\alpha_4^2}{\pi m^4} \frac{m^2}{m_1^2} \chi_1^2 \left[1 - \frac{186\,607}{62\,669} (\hat{S}_1 \cdot \hat{L})^2 \right] + \frac{99\,625}{316\,416} \frac{\alpha_4^2}{\pi m^4} \frac{\chi_1 \chi_2}{\eta} \left[(\hat{S}_1 \cdot \hat{S}_2) - \frac{8327}{3985} (\hat{S}_1 \cdot \hat{L})(\hat{S}_2 \cdot \hat{L}) \right] + (1 \leftrightarrow 2). \quad (5.29)$$

Finally, we come to observable (iii), which is the shift in the gravitational waveform, relevant to ground-based detectors such as Advanced LIGO. By the time a binary gets into the frequency band relevant to these detectors, it is assumed that most eccentricity will have been damped out, and so for quadratic theories these calculations have only been done for quasi-circular orbits (see section 7.3). Since the phase of a gravitational waveform is measured with much more precision than the amplitude, most of the attention has been paid to the phase. This is parameterized in the PPE formalism in terms of β_{PPE} and b_{PPE} via

$$\Psi_{\text{PPE}} = \Psi_{\text{GR}} + \beta_{\text{PPE}} (\pi \mathcal{M} f)^{b_{\text{PPE}}}, \quad (5.30)$$

where the chirp mass is $\mathcal{M} \equiv m \eta^{3/5}$.

For even-parity theories, the dominant physical effect comes from (iii), the dipolar scalar radiation. This was computed for BH–BH binaries in [549] as

$$\beta_{\text{PPE}} = -\frac{5}{7168} \frac{\alpha_3^2}{\pi m^4} \frac{\delta m^2}{m^2} \eta^{-18/5}, \quad b_{\text{PPE}} = -7/3. \quad (5.31)$$

Meanwhile, effects (i)–(iv) all contribute for the dCS calculation. In [262], this was computed for circular BH–BH binaries as

$$\beta_{\text{PPE}} = -\frac{15}{64} \delta C \eta^{-4/5}, \quad b_{\text{PPE}} = -\frac{1}{3}, \quad (5.32)$$

where δC was given in equation (5.29).

5.4. Lorentz-violating theories

As discussed in section 4.9, in Lorentz-violating theories strongly gravitating objects are characterized by ‘sensitivities’ (or \mathcal{A} ether or khronon ‘charges’). As a result, the motion of these objects does not follow geodesics of the background geometry, but rather depends on the numerical values of the sensitivities, and thus ultimately on the object's nature. This means that the universality of free fall and the SEP are violated in these theories. More specifically, the sensitivities enter the equations of motion already at Newtonian level, where

the acceleration of the body A in a binary system is given by

$$\dot{v}_A^i = -\frac{G_N \tilde{m}_B \hat{n}_{AB}^i}{(1 + \sigma_A) r_{AB}^2}, \quad (5.33)$$

with $r_{AB} = |\mathbf{x}_A - \mathbf{x}_B|$ and $\hat{n}_{AB}^i = (x_A^i - x_B^i)/r_{AB}$, and σ_A the sensitivity parameter of body A (see equation (4.30)). This expression can be re-written as [635]

$$\dot{v}_A^i = -\frac{\mathcal{G} m_B \hat{n}_{AB}^i}{r_{AB}^2}, \quad (5.34)$$

where one defines the *active* gravitational masses

$$m_B \equiv \tilde{m}_B (1 + \sigma_B) \quad (5.35)$$

and the ‘effective’ gravitational constant

$$\mathcal{G} \equiv \frac{G_N}{(1 + \sigma_A)(1 + \sigma_B)}. \quad (5.36)$$

Similarly, the sensitivities appear in the equations of motion at higher PN orders in the conservative dynamics [635].

The sensitivities enter also in the dissipative sector of the motion of binary systems, causing both the emission of dipolar fluxes, as well as modifications of the quadrupolar emission of GWs that takes place already in GR. More specifically, the most relevant quantity for binary systems (and in particular for binary pulsars) is the rate of change of the orbital period. For systems whose orbital dynamics is determined by equation (5.34), denoting the orbital period by P_b and the binary’s binding energy by E_b , this quantity can be expressed as

$$\frac{\dot{P}_b}{P_b} = -\frac{3 \dot{E}_b}{2 E_b}, \quad (5.37)$$

which can be further manipulated by writing the binding energy’s rate of change in terms of the total flux of energy \mathcal{F} carried away by GWs, i.e. $\dot{E}_b = -\mathcal{F}$. This flux can be calculated explicitly from the sensitivities and the binary’s orbital parameters, yielding [48, 49]

$$\frac{\dot{P}_b}{P_b} = -\frac{192\pi}{5} \left(\frac{2\pi Gm}{P_b} \right)^{5/3} \frac{\mu}{m P_b} \langle \mathcal{A} \rangle, \quad (5.38)$$

where as usual $\mu = m_1 m_2 / m$ is the reduced mass, $m = m_1 + m_2$ is the total mass, and we have defined

$$\begin{aligned} \langle \mathcal{A} \rangle = & \frac{5}{32} (s_1 - s_2)^2 \mathcal{A}_4 \left(\frac{P_b}{2\pi Gm} \right)^{2/3} \\ & + \left[(1 - s_1)(1 - s_2) \right]^{2/3} (\mathcal{A}_1 + \mathcal{S} \mathcal{A}_2 + \mathcal{S}^2 \mathcal{A}_3) \\ & + \mathcal{O}(1/c^2). \end{aligned} \quad (5.39)$$

Also, $s_A = \sigma_A / (1 + \sigma_A)$ are rescaled sensitivities, $\mathcal{S} = m_1 s_2 / m + m_2 s_1 / m$ and $(\mathcal{A}_1, \mathcal{A}_2, \mathcal{A}_3, \mathcal{A}_4)$ are functions of the coupling constants $((c_+, c_-)$ in Einstein-Æther theory and (β, λ) in khronometric gravity).

Two comments are in order at this stage. First, in the GR limit one obtains $\mathcal{A} = 1$, thus recovering the usual quadrupole formula. Second, for widely separated systems (such as all observed binary pulsars) the decay rate of the orbital period is dominated by the terms appearing at the lowest PN order, i.e. with the least powers of Gm/P_b . Therefore, the last term

in equation (5.39) (the dipolar emission term) dominates the orbital decay rate unless $s_1 - s_2 \approx 0$. This provides a way to constrain Lorentz violations in gravity with white dwarf-pulsar systems (see section 6.1). Nevertheless, in the case $s_1 \approx s_2$ (relevant for instance for the relativistic double pulsar, see section 6.1), even though dipolar emission is suppressed, the sensitivities still produce changes to the quadrupole formula of GR (i.e., $\mathcal{A} \neq 1$).

Hansen *et al* [674] computed the characteristics of gravitational radiation from NS binary inspirals using as a starting point the energy flux described above. The evolution of the orbital frequency F is related to the energy flux via

$$\dot{F}(u) = \dot{F}_{\text{GR}}(u)[1 + \delta_{\dot{F}}(u)], \quad (5.40)$$

where \dot{F}_{GR} is the GR prediction, $u \equiv (2\pi GMF)^{1/3}$ and

$$\delta_{\dot{F}}(u) = \frac{7}{4}\eta^{2/5}\dot{E}_{-1\text{PN}}u^{-2} + \dot{E}_{0\text{PN}} \quad (5.41)$$

is the Lorentz-violating correction to the evolution of F . $\dot{E}_{-1\text{PN}}$ and $\dot{E}_{0\text{PN}}$ represent the Lorentz-violating correction to the energy flux due to the dipolar and quadrupolar radiation, respectively. They are given by

$$\dot{E}_{-1\text{PN}} = -\frac{5}{56}\mathcal{G}(s_1 - s_2)^2\mathcal{A}_4, \quad \dot{E}_{0\text{PN}} = \mathcal{G}(\mathcal{A}_1 + \mathcal{S}\mathcal{A}_2 + \mathcal{S}^2\mathcal{A}_3) - 1. \quad (5.42)$$

From equation (5.40) one can calculate the gravitational waveform in Fourier space using the stationary-phase approximation. In particular, the phase is given by

$$\Psi = \Psi_{\text{GR}} - \frac{3}{128}u^{-5}\left[\dot{E}_{-1\text{PN}}\eta^{2/5}u^{-2} + \dot{E}_{0\text{PN}} + \mathcal{O}(c^{-2})\right]. \quad (5.43)$$

5.5. Massive gravity

Radiation from binary pulsars in the inspiral phase was studied for the Cubic Galileon in [53] and for the general case in [310]. The calculation was done by approximating the time dependence of the source as small: $T = T_0 + \delta T$, where $T_0 = -M\delta^3(\vec{x})$ and $\delta T(\vec{x}, t)$ carries the time dependence of the inspiraling pulsars. Then upon splitting $\pi = \pi_0 + \phi$, the background profile π_0 sourced by T_0 is responsible for Vainshtein screening. The radiation in the Galileon ϕ sourced by δT in the background of π_0 was then computed using the effective action techniques proposed by [675].

For the Cubic Galileon, the dominant channel is the quadrupole ($\ell = 2$)⁵⁷. The power radiated is given by

$$\frac{P_{\text{cubic}}^{\ell=2}}{P_{\text{GR}}^{\ell=2}} \sim v^{-1}(\Omega r_V)^{-3/2}, \quad (5.44)$$

where v is the velocity of the pulsar, Ω its orbital angular velocity and r_V is the Vainshtein radius (see section 2.4). Using parameters from the Hulse–Taylor pulsar as a fiducial example [676] yields $P_{\text{cubic}}/P_{\text{GR}} \sim 10^{-7}$, well below the observational precision $\sigma \sim 10^{-3}$. It is interesting to note, however, that the time dependence in the system makes the Vainshtein screening less effective compared to the static case; the force on the two pulsars is suppressed by $(\bar{r}/r_V)^{3/2}$, where \bar{r} is the separation.

⁵⁷ Because the Galileon is a scalar mode, there is also monopole radiation. However the monopole is suppressed relative to the quadrupole order effect because the monopole enters as a relativistic correction: $P_{\text{cubic}}^{\ell=0}/P_{\text{cubic}}^{\ell=2} \sim v \sim 10^{-3}$, see [53].

For the Quartic Galileon the situation is more subtle. For a given multipole, there is more Vainshtein suppression, $P_{\text{quartic}}^l/P_{\text{GR}}^l \sim v^{-2}(\Omega_{\text{rv}})^{-2}$. However, in this case the approximation of a spherically symmetric background is not good, because higher order multipoles are not suppressed effectively. More work is needed to understand this case, e.g. by taking the time dependence into account in the background.

More recently, Narikawa *et al* [677] reported on the prospects for GW detection from coalescing compact binaries in some models of bimetric massive gravity [304]. They find that, in a certain region of the parameter space, the gravitational waveform can display large-amplitude modulations induced by the interference between two modes. The peak amplitude can be up to an order of magnitude larger than its GR value at a given frequency, and such frequency depends on the parameters of the theory. By using Bayesian methods (see section 7.2), Narikawa *et al* evaluate the detectability of these deviations in the waveforms by an advanced laser interferometer, finding that there is a region of the parameter space of the bimetric gravity theory where the deviations can be significant. The detectable region depends on the specific model, but typically corresponds to a graviton mass $\mu \gtrsim 10^{-22}$ eV [677]. Remarkably, this value overlaps with the bounds on the graviton mass derived through the superradiant instability of supermassive Kerr BHs in massive gravity [110, 503] (see section 3.10.2). It is notable that comparable bounds could follow from GW observations of *stellar-mass* objects.

5.6. Open problems

- It has been shown that the dynamics of a BH binary system (with a nonextreme mass ratio) in Bergmann–Wagoner theory coincides with that of GR up to 2.5PN order. Does this result hold at all PN orders? If it does not, at which PN order does it break down?
- Can we extend numerical relativity to modified theories of gravity other than scalar–tensor theory? What is the signature of nonlinear effects in the late inspiral and merger?
- How do spontaneous scalarization and dynamical scalarization generalize to Horndeski theories or tensor-multiscalar theories? Are there similar nonlinear effects that could produce sensible deviations from GR in quadratic gravity theories, Lorentz violating theories or massive gravity?

6. Binary pulsar and cosmological tests of GR

6.1. Tests of gravity from radio pulsars

Overview. Before the 1970s, precision tests for gravity theories were constrained to the weak-field, slow-motion environment of the Solar System. In terms of relativistic equations of motion, the Solar System gave access to the first order corrections to Newtonian dynamics, notably the well-measured anomalous precession of Mercury’s orbit and the deflection of light by the Sun [2]. Testing anything beyond the first PN contributions, like the emission of GWs, was for a long time out of reach.

The discovery of the first radio pulsar in a binary system, PSR B1913+16, by Russell Hulse and Joseph Taylor in the summer of 1974 [678] initiated a completely new field for testing relativistic gravity. For the first time, the back reaction of GW emission on the binary motion could be studied, which gave the first evidence for the existence of GWs as predicted by Einstein’s theory. Furthermore, the Hulse–Taylor pulsar provided the first test bed for the gravitational interaction of strongly self-gravitating bodies.

To date, there are a number of known radio pulsars that can be utilized for precision tests of gravity. Depending on their orbital properties and their companion, these pulsars provide tests for various different aspects of gravity, for instance (see [8], and references therein):

- GR's quadrupole formula for GW emission. The best test (with accuracy better than 0.1%) comes from the Double Pulsar.
- Emission of dipolar radiation. The best bounds come from relativistic pulsar-white dwarf systems, most notably PSR J1738+0333 and PSR J0348+0432, with constraints of order 10^{-5} .
- Limits on the violation of the universality of free fall for strongly self-gravitating bodies (i.e., tests of the SEP). The best tests (better than 1%) are provided by wide pulsar-white dwarf systems.
- Limits on the violation of local Lorentz invariance of gravity from binary as well as isolated pulsars. In this context, the bounds are better than 10^{-8} for some effects.

Besides tests of specific theories (GR, scalar–tensor gravity, vector-tensor gravity, TeVeS, etcetera) these and other pulsars allow for generic constraints on deviations of gravity from GR in the quasi-stationary strong-field regime, and in the generation of GWs, in particular systems where the (effective gravitating) masses of the system can be determined in a theory-independent way.

In the future, the development of new instruments and larger radio telescopes, like the square kilometre array (SKA)⁵⁸, will greatly enhance our capabilities to test gravity with radio pulsars. On the one hand, the greatly improved timing precision will allow for better and new tests with existing systems. On the other hand, new instruments and survey techniques promise the discovery of new 'gravity labs,' like a pulsar-BH system. Furthermore, a SKA based pulsar timing array that utilizes several hundred millisecond pulsars to form a 'multi-armed' GW detector will, for the first time, provide tests in the nano-Hz GW band.

Main results. Radio pulsars are rotating NSs that emit beams of radio waves along their magnetic poles, and due to their rotation act as 'cosmic light-houses.' Some of the 'recycled' pulsars have rotational stabilities that are comparable to the stability of the best atomic clocks on Earth [679]. Presently there are more than 2000 radio pulsars known, where about 10% of them are members of binary systems [680]. The observation of the rotational phase of a pulsar with a radiotelescope is basically a 'clock-comparison' experiment in a spacetime that contains the binary system with the 'pulsar clock' on the one hand, and the radio telescope with its atomic clock as part of the Solar System on the other hand. The world-line of the pulsar and the world-line of the telescope are connected by the radio signals of the pulsar, propagating through curved spacetime. By this one directly probes the solutions of field equations of different gravity theories. The technique used is the so-called *pulsar timing*, which basically consists of measuring the exact arrival time of pulses at the radio telescope on Earth and fitting an appropriate timing model to these arrival times to obtain a phase-coherent solution, that accounts for every observed rotation of the pulsar. For some pulsars, that phase-coherent solution stretches over several decades, allowing for an extremely precise measurement of the key parameters. For instance, some pulsar periods are known to atto-seconds precision, and some orbital periods of binary pulsars have uncertainties below a micro-second (see table 1 of [681] and references therein).

For binary pulsar experiments that test the quasi-stationary strong-field regime and the GW damping, a phenomenological parametrization, the so-called parametrized post-

⁵⁸ <http://skatelescope.org/>

Keplerian (PPK) formalism, has been introduced by Damour [682] and extended by Damour and Taylor [683]. The PPK formalism generically parametrizes the observable relativistic effects that can be extracted independently from binary pulsar timing and pulse-structure data ('post-Keplerian (PK) parameters'). Consequently, the PPK formalism allows us to obtain theory-independent information from binary pulsar observations by fitting for a set of Keplerian and PK parameters. The most important PK parameters are [684]:

- $\dot{\omega}$: relativistic precession of periastron.
- γ : amplitude of the time dilation of the 'pulsar clock' (compared to an averaged time). It is a combination of the second-order Doppler shift and the redshift caused by the gravitational field of the companion.
- r and s : *range* and *shape* of the Shapiro delay, caused by the gravitational field of the companion.
- \dot{P}_b : change in the orbital period due to GW damping.

Depending on the nature of the companion and the size of the orbit, different aspects of relativistic gravity can be tested with binary pulsars. In the following, we briefly highlight the most important systems and some of the tests that have been performed with them.

PSR B1913+16 (Hulse–Taylor pulsar) was the first binary pulsar to be discovered [678]. It is in a 7.8 h, high-eccentricity ($e = 0.62$) orbit with another NS. This system allows the measurement of three PK parameters ($\dot{\omega}$, γ , \dot{P}_b), and led to the first proof of the existence of GWs as predicted by GR [685]. Presently, it gives a 0.2% verification of GR's quadrupole formula, a precision which currently, however, cannot be further improved due to uncertainties in the distance to PSR B1913+16 [686].

PSR J0737–3039A/B (Double pulsar) was the first, and so far only, binary pulsar system found to consist of two active radio pulsars [687, 688]. Pulsar A is a fast-rotating (23 ms) pulsar in a mildly eccentric ($e = 0.088$), 2.5 h orbit. Until 2008 its companion (pulsar B) was also visible as an active radio pulsar with a rotational period of about 2.8 s. The timing of both pulsars allowed an immediate determination of the mass ratio from the projected semi-major axes of the two pulsar orbits. In the double pulsar all PK parameters listed above have been measured, some of them with exquisite precision. Most importantly, the change in the orbital period \dot{P}_b due to GW damping has by now been tested to agree with the quadrupole formula of GR to better than 0.1%, giving the best test for the existence of GWs as predicted by GR [681]. As a result of geodetic precession, pulsar B has in the meantime turned away from our line-of-sight and is no longer visible [689]. Due to the high inclination of the orbital plane (close to 90°), pulsar A is getting eclipsed by the plasma-filled magnetosphere of pulsar B every $2\frac{1}{2}$ h, for about 30 s around superior conjunction. Changes in the eclipse pattern could be used to determine the rate of geodetic precession, Ω_B , with a precision of about 13% [690]. The obtained value is in good agreement with GR. All these tests are summarized in form of a mass–mass diagram in figure 35.

PSR J1738+0333 is a pulsar in a nearly circular ($e \sim 3 \times 10^{-7}$), 8.5 h orbit with an optically bright white dwarf. High-resolution spectroscopy allowed the determination of the white dwarf mass (based on white dwarf models) and the motion of the white dwarf around the common center of mass (Doppler shifts). In combination with the timing observations, one immediately gets the masses of the system, valid for a large class of gravity theories: $m_p = 1.47_{-0.06}^{+0.07} M_\odot$ and $m_c = 0.181_{-0.006}^{+0.007} M_\odot$ [691]. The corresponding change in the orbital period due to the emission of GWs as predicted by GR agrees well with the observed value ($\sim 13\%$ precision) [37]. Although the precision is significantly worse than in the GW test with the Double Pulsar, the high asymmetry in the compactness/binding energy of the bodies in

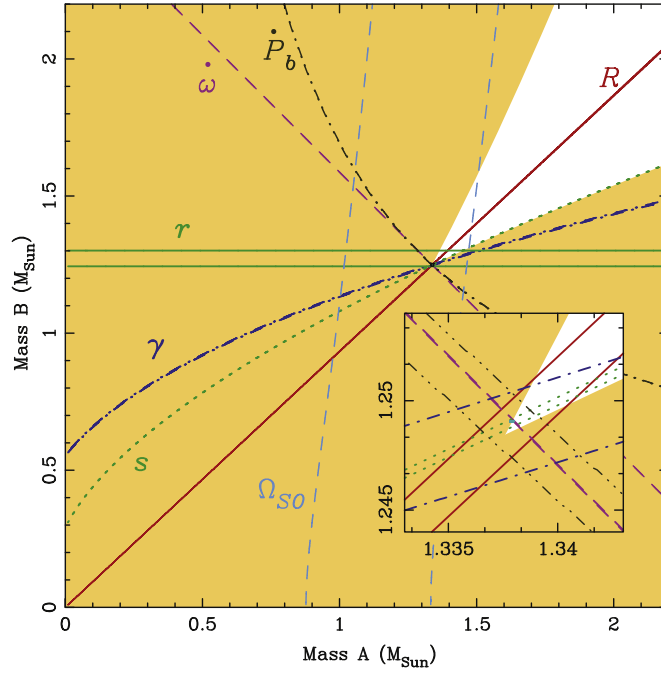


Figure 35. GR mass–mass diagram for the double pulsar with six PK parameters ($\dot{\omega}$, γ , \dot{P}_b , r , s , Ω_{SO}) and the mass ratio (R). All constraints agree on a small common region (see inset), meaning that GR has passed this test of several relativistic effects (quasi-stationary strong-field as well as radiative). (Figure courtesy of Michael Kramer.)

the system makes this test particularly sensitive to gravitational dipolar radiation. As a consequence, PSR J1738+0333 provides the best test for scalar–tensor gravity for most values of β_0 , in particular for the range $\beta_0 \gtrsim 3$ (see figure 37).

The small eccentricity and comparably (unmeasured) high rate of periastron advance ($\sim 1.6 \text{ deg yr}^{-1}$) allows for a test of preferred-frame effects in the orbital motion, and in particular sets the best limit on the strong-field generalization of the PPN parameter α_1 : $\hat{\alpha}_1 = -0.4_{-3.1}^{+3.7} \times 10^{-5}$ at 95% confidence level⁵⁹[692]. An important piece of information for this test is the motion of the system with respect to the frame of reference defined by the cosmic microwave background, which is known for the PSR J1738+0333 system, since one also has the systemic radial velocity derived from the spectroscopy of the white dwarf.

PSR J0348+0432 is the first, and so far only (unambiguously identified) massive pulsar in a relativistic orbit. The pulsar has a mass of $2.01 \pm 0.04 M_\odot$ and is in a 2.5 h orbit with a low-mass white dwarf [551]. The white-dwarf companion is optically bright, and therefore allows for high-resolution spectroscopy, which, like for PSR J1738+0333, was used to determine the masses of the white dwarf and the pulsar. In parallel, high-precision timing led to the measurement of an orbital decay of $\dot{P}_b = -8.6 \pm 1.4 \mu\text{s yr}^{-1}$. The measured value is

⁵⁹ The hat denotes the fact that α_1 can be modified by strong-field contributions: see e.g. equations (194) and (196) in [49].

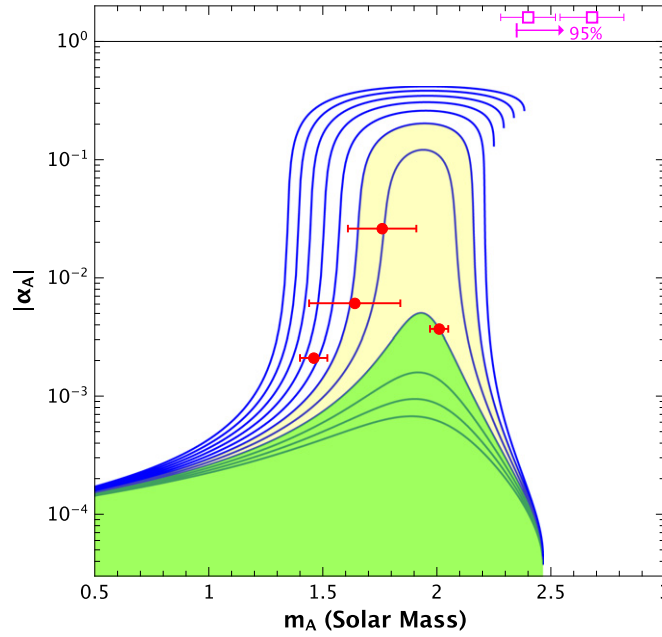


Figure 36. Upper limits on the effective scalar coupling α_A (red dots) for four different pulsars (increasing in mass): PSR J1738+0333, PSR J1012+5307, PSR J0437-4715, and PSR J0348+0432. The blue lines are plotted for $\alpha_0 = 10^{-4}$, while β_0 runs from -5.0 to -4.0 in steps of 0.1 , with the largest $|\alpha_A|$ reached for $\beta_0 = -5.0$. Without PSR J0348+0432 the green and yellow areas would be allowed, and massive NSs could be highly scalarized. This is now excluded with the limit from PSR J0348+0432. The pink measurements at the top of the figure are (less robust) mass constraints for three high-mass pulsar candidates. All three of them do not allow for a gravity test, but indicate the need for a rather stiff equation of state.

in good agreement with GR, and excludes any significant contribution from dipolar radiation: $|\alpha_{\text{PSR}} - \alpha_0| < 0.005$ with 95% confidence⁶⁰ [551]. Although that limit is weaker than the one of PSR J1738+0333 above, it is independently important, since PSR J0348+0432 has a significantly larger gravitational binding energy than other binary pulsars used to test gravity theories. Consequently, PSR J0348+0432 constrains deviations from GR that would only occur in the strong internal fields of more massive NSs, like certain types of spontaneous scalarization (see figure 36).

Even binary-pulsar systems that are not very relativistic ($P_b \gtrsim 1$ d) can be used to test gravity theories. For instance, a violation of the SEP is best tested with pulsars in a wide orbit with a white dwarf companion. If the strongly self-gravitating pulsar felt a different acceleration in the gravitational field of the Milky Way than the white dwarf, a polarizing force would change the orbital eccentricity in a characteristic way. Damour and Schäfer suggested a statistical test, based on Galactic small-eccentricity binary pulsars to constrain a violation of SEP by strongly self-gravitating bodies [694]. The best constraint is based on an

⁶⁰ The quantity α_{PSR} denotes the effective (e.g. scalar) coupling of the pulsar, and α_0 the effective coupling of weakly self-gravitating bodies (e.g. white dwarfs).

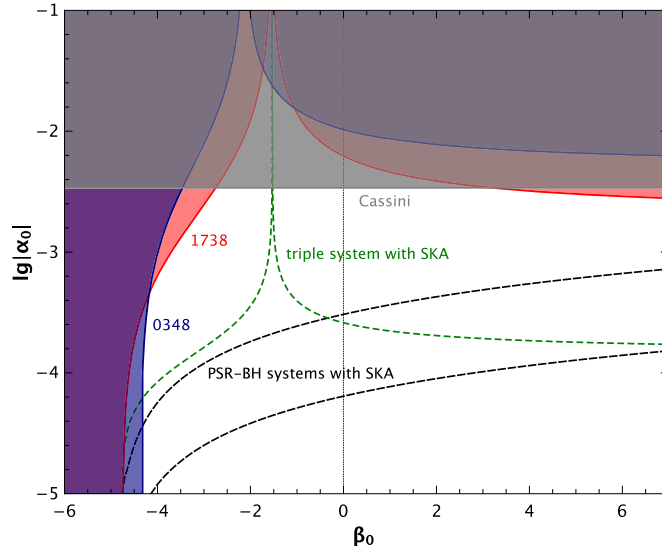


Figure 37. Constraints in the α_0 - β_0 plane of scalar-tensor theories by present experiments (Cassini, PSR J1738+0333, PSR J0348+0432) and selected future tests (dashed curves). The black dashed lines show upper limits from two different (hypothetical) pulsar-BH systems, with $P_b = 5$ d, $e = 0.8$ (upper) and $P_b = 0.5$ d, $e = 0.1$ (lower), observed with the SKA. The dashed green line shows the expected upper limits from timing the triple-system pulsar (PSR J0337+1715) with the SKA. Calculations are based on a stiff equation of state, and therefore conservative. For negative β_0 , PSR J0348+0432 is the most constraining system, due to its high mass. The vertical line at $\beta_0 = 0$ corresponds to Jordan-Fierz-Brans-Dicke gravity. This figure is an updated version of previous studies by Damour and Esposito-Farèse (see [693] and references therein).

ensemble of small-eccentricity binary pulsars, and gives $|\Delta_{\text{SEP}}| < 0.0056$ with 95% confidence⁶¹ [695]. The newly discovered millisecond pulsar PSR J0337+1715 in a stellar triple system [697], where an inner pulsar-white dwarf binary ($P_b = 1.63$ d) is orbited by an outer white dwarf in just 327 d, promises a much better test of the SEP [697, 698]. In particular, with the help of future radio telescopes like the SKA, this system could provide one of the most constraining tests for scalar-tensor gravity (see figure 37). However pure strong-field deviations from GR, like spontaneous scalarization in scalar-tensor gravity, cannot be tested with the triple system pulsar, due to the weak-field nature of the other two bodies.

Binary pulsar constraints on Lorentz violations in gravity. As reviewed in section 2.5, Solar System tests impose tight constraints on *some* combinations of the coupling parameters of both Einstein-Æther theory and khronometric gravity. More specifically, once the constraints on the preferred-frame parameters α_1 and α_2 are imposed (i.e. when one requires $|\alpha_1| \lesssim 10^{-4}$ and $|\alpha_2| \lesssim 10^{-7}$ [2]), both theories remain characterized (to leading order in α_1 and α_2) by only two dimensionless coupling constants, which we denote by

⁶¹ Note that the somewhat better limit given by [696] is heavily based on a binary pulsar that does not fulfill the criteria for the Damour-Schäfer test, and is therefore clearly less robust.

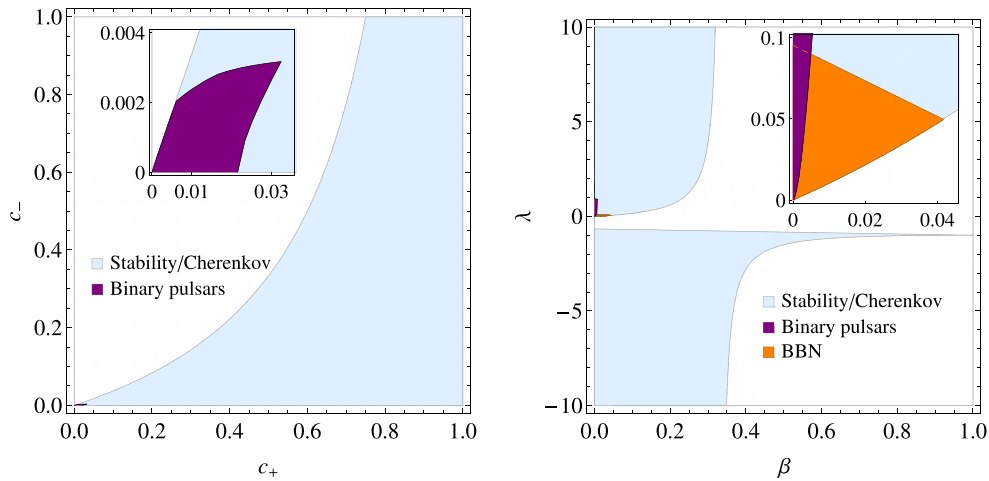


Figure 38. Experimental constraints on Einstein-Æther (left) and khronometric theory (right). (Adapted from [48, 49].)

c_+ and c_- in Einstein-Æther theory and λ and β in khronometric gravity (see section 2.5 for details).

The parameter space for these coupling constants is further constrained by theoretical requirements (absence of ghosts and gradient instabilities), as well as by the requirement that gravitational excitations propagate with speeds larger than the speed of light, in order to avoid the production of gravitational Cherenkov radiation by photons and relativistic particles [278]. Also, in the case of khronometric gravity, further constraints arise from the requirements that the observed primordial element abundances match the predictions of Big Bang nucleosynthesis [48, 49, 276]. Note that Big Bang nucleosynthesis gives much weaker constraints on Einstein-Æther theory [47, 276].

All the above constraints are summarized in figure 38. Also, as discussed in section 5.4, competitive constraints can be placed on the coupling parameters by requiring that the rate of change of binary-pulsar systems matches the observations (as well as by requiring that isolated pulsars show no anomalous precession, which would be induced by Lorentz violations) [48, 49]. In particular, the purple region in figure 38 is obtained by imposing agreement with the observations of PSR J1141–6545 [699], PSR J0348+0432 [551], PSR J0737–3039 [700] and PSR J1738+0333 [37, 691]. Finally, we should stress that additional constraints on Lorentz violations in gravity come from cosmological observations such as the CMB and the large-scale structure, *if* a direct coupling between the Lorentz-violating field and the Dark Sector is introduced [701, 702].

6.1.1. Open problems. In the near future, radio astronomy will benefit from the operation of new radio telescopes with significantly larger collecting area. By the end of 2016 the FAST [703] should see ‘first light,’ and in the early 2020s the SKA should reach its design sensitivity, greatly enhancing timing precision of known pulsars (up to a factor of 100 for many of them) and increasing the number of known pulsars by an order of magnitude [704]. In terms of gravity tests with pulsars, this means a leap in the precision of current tests, various qualitatively new tests with already known systems, and the discovery of many new ‘pulsar laboratories.’

Concerning the known systems, for the first time we will be able to test relativistic effects in binary pulsars beyond the leading order. For instance, in the double pulsar we will be able to test the mass-octupole and current-quadrupole corrections to the quadrupole formula [602, 705]. In the double pulsar, we should also be able to extract the Lense–Thirring drag from the total $\dot{\omega}$, and by this measure the moment-of-inertia of pulsar A: see equation (5.23) of [706]. Since the moment of inertia of a NS depends on its compactness and therefore on the EOS of NS matter, this measurement will test competing NS matter models, and give insight into the properties of matter at very high densities ($\sim 10^{15}$ g cm $^{-3}$) [552, 602].

Qualitatively, new tests could come from the discovery of a pulsar-BH system, either a pulsar in orbit with a stellar mass BH or in orbit around the supermassive BH in the center of our Galaxy. If intermediate-mass BHs do exist in some of the dense cores of globular clusters, this might be a third option to find such a test system. The ranging capability that comes with the timing of a pulsar would provide a unique probe for the BH spacetime, and allow for tests of the frame dragging and the no-hair theorem [707–710]. But even for theories that predict the same BHs as GR, a pulsar-BH system could be a unique ‘laboratory’ (see figure 37).

A completely different type of test could come from pulsar timing arrays, which are presently used in the effort to detect nano-Hz GWs [711]. With the timing capabilities of the SKA, one can hope to probe the polarization and propagation properties of these long-wavelength GWs [712], or even study the evolution of a single supermassive BH binary [713, 714].

6.2. Testing GR with cosmology

The past three decades have witnessed remarkable progress in relativistic cosmology. Cosmological data constraining the expansion rate of the Universe, allied with accurate maps of large-scale structure and the cosmic microwave background, have been used to place ever-tightening constraints on cosmological parameters [715]. In parallel with observational progress, publicly available tools, that can be used to predict cosmological observables for general relativistic cosmologies and their extensions, have been developed. The field is alive and well with a plethora of new, extremely powerful experiments and observatories in the planning stage that will come to fruition at the end of this decade.

Crucial to the successes of modern cosmology has been the realization that the morphology and evolution of large-scale structures—that is, the cosmic web of galaxies, clusters, voids and filaments—should contain a wealth of information about various fundamental properties of the Universe [716]. What was initially a niche area developed by Peebles, Zel’dovich, Silk and others has become a powerhouse of exploration and one of the leading areas of research in modern astrophysics. The theory and observation of anisotropies in the cosmic microwave background are the jewels in the crown of this field of research, and have been used to place precise constraints on properties such as the geometry of the Universe, its material constituents and the initial conditions that seeded structure. A bizarre picture of the Universe has emerged in which, if GR is assumed to be the underlying theory of gravity, 96% of the material content of the Universe is in a dark sector—dark matter and dark energy. A plethora of models has been proposed that try to account for this dark sector [717].

Given that the evidence for the dark sector is purely gravitational, there have been, in the past few years, attempts at finding theories in which it can arise from modifications of gravity [15]. These modifications affect the expansion rate of the Universe, but should also affect gravitational clustering in a way that might be distinguishable from GR. This idea has led to the proposal of a number of different theories (as discussed at length in section 2) but has also focused observational programs to target deviations from GR. It is fair to say that the

cosmological tests of modified gravity are now the primary driver for future surveys of large scale structure.

6.2.1. Theory: the linear regime. Faced with the proliferation of ever-more exotic gravity theories, the conventional process of testing models on an individual basis is not the optimal way of testing GR on cosmological scales. Not only is the theory population too large to tackle (and growing still), but progress is slowed by the increasing mathematical complexity of the most popular ideas. It was for these reasons that, several years ago, a number of groups turned to the strategy of devising model-independent tests of gravity. Effectively, one attempts to build a template for what viable beyond-GR theories can look like, in terms of a minimal set of unknown parameters and functions. One then builds up a ‘translation dictionary,’ that is, a correspondence of how the parameters involved in the general formalism relate to the parameters of specific theories. With this dictionary in hand, testing the unified framework provides an efficient way to test many theories simultaneously. However, the framework is more general than this, because it also covers regions of parameter space for which no corresponding theory has been established yet. Constraints on this part of the parameter space can be used to guide the direction of *future* theoretical work.

While the PPN formalism [718] is an example of one such model-independent framework, it is limited to small-scale tests of gravity, say, in the Solar System or using compact object binaries. There is a need for an analogous formalism that can be applied to cosmological observables. This is a formidable task, so most work to date has focused on formalisms that capture the regime of linear cosmological perturbation theory only.

Let us consider, for a moment, the properties we would like a cosmological equivalent to PPN to have:

- (1) It should encapsulate a large portion of the existing theory space.
- (2) Existing theories should map onto it *exactly*, rather than only as an approximation.
- (3) The parameters of the formalism should have physical meaning, rather than simply denoting mathematical terms.
- (4) The parameters (or combinations thereof) should be constrainable by near-future data.
- (5) The formalism should achieve all of the above with the minimum number of new parameters and/or free functions.

There is no obvious, unique way to meet all of the above criteria. Instead, three species of parametrizations have been put forward in response to the challenge. One can think of these three formulations as corresponding to three manifestations of a gravity theory: its fundamental action, the field equations derived from that action, and the combinations of those field equations which directly influence observable quantities. We will now describe each of these formalisms briefly in turn.

Action-based approaches. To derive linearized gravitational field equations, one needs an action that is quadratic in perturbations. One way to parametrize gravity is to construct the most general quadratic action with a given field content that is consistent with some desirable symmetries. Placing a restriction on the derivative order of the field equations terminates the potentially infinite series of terms that could be constructed. A coefficient of appropriate mass dimensions is assigned to each term; these represent the ‘dials’ of the formalism that can be tuned to match a specific theory.

This concept can, to a certain extent, be thought of as an EFT for modified gravity (see section 2.8), although the analogy with particle physics EFTs should not be taken too far. To

date, nearly all work has focused on actions constructed from the metric and a single scalar degree of freedom [719, 720], though a bi-scalar case recently appeared in [721].

Such parametrized actions can quickly grow to contain large numbers of terms. However, the authors of [722–726] have made use of a clever device to simplify the procedure. They first consider the situation as viewed from the *unitary gauge*, in which the time coordinate is chosen such as to eliminate perturbations of the scalar field. As a result of having used up one gauge freedom in this way, the metric is left with three spin-0 perturbations instead of the usual two (after gauge fixing); one might say that the metric has ‘eaten’ the scalar field.

Given the preferred space–time slicing, it is then natural to reformulate metric perturbations in the ADM formalism. An example of a resulting action is [724]:

$$\begin{aligned}
S_{\text{EFT}} = \int d^4x \sqrt{-g} & \left[\frac{M_P^2}{2} f(\eta) R - \Lambda(\eta) - c(\eta) g^{00} + \frac{M_2^4}{2} (\delta g^{00})^2 \right. \\
& - \frac{m_1^3}{2} \delta K \delta g^{00} - \frac{\bar{M}_2^2}{2} \delta K^2 - \frac{\bar{M}_3^2}{2} \delta K_\nu^\mu \delta K_\mu^\nu + \frac{\mu_1^2{}^{(3)}}{2} R \delta g^{00} \\
& \left. + \frac{\bar{m}_5^{(3)}}{2} R \delta K + \frac{\lambda_1^{(3)}}{2} R^2 + \frac{\lambda_2^{(3)}}{2} R_\nu^\mu {}^{(3)} R_\mu^\nu \right], \quad (6.1)
\end{aligned}$$

where $K_{\mu\nu}$ is the extrinsic curvature of the spatial hypersurfaces defined by the foliation, and ${}^{(3)}R$ is their three-dimensional intrinsic curvature. The metric component g^{00} is related to the usual ADM lapse function by $g^{00} = -1/N^2$. Performing a Stuckelberg transformation [727] on the time coordinate will exit the unitary gauge and cause the scalar field to reappear in the action. The action can then be varied in the usual manner.

The advantage of this EFT-inspired approach is that it directly parametrizes the action, and therefore, constraints on the EFT coefficients would have direct implications for which kinds of theories are allowed by the data. The disadvantages are that (i) it is necessary to fix the field content allowed by the parametrization, and (ii) the combinations of EFT parameters that filter through to observable quantities (say, the modified growth rate or weak lensing kernel) are cumbersome combinations of the action-level parameters. With regards to (i), we emphasize that nearly all work to date has focused on a single scalar field. Clearly this covers only part of the broad space of gravity theories.

Field equation approaches. An alternative method is to directly parametrize the linearized gravitational field equations, the dynamical tools of a theory. After some consideration, one realizes that there are only three kinds of new terms that can appear in the field equations: perturbations of the metric, perturbations of the matter stress–energy tensor, and perturbations of any new degrees of freedom that a theory might add to GR.

An example in this category is the parametrized post-Friedmann formalism (PPF) [728]. For simplicity, we consider here the parametrization of the spin-0 field equations, restricting them to be of second order in time derivatives. We will not show the full framework, but as a representative example the extended 00—component of the field equations in the conformal Newtonian gauge is:

$$\begin{aligned}
-a^2 \delta G_0^0 = 8\pi G_N a^2 \rho_M \delta_M + A_0(k, a) k^2 \Phi + F_0(k, a) k^2 \Gamma \\
+ \alpha_0(k, a) k^2 \chi + \alpha_1(k, a) k^2 \dot{\chi}, \quad (6.2)
\end{aligned}$$

where $\Gamma = (\dot{\Phi} + H\Psi)/k$, δG_ν^μ is the usual linearized Einstein tensor and χ is a template variable representing a new spin-0 degree of freedom; only one new degree of freedom is shown above, but in principle more could be added. The new degree of freedom does not

have to be a simple scalar field: for example, when the parametrization is used to describe Einstein-Æther theory, χ represents the spatial spin-0 perturbation of a vector.

$A_0(k, a)$, $F_0(k, a)$, $\alpha_0(k, a)$ and $\alpha_1(k, a)$ are the free functions of time and scale that act as the ‘dials’ of the parametrization in this case. In fact, the scale-dependence of $A_0 \dots \alpha_1$ is fixed by Lorentz symmetry and the derivative order of the parametrization—they can only contain powers like k^{2n} .

The other components of the spin-0 field equations follow an analogous pattern, see [728] for details. Naively, it appears that 22 free functions are needed to map out all possible extensions to the field equations. In reality, this is too much freedom—not all of these 22 PPF coefficients are independent. By connecting the PPF approach to the action-based parametrizations described above, one determines that only ~ 5 – 9 independent functions are needed to describe a simple scalar field theory (the exact number depends on assumptions made about Lorentz symmetry and whether one fixes the background expansion rate or not). The advantage of field equation approaches such as PPF is that they can encapsulate numerous gravity theories without requiring any assumptions about field content. The disadvantage is that, at face value, the parametrization contains redundant freedoms that could cause problematic degeneracies for a constraint analysis.

Quasistatic approaches. The final approach to parametrizing deviations from GR is the simplest, and therefore the easiest to constrain, but also the least comprehensive from a formal standpoint. It makes use of the *quasistatic approximation*. To implement this, we focus on a restricted range of distance scales that are considered to be significantly smaller than the cosmological horizon, but sufficiently large that [729]:

- (1) Perturbations are in the linear regime.
- (2) $H/k \ll 1$, so any term in the field equations containing this prefactor can be dropped.
- (3) The time derivatives of perturbations are negligible compared to their spatial derivatives on these scales.

In GR, it can be shown that (3) follows as a consequence of (2). In modified theories this is no longer necessarily the case; instead it must be *assumed* that (3) applies to any new fields introduced by a theory, as well as to the metric itself. The majority of theory-specific simulations to date support this set of assumptions [730–733], but see [734, 735] for counter-examples.

By making the above approximations (and taking appropriate combinations of the field equations), one finds that in the quasistatic regime many theories of gravity can be reduced to the simple form:

$$\nabla^2 \Psi = 4\pi G_N a^2 \mu(k, a) \rho_M \Delta_M, \quad (6.3)$$

$$\gamma(k, a) = \frac{\Phi}{\Psi}, \quad (6.4)$$

where Δ_M is a gauge-invariant matter density perturbation and, as in the previous subsection, $\mu(k, a)$ and $\gamma(k, a)$ are functions of time with fixed scale dependence of the form k^{2n} (in the majority of cases). In particular, one can show that in the case of Horndeski gravity, which is the most general theory of a single scalar field with second-order field equations, μ and γ have the form [736, 737]:

$$\mu(k, a) = h_1(a) \left(\frac{1 + h_5(a)k^2}{1 + h_3(a)k^2} \right), \quad (6.5)$$

$$\gamma(k, a) = h_2(a) \left(\frac{1 + h_4(a)k^2}{1 + h_5(a)k^2} \right), \quad (6.6)$$

where $h_i(a)$ are pure functions of time.

This parametrized Poisson equation and ‘slip relation’ (the ratio of Φ and Ψ) are all that is needed to start calculating observable quantities, such as Galaxy weak lensing and the growth rate of large-scale structure [738, 739]. Example forecasts for constraints on μ and γ with the large synoptic survey telescope [740] can be found in [741]. Recent measurements using the 6dF peculiar velocity survey did not find any evidence for scale dependence in the growth rate of large-scale structure [742], which places a lower limit on any new mass scale involved in theories described by equations (6.5) and (6.6) [738].

The advantage of the quasistatic parametrization is clearly its simplicity and direct connection to observations. Its chief disadvantage is that it is an approximation with a limited regime of applicability, and does not exactly match the form of the underlying space of gravity theories. This obscures attempts to work out what constraints on μ and γ really mean for a particular theory of interest.

6.2.2. Theory: the nonlinear regime. Calculating the effects of modified gravity becomes significantly harder as we move into the nonlinear regime. Local (laboratory and Solar System) experiments place strong constraints on any deviation from GR: the results of such experiments require any new gravitational fifth force to be either very weakly coupled to matter or very short-ranged in the environments where the experiments have been performed. To avoid these strong experimental constraints, and at the same time give rise to interesting observable cosmological signatures, a screening mechanism is required. By screening we mean a way of hiding the modifications of gravity in our local (high-density) environments where high-precision gravity experiments have been performed, while at the same time allowing for potentially large deviations in regions of spacetime where the average density is much lower. We will briefly explain how screening works and which theories have some form of screening.

Most of the known screening mechanisms for scalar–tensor theories are encompassed by the general (Einstein-frame) Lagrangian:

$$\mathcal{L} = \frac{R}{2} M_{\text{Pl}}^2 + \mathcal{L}(\phi, \partial\phi, \partial\partial\phi) + \mathcal{L}_m(A^2(\phi)g_{\mu\nu}, \psi_m). \quad (6.7)$$

The matter fields are coupled to a metric $\tilde{g}_{\mu\nu} = g_{\mu\nu}A^2(\phi)$ that is conformally related to the space–time metric $g_{\mu\nu}$. In the nonrelativistic limit, such a theory gives rise to a fifth force given by:

$$\vec{F}_\phi = \frac{\beta(\phi)}{M_{\text{Pl}}} \vec{\nabla}\phi, \quad \beta(\phi) \equiv \frac{d \log A}{d\phi} M_{\text{Pl}}. \quad (6.8)$$

If the field equation for ϕ is linear, then the superposition principle is in play and screening cannot be achieved, so a fundamental requirement for a screening mechanism to work is nonlinear field equations. There are three ways of achieving this: with a self-interacting potential, in the coupling to matter or in the kinetic terms. To see the different ways screening can emerge we expand the Lagrangian about a field value ϕ_0 :

$$\mathcal{L} \simeq \frac{R}{2} M_{\text{Pl}}^2 + Z^{\mu\nu}(\phi_0) \delta\phi_{,\mu} \delta\phi_{,\nu} + m^2(\phi_0) \delta\phi + \frac{\beta(\phi_0) \rho_m}{M_{\text{Pl}}} + \dots \quad (6.9)$$

In a low-density environment, the field sits at some value $\phi_0 = \phi_A$ and the scalar field produces a fifth force on a test mass with strength $\alpha \propto \beta^2(\phi_A)$ relative to the gravitational force. Consider now a high-density region of space where $\phi_0 = \phi_B \neq \phi_A$. One way to reduce the effect of the fifth force is by having the field ϕ acquire a large local mass $m(\phi_B) \gg m(\phi_A)$, which implies a very short interaction range—this is the chameleon mechanism [743, 744]. If the matter coupling is small, $\beta(\phi_B) \ll \beta(\phi_A)$, the fifth force will be suppressed—the symmetron mechanism [745]. Lastly, the condition $|Z^{\mu\nu}(\phi_B)| \gg |Z^{\mu\nu}(\phi_A)|$ leads, after canonical normalization, to a weakened matter source and therefore also a weakened fifth force—the Vainshtein mechanism [308, 746].

In the nonlinear regime of structure formation the screening effect will be in operation and must be taken into account to obtain reliable theory predictions. Linear perturbation theory is unable to account for screening, as it is a purely nonlinear effect, and to understand structure formation in screened theories one is therefore led to N -body simulations. In such simulations one solves for the full evolution of the scalar field in the simulation box just as one does for the metric potential, though one can often apply the quasi-static approximation (see previous section) to simplify the field equation. The N -body equations of motion are given by: (i) the particle displacement equation:

$$\ddot{\mathbf{x}} + \left(2H + \frac{\beta(\phi)\dot{\phi}}{M_{\text{Pl}}} \right) \dot{\mathbf{x}} = -\frac{1}{a^2} \vec{\nabla} \Phi - \frac{1}{a^2} \frac{\beta(\phi)}{M_{\text{Pl}}} \vec{\nabla} \phi, \quad (6.10)$$

where the last term represents the scalar fifth force, and (ii) the Poisson equation for the metric potential:

$$\nabla^2 \Phi = 4\pi G_{\text{N}} a^2 \delta\rho_{\text{eff}}, \quad (6.11)$$

where $\delta\rho_{\text{eff}}$ is the perturbed total effective energy density, which contains contributions from matter and modifications to the Einstein tensor due to modified gravity. Lastly we have the field equation for ϕ , which is model-dependent. Due to the nonlinearities in this equation, the method of choice for solving it is (Newton–Gauss–Seidel) relaxation. Accurately solving the field equation for the scalar field is by far the most challenging and time-consuming part of such simulations. To date several different models with different kinds of screening mechanism have been simulated, including

- Chameleon screening: chameleon models [732] and $f(R)$ gravity [730, 747–749].
- Symmetron screening: symmetron models [733, 750].
- Vainshtein screening: Dvali–Gabadadze–Porrati (DGP) [314, 751, 752] and Galileon models [753].

The results from such simulations have so far mostly been used to map out potential signatures rather than computing explicit constraints. An exception is [754], which constrains $f(R)$ gravity using cluster abundances, however the constraints found are not yet compatible with those found from taking local experiments into account.

The first key observable where the effects of modified gravity are seen is the matter power spectrum. When measured relative to Λ CDM, one typically finds an enhancement: a bump around $k \sim 1 \text{ h/Mpc}$, as seen in figure 39. N -body simulations have shown the importance of taking screening into account when making predictions: linear theory (or simulations with a linearized field equation for the scalar field) produces way too much clustering, and the power spectrum on nonlinear scales can be off by several tens of percent

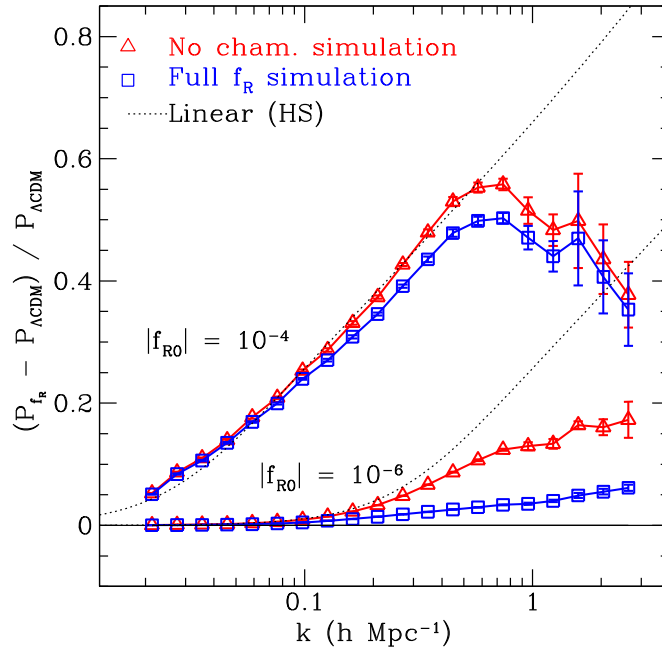


Figure 39. Relative power spectrum enhancement over Λ CDM at $a = 1$ for the full $f(R)$ simulation compared with the no-chameleon (simulations with a linearized field equation) simulations and linear perturbation theory. At high k , linear theory overestimates the relative enhancement. Without the chameleon screening mechanism, power is sharply enhanced on scales smaller than the Compton scale in the background. For $|f_{R0}| = 10^{-6}$ the screening is very effective and the fifth force in the simulations is strongly suppressed. For $|f_{R0}| = 10^{-4}$, this suppression is nearly absent except for a residual effect from the chameleon at high redshift. (From [755].)

from the true result, as seen in figure 39. Different screening mechanisms, different models and also different model parameters can give rise to very different results, making the construction of a model-independent parametrization, as presented above for the linear regime, hard to achieve. However, a parametrization valid for a certain sub-class of models (of the chameleon type) has been proposed [420].

Another key observable is the halo mass function, which is also enhanced relative to Λ CDM, see figure 40. When the screening mechanism is working effectively, the enhancement is typically found for low to mid-size halos ($M \sim 10^{12} - 10^{14} M_{\text{Sun}}/h$). A key property of all known screening mechanisms is that they are more effective for more massive halos. This implies that the mass function converges to that of the underlying cosmological model in the high-mass end ($M \gtrsim 10^{15} M_{\text{Sun}}/h$). If the screening mechanism is not very effective then this does not have to happen, and the mass function is enhanced even for the largest halo masses.

Results from N -body simulations have also revealed several smoking-gun signatures of modified gravity. One particularly interesting signature is the difference between dynamical and lensing masses [756]. The mass contained within a dark-matter halo can be found by either gravitational lensing measurements or by some measurement that relies on the dynamics of test masses. Gravitational lensing is determined by the sum of the two metric potentials $\Phi + \Psi$, and the inferred lensing mass in many theories with screening gives the

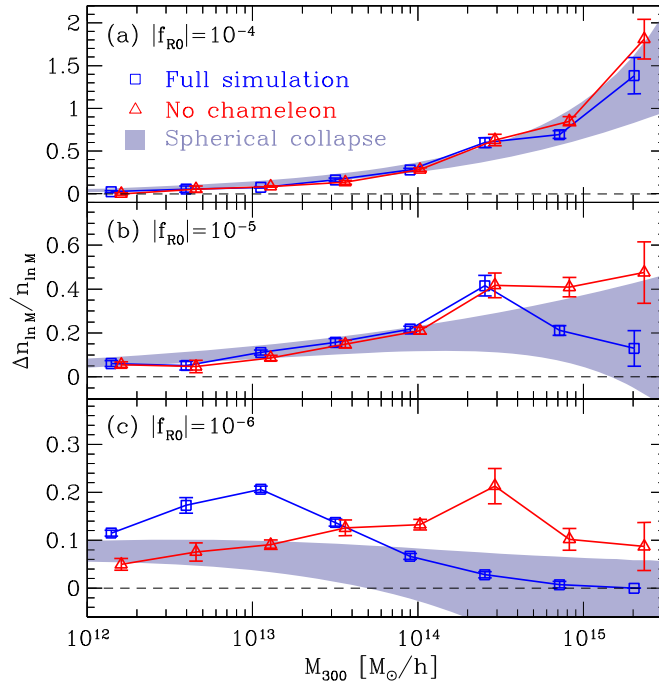


Figure 40. Relative mass-function enhancement over Λ CDM at $a = 1$ for the full $f(R)$ simulation compared with the no-chameleon (simulations with a linearized field equation) simulations and the spherical collapse model. For the lowest value ($|f_{R0}| = 10^{-4}$) the screening mechanism is not much in play, and the mass function is enhanced in the high-mass end. As we go to smaller values of $|f_{R0}|$ the screening mechanism becomes more and more effective, and the mass function is only enhanced for mid-sized halo masses. We also see the importance of solving the full field equation: the no-chameleon simulation significantly overestimates the mass function in the high-mass end for $|f_{R0}| = 10^{-6}$. (From [755].)

same result as in GR. Dynamical masses, on the other hand, are affected by the fifth force, and will consequently be different from the GR versions. Combining lensing and dynamical mass measurements can therefore probe modified gravity. Additionally we have the effect that the amount of screening will depend on the density of the environment a certain massive object lies in. This will give rise to an environment dependence on dynamical mass estimates, and serves as a smoking gun signal for theories with screening. In principle, this effect could also distinguish between different types of screening [757].

Quite often, the strongest effects of modified gravity (measured relative to Λ CDM) are found in the velocity field. Interesting signatures that have been found here include the low-order moments of the pairwise velocity distribution [758] and the full phase space around Galaxy clusters [759].

There are issues related to the nonlinear regime that need to be better understood before we can fully exploit its potential as a probe of modified gravity. For example, when it comes to the matter power spectrum, the modified gravity signal found in simulations is degenerate with several other effects, such as massive neutrinos [760] and baryonic feedback processes, that are not fully understood at the moment. One way around this issue is to look for

observables that are not significantly affected by baryonic physics, or combining observables that allow us to break the degeneracies.

6.2.3. Observations, current and future. There has been remarkable progress in constraining cosmological perturbations, and it is useful to summarize the data sets either in hand or expected over the next decade. The observables of choice are:

- Anisotropies in the CMB; the main statistic is the angular power spectrum of fluctuations, C_ℓ . The current and future experiments are: WMAP, PLANCK, ACT, SPT, ACTPol, SPTPol, Spider, Polarbear, BICEP2, Keck Array.
- Surveys cataloguing the angular positions and redshifts of individual galaxies leading to the power spectrum of fluctuations, $P(k)$, or the two-point correlation function, $\xi(r)$. The current and future experiments are: BOSS, DES, Weave, HETDEX, eBOSS, MS-DESI, LSST, Euclid, SKA, Chime, Baobab, MEERKAT, ASKAP.
- Weak lensing; images of distant galaxies will be distorted and correlated by intervening gravitational potential wells, leading to statistics such as the convergence power spectrum, C_ℓ^c . The current and future experiments are: DES, RCS, KIDS, HSC, LSST, Euclid, SKA.
- Peculiar velocities; by measuring redshifts *and* radial distances of galaxies and clusters it is possible to reconstruct a radially projected map of large-scale motions. Progress in this field will primarily come for the latter method with Planck.

Cosmological data has been used to place constraints on standard scalar–tensor theories [761] and related theories (such as $f(R)$ [762], Galileons and more general Horndeski theories [763]), Einstein-Aether theories [764, 765], braneworld models (specifically DGP) and specific massive gravity models (see e.g. [766, 767] and references therein). There have been preliminary attempts at placing constraints on more generalized parametrizations. If one restricts oneself to the quasi-static functions, μ and γ , constraints are found to be very dependent on assumptions about time- and scale-dependence [741, 768]. So, for example, if these functions are assumed to be constant, constraints are found at the percent level, while freeing up the time evolution (but assuming scale independence) gives constraints of order 50%–100%.

6.2.4. Open problems. Cosmological observations will constrain GR on length scales which are fifteen orders of magnitude greater than current constraints. Current and future data will give us a unique opportunity to do so with remarkable precision. We currently have an excellent understanding of what happens in the linear regime and how it maps onto an incredibly broad family of models. A few self-consistent formulations of how to parametrize GR currently exist which mirror the PPN approach, the workhorse for testing gravity on Solar System scales. Observations will not be able to constrain all the parameters in these approaches, but it should be possible to constrain some of them reasonably well in the quasi-static regime.

There have been attempts at developing such a general framework on nonlinear scales. The inclusion of screening mechanisms has been an essential aspect of this approach. Unlike with the linear regime, a number of theoretical issues remain: how to efficiently and accurately model the nonlinear effects, how to incorporate the uncertainties that arise from baryonic physics—most notably from supernovae and active galactic nuclei feedback—and the more general problem of bias (or how galaxies trace the density field). These are hard problems that need to be understood and solved if we are to use the (abundant) information on smaller length scales.

There have been a number of suggestions for how to test gravity on galactic and cluster scales which may be promising. These involve the transverse Doppler gravitational redshifts in Galaxy clusters [769], the motion of BHs embedded in galaxies [770], constraints from distance indicators [211], galactic brightness [771], cluster abundances [772] and cold tidal streams in galaxies [773]. These would add to, and complement, the constraints arising from large-scale structure.

In conclusion of this section we mention the results of the BICEP2 collaboration [774]. Measurements of the CMB B-mode polarization at 150GHz by the BICEP2 experiment were initially found consistent with a Λ CDM cosmological model plus a spectrum of tensor modes, described by a tensor-to-scalar ratio $r \approx 0.2$. If confirmed, this result would have provided an independent confirmation of the existence of GWs, and placed restrictions on viable inflationary potentials.

However, the interpretation of the measurement in terms of primordial GWs was quickly challenged by several authors (see e.g. [775]). Subsequent polarization data from the ESA Planck satellite [776] (in seven frequency bands between 30 and 353 GHz) revealed the signal contribution from galactic dust in the BICEP2 fields to be much more significant than accounted for by the foreground subtraction performed in [774]. A joint analysis of data from BICEP2, the Keck Array and the ESA Planck satellite reduced the initial detection of r to an upper limit of $r < 0.12$ at 95% confidence (using the standard primordial spectrum pivot scale of 0.05 Mpc^{-1}) [777]. This is consistent with the upper limit obtained from CMB data alone, $r < 0.11$ at 95% confidence (pivot scale 0.002 Mpc^{-1} [778]; the constraint relaxes to $r < 0.15$ if the tensor and scalar spectral indices are allowed to be scale-dependent).

As such, primordial GWs remain undetected. The BICEP2 and Keck array continue to take data, now observing at both 150 and 100 GHz. Upgrades of the Atacama Cosmology Telescope ('Advanced ACTPol' [779]) and the South Pole Telescope ('SPT-3G' [780]) have been proposed to improve the constraint on r .

7. Gravitational wave tests

This section will focus on GW-based tests of GR. There are several comprehensive reviews on the topic, including two excellent and recent *Living Reviews in Relativity* articles: one by Yunes and Siemens [31] (focusing on Earth-based detectors and pulsar timing arrays) and the other by Gair *et al* [32] (focusing on future space-based detectors). We find it unnecessary to reproduce that material in this review.

The consensus is that the ideal astrophysical systems to test strong-field GR are compact objects in merging binaries. Close to merger, the component bodies can reach speeds v very close to the speed of light ($v/c \sim 0.5$). By contrast, the component bodies of radio binary pulsars like J0737-3039 are moving at a small fraction of the speed of light ($v/c \lesssim 10^{-3}$). The leading-order dissipative dynamics in compact binaries, governed by the backreaction due to GW emission, is given by the quadrupole formula—a correction of order $(v/c)^5$ beyond Newtonian gravity. While precise timing of radio pulses has made it possible to measure this leading-order effect, PN corrections to the quadrupole formula are completely negligible in binary pulsars, but they will be very important in the frequency band where GW detectors are most sensitive. Therefore, GW observations of coalescing BHs and NSs should probe the strong-field dissipative dynamics to unprecedented levels of precision and facilitate new tests of strong-field gravity. A thorough introduction to the large and rapidly evolving literature on compact binary waveform modeling within GR (and to the associated systematic errors of

theoretical nature) is beyond the scope of this review. We refer the reader to one of the several recent reviews on this topic [642–647].

In this section we survey the broad range of physics and scales probed by GW tests (section 7.1); the key ideas behind GW measurements (section 7.2) and GW-based tests of GR (section 7.3); the details of one concrete procedure to compare GR with proposed alternatives, i.e., the TIGER pipeline (section 7.3.1); and the challenges and opportunities posed by theoretical and astrophysical systematics (section 7.4) in the context of Earth-based and space-based detectors.

7.1. Science opportunities

There are several ways in which GW observations could provide smoking guns of modified gravitational dynamics in the strong-field regime. Here we list some of them:

Tests of modified dynamics of binary mergers. The most immediate opportunities for GW tests of GR are expected to be provided by Earth-based detectors observing the inspiral and merger of compact binaries. The main target of Earth-based GW detectors like Advanced LIGO and Advanced Virgo is the inspiral and merger of NSs and moderate-mass BHs with masses in the range $[1, 10^3]M_{\odot}$. As described in section 5, these GW signals are very sensitive to the phase evolution of the binary. Therefore they provide an excellent probe of the compact binary’s parameters and properties, and (if present) of modifications to the underlying gravitational theory. The conceptual foundations of these tests, as well as some details of their implementation in a GW data analysis pipeline, are described in detail in sections 7.2 and 7.3 below.

Though potentially powerful, tests of GR based on GW observations from compact binaries are limited by theoretical and astrophysical systematics. Even within GR, only a small submanifold of astrophysically plausible scenarios has been exhaustively explored through inspiral, merger, and ringdown [642–647], particularly when unknown microphysics is involved. For most of the astrophysical parameter space, the natural framework for strong-field tests is the application of robust but approximate models for inspiral (e.g., PN waveforms) and merger (e.g., phenomenological models or QNM decompositions). As described in section 5, the construction of these models is particularly challenging for tests of gravity, as in principle we need comparably accurate calculations of the waveforms from binary BHs and NSs. To quantify the acceptable amount of theoretical error permitted to observe deviations from GR, one must possess sufficiently accurate solutions in both GR and modified gravity. That said, as described in sections 4 and 5, general principles (like the no-hair relations for BHs and the I–Love–Q relations for NSs) provide a promising framework for enabling robust strong-field tests of gravity, particularly for binary NSs, where a knowledge of the merger portion of the signal is not critical. Again, particularly for binary NSs, the dominant effect of many modified-gravity theories seems to be parametrized by a handful of parameters, as explored most comprehensively for the simple case of quasicircular nonspinning inspiral. We will see below (section 7.2) that using these parametrized signal models into a conventional Bayesian model selection and parameter estimation framework enables straightforward tests to identify deviations from GR.

Tests of the spacetime geometry around massive compact objects. The orbits of compact objects plunging into massive BHs are very complex and capture the nonlinear dynamics of gravity. The full multipolar structure of the BH spacetime is imprinted in the emitted signal. From the inspiral signals of an extreme mass-ratio binary one can map out the geometry of the

massive objects that reside in galactic nuclei and test if it agrees with the Kerr geometry [32, 781–784]. The key point is that in the case of BHs the source multipole moments all depend only on two parameters, mass and spin. By measuring more than two multipoles one can check if the spacetime geometry is described by the Kerr metric or if these objects have extra ‘hair’ [428, 781]. The multipole moments and the dissipative dynamics of the system also allow us to test whether the central object possesses an event horizon [457, 462, 785].

An alternative approach to test the Kerr hypothesis consists of looking at BH binary mergers and checking whether the QNM frequencies of the merger remnant are consistent with the predictions of GR [384, 460, 786]. Again, all of these complex frequencies depend only on the mass and spin of the final BH; therefore measuring (say) two oscillation frequencies and one damping time yields one test of GR, and further measurements provide additional consistency checks. The presence of an additional modified-theory parameter characterizing QNMs may also be inferred (at least in principle) by observing ringdown signals with eLISA or a third-generation Earth-based detector, such as ET [787].

Tests of the dark energy EOS. Compact binary sources are natural standard candles [788] or, more appropriately, *standard sirens*. As discussed towards the end of section 6.2, for inspiraling binaries one can measure the source’s luminosity distance from GW observations alone, although weak gravitational lensing would bias distance measurements of individual sources [789]. Methods have been proposed to correct for the bias in the case of eLISA [790], which, unfortunately, will not solve the problem completely, but a large population of events, as in the case of ET, can average out lensing biases [629]. If the host Galaxy of a merger event is identified and its redshift measured, then we can use a population of binary coalescence events to infer cosmological parameters. Indeed, GW observations might also measure the redshift of host galaxies. Tidal effects in NS binaries depend on the density of the NS and not just on its compactness. It turns out that the tidal effect can be used to determine the source’s redshift provided the NS EOS is known [791, 792]. Statistical methods that do not rely on host redshifts have also been proposed to measure cosmological parameters [793–795]. Alternatively, one can use the relation between the luminosity distance and redshift drift to probe cosmology [796–799]. In principle, both quantities can be measured from GW observations alone. One can use such a relation to distinguish inhomogeneous Universe models from Λ CDM [800–803].

Advanced LIGO and Virgo will be able to determine the Hubble parameter to an accuracy of 3% [804]. ET should measure the dark energy EOS parameter to within a few percent [629], and its variation with redshift to within about 20% [805]. By the time ET operates it is likely that most cosmological parameters will have been measured with good accuracy. Nevertheless, it will be very interesting, and important, to have a completely independent way of verifying those numbers.

Tests of alternative polarizations. In contrast to GR, where GWs are characterized by two polarization modes (the ‘plus’ and ‘cross’ polarizations), in alternative theories of gravity GWs could have up to four additional modes. For example, a scalar–tensor theory of gravity such as Brans–Dicke theory [222, 223] has a transverse scalar mode in addition to the plus and cross polarizations. Such a mode causes ‘breathing’ deformation of the test masses transverse to the direction of propagation of the waves [2], as opposed to the differential or quadrupolar deformation caused by the plus and cross polarizations. Interferometric detectors are built to explicitly take advantage of the differential displacements; even so, the presence of extra modes in a transient signal could be detected by a network consisting of a suitably large number of detectors. For example, a network of three noncollocated detectors can infer

the presence of an additional scalar mode [712, 806–812] (see [31] for a review). A single detector, however, should suffice for a continuous signal, since it can sample the different polarizations as the detector changes its orientation relative to the source as the Earth revolves around the Sun.

Though difficult to distinguish from instrumental sources of excess power, the absence of these extra polarizations would weakly constrain alternative theories of gravity. In particular, Hayama and Nishizawa have proposed a theory-independent method to reconstruct an arbitrary number of polarization modes using the time-series data of an advanced detector network [813]. They consider GWs from a supernova simulation and use a network of four detectors to recover all the polarization modes. Future GW observations could also help place further constraints on scalar–tensor theory if they fail to detect scalar modes. The challenge, however, is to produce accurate waveforms in alternative theories of gravity for different GW sources such as supernovae, compact binary coalescences, etcetera.

7.2. Parameter estimation and model selection

A brief introduction to the basic principles of GW data analysis is useful to understand how GR can be tested within a Bayesian model selection framework.

Given a set of compact binary merger observations from GW detectors, the distribution of parameters $\vec{\theta}$ consistent with the data d can be inferred by comparing the predicted GW strain in each instrument with the data. Let $h(\vec{\theta})$ be the waveform family associated with the model H . If the detector noise n is Gaussian and stationary, noting that $n = d - h$, then

$$p(d|H, \vec{\theta}) = \mathcal{N} e^{-\frac{1}{2}\langle d-h|d-h \rangle}, \quad (7.1)$$

where \mathcal{N} is a data-realization-independent normalization constant, and the inner product between the real-valued time series $A(t)$ and $B(t)$ is defined as

$$\langle A|B \rangle \equiv 4\Re \int_0^\infty df \frac{\tilde{A}^*(f)\tilde{B}(f)}{S_n(f)}. \quad (7.2)$$

Here a tilde indicates the Fourier transform, and $S_n(f)$ is the one-sided noise power spectral density (for more details, see e.g. [814–816]).

Bayesian inference is used to turn the templates $h(\vec{\theta})$ and detector data d into posterior probability distributions $p(\vec{\theta}|d, H)$ for the physical parameters which describe the observation via Bayes' theorem:

$$p(\vec{\theta}|d, H) = \frac{p(d|\vec{\theta}, H)p(\vec{\theta}|H)}{p(d|H)}, \quad (7.3)$$

where $p(d|\vec{\theta}, H)$ is the *likelihood* or ‘goodness-of-fit’ statistic, $p(\vec{\theta}|H)$ is the *prior* distribution for the model parameters, and $p(d|H)$ is the *marginalized likelihood* or *evidence* for the model or ‘hypothesis’ H . We use the notation that $p(a|b)$ is the conditional probability density of a , assuming that b is true. Notice that every term in equation (7.3) is conditional on our model H being correct. The model H contains all of our assumptions about the signal, including the physics of gravitational radiation production and propagation, the astrophysics of how these systems form (thereby guiding our choice of parameterization and prior distributions), the response of our detectors to incident GWs, and the instrumental noise with which the signal must compete. More succinctly: in the matched filtering paradigm, conclusions drawn from the data are conditional on our model for the data—including both the GWs and the detectors—being correct.

Bayes' theorem provides the conceptual foundation for parameter estimation and model selection in general, and for GW tests of GR in particular. General hypothesis tests follow by applying Bayes' theorem (7.3) to a collection of hypotheses $\{H_1, \dots, H_N\}$:

$$p(H_k|d) = \frac{p(d|H_k)p(H_k)}{p(d)}. \quad (7.4)$$

where $p(H_k)$ are prior probabilities for the models H_k . The *evidence* $p(d|H)$ can be computed by integrating the likelihood $p(d|\vec{\theta}_k, H_k)$ of the parameters $\vec{\theta}_k$ times the prior probabilities $p(\theta_k|H_k)$ for these parameters within the model H_k :

$$p(d|H_k) \equiv \int d\vec{\theta}_k p(d|\vec{\theta}_k, H_k) p(\theta_k|H_k). \quad (7.5)$$

The probability of the data $p(d)$ depends on all the hypotheses under consideration: $p(d) = \sum_k p(d|H_k)p(H_k)$. That said, in practice this overall probability never appears, since models are compared using *odds ratios* O_{ij} between probabilities for two different hypotheses:

$$O_{ij} = \frac{p(H_i|d)}{p(H_j|d)}. \quad (7.6)$$

In the context of testing GR, we consider multiple models: (a) a model H_{GR} , where GR is correct; and (b) one or more 'modified GR' models H_{modGR} including additional parameters in the signal model, and usually reducing to GR in a suitable limit. For the purposes of model selection, these parameters can—but need not—be connected to an underlying physical theory (e.g., a Lagrangian). In practice, the most-often used 'extended' model parameters describe ad hoc changes to the GW orbital dynamics (e.g., phase).

Ideally, one of our models H perfectly matches reality. In this case the posterior has some finite width, which, to first order, scales as the inverse of the signal-to-noise ratio (SNR). The width of the posterior is the statistical error of the model: for example, the 90% credible interval of $p(\theta|d, H)$ will contain the 'true' model parameters 90% of the time. As the SNR increases (either by finding closer sources or improving the sensitivity of the detector) credible intervals shrink and the distributions (typically) become more Gaussian, allowing for more precise statements to be made about the observations.

In practice, our models H will not fully describe the source physics and the detector. The best-fit model and parameters will be systematically biased, as optimization invites parameters to flex away from the true values in an attempt to overcome our model's shortcomings in matching the data. Systematic errors are less strongly dependent on the signal strength. Hence, relative to statistical errors, the impact of systematic errors increases strongly with signal amplitude and it becomes important as instruments become more sensitive (see e.g. [817, 818]). In other words, the potentially most informative signals require the greatest care.

7.3. Direct versus parametrized tests of gravity

The approaches developed to test GR with compact binaries come in two flavors, that we will call 'direct' and 'parametrized' tests. While both approaches adopt a parametrized model to characterize deviations from GR, they are distinguished by the role of the null hypothesis and the significance of non-GR parameters.

Direct tests with inspiral waves. A direct test assumes that GR is the correct theory of gravity, introduces a systematic (but not necessarily physical) modification to the dynamics and to the resulting GW signal, and evaluates support for the null hypothesis. An example of the direct

approach is as follows. At leading order in the PN approximation, the observed strain amplitude from a nonspinning binary moving on a quasi-circular orbit is given by [639]

$$h(t) = \frac{4GC\eta M}{c^4 R} [GM\omega(t)]^{2/3} \cos 2\phi(t), \quad (7.7)$$

where as usual M and η denote the total mass and symmetric mass ratio; $C < 1$ is a number that depends on the position of the source on the sky, the position of the orbital plane with respect to the line of sight, the polarization of the waves and the distance to the binary; $\phi(t)$ and $\omega(t)$ are the orbital phase and frequency, respectively, obtained by solving the balance equation $\dot{\omega} = -\mathcal{L}/(dE/d\omega)$, where $E(v)$ and $\mathcal{L}(v)$ are the gravitational binding energy (per unit mass) and GW luminosity of the system. It is often convenient to work with the Fourier transform of the waveform, which, in the stationary-phase approximation, is given by [819–821]

$$H(f) = \sqrt{\frac{5\eta}{24}} \frac{\mathcal{C}(GM)^{5/6}}{\pi^{2/3} c^{3/2} R} f^{-7/6} e^{i\psi_{\text{SPA}}(f)}, \quad (7.8)$$

$$\psi_{\text{SPA}}(f) = 2\pi f t_c - \phi_c - \frac{\pi}{4} + \frac{3}{128 \eta v_f^5} \sum_{k=0}^7 \psi_{(k/2)\text{PN}} v_f^k, \quad (7.9)$$

where we denote $v_f = (\pi GMf)^{1/3}$, and the subscript ‘SPA’ obviously stands for ‘stationary-phase approximation.’ The coefficients $\psi_{(k/2)\text{PN}}$ ’s ($k = 0, \dots, 7$) in the Fourier phase are computed in a PN series through the equation

$$\psi(f) = 2\pi f t_c - \phi_c - \frac{\pi}{4} + 2 \int_v^{v_c} (v_c^3 - v^3) \frac{E'(v)}{\mathcal{L}(v)} dv, \quad (7.10)$$

by expanding the binary center-of-mass energy E and the GW luminosity \mathcal{L} through the appropriate PN order; t_c and ϕ_c are the time and phase at coalescence and $v_c = (\pi GMf_c)^{1/3}$, with f_c the cutoff frequency.

Inspiral phasing is currently known to 3.5PN order (i.e., order $(v/c)^7$) beyond the leading-order quadrupole formula. If spins are negligible, which would be a good approximation for binary NSs, all the PN coefficients ψ_k in equation (7.10) (9 of them including logarithmic terms) depend only on the component masses. More in general, the PN coefficients in the GW phasing of a coalescing binary only depend on the component masses and spins, and therefore only a limited number of them are independent, so that a very generic test could be to check for consistency between the measured coefficients. A first proposal in this direction was put forward by Arun *et al* [822–824]. As described in section 7.3.1 below, one approach treats three of the coefficients (say ψ_0 , ψ_2 and ψ_3) as independent, and asks if the measurement of the third is consistent with the first two [824, 825]. The conclusion is that, for Advanced LIGO/Virgo, a single loud event with $\text{SNR} > 20$ would detect a departure of ψ_3 from its GR value by about 2.5% [826].

A drawback of such an approach is that it is difficult to combine information from multiple sources in this way so as to arrive at a stronger test: deviations in the PN coefficients can be different from one source to the next if they themselves depend on masses, spins, and whatever additional charges may be present in an alternative theory of gravity. This problem can be circumvented by searching for GR violations using Bayesian *model selection*, rather than parameter estimation. For instance, one could introduce parametrized deformations in the waveforms predicted by GR, and compare the resulting waveform model with the GR prediction. Del Pozzo *et al* [827] adopted this approach (using a single extra parameter) in the context of binary inspiral, and Gossan *et al* [787] used a similar strategy in the context of

ringdown, considering multiple additional parameters. With model selection it becomes possible to combine information from multiple sources and build up evidence for or against GR, even if deviations manifest themselves in a different way for each source. On the other hand, when the ‘non-GR’ model is insufficiently parsimonious—i.e., it has too many additional free parameters—it may be penalized if the true theory involves only a small number of parameters.

Direct tests with QNMs. The BH remnant resulting from the merger of two compact objects (either BHs or NSs) is initially highly deformed, but it soon settles down to a quiescent state by emitting ringdown radiation, which consists of a superposition of QNMs [828] (for a review see, e.g., [384]). A Kerr BH is characterized only by its mass and angular momentum, and so are the complex frequencies of its QNM oscillations [381, 829], although the relative amplitudes of the modes depend on the specific details of the excitation.

Detection of the characteristic ringdown GW signal of a BH would, therefore, allow a direct test of the no-hair theorem [830], and hence GR, through the comparison of frequencies and decay times of these modes with the predictions of GR for a BH with certain mass and spin. In practice, the detection and discrimination of multiple modes is essential, as it is first necessary to infer the mass and spin of the BH before checking for consistency between the modes. If any of the modes have some parameter dependence, other than mass and spin, then the mass and spin obtained from these modes will not be consistent with that obtained from the others, and thus the source of emission must be different from a Kerr BH. Departures from GR in the QNM spectrum can be encoded in extra parameters to be identified by Bayesian model selection or parameter estimation.

The idea of treating BHs as ‘gravitational atoms,’ and their QNM spectra as the GW analog of atomic lines, dates back to a seminal paper by Detweiler [831]. Dreyer *et al* introduced a formalism for testing GR with QNMs [830], and made a concrete suggestion to test the no-hair theorem through the measurement of more than one mode. Berti *et al* [460, 786] investigated the accuracy of measurement of individual mode parameters using a Fisher matrix analysis and estimated the resolvability of individual modes in the complete signal as a function of SNR. They concluded that the presence of a second mode can be inferred as long as the SNR is larger than a critical value, under the assumption that the presence of a ringdown signal has been confirmed and the parameters of the dominant modes are reliably measured. The critical SNR depends on the mass ratio of the progenitor binary, but an SNR of 20 should suffice if the mass ratio of the progenitor binary is $q = m_1/m_2 \gtrsim 2$. Kamaretsos *et al* showed that using BH ringdown signals following a nonspinning binary merger, it might be possible to recover the mass ratio of the progenitor binary from the relative amplitudes of the QNMs [832].

Using a limited set of sources, Gossan *et al* [787] conducted a proof-of-concept Bayesian model selection calculation for modified gravity using the ringdown signal. Specifically, they applied Bayesian model selection to obtain a more robust and quantitative measure of the consistency of the data with GR, as opposed to a generalized theory where the mode parameters depended on an extra parameter other than the BH mass and spin (i.e., ‘hairy’ BHs). Using this technique, for the sources in their catalog, they can measure deviations at the 10% level in the fundamental $l = m = 2$ frequency parameter $\hat{\omega}_{22}$ out to $\simeq 6$ Gpc for a $500M_\odot$ source with ET. With a space-based detector like LISA it is possible to measure deviations at the 10% level at 6 Gpc with a $10^6 M_\odot$ source, and at the 0.6% level at $z \sim 5$ with a $10^8 M_\odot$ source. This proof-of-concept calculation adopted aggressive simplifying assumptions (a known source location and source orientation) and explored only a handful of candidate sources, very specific source location, orientation and mass ratio of the progenitor binary.

More recently, eliminating these highly simplifying assumptions and using improved waveform models, the TIGER pipeline (discussed in section 7.3.1 below) showed that modifications to gravity could be identified using as few as 10 astrophysically plausible sources seen by ET [833]. Specifically, these authors used a QNM model that is matched to numerical simulations of coalescing BH binaries where BH spins are aligned with the orbital angular momentum. Their model consists of a superposition of the four dominant modes $(\ell, m) = (2, 2), (2, 1), (3, 3)$ and $(4, 4)$ used in Kamaretsos *et al* [834], where the mode amplitudes are given by

$$A_{22}(\eta) = 0.864\eta, \quad (7.11)$$

$$A_{21}(\eta) = 0.43 \left[\sqrt{1 - 4\eta} - \chi_{\text{eff}} \right] A_{22}(\eta), \quad (7.12)$$

$$A_{33}(\eta) = 0.44(1 - 4\eta)^{0.45} A_{22}(\eta), \quad (7.13)$$

$$A_{44}(\eta) = \left[5.4(\eta - 0.22)^2 + 0.04 \right] A_{22}(\eta), \quad (7.14)$$

and χ_{eff} is a single effective spin parameter, that is a specific combination of the two progenitor BH dimensionless spins (χ_1, χ_2) weighted by their masses (m_1, m_2) :

$$\chi_{\text{eff}} = \frac{1}{2} \left(\sqrt{1 - 4\eta} \chi_1 + \chi_- \right), \quad \chi_- = \frac{m_1 \chi_1 - m_2 \chi_2}{M_{\text{in}}}. \quad (7.15)$$

Here M_{in} is the initial total mass of the binary, assumed equal to the mass of the final BH. The frequencies ω_{lm} and damping times τ_{lm} are related through the *quality factors* $Q_{lm} = \omega_{lm} \tau_{lm} / 2$:

$$M\omega = f_1 + f_2(1 - j)^{f_3}, \quad Q = q_1 + q_2(1 - j)^{q_3}, \quad (7.16)$$

and the coefficients $f_1, f_2, f_3, q_1, q_2, q_3$ were fitted to QNM data in [835]. The spin j of the remnant BH can also be written in terms of the binary component masses (m_1, m_2) and spins $(\vec{\chi}_1, \vec{\chi}_2)$ (see e.g. [836]).

Denote the free parameters corresponding to the hypothesis that GR is correct by $\vec{\theta}_{\text{GR}}$. For the non-GR hypothesis, one can use one or more deviations of the QNM frequencies and damping times. Meidam *et al* [833] considered the following different hypotheses and corresponding additional parameters: $H_1 \leftrightarrow \{\vec{\theta}_{\text{GR}}, \delta\hat{\omega}_{22}\}$, $H_2 \leftrightarrow \{\vec{\theta}_{\text{GR}}, \delta\hat{\omega}_{33}\}$, $H_3 \leftrightarrow \{\vec{\theta}_{\text{GR}}, \delta\hat{\tau}_{22}\}$, $H_{12} \leftrightarrow \{\vec{\theta}_{\text{GR}}, \delta\hat{\omega}_{22}, \delta\hat{\omega}_{33}\}$, $H_{13} \leftrightarrow \{\vec{\theta}_{\text{GR}}, \delta\hat{\omega}_{22}, \delta\hat{\tau}_{22}\}$, $H_{23} \leftrightarrow \{\vec{\theta}_{\text{GR}}, \delta\hat{\omega}_{33}, \delta\hat{\tau}_{22}\}$, $H_{123} \leftrightarrow \{\vec{\theta}_{\text{GR}}, \delta\hat{\omega}_{22}, \delta\hat{\omega}_{33}, \delta\hat{\tau}_{22}\}$. Here $\delta\hat{\omega}_{22}, \delta\hat{\omega}_{33}$ and $\delta\hat{\tau}_{22}$ are deviations of the two dominant mode frequencies and of the dominant mode's damping time from their GR values. These are, in essence, extra ‘hair’ parameters of the remnant BH. Using such a model and combining the different hypotheses, Meidam *et al* concluded that deviations from GR at the level of 10% in $\delta\hat{\omega}_{22}$ and $\delta\hat{\omega}_{33}$ could be inferred with ~ 20 intermediate-mass binary BH merger events seen up to a distance of 60 Gpc. To confirm deviation of the same order in $\delta\hat{\tau}_{22}$ would require ~ 50 detections. If one assumes that GR is the correct theory, then ~ 20 detections would be good enough to constrain $\delta\hat{\omega}_{22}$ and $\delta\hat{\omega}_{33}$ to within 0.5% and $\delta\hat{\tau}_{22}$ to within 5% of their GR values (see figure 8 of [833]).

Just like inspiral tests, ringdown-based tests can also be limited by theoretical and astrophysical systematics. The presence of precessing spins is well known to significantly alter the relative QNM amplitude. Indeed, several authors have argued that ringdown radiation can be used to draw inferences about the pre-merger spins [832, 837, 838]. Additionally, many authors adopt simplifying assumptions about the angular distribution of QNMs, even though the asymptotic behavior at late time is well known to involve a superposition of several spin-weighted spherical harmonics [839]. These simplifications are

expected to impact inferences about the mass ratio, inclination, spins, amplitude of precession, and presence or absence of GR modifications, and need to be included in future studies.

Parametrized tests. Yunes and Pretorius proposed a model-independent way of testing alternative theories of gravity [840]. The basic idea is to use as a template for the inspiraling, weak-field regime the phasing formula $H(f)(1 + \alpha f^{a/3})e^{i\beta f^{b/3}}$, $H(f)$ being the GR template of equation (7.8). The coefficients α , β , a and b are called ‘parametrized post-Einsteinian’ (PPE) parameters [840], in analogy with the PPN parameters that measure deviations from GR in the weak-field, slow-motion regime [2]. As in the PPN framework, the PPE parameters depend on the specific theory of gravity, and their values are known in some theories. The PPE framework (or extensions thereof) can capture the predictions of most extensions of GR discussed in this review, and it has been generalized to include more generic corrections to the waveform, such as the presence of higher harmonics, modified GW propagation effects and ringdown radiation. We refer the interested reader to section 5.3.4 of the recent review by Yunes and Siemens [31].

An advantage of parametrized, PPE-like searches is that they would avoid what Yunes and collaborators call ‘fundamental bias,’ by allowing the data to select the correct theory of gravity through a systematic study of statistically significant anomalies. A more subtle concern is that if GR happened to be wrong in the strong-field regime and we observe low-SNR signals (as expected for the first GW detections in Advanced LIGO/Virgo), GR-based GW detection templates could still extract the signal with the wrong parameters, without being able to identify that there is a non-GR anomaly in the data. Vallisneri and Yunes [841] found that this insidious ‘stealth bias’ is indeed possible in a certain region of parameter space.

A practical limitation of the PPE framework is that, if deviations from GR are present in the weak-field regime, they might be already well constrained in a PPN sense by pulsar timing observations. By contrast, if GR deviations affect only the strong-field regime (i.e., the very last stages of inspiral, merger and ringdown), their signal might not be a small deviation away from the GR template. In this scenario, only direct measurements of strong-field sources (e.g., GWs from merging binaries) would enable us to detect and constrain the parameters of the theory. Alternative theories of gravity of this kind might be difficult to conceive, but scalar-tensor theories with dynamical scalarization are an interesting example (see sections 4.2 and 5.1).

7.3.1. Implementation of direct tests: the TIGER pipeline. The TIGER (Test Infrastructure for GEneral Relativity) data analysis pipeline provides a ‘direct test’ of GR via the GW coalescence waveform [826, 833, 842–845]. Broadly speaking, the framework assesses the evidence for ‘generic’ deviations from GR in the signal. Starting from waveform deformations characterized by an (in principle) arbitrarily large number of additional parameters $\delta\xi_1, \delta\xi_2, \dots, \delta\xi_N$ (assumed to be zero if GR is correct), the algorithm asks the question: ‘Do one or more of the $\delta\xi_i$ ($i = 1, 2, \dots, N$) differ from zero?’ Although the method is not tied to any particular part of the coalescence process (indeed, as anticipated in section 7.3, it was applied to ringdown tests [833]), in this section we will focus on the case of inspirals, for which a robust analysis pipeline is available [845]. Parametrized deformations can be introduced in the PN coefficients ψ_i of the GW phase [822, 826], e.g. by setting

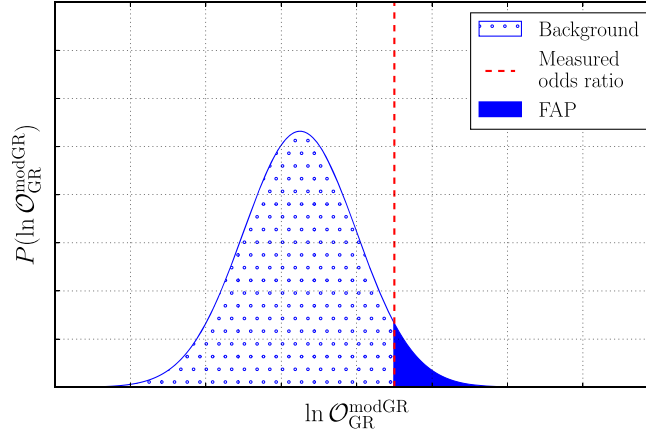


Figure 41. Example of a odds ratio background (blue curve), measured odds ratio (red dashed line), and the false alarm probability associated to the measured odds ratio (blue shaded area).

$$\psi_i = \psi_i^{\text{GR}}(m_1, m_2, \vec{S}_1, \vec{S}_2) [1 + \delta\xi_i], \quad (7.17)$$

where $\psi_i^{\text{GR}}(m_1, m_2, \vec{S}_1, \vec{S}_2)$ describes the functional dependence of the PN coefficients on the component masses m_1, m_2 and spins \vec{S}_1, \vec{S}_2 that is predicted by GR. Given GW observations, TIGER compares two hypotheses:

- The GR (null) hypothesis, denoted by H_{GR} , is the hypothesis that GR is the correct theory of gravity.
- The hypothesis H_{modGR} assumes that there is some deviation from GR. On first consideration, one might be inclined to make this the negation of the GR hypothesis. However, H_{modGR} would then be associated with a family of waveforms that can not be parametrized by a finite number of parameters: literally any waveform outside the family predicted by GR would be allowed. In practice, only a finite number of deformation parameters can be considered. Call these $\delta\xi_1, \delta\xi_2, \dots, \delta\xi_N$ as above, with the understanding that the GR waveform corresponds to $\delta\xi_i = 0$ for $i = 1, \dots, N$. We then define H_{modGR} as follows:

H_{modGR} is the hypothesis that one or more of the deformation parameters $\delta\xi_i$ in the waveform is different from zero, without specifying which.

The odds ratio of interest is then:

$$O_{\text{GR}}^{\text{modGR}} \equiv \frac{p(H_{\text{modGR}}|d)}{p(H_{\text{GR}}|d)}. \quad (7.18)$$

In principle the odds ratio has a straightforward interpretation: if $O_{\text{GR}}^{\text{modGR}} < 1$, GR is favored by the data; if $O_{\text{GR}}^{\text{modGR}} > 1$, the data tell us that a different theory of gravity is favored.

This Bayesian method has a number of attractive features: any waveform model or any particular part of the coalescence process can be employed; information from multiple sources can trivially be combined; sources with small or marginal SNRs can be included without penalty; and the Bayesian Occam's razor naturally accounts for (and where appropriate, penalizes) increasing model dimension. Crucially, as illustrated below, the approach can

identify the presence of deviations from GR that are not included in the chosen parametrized waveform family.

Frequentist approach and nontrivial systematics. Like all parametrized tests, the TIGER pipeline can be limited by observational, astrophysical, and theoretical systematics. Because exact and generic binary merger solutions are generally unavailable, to make progress, the TIGER pipeline has adopted a phenomenological and frequentist approach, usually adopting simplified waveform models (e.g., neglecting spin precession). Real detector noise is nonGaussian and could mimic a violation of GR in a sufficiently large sample of events. For this reason, the pipeline does not adhere to a strictly Bayesian interpretation of these odds ratios; instead, the odds ratios are used as frequentist statistics.

To assign a significance to the measured odds ratio as a statistic, the pipeline evaluates the background distribution of the odds ratio. Specifically, it evaluates the odds ratios for a large number of (catalogs of) simulated signals that are put in the noise, each of them being in accordance with GR⁶². Figure 41 schematically illustrates how a (normalized) background distribution can be used to assign a false alarm probability to the odds ratio computed from the actual, measured signals: it is simply the area under the background distribution for the range of odds ratios that are larger than the measured one. We note that in practice it is convenient to work with the logarithm of the odds ratio, $\ln O_{\text{GR}}^{\text{modGR}}$.

Finally, to assess the effectiveness of the pipeline as a test for the presence of modified gravity, the background distribution is compared with a foreground distribution: the distribution of the detection statistic for a distribution of sources, given a particular modification of gravity. The degree of overlap between foreground and background then tells us how easy or difficult it will be to confidently discover the given violation of GR. This can be formalized by introducing the notion of efficiency, defined as the fraction of the foreground that is above a pre-determined fraction (e.g. 95%) of the background. For details, see [826, 842, 845].

Decomposing and evaluating the odds ratio. By construction, no waveform model is associated with H_{modGR} . Instead, the hypothesis can be broken up into auxiliary hypotheses, each of which *does* come with a concrete waveform model:

$H_{i_1 i_2 \dots i_k}$ is the hypothesis that the parameters $\{\delta\xi_{i_1}, \delta\xi_{i_2}, \dots, \delta\xi_{i_k}\}$ differ from zero, but all the other $\delta\xi_j$, $j \notin \{i_1, i_2, \dots, i_k\}$, are zero. In terms of these hypotheses, H_{modGR} is the logical ‘or’ of all these auxiliary hypotheses:

$$H_{\text{modGR}} = \bigvee_{i_1 < i_2 < \dots < i_k; k \leq N} H_{i_1 i_2 \dots i_k}. \quad (7.19)$$

Note that the hypotheses $H_{i_1 i_2 \dots i_k}$ and $H_{j_1 j_2 \dots j_l}$ for $\{i_1 i_2 \dots i_k\} \neq \{j_1 j_2 \dots j_l\}$ are *mutually exclusive*, or logically disjoint. This implies that the probability of the union of the auxiliary hypotheses equals the sum of the probabilities associated to individual auxiliary hypotheses. The odds ratio in equation (7.18) then becomes

$$O_{\text{GR}}^{\text{modGR}} = \sum_{k=1}^N \sum_{i_1 < i_2 < \dots < i_k} \frac{p(H_{i_1 i_2 \dots i_k} | d)}{p(H_{\text{GR}} | d)}. \quad (7.20)$$

If there are multiple detected sources—which will together be referred to as a *catalog*—in stretches of data d_1, d_2, \dots, d_N , then the definition of the odds ratio (7.18) can trivially be

⁶² For a comparison of analytic and numerical methods, see [846].

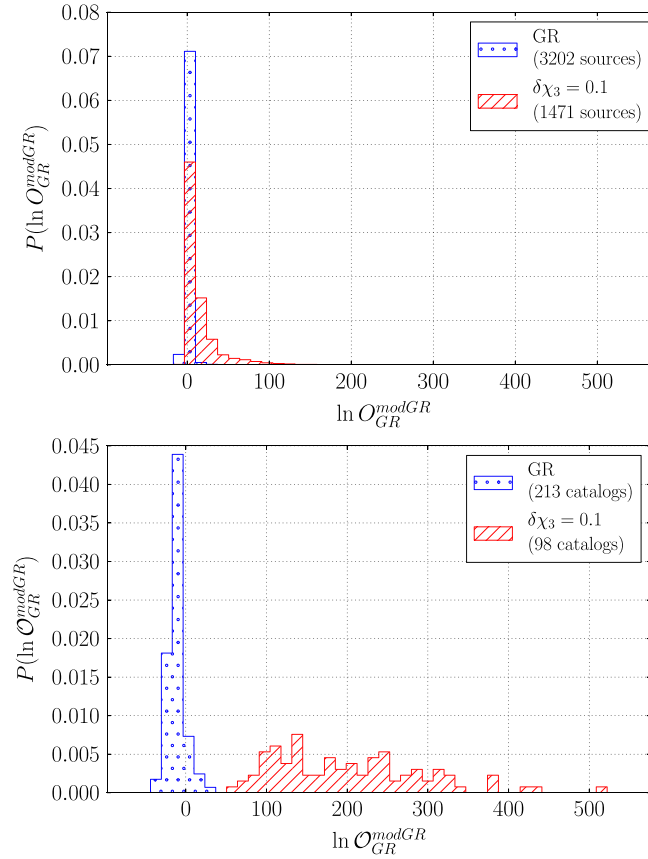


Figure 42. Background (blue) and foreground (red) for deviation of 10% in the 1.5PN phase coefficient ψ_3 . The top plot shows the odds ratio distributions for single sources, whereas the bottom plot shows the results for catalogs of 15 sources each.

generalized, and a result like equation (7.20) will again hold:

$$\begin{aligned} \mathcal{O}_{\text{GR}}^{\text{modGR}} &\equiv \frac{p(H_{\text{modGR}} | d_1, d_2, \dots, d_N)}{p(H_{\text{GR}} | d_1, d_2, \dots, d_N)} \\ &= \sum_{k=1}^N \sum_{i_1 < i_2 < \dots < i_k} \frac{p(H_{i_1 i_2 \dots i_k} | d_1, d_2, \dots, d_N)}{p(H_{\text{GR}} | d_1, d_2, \dots, d_N)}. \end{aligned} \quad (7.21)$$

We refer the reader to [826] for further discussions on the calculation of the odds ratio and the computational details.

Application to NS–NS binaries. We here demonstrate that TIGER is an effective test for a broad spectrum of modifications to gravity, using binary NS sources. Specifically, we show results from simulations where the sources had component masses in the NS–NS range, $m_1, m_2 \in [1, 2] M_\odot$, and were distributed uniformly in co-moving volume, with arbitrary orientations. Having used astrophysically realistic populations of sources and assuming Advanced LIGO and Advanced Virgo operating at design sensitivity, these examples

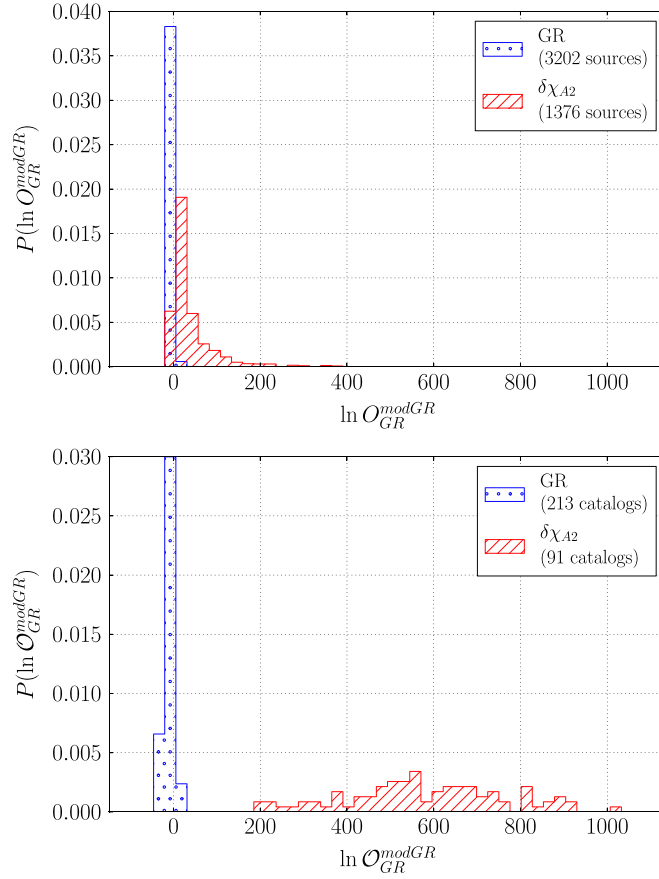


Figure 43. Background (blue) and the foreground (red) for a deviation as in equation (7.22). The top plot show the results for single sources, whereas the bottom plot shows the results for catalogs of 15 sources.

demonstrate the ability to identify modifications to gravity in an astrophysically plausible scenario, where most sources have low SNR and are close to the detection threshold.

For these sources, TIGER is sensitive to deviations in the PN phase coefficients even at high PN order, where no other astrophysical bounds (e.g., from the binary pulsar [847]) exist. For example, consider a deviation in the phase coefficient ψ_3 at 1.5PN, which is the lowest order at which the dynamical nonlinearity of GR manifests itself through the so-called tail terms [825, 848]. For the calculation of the odds ratio, the auxiliary hypotheses corresponded to shifts in different PN phase coefficients, as in equation (7.17). Figure 42 shows the results for a constant 10% relative shift in ψ_3 , which is far beyond the reach of any current observation. Even with a single detection (top panel), one could plausibly detect the deviation. When we combine information from 15 sources (bottom panel) the result is a complete separation between the background and foreground, which means that the given deviation can be detected with near-certainty.

Despite having adopted a parametrized phase model for the PN phase $\Psi(f)$, TIGER is also demonstrably sensitive to modifications of gravity outside its model space. In the present example, these would be GR violations that do not take the form of simple shifts in the phase

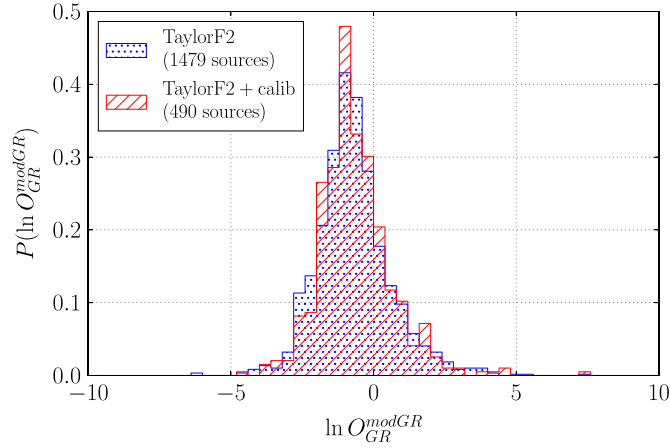


Figure 44. Single-source background distributions where the simulated detector outputs are generated with (red) and without (blue) detector calibration uncertainties.

coefficients, as in equation (7.17). As an extreme example, we can consider a deviation of the form

$$\Psi^{\text{GR}}(M, \eta; f) \rightarrow \Psi^{\text{GR}}(M, \eta; f) + \frac{3}{128\eta} (\pi M f)^{-2+M/(3M_{\odot})}, \quad (7.22)$$

where $\Psi^{\text{GR}}(M, \eta; f)$ is the GR phase in the frequency domain. For a system with $m_1 = m_2 = 1.5 M_{\odot}$, the change in phase at $f = 150$ Hz is about the same as for a 10% shift in ψ_3 . Figure 43 shows the distribution of odds ratio for both single sources and catalogs of 15 sources. The trend is similar to that seen in figure 42: there is a moderate separation between background and foreground for single sources, and a complete separation in the case of 15 sources per catalog.

Other specific kinds of deviations were considered in [826, 842]. So far, all results have indicated that TIGER should be able to discern very generic deviations from GR. Moreover, they show that the results are strengthened by the combination of multiple sources, even if the majority of the sources are near the detection threshold. An open problem is how to identify the exact underlying nature of a GR violation, should one be found: see the discussions in [827, 840, 849, 850].

Assessing theoretical, astrophysical, and instrumental systematics. As described below, in general both theoretical and astrophysical systematics are a common concern for any parameter estimation pipeline. On the one hand, the PN approximation has limited ability to accurately evaluate the waveform for any set of parameters. As described in section 7.4.1, these PN uncertainties have little impact on TIGER's conclusions. On the other hand, TIGER has adopted a simplified (nonprecessing, point-particle) model for binary NSs. To address these astrophysical systematics, tests have been conducted [845] to gauge the effects of ignoring the misalignment of the spins of the component objects and ignoring the tidal deformability of NSs. The impact on the background distribution of all of these effects was found to be negligible compared to the deviations from GR considered in the tests (see figures 42 and 43). This does not guarantee that the background distribution in the advanced detector era will be robust against these effects, but it does give us some confidence that sensitive tests of GR can be performed.

Another spurious effect that could impact a test of GR is the calibration uncertainty of the detector. The strain reported for data analysis is conditioned on calibration measurements. However, these calibration measurements are subject to errors, which propagate to uncertainties in the strain. To probe the influence of this effect on the background distribution, calibration measurement uncertainties can be modeled using existing LIGO/Virgo data [851, 852]. Background distributions are then calculated with and without the introduction of these calibration errors. The results for the single-source background distribution are shown in figure 44: the effects of detector calibration uncertainty are limited. Although it is impossible to predict the behavior of the calibration system for Advanced LIGO/Virgo, there is no indication that calibration uncertainty will have a significant effect on the background distribution.

The robustness tests described above and the additional ones in [845] used simulated stationary, Gaussian noise. By contrast, real data will contain departures from stationarity through short-duration ‘glitches’ caused by various instrumental and environmental noise sources. Preliminary studies of the effects of glitches on the background indicate that, with the implementation of appropriate instrumental ‘vetoes’ (such as those used in the detection effort itself), glitches will not pose any real problems.

7.4. *Waveform and astrophysical systematics*

Estimates of the accuracy of GW detectors in measuring binary parameters, including hypothetical effects from extensions of GR, often assume that the sources are isolated point particles in quasicircular orbits in vacuum, inspiraling and radiating exclusively due to gravitational radiation reaction. Both for stellar-mass objects and supermassive BHs, these assumptions neglect astrophysical realities, ignoring the possibility of nonzero eccentricity and spin precession, the impact of the surrounding environment, and the composition of the object in the case of NSs.

Additionally, these calculations assume that GR waveforms are perfectly known. In practice, particularly for a wide range of astrophysically plausible sources, the solution to the binary problem in GR is known only approximately.

In this section we will first address the impact of astrophysical and waveform systematics on stellar-mass BHs and NSs, and then the corresponding challenges for supermassive BHs.

7.4.1. *Stellar mass objects.* For stellar-mass compact binaries, the assumptions listed above neglect the delicate but nontrivial impact of composition and initial conditions, modifying the expected signal at both high and low frequencies. Just as these effects mimic or mask our ability to measure parameters (see e.g. [853]), they can also mimic or mask modifications to GR, weakening our ability to test it with real astrophysical systems. Conversely, astrophysical processes like precessing spins and eccentricity [854–859] introduce more structure in the gravitational waveforms, potentially enabling stronger and new constraints on both astrophysics and modified gravity.

As outlined above, existing proposals to test modified theories of gravity with second-generation GW detectors such as Advanced LIGO and Advanced Virgo rely on carefully monitoring the phase evolution of the leading-order GW harmonic (see e.g. [850, 860]). NS–NS binaries are the preferred laboratory for testing GR because (a) they have been observed in the electromagnetic spectrum, and therefore (unlike stellar-mass BH binaries) their rates are constrained by observations [861, 862]; (b) most of the SNR is accumulated during the inspiral, which is both analytically tractable and less sensitive to systematic effects, due to uncertainties in the modeling of the late inspiral and merger; and (c) for most formation

scenarios, astrophysics suggests that the gravitational waveforms will be relatively simple (e.g., the eccentricity of the orbit and the spin of NSs is small). Individual events with large SNR could prove definitive, but some techniques to test GR build statistical confidence by ‘stacking’ many individual events, searching for a common signature [860, 863, 864]. Astrophysical effects not included in these models, if sufficiently common, might mimic or mask the effects of modified gravity. Conversely, the near-universal ‘I–Love–Q’ relationships discussed in section 4.8 suggest that, to leading order, EOS-dependent effects can be encapsulated in a handful of parameters [27, 29, 167], potentially enabling direct tests of strong-field gravity even in the presence of nontrivial and poorly constrained matter physics.

According to the above discussion, a test of strong-field gravity would seem to require a detailed understanding of all possible astrophysical influences, including the nuclear EOS and tidal deformability of NSs. In fact, as discussed in section 4.8, strong relationships exist between matter-sourced ‘tidal’ multipoles of different orders, both in GR and in a broad class of modified-gravity theories. Specifically, the Q–Love relation may help us to break the degeneracy between the NS spin and quadrupole moment in GW observations.

To see this, let us consider GWs from a NS–NS binary. The quadrupole moment first enters at 2PN order in the waveform phase [865, 866], together with the NS spin–spin coupling term [866–868], which leads to a strong degeneracy between the NS quadrupole moment and spin. On the other hand, the NS finite-size effect enters first at 5PN order [869] through the tidal Love number, which can be measured with second-generation ground-based interferometers such as Advanced LIGO [601, 628, 853, 863, 864, 869–874]. The Q–Love relation allows us to express the quadrupole moment in terms of the Love number, leading to degeneracy breaking. This observation suggests that strong-field gravity could be coarsely tested even *without knowing the nuclear EOS*.

Since (with notable exceptions, such as scalar–tensor theories and EiBI theory) the functional form of the I–Love–Q relations depends on the underlying gravitational theory, if one can measure *any two* of the I–Love–Q quantities independently, one can in principle perform a model-independent consistency test of GR or test a specific alternative theory. These tests could exploit combined observations of binary pulsars in the electromagnetic spectrum and binary inspirals in the GW spectrum. For example, future observations of the double binary pulsar [687, 688] may measure the NS moment of inertia to an accuracy $\sim 10\%$ [552, 602], and the tidal Love number may be measured to an accuracy $\sim 60\%$ with GW observations [167]. These measurements would identify a measurement point with an error box in the I–Love plane (see the left panel of figure 25). If the I–Love relation is modified from GR in a specific alternative theory, such a theory can only be valid if the ‘modified I–Love relation’ is consistent with the error box. A problem with this idea is that (in the example considered here) the double binary pulsar and the hypothetical GW observations would target different NSs, while the universal relations are valid for any single star. However, since the parameter that is fixed for different models satisfying the universal relation is the NS mass (or compactness), the relations would still hold if the NSs in the two systems have the same mass. This is not too unlikely, given that NSs have a rather peaked mass distribution [517, 875]. Moreover, even if the two NSs have different masses, it turns out that the EOS-universality is preserved to good accuracy for NS models with fixed mass ratio [167].

To exploit these opportunities, then, requires care in identifying possible confusing astrophysical degrees of freedom, their expected magnitude, and methods to robustly disentangle them from the signatures of modified gravity. A useful way to illustrate how different astrophysical degrees of freedom come into play in different frequency bands is shown in figure 45. Using a Fisher matrix approximation to parameter estimation accuracy,

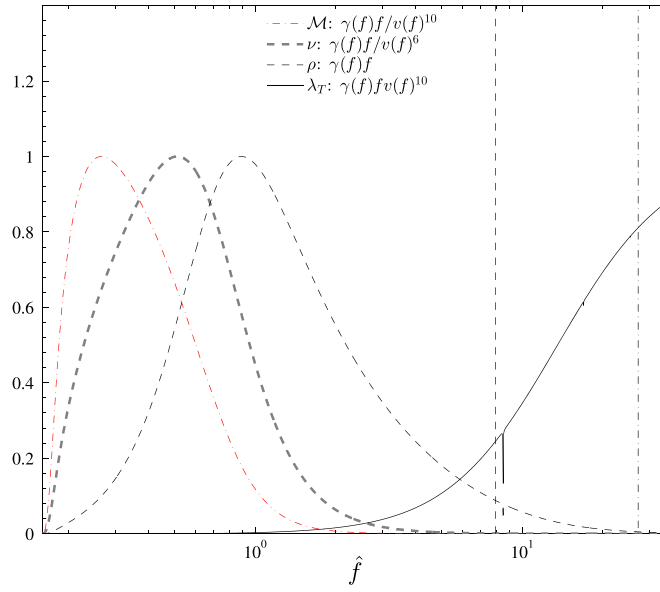


Figure 45. Integrands, per frequency octave, of the integrals determining the SNR ρ and the measurement accuracy of the chirp mass \mathcal{M} , the symmetric mass ratio (denoted by ν in the figure legend, and by η elsewhere in this review), and the tidal parameter $\lambda_T \propto \kappa_2^T$. These integrands are plotted as a function of the rescaled frequency $\hat{f} = f/(56.56 \text{ Hz})$ for a typical $1.4M_\odot + 1.4M_\odot$ binary of two NSs with equal compactness M/R (M and R being the mass and the radius of each star). While most of the SNR is gathered around frequencies $\hat{f} \sim 1$, the measurability of \mathcal{M} and η is concentrated towards lower frequencies ($\hat{f} < 1$), and that of the tidal parameter λ_T gets its largest contribution from the late inspiral up to the merger. The rightmost vertical line indicates the merger frequency, while the leftmost vertical line corresponds to a GW frequency of 450 Hz. (From [863].)

this figure illustrates that different frequency bands of the GW signal encode information about different astrophysical parameters, namely the chirp mass, the symmetric mass ratio and the tidal (Love) parameter. Extending this argument to eccentricity [876–879], precession [880] and merger, one finds the following hierarchy: information on small residual eccentricity and chirp mass is encoded at low frequencies (being tied to the overall number of cycles); information on mass ratio and spin is encoded at intermediate frequencies; finally, information on tidal interactions and strong-field effects comes mostly from the highest frequencies. Similarly—and roughly speaking—different modifications to gravity also predominantly occur at different frequencies, i.e., at different PN orders (see section 7.3). Qualitatively, each frequency scale couples strongly to itself and neighboring scales; for example, mass ratio and (aligned) spins are strongly degenerate [881]. For this physical reason, we expect that confusing effects of astrophysical phenomena are principally entangled with modifications to gravity that dominate at the corresponding frequency interval or PN order (along with all other strongly coupled degrees of freedom). However, because each process has distinctive radiation content (e.g., higher harmonics; precession-induced modulations), astrophysical calculations within GR suggest that these degeneracies can be broken. This will require more precise modeling of gravitational waveforms in various proposed extensions of GR, and further study to quantify precisely what beyond-GR

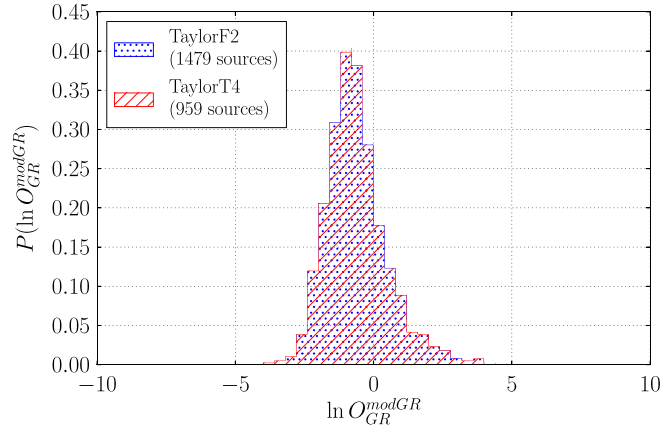


Figure 46. Single-source background distributions where the simulated sources are generated by the `TaylorF2` waveform approximant (blue) or by the `TaylorT4` approximant (red).

properties are accessible to experiment in the presence of all astrophysical parameters that may contaminate the signal.

In the case of NS–NS coalescence, accurate waveforms have been available for some time now. As shown in [882], in the NS–NS mass regime the PN waveform approximants agree with each other and with effective-one-body waveforms to a high degree of accuracy. Nevertheless, it was checked explicitly that (at least for NS–NS sources) the remaining small differences between approximants will not cause one to declare a violation of GR when none is present. Figure 46 shows single-source background distributions where the sources are simulated using the `TaylorF2` waveform family (red) and the `TaylorT4` waveform family (blue). We see that the impact of the waveform mismatch on the background distribution indeed appears to be minimal.

To summarize, binary NSs provide a relatively clean laboratory to investigate modifications to strong-field GR. Unfortunately, in these systems, non-GR deviations in the GW signal could be degenerate with tidal effects, eccentricity and spin. While tidal effects are strong and EOS-dependent at late times, tidal interactions seem to be relatively universal, potentially enabling tests of GR without detailed knowledge of the properties of nuclear matter.

Higher-mass objects: future directions. Quasicircular NS–NS binaries are not the only target of Earth-based GW interferometers. Binaries containing BHs have larger total mass than NS–NS binaries, and their GW signal encodes more nonlinear strong-field dynamics in the LIGO sensitivity band. Fortunately, even though massive binaries may be intrinsically rare, GW detectors are expected to be much more likely to observe them [861, 862].

NS–NS coalescences are relatively simple from the observational point of view: it is mostly the inspiral part that is visible in the detectors’ sensitive frequency band, and NSs in binaries are expected to have small spins. By contrast, for NS–BH and BH–BH coalescences the full process of inspiral, merger, and ringdown will be visible. Moreover, BH spins will likely be large and strongly precessing. Hence NS–BH and BH–BH events are dynamically much richer than NS–NS, but this also makes it more challenging to use them in tests of GR. One problem has been the unavailability of accurate and faithful (semi-)analytical waveform

Table 5. Upper limit on (1) the relative correction to the periastron shift of an EMRI (δ_{per}), and (2) the absolute corrections to the GW phase (δ_{φ}) due to a variety of environmental effects, over a typical eLISA mission duration of one year. We consider two BHs with masses ($10M_{\odot}$, $M = 10^6M_{\odot}$) on a quasicircular inspiral ending at the innermost stable circular orbit (ISCO) $r = 6M$, whereas the periastron shift is computed at $r = 10M$. Dissipative effects such as GW radiation reaction, dynamical friction and hydrodynamic drag from accretion produce negligible δ_{per} , and therefore they are not shown. The scaling with all relevant parameters can be found in [464]. (Adapted from [888].)

Correction		$ \delta_{\text{per}} $	$ \delta_{\varphi} $ (rads)
Thin disks	Planetary migration	—	10^4
	Dyn. friction/accretion	—	10^2
	Gravitational pull	10^{-8}	10^{-3}
	Magnetic field	10^{-8}	10^{-4}
	Electric charge	10^{-7}	10^{-2}
	Gas accretion	10^{-8}	10^{-2}
	Cosmological effects	10^{-31}	10^{-26}
Thick disks	Dyn. friction/accretion	—	10^{-9}
	Gravitational pull	10^{-16}	10^{-11}
	Accretion	—	$10^{-8} \rho_3^{\text{DM}}$
Dark matter	Dynamical friction	—	$10^{-14} \rho_3^{\text{DM}}$
	Gravitational pull	$10^{-21} \rho_3^{\text{DM}}$	$10^{-16} \rho_3^{\text{DM}}$

models, though recently there has been great progress in that regard. For instance, Pan *et al* arrived at an effective-one-body model with full precessing spins that appears to have great faithfulness with waveforms obtained from large-scale numerical simulations [883], although it is still rather costly to generate on a computer. Other options could include (improvements of) the phenomenological time-domain `PhenSpin` waveforms of Sturani *et al* [884, 885], or the frequency-domain (and hence computationally cheap) waveforms for precessing spins developed both for inspiral [880] and for inspiral-merger-ringdown [886, 887]. The application of these waveforms to parameter estimation and model selection of alternative theories of gravity is an exciting research topic for the future.

7.4.2. Supermassive BHs. In addition to the ‘intrinsic’ corrections due to uncertainties on the source composition and on the binary parameters, ‘environmental’ effects such as accretion disks, electromagnetic fields, galactic plasma and dark matter distributions around compact objects may also play a role in GW detection and parameter estimation. These effects are usually dismissed on the grounds that they are believed to be negligible for the typical targets of GW detectors. Nonetheless, unmodeled environmental effects on the ‘vacuum’ gravitational waveforms predicted by GR may degrade the SNR, the accuracy of parameter estimation, and our ability to perform tests of gravitational theories and of astrophysical models.

A careful examination of the environment’s impact on GW observables is mandatory to assess whether GW astrophysics can become a precision discipline in the space-based detector era. Investigations in this direction started only recently, and this section is devoted to a brief summary of the main findings. The upshot is that GW sources are among the ‘cleanest’ astrophysical systems: environmental effects are typically too small to affect the

Table 6. Upper limits on the environmental corrections to the BH ringdown frequencies.

Correction	$ \delta_R (\%)$	$ \delta_I (\%)$
Spherical near-horizon distribution	0.05	0.03
Ring at ISCO	0.01	0.01
Electric charge	10^{-5}	10^{-6}
Magnetic field	10^{-8}	10^{-7}
Gas accretion	10^{-11}	10^{-11}
Dark matter halos	$10^{-21} \rho_3^{\text{DM}}$	$10^{-21} \rho_3^{\text{DM}}$
Cosmological effects	10^{-32}	10^{-32}

Note. δ_R and δ_I denote the deviations in the real and imaginary parts of the QNM frequencies due to environmental effects, relative to the case of an isolated BH with the same total mass. The (rather extreme) reference values for the environmental effects are given in the text, and the scaling with the parameters for each effect can be found in [464]. (From [888].)

detection of GW signals and the estimation of the source parameters. The few and rather extreme cases in which environmental effects can leave a detectable imprint should be seen as opportunities, in the sense that (if such effects are adequately modeled) GW observations may be used to study the behavior of matter around compact objects, as routinely done in the electromagnetic spectrum. These conclusions confirm the enormous potential of GW astronomy and justify the excitement for future observations of GWs from compact objects.

Environmental corrections for eLISA sources. A detailed analysis of the impact of the environment on GW observables for an eLISA-like space detector has been recently presented in [464] and summarized in [888]. The authors have modeled the effects of electromagnetic fields, cosmological evolution, accretion disks and dark matter for the inspiral, merger and ringdown of BH binaries. The main results of this study are summarized in tables 5 and 6, which show the environmental corrections to the periastron shift and GW phase of a typical quasicircular EMRI (table 5) and to the ringdown modes of a massive BH (table 6).

As for the inspiral, the largest corrections come from the presence of geometrically thin, radiatively efficient accretion disks, which have been described using a Shakura-Sunyaev disk model with viscosity parameter $\alpha = 0.1$ and Eddington ratio $f_{\text{Edd}} = 1$. During the binary's inspiral, a gaseous disk affects the orbital evolution in three ways [457, 889, 890]: (i) through its own gravitational field that modifies the trajectories of the inspiral, (ii) through accretion of gas that changes the masses and the spins of the compact objects, and (iii) through the gravitational interaction of the compact objects with their own wake in the gaseous medium, which produces dynamical friction and leads to planetary-like migration [891, 892]. As shown in table 5, for thin disks such effects introduce corrections of very different magnitude, with the gravitational pull of the disk being negligible, whereas planetary migration, dynamical friction and accretion can introduce large corrections, which can even dominate over gravitational radiation reaction at separations larger than ~ 60 gravitational radii [888]. In fact, these corrections may be large enough to affect estimates of the source parameters, prevent accurate tests of GR, and possibly even affect the detectability of the signal.

However, radiatively efficient thin disks are mainly expected in AGNs at very high redshifts, while only EMRIs at $z \lesssim 1$ will be detectable by eLISA [502]. In the local Universe most galactic nuclei are quiescent rather than active, so that only a few percent of the EMRIs

detected by eLISA are expected to be significantly affected by thin-disk environmental corrections [888]. On the other hand, BHs in quiescent nuclei are expected to be surrounded by thick, radiatively inefficient disks, which, as shown in table 5, introduce small relative corrections to the GW observables (of the order of 10^{-9} in the most conservative scenario).

Electromagnetic fields and cosmological effects are also negligible. Because of the uncertainties on the value of galactic magnetic fields B and on the charge qM of massive BHs, the upper limits shown in table 5 were obtained using the rather extreme reference values of $q = Q/M = 10^{-3}$ and $B = 10^8$ Gauss, so that actual corrections are expected to be smaller in less extreme (and more realistic) situations.

The effects of dark matter depend strongly on the assumptions made for the dark matter distribution near the galactic center and, more specifically, on the steepness of the dark matter profile near massive BHs. Dark matter ‘spikes’ produced by the adiabatic growth of massive BHs [893] can be efficiently destroyed by various mechanisms (including mergers, dark matter scattering off stars and off-center formation of the BH seeds) [894–896], so that the actual dark matter profiles are believed to display a shallow slope, rather than a spike. In this case, a typical reference value for the dark matter density near BH binaries is $\rho_{\text{DM}} \sim 10^3 M_{\odot} \text{pc}^{-3} \sim 4 \times 10^4 \text{GeV cm}^{-3}$. Using the normalization $\rho_3^{\text{DM}} = \rho_{\text{DM}} / (10^3 M_{\odot} \text{pc}^{-3})$, table 5 shows that any effect of dark matter (including accretion, dynamical friction and gravitational pull) is negligible. A possible exception are EMRIs in satellite galaxies that have never undergone mergers, so that dark matter spikes with densities as large as $\rho_{\text{DM}} \sim 10^{12} M_{\odot} \text{pc}^{-3}$ may survive in these systems [897].

Similar considerations apply to the environmental corrections to the ringdown frequencies of a single massive BH. As discussed above, ringdown tests can be used to estimate the BH mass and spin within fractions of a percent when the object is assumed to be in isolation [384]. Table 6 shows that environmental effects do not change this prospect, the relative corrections being at most of the order of 0.01%, and usually even smaller. These results were obtained for a nonspinning BH, and degeneracy with spin effects would make it even harder to detect imprints of the environment.

Overall, EMRI detection, ringdown tests and parameter estimation with eLISA should only be marginally affected by the environment. The detectability of these effects in the most optimistic scenarios would depend on the actual SNR and require a more sophisticated modeling (e.g. including spin, eccentricity, tidal effects, etcetera) than the ones currently developed.

Ringdown modes versus QNMs. The presence of matter is the prototypical example of an interesting phenomenon of ‘mode camouflage’ which is not widely recognized in BH physics. Specifically, for matter configurations localized far from the BH or very close to its horizon, the deviations from the isolated BH QNMs (as defined by the poles of the relevant Green’s function) are *arbitrarily large*, even for vanishingly small matter densities. This surprising phenomenon was discovered using a thin-shell toy model in [898], but it is actually very generic [464, 888]: it occurs for several matter distributions, for BHs surrounded by light bosonic fields [110, 403, 488–490], for ultracompact horizonless objects [467], and it may also have important implications for detecting GW signatures of ‘firewalls’ near BH horizons [899] (see also [900] for a similar earlier proposal). This effect would have two important corollaries: (i) deviations from the standard Kerr QNMs may be very large, and thus signatures of new physics would be easily detectable; however (ii) any arbitrarily small deviation from the isolated BH case could destroy the mode spectrum, thus making it essentially impossible to use the Kerr modes as a basis for tests of gravity.

This seems in contrast with the results of table 6 and with our previous discussion of ringdown tests. In fact, the situation is much less dramatic. Although the QNM spectrum of various dirty BHs and BH mimickers is totally different from the isolated BH case, nevertheless the ringdown waveforms at early and intermediate times are dominated by the QNMs of the pure, isolated BH geometry, whereas the modes of the composite system get excited only at late times and with very small amplitudes [464, 888]. In other words, for various deformed BH spacetimes the ringdown modes that dominate the waveform are not necessarily the same as the poles of the relevant Green's function. While poles of the Green's function can be dramatically different, only the modes are of direct interest for GW astronomy. This ensures that current GW ringdown searches—which *assume* the source is described by the pure Kerr geometry [901, 902]—are most likely to perform well under all circumstances.

Intrinsic limits to tests of gravity theories. The clean nature of compact binaries as GW sources, as highlighted by the small impact of environmental effects in most situations, is good news for testing strong-field gravity in the GW spectrum. In order to avoid mistaking environmental effects for deviations from GR, it is essential to understand the impact of the environment on strong-field tests of GR, the latter usually assuming that the sources are isolated and that GWs propagate in vacuum.

Indeed, any environmental effect will provide an *intrinsic limit* to the precision of GR tests. Beyond-GR modifications that introduce effects smaller than environmental perturbations will be very hard to detect, unless the environment is precisely modeled. For instance, EMRIs in thin-disk environments are not good laboratories for tests of GR, because in these systems astrophysical effects such as planetary migration, dynamical friction and accretion can be even more important than GW emission, as previously discussed.

On the other hand, the vast majority of GW sources for terrestrial and space detectors turns out to be extremely clean. Using the estimates in tables 5 and 6, references [464, 888] computed the intrinsic lower bounds due to the environment on the coupling parameters of a large class of modified theories of gravity. It turns out that the environmental lower limits are much less stringent than current observational constraints, and even less stringent than projected bounds that will be placed with GW detectors. In other words, environmental effects are too small to affect the accuracy of GW tests of GR in the foreseeable future.

8. Discussion and conclusions

The theoretical necessity to unify GR with quantum mechanics and the puzzling implications of cosmological measurements led to an explosion of activity in the field of modified gravity. This major area of research has been summarized by many outstanding reviews in the recent past [11–18]. Unlike most of these reviews, our focus here was on the astrophysical and phenomenological implications of modified gravity in the *strong-field regime*. Any attempt at completeness would be foolish, given the amount of literature on strong gravity and compact objects. Our hope is that our collective effort will be seen as a useful, practical map for both novices and experts in strong-field gravity.

In these concluding remarks we wish to highlight some parts of this review that should be particularly valuable as roadmaps for future research. Table 1 gives a simple overview of key references on modified gravity theories whose strong-field behavior has been investigated in some depth. Tables 2 and 3 collect work on compact object solutions in these theories and on

their stability. Each question mark in those tables (and there are many!) could lead to a good PhD project.

At the end of each section we have summarized important questions that require further investigation. We hope that some readers of this review will pick up the gauntlet and shed light on our current understanding of modified gravity (section 2.9), the structure and stability of BHs (section 3.11) and NSs (section 4.10), the dynamics of compact binaries (section 5.6), binary pulsar tests (section 6.1.1) and cosmology (section 6.2.4).

We have not even bothered writing down a list of open problems when it comes to GW tests. The fact that Advanced LIGO and Advanced Virgo are coming online in 2015, the year when we celebrate the centenary of Einstein's milestone accomplishment, is particularly meaningful and inspiring. We hope that when we start listening to GWs, the Universe will amaze us and confuse us, as it has so many times in the past when we turned our gaze in new directions; and that out of the confusion will emerge new understanding.

Acknowledgments

This review was conceived during a workshop funded by the FP7-PEOPLE-2011-IRSES Grant No. 295189 'NRHEP' [903]. We thank Marco Cavaglia, Neil Cornish, Luís Crispino and Nicolás Yunes for attending the workshop and for useful discussions. We are also grateful to T rence Delsate and Claudia de Rham for comments, and to Alessandro Nagar, Thibault Damour, Loic Villain, Michael Kramer and Fabian Schmidt for allowing us to use their figures. This work has been supported by the H2020-MSCA-RISE-2015 Grant No. 690904 'StronGrHEP,' the European Union's FP7 ERC Starting Grant 'The dynamics of black holes: testing the limits of Einstein's theory' grant agreement no. DyBHo-256667, H2020 ERC Consolidator Grant 'Matter and strong-field gravity: New frontiers in Einstein's theory' grant agreement no. MaGraTh-646597, the FP7-PEOPLE-2011-CIG Grant No. 293412 'CBHEO,' the FP7-PEOPLE-2011-CIG Grant PCIG11-GA-2012-321608 'GAL-FORMBHS,' the NSF Grants No. PHY-1055103, PHY-1260995, PHY-1306069 and PHY-1300903, the NASA Grant NNX13AH44G, the ERC-2011-StG Grant No. 279363-HiDGR, the FP7/2007-2013 ERC Grant No. 306425 'Challenging General Relativity', the DFG Research Training Group 1620 'Models of Gravity' FP7-PEOPLE-2011-IRSES Grant No. 606096, the STFC GR Consolidator Grant No. ST/L000636/1, the FCT-Portugal projects PTDC/FIS/116625/2010, CERN/FP/116341/2010, CERN/FP/123593/2011, IF/00293/2013, IF/00797/2014/CP1214/CT0012 and CIDMA strategic funding UID/MAT/04106/2013, the Marie Curie IEF contracts aStronGR-2011-298297 and AstroGRAphy-2013-623439, the COST Action MP1304 'NewCompStar,' a UIUC Fortner Fellowship, the S o Paulo Research Foundation (FAPESP) under grants 2011/11973-4 and 2013/14754-7, the NSF XSEDE Grant No. PHY-090003, the Cosmos system, part of DiRAC, funded by STFC and BIS under Grant Nos. ST/K00333X/1, ST/H008586/1, ST/J001341/1 and ST/J005673/1, and the CESGA-ICTS Grant No. 249. Computations have been performed on the 'Baltasar Sete-Sois' cluster at IST, the 'Venus' cluster at YITP, the COSMOS supercomputer, the Trestles cluster at SDSC, the Kraken cluster at NICS, and Finis Terrae at CESGA. T Baker is supported by All Souls College, Oxford. D Doneva would like to thank the Alexander von Humboldt Foundation for support. P G Ferreira acknowledges support from STFC, BIPAC and Oxford Martin School. D Gerosa is supported by the UK STFC and the Isaac Newton Studentship of the University of Cambridge. J Kunz acknowledges support from DFG Research Training Group 1620 'Models of Gravity' and FP7-PEOPLE-2011-IRSES Grant No. 606096. A Matas would like to thank Claudia de Rham and Andrew Tolley for

many useful conversations and support. A Matas is supported by an NSF-GRFP fellowship. B S Sathyaprakash acknowledges the support of the LIGO Visitor Program through the National Science Foundation award PHY-0757058 and STFC grant ST/J000345/1. L C Stein acknowledges that support for this work was provided by the NASA through Einstein Postdoctoral Fellowship Award Number PF2-130101 issued by the Chandra x-ray Observatory Center, which is operated by the Smithsonian Astrophysical Observatory for and on behalf of the National Aeronautics Space Administration under contract NAS8-03060. This research was supported in part by Perimeter Institute for Theoretical Physics. Research at Perimeter Institute is supported by the Government of Canada through Industry Canada and by the Province of Ontario through the Ministry of Economic Development & Innovation.

References

- [1] Poisson E and Will C M 2014 *Gravity: Newtonian, Post-Newtonian, Relativistic* (Cambridge: Cambridge University Press)
- [2] Will C M 2014 *Living Rev. Relativ.* **17** 4
- [3] Stelle K 1977 *Phys. Rev. D* **16** 953–69
- [4] Hawking S and Penrose R 1970 *Proc. R. Soc. A* **314** 529–48
- [5] Weinberg S 1989 *Rev. Mod. Phys.* **61** 1–23
- [6] Deser S 1970 *Gen. Relativ. Gravit.* **1** 9–18
- [7] Wald R M 1986 *Phys. Rev. D* **33** 3613
- [8] Wex N 2014 *Frontiers in Relativistic Celestial Mechanics* ed S Kopeikin vol 2
- [9] Baker T, Psaltis D and Skordis C 2015 *Astrophys. J.* **802** 63
- [10] Psaltis D 2008 *Living Rev. Relativ.* **11** 9
- [11] Sotiriou T P and Faraoni V 2010 *Rev. Mod. Phys.* **82** 451–97
- [12] De Felice A and Tsujikawa S 2010 *Living Rev. Relativ.* **13** 3
- [13] Nojiri S and Odintsov S D 2011 *Phys. Rep.* **505** 59–144
- [14] Capozziello S and De Laurentis M 2011 *Phys. Rep.* **509** 167–321
- [15] Clifton T, Ferreira P G, Padilla A and Skordis C 2012 *Phys. Rep.* **513** 1–189
- [16] Hinterbichler K 2012 *Rev. Mod. Phys.* **84** 671–710
- [17] de Rham C 2014 *Living Rev. Relativ.* **17** 7
- [18] Joyce A, Jain B, Khoury J and Trodden M 2015 *Phys. Rep.* **568** 1–98
- [19] Burgess C 2004 *Living Rev. Relativ.* **7** 5–56
- [20] Burgess C 2007 *Ann. Rev. Nucl. Part. Sci.* **57** 329–62
- [21] Woodard R P 2007 *Lecture Notes Phys.* **720** 403–33
- [22] Narayan R 2005 *New J. Phys.* **7** 199
- [23] Narayan R and McClintock J E 2015 *General Relativity and Gravitation: A Centennial Perspective* ed A Ashtekar et al (Cambridge, UK: Cambridge University Press)
- [24] Abramowicz M A, Kluzniak W and Lasota J P 2002 *Astron. Astrophys. Lett.* **396** L31–34
- [25] Johannsen T 2013 *Phys. Rev. D* **87** 124017
- [26] Damour T and Esposito-Farèse G 1993 *Phys. Rev. Lett.* **70** 2220–3
- [27] Yagi K and Yunes N 2013 *Science* **341** 365–8
- [28] Pappas G and Apostolatos T A 2014 *Phys. Rev. Lett.* **112** 121101
- [29] Yagi K, Kyutoku K, Pappas G, Yunes N and Apostolatos T A 2014 *Phys. Rev. D* **89** 124013
- [30] Taylor J H, Wolszczan A, Damour T and Weisberg J M 1992 *Nature* **355** 132–6
- [31] Yunes N and Siemens X 2013 *Living Rev. Relativ.* **16** 9
- [32] Gair J R, Vallisneri M, Larson S L and Baker J G 2013 *Living Rev. Relativ.* **16** 7
- [33] Misner C, Thorne K and Wheeler J 1973 *Gravitation* (San Francisco, CA: W. H. Freeman)
- [34] Salgado M, Rio D M d, Alcubierre M and Nunez D 2008 *Phys. Rev. D* **77** 104010
- [35] Bertotti B, Iess L and Tortora P 2003 *Nature* **425** 374
- [36] Alsing J, Berti E, Will C M and Zaglauer H 2012 *Phys. Rev. D* **85** 064041
- [37] Freire P C et al 2012 *Mon. Not. R. Astron. Soc.* **423** 3328
- [38] Choquet-Bruhat Y 2009 *General Relativity and the Einstein Equations* (Oxford: Oxford University Press)
- [39] Damour T and Esposito-Farèse G 1992 *Class. Quantum Grav.* **9** 2093–176

- [40] Lanahan-Tremblay N and Faraoni V 2007 *Class. Quantum Grav.* **24** 5667–80
- [41] Paschalidis V, Halataei S M, Shapiro S L and Sawicki I 2011 *Class. Quantum Grav.* **28** 085006
- [42] Berry C P and Gair J R 2011 *Phys. Rev. D* **83** 104022
- [43] Yagi K 2012 *Phys. Rev. D* **86** 081504
- [44] Delsate T, Hilditch D and Witek H 2015 *Phys. Rev. D* **91** 024027
- [45] Ali-Haimoud Y and Chen Y 2011 *Phys. Rev. D* **84** 124033
- [46] Foster B Z and Jacobson T 2006 *Phys. Rev. D* **73** 064015
- [47] Jacobson T 2007 *PoS QG-PH* 020
- [48] Yagi K, Blas D, Yunes N and Barausse E 2014 *Phys. Rev. Lett.* **112** 161101
- [49] Yagi K, Blas D, Barausse E and Yunes N 2014 *Phys. Rev. D* **89** 084067
- [50] Blas D, Pujolas O and Sibiryakov S 2011 *J. High Energy Phys.* JHEP04(2011)018
- [51] Blas D and Sanctuary H 2011 *Phys. Rev. D* **84** 064004
- [52] Coelho F S, Herdeiro C, Hirano S and Sato Y 2014 *Phys. Rev. D* **90** 064040
- [53] de Rham C, Tolley A J and Wesley D H 2013 *Phys. Rev. D* **87** 044025
- [54] Iorio L and Saridakis E N 2012 *Mon. Not. R. Astron. Soc.* **427** 1555
- [55] Hawking S 1972 *Commun. Math. Phys.* **25** 167–71
- [56] Heusler M 1995 *Class. Quantum Grav.* **12** 2021–36
- [57] Jacobson T 1999 *Phys. Rev. Lett.* **83** 2699–702
- [58] Heusler M 1996 *Black Hole Uniqueness Theorems* (Cambridge: Cambridge University Press)
- [59] Sotiriou T P and Faraoni V 2012 *Phys. Rev. Lett.* **108** 081103
- [60] Graham A A H and Jha R 2014 *Phys. Rev. D* **90** 041501
- [61] Anabalon A, Bičák J and Saavedra J 2014 *Phys. Rev. D* **90** 124055
- [62] Damour T, Deruelle N and Ruffini R 1976 *Lett. Nuovo Cimento* **15** 257–62
- [63] Detweiler S L 1980 *Phys. Rev. D* **22** 2323–6
- [64] Zouros T and Eardley D 1979 *Ann. Phys.* **118** 139–55
- [65] Cardoso V, Dias O J C, Lemos J P S and Yoshida S 2004 *Phys. Rev. D* **70** 044039
- [66] Shlapentokh-Rothman Y 2014 *Commun. Math. Phys.* **329** 859–91
- [67] Cardoso V 2013 *Gen. Relativ. Gravit.* **45** 2079–97
- [68] Herdeiro C A R and Radu E 2014 *Phys. Rev. Lett.* **112** 221101
- [69] Herdeiro C and Radu E 2015 *Class. Quantum Grav.* **32** 144001
- [70] Hersh J and Ove R 1985 *Phys. Lett. B* **156** 305
- [71] Nzioki A M, Goswami R and Dunsby P K S 2014 arXiv:1408.0152
- [72] Mignemi S and Stewart N 1993 *Phys. Rev. D* **47** 5259–69
- [73] Kanti P, Mavromatos N, Rizos J, Tamvakis K and Winstanley E 1996 *Phys. Rev. D* **54** 5049–58
- [74] Yunes N and Stein L C 2011 *Phys. Rev. D* **83** 104002
- [75] Pani P and Cardoso V 2009 *Phys. Rev. D* **79** 084031
- [76] Ayzenberg D and Yunes N 2014 *Phys. Rev. D* **90** 044066
- [77] Kleihaus B, Kunz J and Radu E 2011 *Phys. Rev. Lett.* **106** 151104
- [78] Torii T and Maeda K i 1998 *Phys. Rev. D* **58** 084004
- [79] Ayzenberg D, Yagi K and Yunes N 2014 *Phys. Rev. D* **89** 044023
- [80] Pani P, Macedo C F, Crispino L C and Cardoso V 2011 *Phys. Rev. D* **84** 087501
- [81] Maselli A, Gualtieri L, Pani P, Stella L and Ferrari V 2015 *Astrophys. J.* **801** 115
- [82] Kleihaus B, Kunz J and Mojica S 2014 *Phys. Rev. D* **90** 061501
- [83] Yunes N and Pretorius F 2009 *Phys. Rev. D* **79** 084043
- [84] Konno K, Matsuyama T and Tanda S 2009 *Prog. Theor. Phys.* **122** 561–8
- [85] Yagi K, Yunes N and Tanaka T 2012 *Phys. Rev. D* **86** 044037
- [86] Stein L C 2014 *Phys. Rev. D* **90** 044061
- [87] Cardoso V and Gualtieri L 2009 *Phys. Rev. D* **80** 064008
- [88] Molina C, Pani P, Cardoso V and Gualtieri L 2010 *Phys. Rev. D* **81** 124021
- [89] Garfinkle D, Pretorius F and Yunes N 2010 *Phys. Rev. D* **82** 041501
- [90] Konno K and Takahashi R 2014 *Phys. Rev. D* **90** 064011
- [91] Vincent F 2013 *Class. Quantum Grav.* **31** 025010
- [92] Sotiriou T P and Zhou S Y 2014 *Phys. Rev. Lett.* **112** 251102
- [93] Sotiriou T P and Zhou S Y 2014 *Phys. Rev. D* **90** 124063
- [94] Babichev E and Charmousis C 2014 *J. High Energy Phys.* JHEP08(2014)106
- [95] Kobayashi T, Motohashi H and Suyama T 2012 *Phys. Rev. D* **85** 084025
- [96] Kobayashi T, Motohashi H and Suyama T 2014 *Phys. Rev. D* **89** 084042
- [97] Eling C and Jacobson T 2006 *Class. Quantum Grav.* **23** 5643–60

- [98] Barausse E, Jacobson T and Sotiriou T P 2011 *Phys. Rev. D* **83** 124043
- [99] Barausse E and Sotiriou T P 2013 *Class. Quantum Grav.* **30** 244010
- [100] Wang A 2013 *Phys. Rev. Lett.* **110** 091101
- [101] Barausse E and Sotiriou T P 2013 *Phys. Rev. D* **87** 087504
- [102] Blas D and Sibiriyakov S 2011 *Phys. Rev. D* **84** 124043
- [103] Herdeiro C, Hirano S and Sato Y 2011 *Phys. Rev. D* **84** 124048
- [104] Coelho F S, Herdeiro C and Wang M 2013 *Phys. Rev. D* **87** 047502
- [105] Brito R, Cardoso V and Pani P 2013 *Phys. Rev. D* **88** 064006
- [106] Babichev E and Fabbri A 2014 *J. High Energy Phys.* **JHEP07(2014)016**
- [107] Babichev E and Fabbri A 2014 *Phys. Rev. D* **90** 084019
- [108] Volkov M S 2015 *Lecture Notes Phys.* **892** 161–80
- [109] Babichev E and Fabbri A 2013 *Class. Quantum Grav.* **30** 152001
- [110] Brito R, Cardoso V and Pani P 2013 *Phys. Rev. D* **88** 023514
- [111] Brito R, Cardoso V and Pani P 2013 *Phys. Rev. D* **87** 124024
- [112] Babichev E and Fabbri A 2014 *Phys. Rev. D* **89** 081502
- [113] Hui L and Nicolis A 2013 *Phys. Rev. Lett.* **110** 241104
- [114] Salmona A 1967 *Phys. Rev.* **154** 1218–23
- [115] Hillebrandt W and Heintzmann H 1974 *Gen. Relativ. Gravit.* **5** 663–72
- [116] Damour T and Esposito-Farese G 1996 *Phys. Rev. D* **54** 1474–91
- [117] Tsuchida T, Kawamura G and Watanabe K 1998 *Prog. Theor. Phys.* **100** 291–313
- [118] Salgado M, Sudarsky D and Nucamendi U 1998 *Phys. Rev. D* **58** 124003
- [119] Sotani H 2012 *Phys. Rev. D* **86** 124036
- [120] Pani P and Berti E 2014 *Phys. Rev. D* **90** 024025
- [121] Doneva D D, Yazadjiev S S, Stergioulas N and Kokkotas K D 2013 *Phys. Rev. D* **88** 084060
- [122] Doneva D D, Yazadjiev S S, Stergioulas N, Kokkotas K D and Athanasiadis T M 2014 *Phys. Rev. D* **90** 044004
- [123] Doneva D D, Yazadjiev S S, Staykov K V and Kokkotas K D 2014 *Phys. Rev. D* **90** 104021
- [124] Scheel M A, Shapiro S L and Teukolsky S A 1995 *Phys. Rev. D* **51** 4208–35
- [125] Scheel M A, Shapiro S L and Teukolsky S A 1995 *Phys. Rev. D* **51** 4236–49
- [126] Shibata M, Nakao K and Nakamura T 1994 *Phys. Rev. D* **50** 7304–17
- [127] Harada T, Chiba T, Nakao K I and Nakamura T 1997 *Phys. Rev. D* **55** 2024–37
- [128] Novak J 1998 *Phys. Rev. D* **57** 4789–801
- [129] Novak J 1998 *Phys. Rev. D* **58** 064019
- [130] Kerimo J and Kalligas D 1998 *Phys. Rev. D* **58** 104002
- [131] Novak J and Ibanez J M 2000 *Astrophys. J.* **533** 392–405
- [132] Zaglauer H 1992 *Astrophys. J.* **393** 685–96
- [133] Nutku Y 1969 *Astrophys. J.* **155** 999
- [134] Harada T 1997 *Prog. Theor. Phys.* **98** 359–79
- [135] Harada T 1998 *Phys. Rev. D* **57** 4802
- [136] Sotani H and Kokkotas K D 2004 *Phys. Rev. D* **70** 084026
- [137] Sotani H and Kokkotas K D 2005 *Phys. Rev. D* **71** 124038
- [138] Lima W C, Matsas G E and Vanzella D A 2010 *Phys. Rev. Lett.* **105** 151102
- [139] Pani P, Cardoso V, Berti E, Read J and Salgado M 2011 *Phys. Rev. D* **83** 081501
- [140] Mendes R F, Matsas G E and Vanzella D A 2014 *Phys. Rev. D* **89** 047503
- [141] Landulfo A G S, Lima W C C, Matsas G E A and Vanzella D A T 2015 *Phys. Rev. D* **91** 024011
- [142] Sotani H 2014 *Phys. Rev. D* **89** 064031
- [143] Silva H O, Sotani H, Berti E and Horbatsch M 2014 *Phys. Rev. D* **90** 124044
- [144] DeDeo S and Psaltis D 2004 arXiv:[astro-ph/0405067](https://arxiv.org/abs/astro-ph/0405067)
- [145] Kobayashi T and Maeda K 2008 *Phys. Rev. D* **78** 064019
- [146] Cooney A, DeDeo S and Psaltis D 2010 *Phys. Rev. D* **82** 064033
- [147] Upadhye A and Hu W 2009 *Phys. Rev. D* **80** 064002
- [148] Babichev E and Langlois D 2009 *Phys. Rev. D* **80** 121501
- [149] Babichev E and Langlois D 2010 *Phys. Rev. D* **81** 124051
- [150] Miranda V, Joras S E, Waga I and Quartin M 2009 *Phys. Rev. Lett.* **102** 221101
- [151] Jaime L G, Patino L and Salgado M 2011 *Phys. Rev. D* **83** 024039
- [152] Astashenok A V, Capozziello S and Odintsov S D 2013 *J. Cosmol. Astropart. Phys.* **JCAP12(2013)040**
- [153] Astashenok A V, Capozziello S and Odintsov S D 2014 *Phys. Rev. D* **89** 103509

- [154] Astashenok A V, Capozziello S and Odintsov S D 2015 *Astrophys. Space Sci.* **355** 333–41
- [155] Yazadjiev S S, Doneva D D, Kokkotas K D and Staykov K V 2014 *J. Cosmol. Astropart. Phys.* [JCAP06\(2014\)003](#)
- [156] Arapoglu A S, Deliduman C and Eksi K Y 2011 *J. Cosmol. Astropart. Phys.* [JCAP07\(2011\)020](#)
- [157] Alavirad H and Weller J M 2013 *Phys. Rev. D* **88** 124034
- [158] Staykov K V, Doneva D D, Yazadjiev S S and Kokkotas K D 2014 *J. Cosmol. Astropart. Phys.* [JCAP10\(2014\)006](#)
- [159] Yazadjiev S S, Doneva D D and Kokkotas K D 2015 *Phys. Rev. D* **91** 084018
- [160] Cembranos J, de la Cruz-Dombriz A and Montes Nunez B 2012 *J. Cosmol. Astropart. Phys.* [JCAP04\(2012\)021](#)
- [161] Borisov A, Jain B and Zhang P 2012 *Phys. Rev. D* **85** 063518
- [162] Seifert M D 2007 *Phys. Rev. D* **76** 064002
- [163] Kainulainen K and Sunhede D 2008 *Phys. Rev. D* **78** 063511
- [164] Pani P, Berti E, Cardoso V and Read J 2011 *Phys. Rev. D* **84** 104035
- [165] Yunes N, Psaltis D, Ozel F and Loeb A 2010 *Phys. Rev. D* **81** 064020
- [166] Yagi K, Stein L C, Yunes N and Tanaka T 2013 *Phys. Rev. D* **87** 084058
- [167] Yagi K and Yunes N 2013 *Phys. Rev. D* **88** 023009
- [168] Eling C and Jacobson T 2006 *Class. Quantum Grav.* **23** 5625–42
- [169] Eling C, Jacobson T and Miller M C 2007 *Phys. Rev. D* **76** 042003
- [170] Garfinkle D, Eling C and Jacobson T 2007 *Phys. Rev. D* **76** 024003
- [171] Greenwald J, Papazoglou A and Wang A 2010 *Phys. Rev. D* **81** 084046
- [172] Babichev E, Deffayet C and Ziour R 2010 *Phys. Rev. D* **82** 104008
- [173] Gruzinov A and Mirbabayi M 2011 *Phys. Rev. D* **84** 124019
- [174] Chagoya J, Koyama K, Niz G and Tasinato G 2014 *J. Cosmol. Astropart. Phys.* [JCAP10\(2014\)055](#)
- [175] Bellini E, Bartolo N and Matarrese S 2012 *J. Cosmol. Astropart. Phys.* [JCAP06\(2012\)019](#)
- [176] Barreira A, Li B, Baugh C M and Pascoli S 2013 *J. Cosmol. Astropart. Phys.* [JCAP11\(2013\)056](#)
- [177] Kainulainen K, Reijonen V and Sunhede D 2007 *Phys. Rev. D* **76** 043503
- [178] Kainulainen K, Pilonen J, Reijonen V and Sunhede D 2007 *Phys. Rev. D* **76** 024020
- [179] Barausse E, Sotiriou T P and Miller J C 2008 *Class. Quantum Grav.* **25** 062001
- [180] Barausse E, Sotiriou T and Miller J 2008 *Class. Quantum Grav.* **25** 105008
- [181] Olmo G J 2008 *Phys. Rev. D* **78** 104026
- [182] Pani P, Cardoso V and Delsate T 2011 *Phys. Rev. Lett.* **107** 031101
- [183] Pani P, Delsate T and Cardoso V 2012 *Phys. Rev. D* **85** 084020
- [184] Pani P and Sotiriou T P 2012 *Phys. Rev. Lett.* **109** 251102
- [185] Sham Y, Leung P and Lin L 2013 *Phys. Rev. D* **87** 061503
- [186] Harko T, Lobo F S N, Mak M and Sushkov S V 2013 *Phys. Rev. D* **88** 044032
- [187] Sotani H 2014 *Phys. Rev. D* **89** 104005
- [188] Casanellas J, Pani P, Lopes I and Cardoso V 2012 *Astrophys. J.* **745** 15
- [189] Sham Y H, Lin L M and Leung P 2012 *Phys. Rev. D* **86** 064015
- [190] Sotani H 2014 *Phys. Rev. D* **89** 124037
- [191] Lovelock D 1971 *J. Math. Phys.* **12** 498–501
- [192] Lovelock D 1972 *J. Math. Phys.* **13** 874–6
- [193] Cartan E 1922 *J. Math. Pures Appl.* **1** 141–204
- [194] Sotiriou T P, Liberati S and Faraoni V 2008 *Int. J. Mod. Phys. D* **17** 399–423
- [195] Di Casola E, Liberati S and Sonego S 2014 *Phys. Rev. D* **89** 084053
- [196] Sotiriou T P 2015 *Lecture Notes Phys.* **892** 3–24
- [197] Pani P, Sotiriou T P and Vernieri D 2013 *Phys. Rev. D* **88** 121502
- [198] Banados M and Ferreira P G 2010 *Phys. Rev. Lett.* **105** 011101
- [199] Olmo G J 2011 *Int. J. Mod. Phys. D* **20** 413–62
- [200] Horava P 2009 *Phys. Rev. D* **79** 084008
- [201] Jacobson T, Liberati S and Mattingly D 2006 *Ann. Phys.* **321** 150–96
- [202] Choquet-Bruhat Y 1988 *J. Math. Phys.* **29** 1891–5
- [203] Reall H, Tanahashi N and Way B 2014 *Class. Quantum Grav.* **31** 205005
- [204] Willison S 2015 *Class. Quantum Grav.* **32** 022001
- [205] Kanti P 2004 *Int. J. Mod. Phys. A* **19** 4899–951
- [206] Bertolami O, Boehmer C G, Harko T and Lobo F S 2007 *Phys. Rev. D* **75** 104016

- [207] Schlamminger S, Choi K Y, Wagner T, Gundlach J and Adelberger E 2008 *Phys. Rev. Lett.* **100** 041101
- [208] Burrage C, Copeland E J and Hinds E 2015 *J. Cosmol. Astropart. Phys.* **JCAP03(2015)042**
- [209] Hamilton P *et al* 2015 *Science* **349** 849–51
- [210] Steffen J H *et al* (GammeV) 2010 *Phys. Rev. Lett.* **105** 261803
- [211] Jain B, Vikram V and Sakstein J 2013 *Astrophys. J.* **779** 39
- [212] Chiba T, Harada T and Nakao K i 1997 *Prog. Theor. Phys. Suppl.* **128** 335–72
- [213] Fujii Y and Maeda K I 2003 *The Scalar–Tensor Theory of Gravitation* (Cambridge: Cambridge University Press)
- [214] Faraoni V 2004 *Cosmology in Scalar Tensor Gravity* (Berlin: Springer)
- [215] Polchinski J 1998 *String Theory* (Cambridge: Cambridge University Press)
- [216] Duff M 1995 *The Oscar Klein Centenary: Proc. Symp. (19–21 September 1994, Stockholm, Sweden)* ed U Lundstrom (Singapore: World Scientific)
- [217] Randall L and Sundrum R 1999 *Phys. Rev. Lett.* **83** 3370–3
- [218] Randall L and Sundrum R 1999 *Phys. Rev. Lett.* **83** 4690–3
- [219] Bergmann P G 1968 *Int. J. Theor. Phys.* **1** 25–36
- [220] Wagoner R V 1970 *Phys. Rev. D* **1** 3209–16
- [221] Jordan P 1959 *Z. Phys.* **157** 112–21
- [222] Fierz M 1956 *Helv. Phys. Acta* **29** 128–34
- [223] Brans C and Dicke R 1961 *Phys. Rev.* **124** 925–35
- [224] Goenner H 2012 *Gen. Relativ. Gravit.* **44** 2077–97
- [225] Brans C H 2008 *AIP Conf. Proc.* **1083** 34–46
- [226] Brans C H 2005 arXiv:gr-qc/0506063
- [227] Flanagan E E 2004 *Class. Quantum Grav.* **21** 3817
- [228] Eardley D M 1975 *Astrophys. J. Lett.* **196** L59–62
- [229] Will C 1993 *Theory and Experiment in Gravitational Physics* (Cambridge: Cambridge University Press) ISBN 9780521439732
- [230] Damour T and Esposito-Farese G 1996 *Phys. Rev. D* **53** 5541–78
- [231] Will C M and Zaglauer H W 1989 *Astrophys. J.* **346** 366
- [232] Cardoso V, Chakrabarti S, Pani P, Berti E and Gualtieri L 2011 *Phys. Rev. Lett.* **107** 241101
- [233] Mirshekari S and Will C M 2013 *Phys. Rev. D* **87** 084070
- [234] Yunes N, Pani P and Cardoso V 2012 *Phys. Rev. D* **85** 102003
- [235] Horndeski G W 1974 *Int. J. Theor. Phys.* **10** 363–84
- [236] Deffayet C, Gao X, Steer D and Zahariade G 2011 *Phys. Rev. D* **84** 064039
- [237] Carroll S M 2001 *Living Rev. Relativ.* **4** 1
- [238] Martin J 2012 *C. R. Phys.* **13** 566–665
- [239] Schmidt H J 2006 *eConf C* **0602061** 12
- [240] Teyssandier P and Tourrenc P 1983 *J. Math. Phys.* **24** 2793
- [241] Barrow J D 1988 *Nucl. Phys. B* **296** 697–709
- [242] Barrow J D and Cotsakis S 1988 *Phys. Lett. B* **214** 515–8
- [243] Wands D 1994 *Class. Quantum Grav.* **11** 269–80
- [244] O’Hanlon J 1972 *Phys. Rev. Lett.* **29** 137–8
- [245] Fiziev P 2000 *Mod. Phys. Lett. A* **15** 1977
- [246] Sotiriou T P 2006 *Class. Quantum Grav.* **23** 5117–28
- [247] Biswas T, Gerwick E, Koivisto T and Mazumdar A 2012 *Phys. Rev. Lett.* **108** 031101
- [248] Talaganis S, Biswas T and Mazumdar A 2015 *Class. Quantum Grav.* **32** 215017
- [249] Moura F and Schiappa R 2007 *Class. Quantum Grav.* **24** 361–86
- [250] Ashtekar A, Balachandran A and Jo S 1989 *Int. J. Mod. Phys. A* **4** 1493–514
- [251] Chen T j, Fasiello M, Lim E A and Tolley A J 2013 *J. Cosmol. Astropart. Phys.* **JCAP02(2013)042**
- [252] Chen T j and Lim E A 2014 *J. Cosmol. Astropart. Phys.* **JCAP05(2014)010**
- [253] Psaltis D, Perrodin D, Dienes K R and Mocioiu I 2008 *Phys. Rev. Lett.* **100** 091101
- [254] Yunes N and Sopuerta C F 2008 *Phys. Rev. D* **77** 064007
- [255] Barausse E and Sotiriou T P 2008 *Phys. Rev. Lett.* **101** 099001
- [256] Gross D J and Sloan J H 1987 *Nucl. Phys. B* **291** 41–89
- [257] Kobayashi T, Yamaguchi M and Yokoyama J 2011 *Prog. Theor. Phys.* **126** 511–29
- [258] Alexander S and Yunes N 2009 *Phys. Rep.* **480** 1–55
- [259] Grumiller D and Yunes N 2008 *Phys. Rev. D* **77** 044015

- [260] Everitt C *et al* 2011 *Phys. Rev. Lett.* **106** 221101
- [261] Canizares P, Gair J and Sopuerta C 2012 *J. Phys. Conf. Ser.* **363** 012019
- [262] Yagi K, Yunes N and Tanaka T 2012 *Phys. Rev. Lett.* **109** 251105
- [263] Shafee R, McClintock J E, Narayan R, Davis S W, Li L X and Remillard R A 2006 *Astrophys. J. Lett.* **636** L113–6
- [264] Kosteley V A 2004 *Phys. Rev. D* **69** 105009
- [265] Kosteley V A and Russell N 2011 *Rev. Mod. Phys.* **83** 11–31
- [266] Mattingly D 2005 *Living Rev. Relativ.* **8** 5
- [267] Liberati S 2013 *Class. Quantum Grav.* **30** 133001
- [268] Blas D and Lim E 2015 *Int. J. Mod. Phys. D* **23** 1443009
- [269] Colladay D and Kosteley V A 1998 *Phys. Rev. D* **58** 116002
- [270] Bailey Q G and Kosteley V A 2006 *Phys. Rev. D* **74** 045001
- [271] Kosteley V A and Tasson J D 2011 *Phys. Rev. D* **83** 016013
- [272] Shao L 2014 *Phys. Rev. Lett.* **112** 111103
- [273] Shao L 2014 *Phys. Rev. D* **90** 122009
- [274] Jacobson T and Mattingly D 2001 *Phys. Rev. D* **64** 024028
- [275] Eling C, Jacobson T and Mattingly D 2006 *Deserfest: A Celebration of the life and Works of Stanley Deser* ed J T Liu *et al* (Singapore: World Scientific)
- [276] Carroll S M and Lim E A 2004 *Phys. Rev. D* **70** 123525
- [277] Jacobson T and Mattingly D 2004 *Phys. Rev. D* **70** 024003
- [278] Elliott J W, Moore G D and Stoica H 2005 *J. High Energy Phys.* **JHEP08(2005)066**
- [279] Blas D, Pujolas O and Sibiryakov S 2010 *Phys. Rev. Lett.* **104** 181302
- [280] Jacobson T 2010 *Phys. Rev. D* **81** 101502
- [281] Barausse E and Sotiriou T P 2012 *Phys. Rev. Lett.* **109** 181101
- Barausse E and Sotiriou T P 2013 *Phys. Rev. Lett.* **110** 039902 (erratum)
- [282] Liberati S, Maccione L and Sotiriou T P 2012 *Phys. Rev. Lett.* **109** 151602
- [283] Froggatt C and Nielsen H B 1991 *Origin of Symmetries* (Singapore: World Scientific)
- [284] Groot Nibbelink S and Pospelov M 2005 *Phys. Rev. Lett.* **94** 081601
- [285] Chadha S and Nielsen H B 1983 *Nucl. Phys. B* **217** 125
- [286] Bednik G, Pujolàs O and Sibiryakov S 2013 *J. High Energy Phys.* **JHEP11(2013)064**
- [287] Pospelov M and Shang Y 2012 *Phys. Rev. D* **85** 105001
- [288] Papazoglou A and Sotiriou T P 2010 *Phys. Lett. B* **685** 197–200
- [289] Kimpton I and Padilla A 2010 *J. High Energy Phys.* **JHEP07(2010)014**
- [290] Blas D, Pujolas O and Sibiryakov S 2010 *Phys. Lett. B* **688** 350–5
- [291] Herdeiro C and Hirano S 2012 *J. Cosmol. Astropart. Phys.* **JCAP05(2012)031**
- [292] Arnowitt R L, Deser S and Misner C W 1960 *Phys. Rev.* **117** 1595–602
- [293] Coelho F S, Herdeiro C, Hirano S and Sato Y 2012 *Phys. Rev. D* **86** 064009
- [294] Alcubierre M 2008 *Introduction to 3 + 1 Numerical Relativity* (Oxford: Oxford University Press)
- [295] Pauli W and Fierz M 1939 *Helv. Phys. Acta* **12** 297–300
- [296] Boulware D and Deser S 1972 *Phys. Rev. D* **6** 3368–82
- [297] de Rham C and Gabadadze G 2010 *Phys. Rev. D* **82** 044020
- [298] de Rham C, Gabadadze G and Tolley A J 2011 *Phys. Rev. Lett.* **106** 231101
- [299] Groot Nibbelink S, Peloso M and Sexton M 2007 *Eur. Phys. J. C* **51** 741–52
- [300] Hinterbichler K and Rosen R A 2012 *J. High Energy Phys.* **JHEP07(2012)047**
- [301] Hassan S, Rosen R A and Schmidt-May A 2012 *J. High Energy Phys.* **JHEP02(2012)026**
- [302] Hassan S and Rosen R A 2012 *Phys. Rev. Lett.* **108** 041101
- [303] Bernard L, Deffayet C and von Strauss M 2015 *Phys. Rev. D* **91** 104013
- [304] Hassan S and Rosen R 2012 *J. High Energy Phys.* **JHEP02(2012)126**
- [305] Nicolis A, Rattazzi R and Trincherini E 2009 *Phys. Rev. D* **79** 064036
- [306] van Dam H and Veltman M 1970 *Nucl. Phys. B* **22** 397–411
- [307] Zakharov V 1970 *JETP Lett.* **12** 312
- [308] Vainshtein A 1972 *Phys. Lett. B* **39** 393–4
- [309] Babichev E and Deffayet C 2013 *Class. Quantum Grav.* **30** 184001
- [310] de Rham C, Matas A and Tolley A J 2013 *Phys. Rev. D* **87** 064024
- [311] Chow N and Khoury J 2009 *Phys. Rev. D* **80** 024037
- [312] de Rham C and Heisenberg L 2011 *Phys. Rev. D* **84** 043503
- [313] Li B *et al* 2013 *J. Cosmol. Astropart. Phys.* **JCAP11(2013)012**
- [314] Li B, Zhao G B and Koyama K 2013 *J. Cosmol. Astropart. Phys.* **JCAP05(2013)023**

- [315] Hiramatsu T, Hu W, Koyama K and Schmidt F 2013 *Phys. Rev. D* **87** 063525
- [316] Falck B, Koyama K, Zhao G b and Li B 2014 *J. Cosmol. Astropart. Phys.* JCAP07(2014)058
- [317] Falck B, Koyama K and Zhao G b 2015 *J. Cosmol. Astropart. Phys.* JCAP07(2015)049
- [318] Nicolis A and Rattazzi R 2004 *J. High Energy Phys.* JHEP06(2004)059
- [319] Brito R, Terrana A, Johnson M and Cardoso V 2014 *Phys. Rev. D* **90** 124035
- [320] Jaccard M, Maggiore M and Mitsou E 2013 *Phys. Rev. D* **88** 044033
- [321] Maggiore M 2014 *Phys. Rev. D* **89** 043008
- [322] Dvali G, Gruzinov A and Zaldarriaga M 2003 *Phys. Rev. D* **68** 024012
- [323] Lue A and Starkman G 2003 *Phys. Rev. D* **67** 064002
- [324] Tseytlin A A 1999 *The Many Faces of the Superworld* ed M A Shifman (Singapore: World Scientific)
- [325] Deser S and Gibbons G 1998 *Class. Quantum Grav.* **15** L35–39
- [326] Vollick D N 2004 *Phys. Rev. D* **69** 064030
- [327] Olmo G J, Rubiera-Garcia D and Sanchis-Alepuz H 2014 *Eur. Phys. J. C* **74** 2804
- [328] Barragan C, Olmo G J and Sanchis-Alepuz H 2009 *Phys. Rev. D* **80** 024016
- [329] Delsate T and Steinhoff J 2012 *Phys. Rev. Lett.* **109** 021101
- [330] Barausse E, Sotiriou T P and Miller J C 2008 *EAS Publ. Ser.* **30** 189–92
- [331] Sotiriou T P 2008 *Phys. Lett. B* **664** 225–8
- [332] Kim H C 2014 *Phys. Rev. D* **89** 064001
- [333] Flanagan E E 2004 *Phys. Rev. Lett.* **92** 071101
- [334] Vollick D N 2004 *Class. Quantum Grav.* **21** 3813–6
- [335] Li B, Mota D F and Shaw D J 2008 *Phys. Rev. D* **78** 064018
- [336] Goldberger W D 2007 *Particle Physics and Cosmology: The Fabric of Spacetime (31 July to 25 August 2006)* ed F Bernardeau *et al* (Elsevier)
- [337] Donoghue J F 2012 *AIP Conf. Proc.* **1483** 73–94
- [338] Polchinski J 2007 *The Quantum Structure of Space and Time* ed D Gross *et al* (Singapore: Elsevier)
- [339] Burgess C 2015 *Post-Planck Cosmology* ed C Deffayet *et al* (Oxford: Oxford University Press)
- [340] DeWitt B S 1967 *Phys. Rev.* **160** 1113–48
- [341] DeWitt B S 1967 *Phys. Rev.* **162** 1195–239
- [342] DeWitt B S 1967 *Phys. Rev.* **162** 1239–56
- [343] Dunbar D C and Norridge P S 1995 *Nucl. Phys. B* **433** 181–208
- [344] Weinberg S 1965 *Phys. Rev.* **140** B516–24
- [345] Donoghue J F and Torma T 1999 *Phys. Rev. D* **60** 024003
- [346] Weinberg S 1979 *Physica A* **96** 327
- [347] Burgess C 2012 *Proc. Foundations of Space and Time: Reflections on Quantum Gravity* ed J Murugan, A Weltman and G F R Ellis (Cambridge: Cambridge University Press) pp 50–68
- [348] Burgess C and Williams M 2014 *J. High Energy Phys.* JHEP08(2014)074
- [349] Clifton T, Dunsby P, Goswami R and Nzioki A M 2013 *Phys. Rev. D* **87** 063517
- [350] Clifton T and Dunsby P K 2015 *Phys. Rev. D* **91** 103528
- [351] Mannheim P D and Kazanas D 1989 *Astrophys. J.* **342** 635–8
- [352] Varieschi G U 2014 *Gen. Relativ. Gravit.* **46** 1741
- [353] Visser M 2009 *Phys. Rev. D* **80** 025011
- [354] D’Amico G *et al* 2011 *Phys. Rev. D* **84** 124046
- [355] Gratia P, Hu W and Wyman M 2012 *Phys. Rev. D* **86** 061504
- [356] Fasiello M and Tolley A J 2013 *J. Cosmol. Astropart. Phys.* JCAP12(2013)002
- [357] De Felice A, Gümrukçüoğlu A E, Mukohyama S, Tanahashi N and Tanaka T 2014 *J. Cosmol. Astropart. Phys.* JCAP06(2014)037
- [358] D’Amico G, Gabadadze G, Hui L and Pirtskhalava D 2013 *Phys. Rev. D* **87** 064037
- [359] De Felice A and Mukohyama S 2014 *Phys. Lett. B* **728** 622–5
- [360] Sotiriou T P and Liberati S 2007 *Ann. Phys.* **322** 935–66
- [361] Bekenstein J D 1997 *Proc. Second International A. D. Sakharov Conf. on Physics (Moscow, Russia; 20–24 May 1996)* ed I M Dremin and A M Semikhatov (Singapore: World Scientific)
- [362] Carter B 1999 *Proc. 8th Marcel Grossmann Meeting (Jerusalem, Israel; 22–27 June 1997)* ed T Piran (Singapore: World Scientific) pp 136–155
- [363] Chrusciel P T, Costa J L and Heusler M 2012 *Living Rev. Relativ.* **15** 7
- [364] Robinson D 2009 *Four Decades of Black Holes Uniqueness Theorems* (Cambridge: Cambridge University Press)

- [365] Gibbons G W 1975 *Commun. Math. Phys.* **44** 245–64
- [366] Goldreich P and Julian W H 1969 *Astrophys. J.* **157** 869
- [367] Ruderman M A and Sutherland P G 1975 *Astrophys. J.* **196** 51–72
- [368] Blandford R D and Znajek R L 1977 *Mon. Not. R. Astron. Soc.* **179** 433–56
- [369] Kerr R P 1963 *Phys. Rev. Lett.* **11** 237–8
- [370] Rhoades Clifford E J and Ruffini R J 1974 *Phys. Rev. Lett.* **32** 324–7
- [371] Teukolsky S A 2015 *Class. Quantum Grav.* **32** 124006
- [372] Shapiro S and Teukolsky S 1983 *Black Holes, White Dwarfs, and Neutron Stars: The Physics of Compact Objects* (New York: Wiley)
- [373] Chandrasekhar S 1983 *The Mathematical Theory of Black Holes* (New York: Oxford University Press)
- [374] Frolov V P and Novikov I D 1998 *Black Hole Physics: Basic Concepts and New Developments* (Dordrecht: Kluwer Academic) p 770
- [375] Teukolsky S A 1972 *Phys. Rev. Lett.* **29** 1114–8
- [376] Teukolsky S A 1973 *Astrophys. J.* **185** 635–47
- [377] Press W H and Teukolsky S A 1973 *Astrophys. J.* **185** 649–74
- [378] Teukolsky S A and Press W H 1974 *Astrophys. J.* **193** 443–61
- [379] Whiting B F 1989 *J. Math. Phys.* **30** 1301
- [380] Press W H 1971 *Astrophys. J.* **170** L105
- [381] Leaver E W 1985 *Proc. R. Soc. A* **402** 285–98
- [382] Kokkotas K D and Schmidt B G 1999 *Living Rev. Relativ.* **2** 2
- [383] Nollert H P 1999 *Class. Quantum Grav.* **16** R159–216
- [384] Berti E, Cardoso V and Starinets A O 2009 *Class. Quantum Grav.* **26** 163001
- [385] Konoplya R and Zhidenko A 2011 *Rev. Mod. Phys.* **83** 793–836
- [386] Kay B S and Wald R M 1987 *Class. Quantum Grav.* **4** 893–8
- [387] Dafermos M and Rodnianski I 2013 *Clay Math. Proc.* **17** 97–205
- [388] Dafermos M and Rodnianski I 2010 *XVIth International Congress on Mathematical Physics* ed P Exner (Singapore: World Scientific) pp 421–433
- [389] Dafermos M and Rodnianski I 2010 arXiv:1010.5132
- [390] Dafermos M, Rodnianski I and Shlapentokh-Rothman Y 2014 arXiv:1402.7034
- [391] Dafermos M, Rodnianski I and Shlapentokh-Rothman Y 2014 arXiv:1412.8379
- [392] Aretakis S 2015 *Adv. Theor. Math. Phys.* **19** 507–30
- [393] Lucietti J and Reall H S 2012 *Phys. Rev. D* **86** 104030
- [394] Yang H *et al* 2013 *Phys. Rev. D* **87** 041502
- [395] Yang H *et al* 2013 *Phys. Rev. D* **88** 044047
- [396] Cook G B and Zalutsky M 2014 *Phys. Rev. D* **90** 124021
- [397] Thorne K S and Dykla J J 1971 *Astrophys. J. Lett.* **166** L35
- [398] Chase J 1970 *Commun. Math. Phys.* **19** 276–88
- [399] Bekenstein J 1995 *Phys. Rev. D* **51** 6608–11
- [400] Zel'dovich Y B 1971 *Pis'ma Zh. Eksp. Teor. Fiz.* **14** 270
- [401] Zel'dovich Y B 1972 *Zh. Eksp. Teor. Fiz.* **62** 2076
- [402] Press W H and Teukolsky S A 1972 *Nature* **238** 211–2
- [403] Witek H, Cardoso V, Ishibashi A and Sperhake U 2013 *Phys. Rev. D* **87** 043513
- [404] Okawa H, Witek H and Cardoso V 2014 *Phys. Rev. D* **89** 104032
- [405] Brito R, Cardoso V and Pani P 2015 *Class. Quantum Grav.* **32** 134001
- [406] Pena I and Sudarsky D 1997 *Class. Quantum Grav.* **14** 3131–4
- [407] Hod S 2012 *Phys. Rev. D* **86** 104026
Hod S 2012 *Phys. Rev. D* **86** 129902
- [408] Hod S 2013 *Eur. Phys. J. C* **73** 2378
- [409] Benone C L, Crispino L C, Herdeiro C and Radu E 2014 *Phys. Rev. D* **90** 104024
- [410] Herdeiro C, Radu E and Runarsson H 2014 *Phys. Lett. B* **739** 302–7
- [411] Herdeiro C A R and Radu E 2014 *Int. J. Mod. Phys. D* **23** 1442014
- [412] Yoshida S and Eriguchi Y 1997 *Phys. Rev. D* **56** 762–71
- [413] Kleihaus B, Kunz J and List M 2005 *Phys. Rev. D* **72** 064002
- [414] Ryan F D 1997 *Phys. Rev. D* **55** 6081–91
- [415] Herdeiro C and Radu E 2014 *Phys. Rev. D* **89** 124018
- [416] Webpages with numerical data and Mathematica notebooks: <http://www.phy.olemiss.edu/~berti/research> <http://centra.tecnico.ulisboa.pt/network/grit/files/>

- [417] Cardoso V, Carucci I P, Pani P and Sotiriou T P 2013 *Phys. Rev. Lett.* **111** 111101
- [418] Cardoso V, Carucci I P, Pani P and Sotiriou T P 2013 *Phys. Rev. D* **88** 044056
- [419] Davis A C, Gregory R, Jha R and Muir J 2014 *J. Cosmol. Astropart. Phys.* **JCAP08(2014)033**
- [420] Brax P, Davis A C, Li B and Winther H A 2012 *Phys. Rev. D* **86** 044015
- [421] Maselli A, Cardoso V, Ferrari V, Gualtieri L and Pani P 2013 *Phys. Rev. D* **88** 023007
- [422] Cardoso V, Miranda A S, Berti E, Witek H and Zanchin V T 2009 *Phys. Rev. D* **79** 064016
- [423] Geroch R P 1970 *J. Math. Phys.* **11** 2580–8
- [424] Hansen R 1974 *J. Math. Phys.* **15** 46–52
- [425] Hoenselaers C and Perjes Z 1990 *Class. Quantum Grav.* **7** 1819–25
- [426] Sotiriou T P and Apostolatos T A 2004 *Class. Quantum Grav.* **21** 5727–33
- [427] Torii T, Yajima H and Maeda K i 1997 *Phys. Rev. D* **55** 739–53
- [428] Ryan F D 1995 *Phys. Rev. D* **52** 5707–18
- [429] Feroci M *et al* 2012 *Exp. Astron.* **34** 415
- [430] Pappas G 2012 *Mon. Not. R. Astron. Soc.* **422** 2581–9
- [431] Kanti P, Mavromatos N E, Rizos J, Tamvakis K and Winstanley E 1998 *Phys. Rev. D* **57** 6255–64
- [432] Bambi C and Barausse E 2011 *Astrophys. J.* **731** 121
- [433] Seoane P A *et al* (eLISA Collaboration) 2013 arXiv:1305.5720
- [434] Berglund P, Bhattacharyya J and Mattingly D 2012 *Phys. Rev. D* **85** 124019
- [435] Cropp B, Liberati S, Mohd A and Visser M 2014 *Phys. Rev. D* **89** 064061
- [436] Gravity group, CENTRA/IST, Lisbon: <http://blackholes.ist.utl.pt/?page=Files>
- [437] Eddington A S 1954 *The Mathematical Theory of Relativity* (Cambridge: Cambridge University Press)
- [438] Will C M and Nordtvedt Kenneth J 1972 *Astrophys. J.* **177** 757
- [439] Nordtvedt K J and Will C M 1972 *Astrophys. J.* **177** 775–92
- [440] Cardoso V, Pani P and Rico J 2014 *Phys. Rev. D* **89** 064007
- [441] Rico J 2013 *The Kerr black hole hypothesis: a review of methods and results* Master's Thesis Instituto Superior Técnico (http://blackholes.ist.utl.pt/fp-content/attachs/thesis_joaoorico.pdf)
- [442] Collins N A and Hughes S A 2004 *Phys. Rev. D* **69** 124022
- [443] Vigeland S J and Hughes S A 2010 *Phys. Rev. D* **81** 024030
- [444] Gair J and Yunes N 2011 *Phys. Rev. D* **84** 064016
- [445] Vigeland S, Yunes N and Stein L 2011 *Phys. Rev. D* **83** 104027
- [446] Glampedakis K and Babak S 2006 *Class. Quantum Grav.* **23** 4167–88
- [447] Manko V S and Novikov I D 1992 *Class. Quantum Grav.* **9** 2477–87
- [448] Gair J R, Li C and Mandel I 2008 *Phys. Rev. D* **77** 024035
- [449] Newman E and Janis A 1965 *J. Math. Phys.* **6** 915–7
- [450] Johannsen T and Psaltis D 2011 *Phys. Rev. D* **83** 124015
- [451] Hansen D and Yunes N 2013 *Phys. Rev. D* **88** 104020
- [452] Bambi C 2014 *Phys. Rev. D* **90** 047503
- [453] Bambi C 2015 *Class. Quantum Grav.* **32** 065005
- [454] Rezzolla L and Zhidenko A 2014 *Phys. Rev. D* **90** 084009
- [455] Broderick A E and Narayan R 2006 *Astrophys. J. Lett.* **638** L21–24
- [456] Liebling S L and Palenzuela C 2012 *Living Rev. Relativ.* **15** 6
- [457] Macedo C F, Pani P, Cardoso V and Crispino L C 2013 *Astrophys. J.* **774** 48
- [458] Mazur P O and Mottola E 2001 arXiv:gr-qc/0109035
- [459] Gimon E G and Horava P 2009 *Phys. Lett. B* **672** 299–302
- [460] Berti E, Cardoso V and Will C M 2006 *Phys. Rev. D* **73** 064030
- [461] Berti E and Cardoso V 2006 *Int. J. Mod. Phys. D* **15** 2209–16
- [462] Kesden M, Gair J and Kamionkowski M 2005 *Phys. Rev. D* **71** 044015
- [463] Pani P, Berti E, Cardoso V, Chen Y and Norte R 2009 *Phys. Rev. D* **80** 124047
- [464] Barausse E, Cardoso V and Pani P 2014 *Phys. Rev. D* **89** 104059
- [465] Friedman J L 1978 *Commun. Math. Phys.* **63** 243–55
- [466] Schutz B F and Comins N 1978 *MNRAS* **182** 69–76
- [467] Cardoso V, Crispino L C B, Macedo C F B, Okawa H and Pani P 2014 *Phys. Rev. D* **90** 044069
- [468] Cardoso V, Pani P, Cadoni M and Cavaglia M 2008 *Phys. Rev. D* **77** 124044
- [469] Chirenti C B and Rezzolla L 2008 *Phys. Rev. D* **78** 084011
- [470] Cardoso V, Pani P, Cadoni M and Cavaglia M 2008 *Class. Quantum Grav.* **25** 195010
- [471] Pani P, Barausse E, Berti E and Cardoso V 2010 *Phys. Rev. D* **82** 044009

- [472] Keir J 2014 arXiv:1404.7036
- [473] Johannsen T 2013 *Astrophys. J.* **777** 170
- [474] Lu R S *et al* 2014 *Astrophys. J.* **788** 120
- [475] Eisenhauer F *et al* 2008 GRAVITY: getting to the event horizon of Sgr A* *Proc. SPIE* **7013** 2A
- [476] Gundlach C and Martin-Garcia J M 2007 *Living Rev. Relativ.* **10** 5
- [477] Bizon P and Rostworowski A 2011 *Phys. Rev. Lett.* **107** 031102
- [478] Dias O J, Horowitz G T and Santos J E 2012 *Class. Quantum Grav.* **29** 194002
- [479] Buchel A, Lehner L and Liebling S L 2012 *Phys. Rev. D* **86** 123011
- [480] Bizoń P and Jalmuzna J 2013 *Phys. Rev. Lett.* **111** 041102
- [481] Buchel A, Liebling S L and Lehner L 2013 *Phys. Rev. D* **87** 123006
- [482] Dias O J, Horowitz G T, Marolf D and Santos J E 2012 *Class. Quantum Grav.* **29** 235019
- [483] Maliborski M and Rostworowski A 2013 *Phys. Rev. Lett.* **111** 051102
- [484] Seidel E and Suen W M 1991 *Phys. Rev. Lett.* **66** 1659–62
- [485] Seidel E and Suen W M 1994 *Phys. Rev. Lett.* **72** 2516–9
- [486] Page D N 2004 *Phys. Rev. D* **70** 023002
- [487] Cardoso V and Yoshida S 2005 *J. High Energy Phys.* JHEP07(2005)099
- [488] Dolan S R 2007 *Phys. Rev. D* **76** 084001
- [489] Pani P, Cardoso V, Gualtieri L, Berti E and Ishibashi A 2012 *Phys. Rev. Lett.* **109** 131102
- [490] Pani P, Cardoso V, Gualtieri L, Berti E and Ishibashi A 2012 *Phys. Rev. D* **86** 104017
- [491] Choptuik M W 1993 *Phys. Rev. Lett.* **70** 9–12
- [492] Brady P R, Chambers C M and Goncalves S M 1997 *Phys. Rev. D* **56** 6057–61
- [493] Okawa H, Cardoso V and Pani P 2014 *Phys. Rev. D* **89** 041502
- [494] Grandclement P, Fodor G and Forgacs P 2011 *Phys. Rev. D* **84** 065037
- [495] Okawa H, Cardoso V and Pani P 2014 *Phys. Rev. D* **90** 104032
- [496] Brito R, Cardoso V and Pani P 2015 *Superradiance* (Berlin: Springer)
- [497] Rosa J G and Dolan S R 2012 *Phys. Rev. D* **85** 044043
- [498] Arvanitaki A, Dimopoulos S, Dubovsky S, Kaloper N and March-Russell J 2010 *Phys. Rev. D* **81** 123530
- [499] Peccei R D and Quinn H R 1977 *Phys. Rev. Lett.* **38** 1440–3
- [500] McClintock J E and Remillard R A 2009 arXiv:0902.3488
- [501] Reynolds C S 2014 *Space Sci. Rev.* **183** 277–94
- [502] Amaro-Seoane P *et al* 2013 *GW Notes* **6** 4–110
- [503] Olive K *et al* (Particle Data Group) 2014 *Chin. Phys. C* **38** 090001
- [504] Arvanitaki A and Dubovsky S 2011 *Phys. Rev. D* **83** 044026
- [505] Arvanitaki A, Baryakhtar M and Huang X 2015 *Phys. Rev. D* **91** 084011
- [506] Kodama H and Yoshino H 2012 *Int. J. Mod. Phys. Conf. Ser.* **7** 84–115
- [507] Brenneman L *et al* 2011 *Astrophys. J.* **736** 103
- [508] East W E, Ramazanoğlu F M and Pretorius F 2014 *Phys. Rev. D* **89** 061503
- [509] Aasi J *et al* (LIGO Scientific Collaboration, Virgo Collaboration) 2013 arXiv:1304.0670
- [510] Rosa J G 2013 *J. High Energy Phys.* JHEP02(2013)014 arXiv:1209.4211
- [511] Rosa J G 2015 *Phys. Lett. B* **749** 226–30
- [512] Yoshino H and Kodama H 2012 *Prog. Theor. Phys.* **128** 153–90
- [513] Lattimer J and Prakash M 2004 *Science* **304** 536–42
- [514] Lattimer J M and Prakash M 2007 *Phys. Rep.* **442** 109–65
- [515] Özel F, Baym G and Guver T 2010 *Phys. Rev. D* **82** 101301
- [516] Steiner A W, Lattimer J M and Brown E F 2010 *Astrophys. J.* **722** 33–54
- [517] Steiner A W, Lattimer J M and Brown E F 2013 *Astrophys. J.* **765** L5
- [518] Hebeler K, Lattimer J, Pethick C and Schwenk A 2013 *Astrophys. J.* **773** 11
- [519] Psaltis D, Özel F and Chakrabarty D 2014 *Astrophys. J.* **787** 136
- [520] Stergioulas N 2003 *Living Rev. Relativ.* **6** 3
- [521] Friedman J L and Stergioulas N 2013 *Rotating Relativistic Stars* (Cambridge: Cambridge University Press)
- [522] Hartle J B 1967 *Astrophys. J.* **150** 1005–29
- [523] Hartle J B and Thorne K S 1968 *Astrophys. J.* **153** 807
- [524] Berti E, White F, Maniopolou A and Bruni M 2005 *Mon. Not. R. Astron. Soc.* **358** 923–38
- [525] Benhar O, Ferrari V, Gualtieri L and Marassi S 2005 *Phys. Rev. D* **72** 044028
- [526] Unno W, Osaki Y, Ando H, Saio H and Shibahashi H 1989 *Nonradial Oscillations of Stars* (Tokyo: University of Tokyo Press)

- [527] Ferrari V and Gualtieri L 2008 *Gen. Relativ. Gravit.* **40** 945–70
- [528] Andersson N *et al* 2011 *Gen. Relativ. Gravit.* **43** 409–36
- [529] Andersson N and Kokkotas K D 1998 *Mon. Not. R. Astron. Soc.* **299** 1059–68
- [530] Benhar O, Ferrari V and Gualtieri L 2004 *Phys. Rev. D* **70** 124015
- [531] Chandrasekhar S 1970 *Phys. Rev. Lett.* **24** 611–5
- [532] Friedman J and Schutz B F 1978 *Astrophys. J.* **222** 281
- [533] Andersson N and Kokkotas K D 2001 *Int. J. Mod. Phys. D* **10** 381–442
- [534] Andersson N and Comer G 2007 *Living Rev. Relativ.* **10** 1
- [535] Horbatsch M and Burgess C 2011 *J. Cosmol. Astropart. Phys.* JCAP08(2011)027
- [536] Stefanov I Z, Yazadjiev S S and Todorov M D 2008 *Mod. Phys. Lett. A* **23** 2915
- [537] Doneva D D, Yazadjiev S S, Kokkotas K D and Stefanov I Z 2010 *Phys. Rev. D* **82** 064030
- [538] Damour T and Esposito-Farese G 1998 *Phys. Rev. D* **58** 042001
- [539] Silva H O, Macedo C F B, Berti E and Crispino L C B 2015 *Class. Quantum Grav.* **32** 145008
- [540] Barausse E, Palenzuela C, Ponce M and Lehner L 2013 *Phys. Rev. D* **87** 081506
- [541] Palenzuela C, Barausse E, Ponce M and Lehner L 2014 *Phys. Rev. D* **89** 044024
- [542] Shibata M, Taniguchi K, Okawa H and Buonanno A 2014 *Phys. Rev. D* **89** 084005
- [543] Taniguchi K, Shibata M and Buonanno A 2015 *Phys. Rev. D* **91** 024033
- [544] Frolov A V 2008 *Phys. Rev. Lett.* **101** 061103
- [545] Khoury J and Weltman A 2004 *Phys. Rev. Lett.* **93** 171104
- [546] Gubser S S and Khoury J 2004 *Phys. Rev. D* **70** 104001
- [547] Starobinsky A A 2007 *JETP Lett.* **86** 157–63
- [548] Hu W and Sawicki I 2007 *Phys. Rev. D* **76** 064004
- [549] Yagi K, Stein L C, Yunes N and Tanaka T 2012 *Phys. Rev. D* **85** 064022
- [550] Demorest P, Pennucci T, Ransom S, Roberts M and Hessels J 2010 *Nature* **467** 1081–3
- [551] Antoniadis J *et al* 2013 *Science* **340** 6131
- [552] Lattimer J M and Schutz B F 2005 *Astrophys. J.* **629** 979–84
- [553] Diaz-Alonso J and Ibañez Cabanell J 1985 *Astrophys. J.* **291** 308–18
- [554] Haensel P and Potekhin A Y 2004 *Astron. Astrophys.* **428** 191–7
- [555] Akmal A, Pandharipande V and Ravenhall D 1998 *Phys. Rev. C* **58** 1804–28
- [556] Douchin F and Haensel P 2001 *Astron. Astrophys.* **380** 151–67
- [557] Shen H, Toki H, Oyamatsu K and Sumiyoshi K 1998 *Nucl. Phys. A* **637** 435–50
- [558] Shen H, Toki H, Oyamatsu K and Sumiyoshi K 1998 *Prog. Theor. Phys.* **100** 1013
- [559] Lattimer J M and Swesty F D 1991 *Nucl. Phys. A* **535** 331–76
- [560] Damour T, Kogan I I and Papazoglou A 2003 *Phys. Rev. D* **67** 064009
- [561] Babichev E, Deffayet C and Ziour R 2009 *Phys. Rev. Lett.* **103** 201102
- [562] Read J S, Lackey B D, Owen B J and Friedman J L 2009 *Phys. Rev. D* **79** 124032
- [563] Avelino P 2012 *Phys. Rev. D* **85** 104053
- [564] Harko T, Lobo F S N, Mak M and Sushkov S V 2015 *Mod. Phys. Lett.* **A30** 1550190
- [565] Stairs I H 2003 *Living Rev. Relativ.* **6** 5
- [566] Benhar O, Berti E and Ferrari V 1999 *Mon. Not. R. Astron. Soc.* **310** 797–803
- [567] Tsui L and Leung P 2005 *Mon. Not. R. Astron. Soc.* **357** 1029–37
- [568] Gaertig E and Kokkotas K D 2011 *Phys. Rev. D* **83** 064031
- [569] Doneva D D, Gaertig E, Kokkotas K D and Krüger C 2013 *Phys. Rev. D* **88** 044052
- [570] Lau H, Leung P and Lin L 2010 *Astrophys. J.* **714** 1234–8
- [571] Ravenhall D G and Pethick C J 1994 *Astrophys. J.* **424** 846–51
- [572] Lattimer J and Prakash M 2001 *Astrophys. J.* **550** 426
- [573] Bejger M and Haensel P 2002 *Astron. Astrophys.* **396** 917
- [574] Urbanec M, Miller J C and Stuchlík Z 2013 *Mon. Not. R. Astron. Soc.* **433** 1903–9
- [575] Lattimer J M and Yahil A 1989 *Astrophys. J.* **340** 426–34
- [576] Prakash M *et al* 1997 *Phys. Rep.* **280** 1–77
- [577] Haensel P, Zdunik J, Bejger M and Lattimer J 2009 *Astron. Astrophys.* **502** 605–10
- [578] Pandharipande V R and Smith R A 1975 *Nucl. Phys. A* **237** 507–32
- [579] Prakash M, Cooke J and Lattimer J 1995 *Phys. Rev. D* **52** 661–5
- [580] Lattimer J M and Lim Y 2013 *Astrophys. J.* **771** 51
- [581] Haskell B, Ciolfi R, Pannarale F and Rezzolla L 2014 *Mon. Not. R. Astron. Soc.* **438** L71–75
- [582] Doneva D D, Yazadjiev S S, Stergioulas N and Kokkotas K D 2013 *Astrophys. J.* **781** L6
- [583] Stergioulas N and Friedman J 1995 *Astrophys. J.* **444** 306
- [584] Chakrabarti S, Delsate T, Gürlebeck N and Steinhoff J 2014 *Phys. Rev. Lett.* **112** 201102

- [585] Martinon G, Maselli A, Gualtieri L and Ferrari V 2014 *Phys. Rev. D* **90** 064026
- [586] Stein L C, Yagi K and Yunes N 2014 *Astrophys. J.* **788** 15
- [587] Lai D, Rasio F A and Shapiro S L 1993 *Astrophys. J. Suppl.* **88** 205–52
- [588] Chatziioannou K, Yagi K and Yunes N 2014 *Phys. Rev. D* **90** 064030
- [589] Seidov Z F and Kuzakhmedov R K 1978 *Sov. Astron.* **22** 711
- [590] Yagi K, Stein L C, Pappas G, Yunes N and Apostolatos T A 2014 *Phys. Rev. D* **90** 063010
- [591] Psaltis D and Özel F 2014 *Astrophys. J.* **792** 87
- [592] Bauböck M, Berti E, Psaltis D and Özel F 2013 *Astrophys. J.* **777** 68
- [593] Gendreau K C, Arzoumanian Z and Okajima T 2012 The Neutron Star Interior Composition Explorer (NICER): an explorer mission of opportunity for soft x-ray timing spectroscopy *Society of Photo-Optical Instrumentation Engineers (SPIE) Conf. Series* **vol 8443**
- [594] Ray P S, Feroci M, den Herder J, Bozzo E, Stella L LOFT Collaboration 2012 The Large Observatory for X-ray Timing (LOFT): an ESA M-class mission concept *American Astronomical Society Meeting Abstracts* vol 219 p 249.06
- [595] Lo K H, Coleman Miller M, Bhattacharyya S and Lamb F K 2013 *Astrophys. J.* **776** 19
- [596] Jackiw R and Pi S Y 2003 *Phys. Rev. D* **68** 104012
- [597] Sham Y H, Lin L M and Leung P 2014 *Astrophys. J.* **781** 66
- [598] Pappas G and Sotiriou T P 2015 *Phys. Rev. D* **91** 044011
- [599] Damour T and Nagar A 2009 *Phys. Rev. D* **80** 084035
- [600] Postnikov S, Prakash M and Lattimer J M 2010 *Phys. Rev. D* **82** 024016
- [601] Hinderer T, Lackey B D, Lang R N and Read J S 2010 *Phys. Rev. D* **81** 123016
- [602] Kramer M and Wex N 2009 *Class. Quantum Grav.* **26** 073001
- [603] Özel F, Guver T and Psaltis D 2009 *Astrophys. J.* **693** 1775–9
- [604] Özel F, Gould A and Guver T 2012 *Astrophys. J.* **748** 5
- [605] Guver T, Özel F, Cabrera-Lavers A and Wroblewski P 2010 *Astrophys. J.* **712** 964–73
- [606] Guver T, Wroblewski P, Camarota L and Özel F 2010 *Astrophys. J.* **719** 1807
- [607] Guver T and Özel F 2013 *Astrophys. J.* **765** L1
- [608] Suleimanov V, Poutanen J and Werner K 2011 *Astron. Astrophys.* **527** A139
- [609] Zamfir M, Cumming A and Galloway D K 2012 *Astrophys. J.* **749** 69
- [610] Becker W *et al* 2003 *Astrophys. J.* **594** 798–811
- [611] Gendre B, Barret D and Webb N A 2003 *Astron. Astrophys.* **403** L11–14
- [612] Guillot S, Rutledge R E and Brown E F 2011 *Astrophys. J.* **732** 88
- [613] Gendre B, Barret D and Webb N A 2003 *Astron. Astrophys.* **400** 521–32
- [614] Catuneanu A, Heinke C O, Sivakoff G R, Ho W C and Servillat M 2013 *Astrophys. J.* **764** 145
- [615] Servillat M, Heinke C O, Ho W C G, Grindlay J E, Hong J, van den Berg M and Bogdanov S 2012 *Mon. Not. R. Astron. Soc.* **423** 1556–61
- [616] Rutledge R E, Bildsten L, Brown E F, Pavlov G G and Zavlin V E 2002 *Astrophys. J.* **578** 405–12
- [617] Guillot S, Rutledge R E, Bildsten L, Brown E F, Pavlov G G and Zavlin V E 2009 *Mon. Not. R. Astron. Soc.* **392** 665–81
- [618] Walter F M, Wolk S J and Neuhäuser R 1996 *Nature* **379** 233–5
- [619] Walter F *et al* 2010 *Astrophys. J.* **724** 669–77
- [620] Pons J A *et al* 2002 *Astrophys. J.* **564** 981–1006
- [621] Heinke C O, Rybicki G B, Narayan R and Grindlay J E 2006 *Astrophys. J.* **644** 1090–103
- [622] Webb N A and Barret D 2007 *Astrophys. J.* **671** 727–33
- [623] Burwitz V, Haberl F, Neuhäuser R, Predehl P, Trümper J and Zavlin V E 2003 *Astron. Astrophys.* **399** 1109–14
- [624] Ho W C G, Kaplan D L, Chang P, van Adelsberg M and Potekhin A Y 2007 *Mon. Not. R. Astron. Soc.* **375** 821–30
- [625] Lattimer J M and Steiner A W 2014 *Astrophys. J.* **784** 123
- [626] Binnington T and Poisson E 2009 *Phys. Rev. D* **80** 084018
- [627] Landry P and Poisson E 2014 *Phys. Rev. D* **89** 124011
- [628] Yagi K 2014 *Phys. Rev. D* **89** 043011
- [629] Sathyaprakash B, Schutz B and Van Den Broeck C 2010 *Class. Quantum Grav.* **27** 215006
- [630] Punturo M *et al* 2010 *Class. Quantum Grav.* **27** 194002
- [631] Sathyaprakash B *et al* 2012 *Class. Quantum Grav.* **29** 124013
- [632] Van Den Broeck C 2014 *J. Phys.: Conf. Ser.* **484** 012008
- [633] Chan T, Sham Y H, Leung P and Lin L M 2014 *Phys. Rev. D* **90** 124023

- [634] Carriere J, Horowitz C and Piekarewicz J 2003 *Astrophys. J.* **593** 463–71
- [635] Foster B Z 2007 *Phys. Rev. D* **76** 084033
- [636] Ganguly A, Gannouji R, Goswami R and Ray S 2014 *Phys. Rev. D* **89** 064019
- [637] Psaltis D and Johannsen T 2012 *Astrophys. J.* **745** 1
- [638] Baubock M, Psaltis D, Ozel F and Johannsen T 2012 *Astrophys. J.* **753** 175
- [639] Blanchet L 2014 *Living Rev. Relativ.* **17** 2
- [640] Damour T 2014 *Frontiers in Relativistic Celestial Mechanics* ed S Kopeikin vol 1
- [641] Buonanno A and Sathyaprakash B 2015 *General Relativity and Gravitation: A Centennial Perspective* ed A Ashtekar *et al* (Cambridge, UK: Cambridge University Press)
- [642] Pretorius F 2007 *Binary Black Hole Coalescence* (New York: Springer) ch 9 (arXiv:0710.1338)
- [643] Centrella J, Baker J G, Kelly B J and van Meter J R 2010 *Rev. Mod. Phys.* **82** 3069
- [644] Sperhake U, Berti E and Cardoso V 2013 *C. R. Phys.* **14** 306–17
- [645] Pfeiffer H P 2012 *Class. Quantum Grav.* **29** 124004
- [646] Hannam M 2014 *Gen. Relativ. Gravit.* **46** 1767
- [647] Lehner L and Pretorius F 2014 *Ann. Rev. Astron. Astrophys.* **52** 661
- [648] Will C 1977 *Astrophys. J.* **214** 826–39
- [649] Lang R N 2014 *Phys. Rev. D* **89** 084014
- [650] Lang R N 2015 *Phys. Rev. D* **91** 084027
- [651] Will C M and Wiseman A G 1996 *Phys. Rev. D* **54** 4813–48
- [652] Pati M E and Will C M 2000 *Phys. Rev. D* **62** 124015
- [653] Pati M E and Will C M 2002 *Phys. Rev. D* **65** 104008
- [654] Healy J *et al* 2012 *Class. Quantum Grav.* **29** 232002
- [655] Berti E, Cardoso V, Gualtieri L, Horbatsch M and Sperhake U 2013 *Phys. Rev. D* **87** 124020
- [656] Krause D, Kloor H T and Fischbach E 1994 *Phys. Rev. D* **49** 6892–906
- [657] Perivolaropoulos L 2010 *Phys. Rev. D* **81** 047501
- [658] Sperhake U 2015 *Class. Quantum Grav.* **32** 124011
- [659] Cardoso V, Gualtieri L, Herdeiro C and Sperhake U 2015 *Living Rev. Relativity* **18** 1
- [660] Baumgarte T W and Shapiro S L 2010 *Numerical Relativity* (Cambridge: Cambridge University Press)
- [661] Salgado M 2006 *Class. Quantum Grav.* **23** 4719–42
- [662] Horbatsch M and Burgess C 2012 *J. Cosmol. Astropart. Phys.* **JCAP05(2012)010**
- [663] Sahni V and Wang L M 2000 *Phys. Rev. D* **62** 103517
- [664] Hu W, Barkana R and Gruzinov A 2000 *Phys. Rev. Lett.* **85** 1158–61
- [665] Nordtvedt K 1968 *Phys. Rev.* **169** 1014–6
- [666] Roll P G, Krotkov R and Dicke R H 1964 *Ann. Phys.* **26** 442–517
- [667] Sampson L *et al* 2014 *Phys. Rev. D* **90** 124091
- [668] Ponce M, Palenzuela C, Barausse E and Lehner L 2015 *Phys. Rev. D* **91** 084038
- [669] Naf J and Jetzer P 2010 *Phys. Rev. D* **81** 104003
- [670] Naf J and Jetzer P 2011 *Phys. Rev. D* **84** 024027
- [671] De Laurentis M and Capozziello S 2011 *Astropart. Phys.* **35** 257–65
- [672] De Laurentis M and De Martino I 2013 *Mon. Not. R. Astron. Soc.* **431** 741–48
- [673] Stein L C and Yagi K 2014 *Phys. Rev. D* **89** 044026
- [674] Hansen D, Yunes N and Yagi K 2015 *Phys. Rev. D* **91** 082003
- [675] Goldberger W D and Rothstein I Z 2006 *Phys. Rev. D* **73** 104029
- [676] Weisberg J M and Taylor J H 2005 *ASP Conf. Ser.* **328** 25
- [677] Narikawa T *et al* 2015 *Phys. Rev. D* **91** 062007
- [678] Hulse R and Taylor J 1975 *Astrophys. J. Lett.* **195** L51–3
- [679] Hobbs G *et al* 2012 *Mon. Not. R. Astron. Soc.* **427** 2780–7
- [680] Manchester R N, Hobbs G B, Teoh A and Hobbs M 2005 *Astron. J.* **129** 1993
- [681] Kramer M 2012 *IAU Proc.* **8** 19–26
- [682] Damour T 1988 Strong-field tests of general relativity and the binary pulsar *Proc. 2nd Canadian Conf. on General Relativity and Relativistic Astrophysics* ed A Coley, C Dyer and T Tupper pp 315–34
- [683] Damour T and Taylor J H 1992 *Phys. Rev. D* **45** 1840–68
- [684] Damour T and Deruelle N 1986 *Ann. Inst. Henri Poincaré Phys. Théor.* **44** 263–92
- [685] Taylor J, Fowler L and McCulloch P 1979 *Nature* **277** 437–40
- [686] Weisberg J, Nice D and Taylor J 2010 *Astrophys. J.* **722** 1030–4
- [687] Burgay M *et al* 2003 *Nature* **426** 531–3

- [688] Lyne A *et al* 2004 *Science* **303** 1153–7
- [689] Perera B *et al* 2010 *Astrophys. J.* **721** 1193
- [690] Breton R P *et al* 2008 *Science* **321** 104–7
- [691] Antoniadis J *et al* 2012 *Mon. Not. R. Astron. Soc.* **423** 3316
- [692] Shao L and Wex N 2012 *Class. Quantum Grav.* **29** 215018
- [693] Esposito-Farèse G 2011 *Fundam. Theor. Phys.* **162** 461–89
- [694] Damour T and Schaefer G 1991 *Phys. Rev. Lett.* **66** 2549–52
- [695] Stairs I H *et al* 2005 *Astrophys. J.* **632** 1060–8
- [696] Gonzalez M *et al* 2011 *Astrophys. J.* **743** 102
- [697] Ransom S M 2014 *Nature* **505** 520–4
- [698] Freire P C, Kramer M and Wex N 2012 *Class. Quantum Grav.* **29** 184007
- [699] Bhat N R, Bailes M and Verbiest J P 2008 *Phys. Rev. D* **77** 124017
- [700] Kramer M *et al* 2006 *Science* **314** 97–102
- [701] Audren B, Blas D, Lesgourgues J and Sibiryakov S 2013 *J. Cosmol. Astropart. Phys.* **JCAP08(2013)039**
- [702] Audren B, Blas D, Ivanov M, Lesgourgues J and Sibiryakov S 2015 *J. Cosmol. Astropart. Phys.* **JCAP03(2015)016**
- [703] Nan R *et al* 2011 *Int. J. Mod. Phys. D* **20** 989–1024
- [704] Lazio T 2013 *Class. Quantum Grav.* **30** 224011
- [705] Blanchet L and Schaefer G 1989 *Mon. Not. R. Astron. Soc.* **239** 845–67
- [706] Damour T and Schäfer G 1988 *Nuovo Cimento B* **101** 127
- [707] Wex N and Kopeikin S 1999 *Astrophys. J.* **514** 388
- [708] Liu K, Wex N, Kramer M, Cordes J and Lazio T 2012 *Astrophys. J.* **747** 1
- [709] Wex N *et al* 2012 *IAU Proc.* **8** 171–6
- [710] Liu K, Eatough R, Wex N and Kramer M 2014 *Mon. Not. R. Astron. Soc.* **445** 3115
- [711] Manchester R 2013 *Class. Quantum Grav.* **30** 224010
- [712] Lee K 2013 *Class. Quantum Grav.* **30** 224016
- [713] Corbin V and Cornish N J 2010 arXiv:1008.1782
- [714] Lee K *et al* 2011 *Mon. Not. R. Astron. Soc.* **414** 3251
- [715] Ade P *et al* (Planck Collaboration) 2014 *Astron. Astrophys.* **571** A16
- [716] Peacock J 1999 *Cosmological Physics (Cambridge Astrophysics)* (Cambridge: Cambridge University Press) ISBN 9780521422703
- [717] Copeland E J, Sami M and Tsujikawa S 2006 *Int. J. Mod. Phys. D* **15** 1753–936
- [718] Will C M 2011 *Proc. Natl Acad. Sci.* **108** 5938
- [719] Battye R A and Pearson J A 2012 *J. Cosmol. Astropart. Phys.* **JCAP07(2012)019**
- [720] Battye R A and Pearson J A 2013 *Phys. Rev. D* **88** 061301
- [721] Gergely L A and Tsujikawa S 2014 *Phys. Rev. D* **89** 064059
- [722] Gubitosi G, Piazza F and Vernizzi F 2013 *J. Cosmol. Astropart. Phys.* **JCAP02(2013)032**
- [723] Bloomfield J K, Flanagan E E, Park M and Watson S 2013 *J. Cosmol. Astropart. Phys.* **JCAP08(2013)010**
- [724] Gleyzes J, Langlois D, Piazza F and Vernizzi F 2013 *J. Cosmol. Astropart. Phys.* **JCAP08(2013)025**
- [725] Gleyzes J, Langlois D and Vernizzi F 2015 *Int. J. Mod. Phys. D* **23** 1443010
- [726] Gao X 2014 *Phys. Rev. D* **90** 081501
- [727] Cheung C, Fitzpatrick A L, Kaplan J, Senatore L and Creminelli P 2008 *J. High Energy Phys.* **JHEP03(2008)014**
- [728] Baker T, Ferreira P G and Skordis C 2013 *Phys. Rev. D* **87** 024015
- [729] Silvestri A, Pogosian L and Buniy R V 2013 *Phys. Rev. D* **87** 104015
- [730] Oyaizu H 2008 *Phys. Rev. D* **78** 123523
- [731] Noller J, von Braun-Bates F and Ferreira P G 2014 *Phys. Rev. D* **89** 023521
- [732] Brax P, Davis A C, Li B, Winther H A and Zhao G B 2013 *J. Cosmol. Astropart. Phys.* **JCAP04(2013)029**
- [733] Brax P, Davis A C, Li B, Winther H A and Zhao G B 2012 *J. Cosmol. Astropart. Phys.* **JCAP10(2012)002**
- [734] Llinares C and Mota D 2013 *Phys. Rev. Lett.* **110** 161101
- [735] Comelli D, Crisostomi M and Pilo L 2014 *Phys. Rev. D* **90** 084003
- [736] De Felice A, Kobayashi T and Tsujikawa S 2011 *Phys. Lett. B* **706** 123–33
- [737] Amendola L, Kunz M, Motta M, Saltas I D and Sawicki I 2013 *Phys. Rev. D* **87** 023501

- [738] Baker T, Ferreira P G, Leonard C D and Motta M 2014 *Phys. Rev. D* **90** 124030
- [739] Leonard C D, Baker T and Ferreira P G 2015 *Phys. Rev. D* **91** 083504
- [740] <http://www.lsst.org/lsst/>
- [741] Hojjati A, Pogosian L, Silvestri A and Zhao G B 2014 *Phys. Rev. D* **89** 083505
- [742] Johnson A *et al* 2014 *Mon. Not. R. Astron. Soc.* **444** 3926
- [743] Khoury J and Weltman A 2004 *Phys. Rev. D* **69** 044026
- [744] Mota D F and Shaw D J 2007 *Phys. Rev. D* **75** 063501
- [745] Hinterbichler K and Khoury J 2010 *Phys. Rev. Lett.* **104** 231301
- [746] Deffayet C, Esposito-Farese G and Vikman A 2009 *Phys. Rev. D* **79** 084003
- [747] Llinares C, Mota D F and Winther H A 2014 *Astron. Astrophys.* **562** A78
- [748] Li B, Zhao G B, Teyssier R and Koyama K 2012 *J. Cosmol. Astropart. Phys.* **JCAP01(2012)051**
- [749] Puchwein E, Baldi M and Springel V 2013 *Mon. Not. Roy. Astron. Soc.* **436** 348
- [750] Davis A C, Li B, Mota D F and Winther H A 2012 *Astrophys. J.* **748** 61
- [751] Schmidt F 2009 *Phys. Rev. D* **80** 123003
- [752] Schmidt F 2009 *Phys. Rev. D* **80** 043001
- [753] Barreira A, Li B, Hellwing W A, Baugh C M and Pascoli S 2013 *J. Cosmol. Astropart. Phys.* **JCAP10(2013)027**
- [754] Schmidt F, Vikhlinin A and Hu W 2009 *Phys. Rev. D* **80** 083505
- [755] Schmidt F, Lima M V, Oyaizu H and Hu W 2009 *Phys. Rev. D* **79** 083518
- [756] Schmidt F 2010 *Phys. Rev. D* **81** 103002
- [757] Zhao G B, Li B and Koyama K 2011 *Phys. Rev. Lett.* **107** 071303
- [758] Hellwing W A, Barreira A, Frenk C S, Li B and Cole S 2014 *Phys. Rev. Lett.* **112** 221102
- [759] Lam T Y, Nishimichi T, Schmidt F and Takada M 2012 *Phys. Rev. Lett.* **109** 051301
- [760] Shim J, Lee J and Baldi M 2014 arXiv:1404.3639
- [761] Avilez A and Skordis C 2014 *Phys. Rev. Lett.* **113** 011101
- [762] Lombriser L, Slosar A, Seljak U and Hu W 2012 *Phys. Rev. D* **85** 124038
- [763] Barreira A, Li B, Baugh C M and Pascoli S 2012 *Phys. Rev. D* **86** 124016
- [764] Zuntz J A, Ferreira P and Zlosnik T 2008 *Phys. Rev. Lett.* **101** 261102
- [765] Koivisto T and Mota D F 2008 *J. Cosmol. Astropart. Phys.* **JCAP08(2008)021**
- [766] Akrami Y, Koivisto T S, Mota D F and Sandstad M 2013 *J. Cosmol. Astropart. Phys.* **JCAP10(2013)046**
- [767] Koennig F, Akrami Y, Amendola L, Motta M and Solomon A R 2014 *Phys. Rev. D* **90** 124014
- [768] Bean R and Tangmatitham M 2010 *Phys. Rev. D* **81** 083534
- [769] Zhao H, Peacock J A and Li B 2013 *Phys. Rev. D* **88** 043013
- [770] Hui L and Nicolis A 2012 *Phys. Rev. Lett.* **109** 051304
- [771] Davis A C, Lim E A, Sakstein J and Shaw D 2012 *Phys. Rev. D* **85** 123006
- [772] Ferraro S, Schmidt F and Hu W 2011 *Phys. Rev. D* **83** 063503
- [773] Penarrubia J, Kuposov S E and Walker M G 2012 *Astrophys. J.* **760** 2
- [774] Ade P *et al* (BICEP2 Collaboration) 2014 *Phys. Rev. Lett.* **112** 241101
- [775] Flauger R, Hill J C and Spergel D N 2014 *J. Cosmol. Astropart. Phys.* **JCAP08(2014)039**
- [776] Adam R *et al* (Planck) 2015 submitted to A&A (arXiv:1502.01588)
- [777] Ade P *et al* (BICEP2, Planck) 2015 *Phys. Rev. Lett.* **114** 101301
- [778] Ade P *et al* (Planck) 2015 submitted to A&A (arXiv:1502.02114)
- [779] Calabrese E *et al* 2014 *J. Cosmol. Astropart. Phys.* **JCAP08(2014)010**
- [780] Benson B *et al* (SPT-3G) 2014 *Proc. SPIE Int. Soc. Opt. Eng.* **9153** 91531P
- [781] Ryan F D 1997 *Phys. Rev. D* **56** 1845–55
- [782] Barack L and Cutler C 2007 *Phys. Rev. D* **75** 042003
- [783] Amaro-Seoane P, Gair J R, Freitag M, Miller M C, Mandel I, Cutler C J and Babak S 2007 *Class. Quantum Grav.* **24** R113–69
- [784] Gair J R 2009 *Class. Quantum Grav.* **26** 094034
- [785] Pani P, Berti E, Cardoso V, Chen Y and Norte R 2010 *Phys. Rev. D* **81** 084011
- [786] Berti E, Cardoso J, Cardoso V and Cavaglia M 2007 *Phys. Rev. D* **76** 104044
- [787] Gossan S, Veitch J and Sathyaprakash B 2012 *Phys. Rev. D* **85** 124056
- [788] Schutz B F 1986 *Nature* **323** 310–1
- [789] Holz D E and Hughes S A 2005 *Astrophys. J.* **629** 15–22
- [790] Shapiro C, Bacon D, Hendry M and Hoyle B 2010 *Mon. Not. R. Astron. Soc.* **404** 858–66
- [791] Messenger C and Read J 2012 *Phys. Rev. Lett.* **108** 091101

- [792] Messenger C, Takami K, Gossan S, Rezzolla L and Sathyaprakash B 2014 *Phys. Rev. X* **4** 041004
- [793] Del Pozzo W 2012 *Phys. Rev. D* **86** 043011
- [794] Taylor S R, Gair J R and Mandel I 2012 *Phys. Rev. D* **85** 023535
- [795] Taylor S R and Gair J R 2012 *Phys. Rev. D* **86** 023502
- [796] Seto N, Kawamura S and Nakamura T 2001 *Phys. Rev. Lett.* **87** 221103
- [797] Takahashi R and Nakamura T 2005 *Prog. Theor. Phys.* **113** 63–71
- [798] Nishizawa A, Yagi K, Taruya A and Tanaka T 2012 *Phys. Rev. D* **85** 044047
- [799] Nishizawa A, Yagi K, Taruya A and Tanaka T 2012 *J. Phys. Conf. Ser.* **363** 012052
- [800] Loeb A 1998 *Astrophys. J.* **499** L111–4
- [801] Quartin M and Amendola L 2010 *Phys. Rev. D* **81** 043522
- [802] Yagi K, Nishizawa A and Yoo C M 2012 *J. Cosmol. Astropart. Phys.* JCAP04(2012)031
- [803] Yagi K, Nishizawa A and Yoo C M 2012 *J. Phys. Conf. Ser.* **363** 012056
- [804] Dalal N, Holz D E, Hughes S A and Jain B 2006 *Phys. Rev. D* **74** 063006
- [805] Zhao W, Van Den Broeck C, Baskaran D and Li T G F 2011 *Phys. Rev. D* **83** 023005
- [806] Krisner T P and Will C M 1985 *Phys. Rev. D* **31** 2480–7
- [807] Gürsel Y and Tinto M 1989 *Phys. Rev. D* **40** 3884–938
- [808] Chatterji S, Lazzarini A, Stein L, Sutton P J, Searle A and Tinto M 2006 *Phys. Rev. D* **74** 082005
- [809] Lee K J, Jenet F A and Price R H 2008 *Astrophys. J.* **685** 1304–19
- [810] Arun K G 2012 *Class. Quantum Grav.* **29** 075011
- [811] Chatziioannou K, Yunes N and Cornish N 2012 *Phys. Rev. D* **86** 022004
- [812] Isi M, Weinstein A J, Mead C and Pitkin M 2015 *Phys. Rev. D* **91** 082002
- [813] Hayama K and Nishizawa A 2013 *Phys. Rev. D* **87** 062003
- [814] Maggiore M 2007 *Gravitational Waves* (Oxford: Oxford University Press) ISBN 9780198570745
- [815] Creighton J D and Anderson W G 2011 *Gravitational-Wave Physics and Astronomy: An Introduction to Theory, Experiment and Data Analysis* (Weinheim, Germany: Wiley-VCH)
- [816] Veitch J *et al* 2015 *Phys. Rev. D* **91** 042003
- [817] Berti E 2006 *Class. Quantum Grav.* **23** S785–98
- [818] Cutler C and Vallisneri M 2007 *Phys. Rev. D* **76** 104018
- [819] Sathyaprakash B and Dhurandhar S 1991 *Phys. Rev. D* **44** 3819–34
- [820] Dhurandhar S and Sathyaprakash B 1994 *Phys. Rev. D* **49** 1707–22
- [821] Finn L S and Chernoff D F 1993 *Phys. Rev. D* **47** 2198–219
- [822] Arun K G, Iyer B R, Qusailah M S S and Sathyaprakash B S 2006 *Class. Quantum Grav.* **23** L37–43
- [823] Arun K G, Iyer B R, Qusailah M S S and Sathyaprakash B S 2006 *Phys. Rev. D* **74** 024006
- [824] Mishra C K, Arun K, Iyer B R and Sathyaprakash B 2010 *Phys. Rev. D* **82** 064010
- [825] Blanchet L and Sathyaprakash B S 1995 *Phys. Rev. Lett.* **74** 1067–70
- [826] Li T G F *et al* 2012 *Phys. Rev. D* **85** 082003
- [827] Del Pozzo W, Veitch J and Vecchio A 2011 *Phys. Rev. D* **83** 082002
- [828] Vishveshwara C 1970 *Phys. Rev. D* **1** 2870–9
- [829] Ruffini R J and Wheeler J A 1971 *Phys. Today* **24** 30
- [830] Dreyer O, Kelly B J, Krishnan B, Finn L S, Garrison D and Lopez-Aleman R 2004 *Class. Quantum Grav.* **21** 787–804
- [831] Detweiler S L 1978 *Astrophys. J.* **225** 687–93
- [832] Kamaretsos I, Hannam M, Husa S and Sathyaprakash B S 2012 *Phys. Rev. D* **85** 024018
- [833] Meidam J, Agathos M, Van Den Broeck C, Veitch J and Sathyaprakash B S 2014 *Phys. Rev. D* **90** 064009
- [834] Kamaretsos I, Hannam M and Sathyaprakash B 2012 *Phys. Rev. Lett.* **109** 141102
- [835] Berti E, Cardoso V and Will C M 2006 *AIP Conf. Proc.* **873** 82–88
- [836] Barausse E and Rezzolla L 2009 *Astrophys. J. Lett.* **704** L40–44
- [837] O’Shaughnessy R, London L, Healy J and Shoemaker D 2013 *Phys. Rev. D* **87** 044038
- [838] Pekowsky L, O’Shaughnessy R, Healy J and Shoemaker D 2013 *Phys. Rev. D* **88** 024040
- [839] London L, Shoemaker D and Healy J 2014 *Phys. Rev. D* **90** 124032
- [840] Yunes N and Pretorius F 2009 *Phys. Rev. D* **80** 122003
- [841] Vallisneri M and Yunes N 2013 *Phys. Rev. D* **87** 102002
- [842] Li T G F *et al* 2012 *J. Phys. Conf. Ser.* **363** 012028

- [843] Van Den Broeck C 2014 Probing dynamical spacetimes with gravitational waves *Springer Handbook of Spacetime* (Berlin: Springer)
- [844] Agathos M *et al* 2015 *Proc. MG13 Meeting on General Relativity* pp 1710–12
- [845] Agathos M, Del Pozzo W, Li T G F, Van Den Broeck C, Veitch J and Vitale S 2014 *Phys. Rev. D* **89** 082001
- [846] Del Pozzo W, Grover K, Mandel I and Vecchio A 2014 *Class. Quantum Grav.* **31** 205006
- [847] Yunes N and Hughes S A 2010 *Phys. Rev. D* **82** 082002
- [848] Blanchet L and Sathyaprakash B S 1994 *Class. Quantum Grav.* **11** 2807–31
- [849] Vitale S and Del Pozzo W 2014 *Phys. Rev. D* **89** 022002
- [850] Sampson L, Cornish N and Yunes N 2014 *Phys. Rev. D* **89** 064037
- [851] Vitale S, Del Pozzo W, Li T G F, Van Den Broeck C, Mandel I, Aylott B and Veitch J 2012 *Phys. Rev. D* **85** 064034
- [852] Vitale S *et al* 2014 *J. Phys. Conf. Ser.* **484** 012026
- [853] Favata M 2014 *Phys. Rev. Lett.* **112** 101101
- [854] Samsing J, MacLeod M and Ramirez-Ruiz E 2014 *Astrophys. J.* **784** 71
- [855] O’Leary R, O’Shaughnessy R and Rasio F 2007 *Phys. Rev. D* **76** 061504
- [856] Downing J M B, Benacquista M J, Giersz M and Spurzem R 2011 *MNRAS* **416** 133–47
- [857] Morscher M, Umbreit S, Farr W M and Rasio F A 2013 *Astrophys. J.* **763** L15
- [858] Antonini F, Murray N and Mikkola S 2014 *Astrophys. J.* **781** 45
- [859] Antognini J M, Shappee B J, Thompson T A and Amaro-Seoane P 2014 *MNRAS* **439** 1079–91
- [860] Del Pozzo W, Li T G F, Agathos M, Van Den Broeck C and Vitale S 2013 *Phys. Rev. Lett.* **111** 071101
- [861] Abadie J *et al* (LIGO Scientific) 2010 *Class. Quantum Grav.* **27** 173001
- [862] Dominik M *et al* 2015 *Astrophys. J.* **806** 263
- [863] Damour T, Nagar A and Villain L 2012 *Phys. Rev. D* **85** 123007
- [864] Wade L *et al* 2014 *Phys. Rev. D* **89** 103012
- [865] Poisson E 1998 *Phys. Rev. D* **57** 5287–90
- [866] Mikoczi B, Vasuth M and Gergely L A 2005 *Phys. Rev. D* **71** 124043
- [867] Kidder L E, Will C M and Wiseman A G 1993 *Phys. Rev. D* **47** 4183–7
- [868] Arun K G, Buonanno A, Faye G and Ochsner E 2009 *Phys. Rev. D* **79** 104023
- [869] Flanagan É É and Hinderer T 2008 *Phys. Rev. D* **77** 021502
- [870] Read J S *et al* 2009 *Phys. Rev. D* **79** 124033
- [871] Lackey B D, Kyutoku K, Shibata M, Brady P R and Friedman J L 2012 *Phys. Rev. D* **85** 044061
- [872] Lackey B D, Kyutoku K, Shibata M, Brady P R and Friedman J L 2014 *Phys. Rev. D* **89** 043009
- [873] Read J S *et al* 2013 *Phys. Rev. D* **88** 044042
- [874] Yagi K and Yunes N 2014 *Phys. Rev. D* **89** 021303
- [875] Lattimer J M 2010 *Prog. Theor. Phys. Suppl.* **186** 1–8
- [876] Yunes N, Arun K, Berti E and Will C M 2009 *Phys. Rev. D* **80** 084001
- [877] Królak A, Kokkotas K D and Schäfer G 1995 *Phys. Rev. D* **52** 2089–111
- [878] Gopakumar A and Schäfer G 2011 *Phys. Rev. D* **84** 124007
- [879] Huerta E, Kumar P, McWilliams S T, O’Shaughnessy R and Yunes N 2014 *Phys. Rev. D* **90** 084016
- [880] Lundgren A and O’Shaughnessy R 2014 *Phys. Rev. D* **89** 044021
- [881] Berti E, Buonanno A and Will C M 2005 *Phys. Rev. D* **71** 084025
- [882] Buonanno A, Iyer B, Ochsner E, Pan Y and Sathyaprakash B S 2009 *Phys. Rev. D* **80** 084043
- [883] Pan Y, Buonanno A, Taracchini A, Boyle M, Kidder L E, Mroué A H, Pfeiffer H P, Scheel M A, Szilágyi B and Zenginoglu A 2014 *Phys. Rev. D* **89** 061501
- [884] Sturani R, Fischetti S, Cadonati L, Guidi G M, Healy J, Shoemaker D M and Viceré A 2010 *J. Phys.: Conf. Ser.* **243** 012007
- [885] Sturani R *et al* 2010 arXiv:1012.5172
- [886] Hannam M *et al* 2014 *Phys. Rev. Lett.* **113** 151101
- [887] Schmidt P, Ohme F and Hannam M 2015 *Phys. Rev. D* **91** 024043
- [888] Barausse E, Cardoso V and Pani P 2015 *J. Phys.: Conf. Ser.* **610** 012044
- [889] Barausse E and Rezzolla L 2008 *Phys. Rev. D* **77** 104027
- [890] Barausse E 2007 *Mon. Not. R. Astron. Soc.* **382** 826–34
- [891] Yunes N, Kocsis B, Loeb A and Haiman Z 2011 *Phys. Rev. Lett.* **107** 171103
- [892] Kocsis B, Yunes N and Loeb A 2011 *Phys. Rev. D* **84** 024032
- [893] Gondolo P and Silk J 1999 *Phys. Rev. Lett.* **83** 1719–22

- [894] Merritt D, Milosavljevic M, Verde L and Jimenez R 2002 *Phys. Rev. Lett.* **88** 191301
- [895] Bertone G and Merritt D 2005 *Phys. Rev. D* **72** 103502
- [896] Ullio P, Zhao H and Kamionkowski M 2001 *Phys. Rev. D* **64** 043504
- [897] Bertone G, Zentner A R and Silk J 2005 *Phys. Rev. D* **72** 103517
- [898] Leung P T, Liu Y T, Suen W M, Tam C Y and Young K 1997 *Phys. Rev. Lett.* **78** 2894–7
- [899] Almheiri A, Marolf D, Polchinski J, Stanford D and Sully J 2013 *J. High Energy Phys.* **JHEP09** (2013)018
- [900] Braunstein S L, Pirandola S and Zyczkowski K 2013 *Phys. Rev. Lett.* **110** 101301
- [901] Abbott B P *et al* (LIGO Scientific) 2009 *Phys. Rev. D* **80** 062001
- [902] Aasi J *et al* (LIGO Scientific Collaboration, VIRGO Collaboration) 2014 *Phys. Rev. D* **89** 102006
- [903] Berti E *et al* 2014 *Webpage of the Workshop Testing General Relativity with Astrophysical Observations (Oxford, MS, 6–10 January 2014)* (<http://www.phy.olemiss.edu/TestGR2014/>)